



NOVEL ELECTROSPUN POLYHYDROXYALKANOATE BASED
HIGH BARRIER AND ACTIVE BIOPAPERS OF INTEREST IN
FOOD PACKAGING

Tesis Doctoral Internacional

Adriane Cherpinski Correa

Valencia, May 2019

Supervisor:
Jose Maria Lagaron



INSTITUTO DE AGROQUÍMICA Y TECNOLOGIA DE ALIMENTOS

Universidad Politécnica de Valencia

Doctorado en Ciencia, Tecnología y Gestión Alimentaria

Tesis Doctoral Internacional

Adriane Cherpinski Correa

NOVEL ELECTROSPUN POLYHYDROXYALKANOATE BASED
HIGH BARRIER AND ACTIVE BIOPAPERS OF INTEREST IN
FOOD PACKAGING

NUEVOS BIOPAPELES BASADOS EN
POLIHIDROXIALCANOATOS CON PROPIEDADES DE
BARRERA PASIVA Y ACTIVA DE APLICACIÓN EN
ENVASADO ALIMENTARIO

Valencia, Mayo 2019

Supervisor:
Jose Maria Lagaron

Abstract

The present PhD thesis aimed to develop novel active fiber based biodegradable layers obtained by electrospinning, so-called biopapers, with water and gas barrier and oxygen scavenging properties for their potential use as paper coatings or packaging interlayers in fiber based packaging.

In a first study, PHB biopapers were obtained by electrospinning, by means of two types of collectors namely, flat plate and rotation drum collectors, to evaluate the influence of the alignment of fibers. Annealing post-processing below the polymer melting point was carried at different temperatures, isothermal times and cooling processes to obtain transparent and pore free continuous films by fibers coalescence which in turn led to interlayer adhesion, enhanced barrier and optical properties.

In a second study, mono and multilayer biopapers comprising PHB, PVOH and PLA were deposited onto a conventional uncoated paper substrate, using the cited two collectors; and the electrospinning processing time was varied to produce different thicknesses. To enhance adhesion to the paper substrate, optical and barrier performance of the multilayer, the biopapers were subjected to an annealed process as described and optimized in the first study. Regarding water barrier, the system paper/PVOH/PHB presented the highest barrier performance.

In a third study, environmentally friendly materials such as cellulose based nanopapers, i.e. gas barrier layers made of cellulose nanofibrils

(CNFs) and lignocellulose nanofibrils (LCNFs), were obtained and coated with the water barrier electrospun PHA biopapers. As a result, the hydrophobic character of the nanopapers was significantly improved by the electrospun biopapers. Moreover, these also exhibited a more balanced mechanical performance.

In a fourth study, active oxygen scavenging PHA biopapers were developed, in which palladium nanoparticles (PdNP) were used as catalysts to scavenge oxygen from the headspace. The main difficulty associated with nanoparticles is to keep them dispersed, so in this work we assessed the use of CTAB and TEOS surfactants as food contact permitted substances to help dispersion and distribution of the PdNP within the PHA fibers. As a result, oxygen scavenging nanocomposite biopapers made of electrospun PHB and PdNP were prepared, followed by annealing treatment to obtain homogeneous and continuous active layers. The oxygen scavenging capacity at 100% relative humidity (RH) of the biopapers in fiber form showed better performance than their annealed specimens as expected, but in general this was not considered optimal.

In order to improve further the oxygen scavenging capacity, even at a low relative humidity and in film form, a fifth study, developed multilayered biopapers made of PCL and PHA coated on conventional cellulose paper. The PCL/PdNP nanocomposites showed much more enhanced oxygen scavenging performance in comparison with the above PHA/PdNP

system. This result is attributed to the higher fractional free volume of the PCL polymer that allows moisture, hydrogen and oxygen permeation to trigger the catalytic scavenging reaction.

Finally, a sixth study, developed a solvent casting high gas barrier and active oxygen scavenging layer concept based on PdNP, CNC and EVOH. Thus, CNC and TEMPO oxidized CNC, were used to produce in situ PdNP, which were incorporated into the EVOH polymer matrix. The TEMPO oxidized CNC exhibited higher oxygen absorption due to the generated carboxylic groups on CNC that created a strong coordination effect with the metal ions, which resulted in improved dispersion.

On the overall, the materials developed in this PhD thesis proposed novel layers and interlayers of potential application interest to design more sustainable and environmentally friendly nanobiocomposites of application interest in coating of fiber based food packaging papers that can replace current conventional materials and processes.

Resumen

La presente tesis doctoral tuvo como objetivo desarrollar nuevos materiales biodegradables hechos a base de fibras obtenidas mediante la técnica de electroestirado, denominadas “biopapers” o biopapeles, con barrera a agua y a gases y propiedades de secuestro de oxígeno para su posible aplicación en recubrimientos de papel o como capas intermedias en envases alimentarios basados en papel y cartón.

En un primer estudio, se desarrollaron biopapeles de PHB mediante electroestirado, usando dos tipos de colectores, colectores de placa plana y rotativo, para evaluar la influencia del alineamiento de las fibras. Con posterioridad se aplicó un tratamiento de recocido por debajo del punto de fusión del polímero a diferentes temperaturas, tiempos y procesos de enfriamiento para obtener películas continuas por coalescencia de las fibras, lo que a su vez condujo a la adhesión entre capas, y a una mejora en las propiedades barrera y ópticas.

En un segundo estudio, se depositaron biopapeles monocapa y multicapa hechos de PHB, PVOH y PLA sobre un sustrato de papel no estucado, utilizando los dos colectores citados; y el tiempo de procesamiento por electrospinning se varió para producir espesores diferentes. Para mejorar la adhesión al sustrato de papel, y las propiedades ópticas y de barrera de las multicapas, los biopapeles se sometieron a un proceso de recocido como se describe y optimiza en el primer estudio. Con respecto a la

barrera al agua, el sistema de papel/ PVOH/PHB presentó las mejores propiedades.

En un tercer estudio, se obtuvieron dos nanopapeles de alta barrera hechos a base de nanofibras de celulosa de dos tipos, nanofibras de celulosa (CNF) y nanofibras de lignocelulosa (LCNF) y se recubrieron con biopapeles de PHA electroestirados con barrera a agua. Como resultado, el carácter hidrófobo de los nanopapeles se mejoró significativamente. Por otra parte, estos también exhibieron un rendimiento mecánico más equilibrado.

En un cuarto estudio, se desarrollaron biopapeles de PHA con capacidad activa de secuestro de oxígeno, para lo cual se usaron nanopartículas de paladio (PdNP) como catalizadores de la respuesta activa. La principal dificultad asociada con las nanopartículas es mantenerlas dispersas, por lo que en este trabajo evaluamos el uso de surfactantes CTAB y TEOS como sustancias permitidas en contacto con alimentos para ayudar a la dispersión y distribución de PdNP dentro de las fibras de PHA. Como resultado, se prepararon nanocompuestos electroestirados con capacidad de secuestro de oxígeno hechos de PHB y PdNP, seguidos de un tratamiento de recocido para obtener capas continuas y autoadhesivas. La capacidad de secuestro de oxígeno de los biopapeles, medida a un 100% de humedad relativa (HR), mostró un mejor rendimiento para el material en forma de fibra que en forma de film. En cualquier caso, los resultados indicaron una cinética de absorción relativamente baja.

Con el fin de mejorar aún más la cinética de secuestro de oxígeno, incluso a una humedad intermedia y en forma de película, un quinto estudio, desarrolló biopapeles multicapa hechos de PCL y PHA aplicados sobre papel no estucado. Los nanocompuestos de PCL/PdNP mostraron una cinética de secuestro de oxígeno mucho mayor que la del sistema PHA / PdNP anterior. Este resultado se atribuye a la mayor fracción de volumen libre del PCL que permite que la humedad, el hidrógeno y la permeación de oxígeno desencadenen la reacción de eliminación catalítica de forma más eficiente.

Finalmente, un sexto estudio, desarrolló un nuevo concepto de capa con capacidad de secuestro de oxígeno y con alta barrera pasiva a gases y vapores orgánicos basado en PdNP, CNC y EVOH. Así, CNC y CNC oxidado con TEMPO (TEMPO oxidized CNC), se utilizaron para producir PdNP in situ sobre el nanorefuerzo, que se incorporaron en la matriz del polímero EVOH. El TEMPO oxidized CNC demostró poseer una mayor absorción de oxígeno debido a los grupos carboxílicos generados en el CNC que posibilitan un fuerte efecto de coordinación con los iones metálicos, efecto que justifica su mejor dispersión.

En general, los materiales desarrollados en esta tesis doctoral propusieron nuevos recubrimientos e intercapas de interés potencial para diseñar nanobiocompuestos más sostenibles y respetuosos con el medio ambiente que puedan tener aplicación en el recubrimiento de papeles de uso

alimentario y que puedan reemplazar a materiales y procesos que se utilizan en la actualidad.

Resum

La present tesi doctoral va tindre com a objectiu desenvolupar noves capes biodegradables actives obtingudes mitjançant electrospinning, denominades "biopapers" o biopapeles, amb barrera a aigua i a gasos i propietats de segrest d'oxigen per a la seua possible aplicació en recobriments de paper o com a capes intermèdies en envasos alimentaris basats en paper i cartó.

En un primer estudi, es van desenvolupar bio-papers de PHB mitjançant electrospinning, utilitzant dos tipus de col·lectors, col·lectors de placa plana i rotatiu, per a avaluar la influència de l'alineament de les fibres. Amb posterioritat es va aplicar un tractament de recuita per davall del punt de fusió del polímer a diferents temperatures, temps i processos de refredament per a obtenir pel·lícules contínues per coalescència de les fibres, la qual cosa al seu torn va conduir a l'adhesió entre capes, i a una millora en les propietats barrera i òptiques.

En un segon estudi, es van depositar bio-papers monocapa i multicapa fets de PHB, PVOH i PLA sobre un substrat de paper no estucat, utilitzant els dos col·lectors citats; i el temps de processament per electrospinning es va variar per a produir grossàries diferents. Per a millorar l'adhesió al substrat de paper, i les propietats òptiques i de barrera de les multicapes, els biopapers es van sotmetre a un procés de recuita com es descriu i optimitza en el primer estudi. Respecte a la barrera a l'aigua, el sistema de paper/PVOH/PHB va presentar les millors propietats.

En un tercer estudi, es van obtenir dos nano-papers d'alta barrera fets a base de nanofibres de cel·lulosa de dos tipus, nanofibres de cel·lulosa (CNF) i nanofibres de lignocel·lulosa (LCNF) i es van recobrir amb bio-papers de PHA electro-estirats amb barrera aigua. Com a resultat, el caràcter hidròfob dels nano-papers es va millorar significativament. D'altra banda, aquests també van exhibir un rendiment mecànic més equilibrat.

En un quart estudi, es van desenvolupar bio-papers de PHA amb capacitat activa de segrest d'oxigen, per a això es van usar nanopartícules de pal·ladi (PdNP) com a catalitzadors de la resposta activa. La principal dificultat associada amb les nanopartícules és mantenir-les disperses, per la qual cosa en aquest treball avaluem l'ús de surfactants CTAB i TEOS com a substàncies permeses en contacte amb aliments per a ajudar la dispersió i distribució de PdNP dins de les fibres de PHA. Com a resultat, es van preparar nano-compostos electro-estirats amb capacitat de segrest d'oxigen fets de PHB i PdNP, seguits d'un tractament de recuita per a obtenir capes contínues i autoadhesives. La capacitat de segrest d'oxigen dels bio-papers, mesurada a un 100% d'humitat relativa (HR), va mostrar un millor rendiment per al material en forma de fibra que en forma de film. En qualsevol cas, els resultats van indicar una cinètica de absorció relativament baixa.

Amb la finalitat de millorar encara més la cinètica de segrest d'oxigen, fins i tot a una humitat intermèdia i en forma de pel·lícula, un cinquè estudi,

va desenvolupar bio-papers multicapa fets de PCL i PHA aplicats sobre paper no estucat. Els nano-compostos de PCL/PdNP van mostrar una cinètica de segrest d'oxigen molt major que la del sistema PHA/PdNP anterior. Aquest resultat s'atribueix a la major fracció de volum lliure del PCL que permet que la humitat, l'hidrogen i la permeància d'oxigen desencadenen la reacció d'eliminació catalítica de forma més eficient.

Finalment, un sisè estudi, va desenvolupar un nou concepte de capa amb capacitat de segrest d'oxigen i amb alta barrera passiva a gasos i vapors orgànics basat en PdNP, CNC i EVOH. Així, CNC i CNC oxidat com TEMPO (TEMPO oxidat CNC), es van utilitzar per a produir PdNP in situ sobre el nano-reforç, que es van incorporar en la matriu del polímer EVOH. El TEMPO oxidat CNC va demostrar posseir una major absorció d'oxigen degut als grups carboxílics generats en el CNC que possibiliten un fort efecte de coordinació amb els ions metàl·lics, efecte que justifica la seua millor dispersió.

En general, els materials desenvolupats en aquesta tesi doctoral van proposar nous recobriments i intercapas d'interès potencial per a dissenyar nanobiocompostos més sostenibles i respectuosos amb el medi ambient que puguen tindre aplicació en el recobriment de papers d'ús alimentari i que puguen reemplaçar a materials i processos que s'utilitzen en l'actualitat.

Index

1. Introduction	1
1.1- Bio-based Packaging	3
1.2- Active Packaging: O ₂ scavengers	6
1.3- Nanometal based O ₂ scavenger	10
1.4- Fiber based Packaging	12
1.5- Coating of Fiber Based Packaging and Nanopapers	13
1.6- Electrospinning as an innovative processing technology: Electrospinning coating technique	17
2. General and specific objectives	35
3. Results	39
Chapter I: Post-processing optimization of electrospun submicron poly(3-hydroxybutyrate) fibers to obtain continuous films of interest in food packaging applications	43
Chapter II: Multilayer Structures Based on Annealed Electrospun Biopolymer Coatings of Interest in Water and Aroma Barrier Fiber-Based Food Packaging Applications	85
Chapter III: Improving the water resistance of nanocellulose-based films with polyhydroxyalkanoates processed by the electrospinning coating technique	125

Chapter IV: Electrospun Oxygen Scavenging Films of Poly(3-hydroxybutyrate) Containing Palladium Nanoparticles for Active Packaging Applications	171
Chapter V: Oxygen-Scavenging Multilayered Biopapers Containing Palladium Nanoparticles Obtained by the Electrospinning Coating Technique	215
Chapter VI: Preparation and evaluation of oxygen scavenging nanocomposite films incorporating poly(ethylene-co-vinyl alcohol), Pd nanoparticles, and cellulose nanocrystals	257
4. General discussion	297
5. Conclusions	309
6. Annexes	315
Annex A: List of publications	317
Annex B: Additional work	329

1. Introduction

1. Introduction

1.1 Bio-based Packaging

Packaging is used, among other roles, as a preservation technology to enhance the shelf-life of foods. Today, glass, metal, paper, paperboard and plastics are being used as packaging materials. However, these conventional food packaging materials, specially plastics and plastic coated paper, have brought up different problems, being the most relevant related to waste management [1]. To cope with this challenge society has led technologists to work on alternative packaging materials in bio-based packaging.

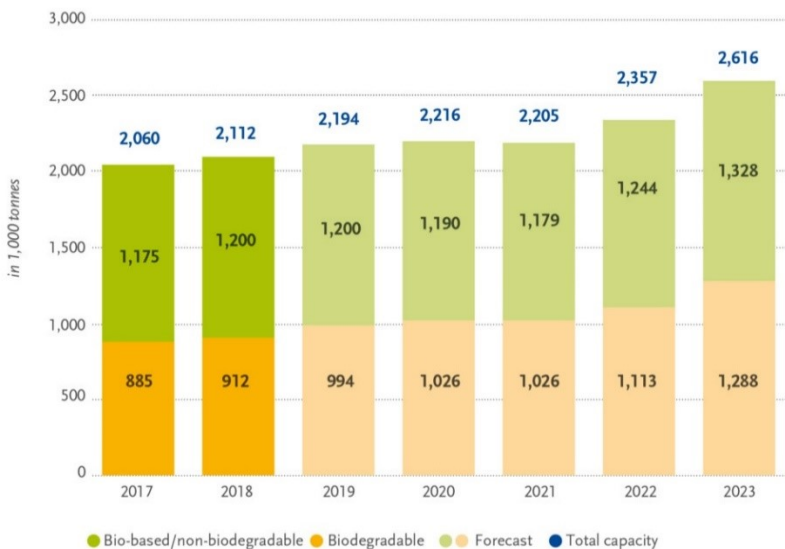
Such type of packaging materials are usually derived from biodegradable renewable resources. According to ASTM D7075-04 standard most of these materials are based on carbon compounds which are derived from non-fossil bio sources, where, these bio polymers generally produce lower carbon dioxide and hence, are more environment friendly in nature [2].

There are three principal ways to produce bio-based polymers using renewable resources: (1) direct extraction or tailored modification of polymers from biomass; (2) polymers produced by microorganisms; (3) bio-polymerization of monomers. Recently, many efforts have been invested towards introducing new bio-based polymers with higher performance and its production capacities are likely to be amplified in near future. [3].

Introduction

The worldwide production capacity of durable plastics in 2016 was almost 75 percent, which is expected to be increased to nearly 80 percent by 2021. Similarly, the production of PLA, PHA and alike polymers are growing as they were reported to be 0.9 million tonnes in 2016 and is expected to be increased to approximately 1.3 million tonnes by 2021 [4]. The PHA production, due to the ramp-up of capacities in Asia and USA as well as the first PHA plant in Europe, is expected to be quadruple in the next five years. In addition, the global production capacity is set to increase from around 2.11 million tonnes in 2018 to approximately 2.62 million tonnes in 2023 [5].

Global production capacities of bioplastics



Source: European Bioplastics, nova-Institute (2018)
More information: www.european-bioplastics.org/market and www.bio-based.eu/markets

However, the barrier properties of these biopolymers, especially against moisture, are somehow challenging. New innovations and efforts are therefore needed to develop new packaging materials to enhance their performance [6].

In the future, the demand of the food industry that are tailored barrier and mechanical properties are most likely to be polymers containing nanoadditives. The research in this area has already been initiated at small commercial scale but the coming decade is expected to observe significant advancement in biopolymers production for food packaging [7].

The barrier properties of bio-based food packaging are extremely important and special attention is needed to be given to their improvement. The hydrophilic nature of these polymers makes them less resistant to moisture and excessive water vapour transmission through these bio-based packaging shortens the shelf life that eventually increases the cost as well as the waste. Typically, polyhydroxybutirates (PHB), polylactic acid (PLA), polyhydroxyalkanoates (PHA) are filled with laminar nanofillers to improve their barrier properties [8]. But still the moisture resistance is a problem that needs be addressed.

The humidity may also affect the gas permeation properties of high gas impermeable materials such as nylon and ethylene vynil alcohol. Therefore, the researchers are focusing on this and future bio-based materials are expected to be considerably more resistant to water vapour. Presently, at high relative humidity conditions, very few bio-based

Introduction

materials retain their properties. [9]. Biomaterials such as PLA and PHA are, however, known to be largely independent on relative humidity.

Among the various bio-based materials used to date, PHA and PLA exhibit some degree of barrier to gas and water vapour and are found to be interesting for a range of food packaging application [10].

PHA in general, having comparatively better oxygen and water vapour barrier as well as better mechanical strength than other widely used biopolymers such as PLA, have emerged as a very promising polymer for different applications. However, they still have certain limitations like comparatively higher costs and limited availability [11], [12], issues that need to be resolved in the near future.

1.2- Active Packaging: O₂ scavengers

To maintain or extend the shelf life of food products along with their quality, some additives may be added to the food packaging and/or food packaging materials to turn them into active packaging technologies. These additives are either added to the packaging matrix directly, coated onto the interior surface of the packaging material or otherwise placed inside the packages in the form of, for instance, sachets [13].

Therefore, some active packaging technologies that can maintain quality, wholesomeness and safety of food products have been developed so far. Similarly, the environmental pollution and problems related to their disposal of food packaging have also been developed. Oxygen scavengers, moisture absorbers, carbon dioxide absorbers/emitters,

ethanol emitters, ethylene absorbers, time-temperature indicators, flavour releasing/absorbing systems and antimicrobial films are some of the examples of active packaging [14, 15].

The active packaging of foods is growing worldwide as more retailers and food processors are being aware of their benefits. These active packaging alternatives are believed to have a significant impact on food packaging and preservation processes [16].

Food's shelf life mainly depends on the oxygen present in the headspace of the food packaging that is responsible for oxidation where subsequently, the flavour, colour, texture and nutritive quality of food product may be altered. Hence the lowering of oxygen concentration or its complete removal from the package is the key factor to control this undesirable effect [17].

This undesirable oxygen concentration in the headspace of food packaging may be controlled either by vacuum sealing or by the provision of the inert gas atmosphere using nitrogen (N_2) and/or carbon dioxide (CO_2) that have the capacity to remove c.a. 90 to 95% of oxygen present in the packaging headspace. Active alternatives to these technologies are the oxygen scavengers (OS), which may reduce the oxygen concentration even up-to 0.01% of its initial concentration [18].

These oxygen scavengers act as an active barrier that actively removes the residual oxygen present in food package thus creating efficient technologies targeting the undesired oxygen concentrations and helping to extend the shelf life of food products [19].

Introduction

Research on oxygen scavengers like ferrous sulfate as moisture absorbing mixture began in 1920s. A patent in 1938 was registered with the British government where Iron, Manganese or Zinc was reported to as oxygen scavenger for canned foods. Most of the research in this area was conducted by the United Kingdom and United States in 1940s for military rations. The first iron oxide based commercial oxygen scavenger was reported by Mitsubishi Gas and Chemical company in Japan in 1970s [20]. Apart from iron powders, researchers also reported the use of Zinc, Manganese, Titanium, Copper and alike transition metals as reducing agents. Their oxidation mechanism has been reported to be similar to that of iron powders but lower reaction capacities, higher cost and toxic nature limited their use as oxygen scavengers at commercial level [21].

Usually the commercially available oxygen scavengers contain iron that absorb oxygen and are marketed in the form of sachets [22] but then a foreign item needs to be inserted in the packaging design, which sometimes may not be accepted by the consumer. Furthermore, they may not be considered as a true active material as the active solution is considered to be independent of the packaging material [23].

The oxygen scavengers were initiated with the use of a sachet inside the food package but the present trend in their commercial applications is to incorporate the active to the packaging material so as to avoid the negative perception by consumers (the risk of accidental rupture of the sachet inside the food packaging) of being ingesting the non-edible content along with the food product [24].

The oxygen scavenging films are alternatives to the sachets, where, low molecular weight ingredients may be dispersed within the polymer matrix or in other cases the plastic material may intrinsically act as an oxygen scavenger. These oxygen scavengers may be incorporated as a solid dispersion in the plastic medium or coated on a surface like enamels, printing ink, lacquer or as adhesive [25].

The prerequisite for these oxygen scavengers in the packaging material is that the system must not be affected by the oxygen before use [26].

Factors like activation mechanisms of the oxygen scavengers, their reaction by-products, their oxidation endpoints and the scavenger's interactions with the product makes the application of scavenging technology somehow complex [27].

The preliminary oxygen scavenging packaging films reported by Kuhn et al. as well as by Warmbier and Wold in 1970s were multilayer systems where palladium metal was used in the can lids. The cans were pre-charged with the mixtures of hydrogen and nitrogen and the residual oxygen could react with hydrogen producing water in the presence of a palladium surface [25].

These oxygen scavengers based "active packaging" technologies play a vital role in optimizing the oxygen concentration inside the food packaging hence preserving and consequently prolongs the shelf life of food products sensitive to oxygen [28].

1.3- Nanometal based O₂ scavenger

Numerous metal based systems have been developed for their use in packaging. Ferrous based oxygen scavengers have most widely been reported as preservation for packaged food [29, 30]. The reported data reveals that approximately 2 grams of ferrous carbonate can absorb at least 100 mL of oxygen [31]. As explained above, most of commercially available oxygen scavengers are in the form of small sachets but current preferences are to incorporate them into the packaging materials [19, 32-35].

To be able to respond to the cited trends and to optimize food safety, quality and improved active properties, the conventional oxygen scavenging materials are being replaced by nanomaterials, where antimicrobial nanomaterials, nanobiosensors and oxygen scavengers are examples of the current research investigations in nanomaterials for food packaging [36]. The application of oxygen scavengers is one of the most important active packaging technologies [37].

Noble metals such as palladium (Pd), gold (Au) and platinum (Pt) nanoparticles due to their large surface area display a strong catalytic hydration, hydrogenation and oxidation type of reactions [38]. These nanoparticles provide remarkable oxygen scavenging properties, which may be of interest in future food packaging applications [39]. Generally oxygen and hydrogen molecules are adsorbed and dissociated onto the

surface of these nanoparticles, where they react as atomic O, H, and OH to form water [40].

The oxidative mode of action of the catalytic system palladium (CSP) is based on the catalytic oxidation of hydrogen in the presence of water [37]. However, the exact mechanism of how the substrate affects the oxygen scavenging reaction is not yet fully understood. It was found out that in the presence of $H_2/H_2O/O_2$, water can be associatively adsorbed directly onto the Pd surface and thereby interact with the adsorbed hydrogen and oxygen to trigger the oxygen scavenging reaction [35].

Ceria (CeO_2) nanoparticles have also been shown to be excellent free radical scavengers with most of their current applications in biological systems but also in active packaging [41, 42].

In comparison with Pd, Ceria is considered to present lower kinetics of oxygen absorption [43].

However, metallic nanoparticles due to their high surface-to-volume ratio aggregate easily and hence lead to a decrease in their respective catalytic properties [44]. Moreover, this agglomeration affects the uniform dispersion of these nanomaterials throughout the matrix that in turn affects the final functionality of the catalyst [45]

To reinforce the dispersion of these nanoparticles, nanocellulose (CN) can be used, where nanocellulose acts as a novel carrier of different types of inorganic nanoparticles [46]. Nanocelluloses have smooth surface having hydroxyl groups along with negatively charged sulfate esters that brings them good colloidal stability in aqueous medium [47].

Introduction

The surface of CNs may act as anchor points to immobilize, for instance palladium nanoparticles (PdNP), through electrostatic interactions, which may prevent the aggregation of the nanoparticles [48]. Of particular interest in this field is the use of the stable nitroxyl radical 2,2,6,6-tetramethylpiperidine-1-oxyl (TEMPO) in combination with a co-oxidant as an alternative to metal based oxidants to modify CNs [49]. When the surface of NCs are fully oxidized using TEMPO, carboxylate functionalities are introduced. All these oxygen containing moieties are very effective metal center stabilizers via the formation of dative bonds [50].

1.4- Fiber based Packaging

Paper is a biodegradable and environmentally friendly packaging material that is widely used in packaging applications. Its microfibrils generally consist of long chains of crystalline cellulose mixed with amorphous phase. However, the cellulose fibres due to their hydrophilic nature are less resistant to moisture and subsequently inadequate for barrier applications [51, 52].

To overcome the barrier problem in cellulose based paper, coatings of different nature have been traditionally applied. For food packaging applications these are typically made of petroleum based polymers. However, the use of biopolymers would be highly desirable to retain a fully biobased origin [53].

Likewise, paperboard that is mechanically stronger compared to the ordinary paper and offers flexibility for its production, also suffers from lack of moisture resistance. Hence, surface treatments need to be carried out to cope with their intrinsic moisture barrier limitations for their improved functionality [54].

In this context, several biopolymers, c.a. starch, chitosan, whey proteins and alike, have been investigated as coating materials for paper based packaging. The development of nanocellulose has also been since more recently considered as a coating material. Microfibrillated Cellulose (MFC), was thus recently reported as a promising coating for paper and paperboard based packaging material [55].

Another recent alternative to the traditional paper and paperboard is the so called nanopapers. Nanopapers are compact films developed from fiber based materials, such as wood pulp that contain highly packed fibrils with upto 100 nm in diameter. They can be produced from various sources such as nanofibrous polymers, cellulose, metallic nanowires and alike nanomaterials [56]. When these fiber based materials are produced from ultra thin fibers made by electrospinning of biopolymers, we have coined the term of biopapers to describe them.

1.5- Coating of Fiber Based Packaging and Nanopapers

Biopolymers from renewable resources have been proposed as barrier coatings for paper applications such as whey protein, corn protein zein, biopolyesters, cellulose, alginates and starch. Some of these biopolymers,

Introduction

proteins and polysaccharides, provide protection against gases, organic vapours and grease, whereas biopolyesters provide barrier to moisture [57].

Using wheat gluten (WG) to coat paper was seen to significantly reduce its water permeability, which decreased by 56% [58]. Whey protein isolate (WPI) based bio-nanocomposite films embedded with zein nanoparticles (ZNP) prepared by solution casting showed significant improvement in the water vapor barrier property, mainly due to the hydrophobic nature of the ZNP [59]. In order to improve the barrier limitation of nanopapers multi-layered emulsion or successive layer coatings have also been reported where hydrocolloid coatings with good gas-barrier properties were combined with lipids with good moisture barrier properties [60]. Similarly, naturally abundant polysaccharides such as cellulose, alginate, carrageenan and chitosan have been used as barrier materials against the migration of mineral oil fractions on paper surface intended for food packaging [61]. In another example, soy protein thanks to its biodegradability, amphiphilic nature and surface activity was proposed as a coating for oil and grease resistance [62]. An inexpensive cellulose derivative carboxymethyl cellulose (CMC) has been often proposed to improve paper quality [63]. CMC produced by the incorporation of carboxymethyl functional groups along the cellulose chain, has shown some good water retention features and consequently has been used by the paper industry as a binder coating [64]. Cellulose-based films and coatings to improve water resistance and oxygen barrier, have been

widely reported but with different levels of barrier protection [65]. Papers coated with microfibrillated cellulose (MFC) demonstrated very low oxygen permeability values at 0% RH in the same range as that provided by PVOH [66]. In another study, paper coated with MFC reduced oxygen and water permeability [67, 68]. Nanofibrillated cellulose (NFC) films showed decreases in water vapour transmission (WVT) and oxygen transmission rate (OTR) [69, 70]. In other works, NCs have been used to, for instance, decrease the water permeability of wheat gluten (WG). Thus, loading of WG with 2.5% CNC decreased optimally its water vapour permeability (WVP) [71]. Wang et al. used soy protein as intercalating agent to achieve highly intercalated montmorillonite nanocomposites to reinforce EVOH. In comparison with the neat EVOH film, the nanocomposites of EVOH based on soy protein and montmorillonite, significantly reduced their oxygen and water vapour permeability [72]. Polyglycolic acid (PGA), a biodegradable, thermoplastic polymer, have also shown some excellent gas barrier properties [73]. The use of lactic acid oligomer-grafted-chitosan (OLLA-g-CH) as a nano-filler to improve multiple properties, including barrier, of poly (lactic acid) (PLA) was also reported [74]. A gas barrier composite film prepared from hydroxypropyl guar (HPG) and TEMPO-oxidized cellulose nanofibrils (TOCNs) by a solution casting method reported excellent oxygen-barrier properties [75].

Regarding polyhydroxybutyrate, this polymer has also been proposed as a potential coating material for paper [76]. PHB has already been widely

Introduction

reported to possess significant water barrier and as such able to potentially provide enhanced water barrier to cellulose paperboard [77-80].

In this context, Follain et al. analysed films of PHB and PHBV polymers, and found that cast films were more permeable than the melt compounded pressed films, as would be expected [81]. In general terms, PHB and PHBV copolymers can be classified as good barrier polymers, having gas and water transport properties similar to thermoplastics such as PVC and PET [82]. Interlayers of zein used to improve the gas barrier properties of PHB and PHBV, exhibited combined values of water vapour and oxygen barrier similar to those obtained for PET [83]. Arrieta et al. also reported that combination of PHB and CNCs improved the oxygen barrier properties of PLA prepared by melt blending [84]. A layered material comprising a thermoplastic starch (TPS) coated onto PHBV, showed that for a coating thickness of 91–115 μm , the system improved oxygen barrier and moisture resistance [85].

PHBV nanobiocomposites with different valerate contents were prepared by incorporating different loadings of bacterial cellulose nanowhiskers (BCNW) by solution casting. The results showed that both water and oxygen barrier decreased as the nanofiller concentration increased, as modelled [86]. In this context, Martinez-Sanz et al. obtained nanopapers of BCNW and coated them with PLA by electrospinning to protect BCNW from moisture. The coated system presented a significant decrease in water permeability and a 74% reduction in oxygen permeability at 80%RH [87].

1.6- Electrospinning as an innovative processing technology: Electrospinning coating technique

The recent interest in the field of nanotechnology has led to the development of various techniques for the synthesis of materials at the nanometer level. Among the various techniques employed for obtaining polymeric fibres with diameters ranging from the nanometer to the micrometer scale, the electrospinning technique has emerged as one of the most efficient techniques used in the field, which has been rapidly developed in the last few decades [88, 89].

The electrospinning technique is based on the principle of applying a high-voltage to a polymer solution, where nanofibers are formed by stretching the solution via electrostatic repulsions of the liquid molecules [90]. The electrospinning process is mainly conducted by adjusting solution parameters and processing parameters [91]. Hence different precursors like biopolymers, water soluble polymers, etc. can easily be electrospun by properly controlling their respective solution and process parameters [92].

Considering the significant potential of the properties of electrospun fibers, such as ultra-fine diameter, huge surface area to volume ratio, large porosity, high aspect ratio of length to diameter, high mechanical properties and the advantage of simple processing, the electrospinning technique has become very attractive and suitable for the development of ultrathin materials in wide-ranging applications.

Introduction

Aside from the development of electrospun polymer fibers of interest in packaging, this versatile technique has also been applied to develop nanofiber materials for different areas, such as scaffolds for tissue engineering [93-95], sensors applications [96-98], textile and clothing concepts [99, 100], membranes applications [101-103], conductive materials [104, 105] and nanofiber-reinforced composites [106, 107], among others. As an example, electrospun fibres produced from polymeric materials and blends making use of PEO, PCL, PVA, PLA and alike have being produced and tested for improving mechanical and thermal properties [108, 109]. Biopolymer based fibrous matrices with improved physico-chemical and functional properties by enhanced dispersion of nano-additives have been reported in the literature [110].

In this context, metal nanoparticles incorporation into polymers and biopolymers is gaining attention to extend the application of such type of polymeric nanocomposites. The metal loaded biopolymeric nanocomposites with enhanced performance and multifunctionalities have potential applications in the fields of biotechnology, optics, environment and electronics as they may otherwise be difficult with macro scale metal particles [111].

Active substances can conveniently also be encapsulated into electrospun fibres having high porosity as well as specific surface area. Metal based active substances with antioxidant and/or antimicrobial features for active packaging systems has been reported by different researchers. Thus metal oxides like ZnO [96], TiO₂ [112], MgO [113] and CuO [114]

were successfully incorporated into biodegradable fibres through electrospinning.

Electrospinning is then an appropriate technique either to fabricate active packaging or to coat conventional packaging materials with nanostructured layers since the non-woven mats of electrospun fibers can be latter turn into continuous films by fiber coalescence after a carefully designed annealing process [115]. For example, problems concerning the barrier and mechanical properties of biopolymers can be overcome by incorporating appropriated nanofillers as discussed above [116-119]. In a similar manner, the oxidation/rancidity process or the growth of pathogens may be reduced or inhibited via coating or interlayering the packaging material with functional ingredients such as antioxidant and/or antimicrobial compounds [120].

References

1. Tang, XZ, P Kumar, S Alavi, and KP Sandeep. "Recent Advances in Biopolymers and Biopolymer-Based Nanocomposites for Food Packaging Materials." *Critical reviews in food science and nutrition* 52, no. 5 (2012): 426-42.
2. Attaran, Seyed Ahmad, Azman Hassan, and Mat Uzir Wahit. "Materials for Food Packaging Applications Based on Bio-Based Polymer Nanocomposites: A Review." *Journal of Thermoplastic Composite Materials* 30, no. 2 (2017): 143-73.
3. Babu, Ramesh P, Kevin O'connor, and Ramakrishna Seeram. "Current Progress on Bio-Based Polymers and Their Future Trends." *Progress in Biomaterials* 2, no. 1 (2013): 8.

4. European-Bioplastics. <https://www.European-Bioplastics.Org/Market-Data-Update-2016/>, Accessed November 05, 2018.
5. — — —. <https://www.European-Bioplastics.Org/Market/>, Accessed March 03, 2019.
6. Hirvikorpi, Terhi, Mika Vähä-Nissi, Tuomas Mustonen, Ali Harlin, and Maarit Karppinen. "Gas and Moisture Barrier on Bio-Based Packaging Materials by Atomic Layer Deposition." Paper presented at the 10th International Conference on Atomic Layer Deposition, ALD 2010 2010.
7. Robertson, Gordon. *State-of-the-Art Biobased Food Packaging Materials*, 2008.
8. Vartiainen, Jari, Mika Vähä-Nissi, and Ali Harlin. "Biopolymer Films and Coatings in Packaging Applications—a Review of Recent Developments." *Materials Sciences and applications* 5, no. 10 (2014): 708.
9. Otles, Serkan, and Semih Otles. "Focus on Principial Properties of Biobased Packaging Materials for the Food Industry." *Acta Scientiarum Polonorum Technologia Alimentaria* 3, no. 2 (2004): 5-12.
10. Weber, CJ, V Haugaard, R Festersen, and G Bertelsen. "Production and Applications of Biobased Packaging Materials for the Food Industry." *Food Additives & Contaminants* 19, no. S1 (2002): 172-77.
11. Bugnicourt, Elodie, Patrizia Cinelli, Andrea Lazzeri, and Vera Alejandra Alvarez. "Polyhydroxyalkanoate (Pha): Review of Synthesis, Characteristics, Processing and Potential Applications in Packaging." (2014).
12. Han, Jia-Wei, Luis Ruiz-Garcia, Jian-Ping Qian, and Xin-Ting Yang. "Food Packaging: A Comprehensive Review and Future Trends." *Comprehensive Reviews in Food Science and Food Safety* 17, no. 4 (2018): 860-77.
13. Restuccia, Donatella, U Gianfranco Spizzirri, Ortensia I Parisi, Giuseppe Cirillo, Manuela Curcio, Francesca Iemma, Francesco Puoci, Giuliana Vinci, and Nevio Picci. "New Eu Regulation Aspects and Global Market of Active and Intelligent Packaging for Food Industry Applications." *Food control* 21, no. 11 (2010): 1425-35.

14. Mlalila, Nichrous, Dattatreya M. Kadam, Hulda Swai, and Askwar Hilonga. "Transformation of Food Packaging from Passive to Innovative Via Nanotechnology: Concepts and Critiques." *Journal of food science and technology* 53, no. 9 (2016): 3395-407.
15. Ozdemir, Murat, and John D Floros. "Active Food Packaging Technologies." *Critical reviews in food science and nutrition* 44, no. 3 (2004): 185-93.
16. Damaj, Ziad, Catherine Joly, and Emmanuel Guillon. "Toward New Polymeric Oxygen Scavenging Systems: Formation of Poly (Vinyl Alcohol) Oxygen Scavenger Film." *Packaging Technology and Science* 28, no. 4 (2015): 293-302.
17. Gaikwad, Kirtiraj K, Suman Singh, and Youn Suk Lee. "A Pyrogallol-Coated Modified Ldpe Film as an Oxygen Scavenging Film for Active Packaging Materials." *Progress in Organic Coatings* 111 (2017): 186-95.
18. Pereira de Abreu, DA, Jose M Cruz, and Perfecto Paseiro Losada. "Active and Intelligent Packaging for the Food Industry." *Food Reviews International* 28, no. 2 (2012): 146-87.
19. Lagarón, J-M, and M-A Busolo. "Multifunctional Nanoclays for Food Contact Applications." In *Multifunctional and Nanoreinforced Polymers for Food Packaging*, 31-42: Elsevier, 2011.
20. Cooksey, Kay. "Oxygen Scavenging Packaging Systems." *Encyclopedia of Polymer Science and Technology* (2002).
21. Solovyov, S.E. "Oxygen Scavengers." In *Kirk-Othmer Encyclopedia of Chemical Technology*, John Wiley & Sons, Inc., pp. 1-31., 2014.
22. Miltz, Joseph, and Michael Perry. "Evaluation of the Performance of Iron-Based Oxygen Scavengers, with Comments on Their Optimal Applications." *Packaging Technology and Science: An International Journal* 18, no. 1 (2005): 21-27.
23. Nerín, C. "Antioxidant Active Food Packaging and Antioxidant Edible Films." *Oxidation in foods and beverages and antioxidant applications. Volume 2: Management in different industry sectors* (2010): 496-515.
24. Suppakul, Panuwatt, Joseph Miltz, Kees Sonneveld, and Stephen W Bigger. "Active Packaging Technologies with an Emphasis on

- Antimicrobial Packaging and Its Applications." *Journal of food science* 68, no. 2 (2003): 408-20.
25. Rooney, ML. "Active Packaging in Polymer Films." In *Active Food Packaging*, 74-110: Springer, 1995.
 26. Kruijf, N De, M Van Beest, Rinus Rijk, Thea Sipiläinen-Malm, P Paseiro Losada, and B De Meulenaer. "Active and Intelligent Packaging: Applications and Regulatory Aspects." *Food Additives & Contaminants* 19, no. S1 (2002): 144-62.
 27. Yam, Kit L. *The Wiley Encyclopedia of Packaging Technology*: John Wiley & Sons, 2010.
 28. Yildirim, Selçuk, Bettina Röcker, Marit Kvalvåg Pettersen, Julie Nilsen-Nygaard, Zehra Ayhan, Ramune Rutkaite, Tanja Radusin, Patrycja Suminska, Begonya Marcos, and Véronique Coma. "Active Packaging Applications for Food." *Comprehensive Reviews in Food Science and Food Safety* 17, no. 1 (2018): 165-99.
 29. Cruz, Renato Souza, Nilda de Fátima Ferreira Soares, and Nélio José de Andrade. "Efficiency of Oxygen: Absorbing Sachets in Different Relative Humidities and Temperatures." *Ciência e Agrotecnologia* 31, no. 6 (2007): 1800-04.
 30. Demirhan, B, and K Candoğan. "Active Packaging of Chicken Meats with Modified Atmosphere Including Oxygen Scavengers." *Poultry science* 96, no. 5 (2017): 1394-401.
 31. Cichello, Simon Angelo. "Oxygen Absorbers in Food Preservation: A Review." *Journal of food science and technology* 52, no. 4 (2015): 1889-95.
 32. Galotto, MJ, SA Anfossi, and A Guarda. "Oxygen Absorption Kinetics of Sheets and Films Containing a Commercial Iron-Based Oxygen Scavenger." *Food Science and Technology International* 15, no. 2 (2009): 159-68.
 33. Matche, Rajeshwar S, RK Sreekumar, and Baldev Raj. "Modification of Linear Low-Density Polyethylene Film Using Oxygen Scavengers for Its Application in Storage of Bun and Bread." *Journal of Applied Polymer Science* 122, no. 1 (2011): 55-63.
 34. Sänglerlaub, Sven, Doris Gibis, Eva Kirchhoff, Melanie Tittjung, Markus Schmid, and Kajetan Müller. "Compensation of Pinhole Defects in Food Packages by Application of Iron-Based Oxygen

- Scavenging Multilayer Films." *Packaging Technology and Science* 26, no. 1 (2013): 17-30.
35. Yildirim, Selçuk, Bettina Röcker, Nadine Rüegg, and Wolfgang Lohwasser. "Development of Palladium-Based Oxygen Scavenger: Optimization of Substrate and Palladium Layer Thickness." *Packaging Technology and Science* 28, no. 8 (2015): 710-18.
 36. Reig, Carmen Sanchez, Antonio Dobon Lopez, Mercedes Hortal Ramos, and Vicente Agustin Cloquell Ballester. "Nanomaterials: A Map for Their Selection in Food Packaging Applications." *Packaging Technology and Science* 27, no. 11 (2014): 839-66.
 37. Röcker, Bettina, Nadine Rüegg, Alexia N Glöss, Chahan Yeretian, and Selçuk Yildirim. "Inactivation of Palladium-Based Oxygen Scavenger System by Volatile Sulfur Compounds Present in the Headspace of Packaged Food." *Packaging Technology and Science* 30, no. 8 (2017): 427-42.
 38. Roucoux, Alain, Jürgen Schulz, and Henri Patin. "Reduced Transition Metal Colloids: A Novel Family of Reusable Catalysts?" *Chemical reviews* 102, no. 10 (2002): 3757-78.
 39. Llorens, Amparo, Elsa Lloret, Pierre A Picouet, Raul Trbojevich, and Avelina Fernandez. "Metallic-Based Micro and Nanocomposites in Food Contact Materials and Active Food Packaging." *Trends in Food Science & Technology* 24, no. 1 (2012): 19-29.
 40. Johansson, Åsa, Michael Försth, and Arne Rosén. "The H₂/O₂ Reaction on a Palladium Model Catalyst Studied with Laser-Induced Fluorescence and Microcalorimetry." *International Journal of Molecular Sciences* 2, no. 5 (2001): 221-29.
 41. Lei, M, TZ Yang, WJ Wang, K Huang, R Zhang, XL Fu, HJ Yang, YG Wang, and WH Tang. "Self-Assembled Mesoporous Carbon Sensitized with Ceria Nanoparticles as Durable Catalyst Support for Pem Fuel Cell." *international journal of hydrogen energy* 38, no. 1 (2013): 205-11.
 42. Xue, Ying, Qingfen Luan, Dan Yang, Xin Yao, and Kebin Zhou. "Direct Evidence for Hydroxyl Radical Scavenging Activity of

- Cerium Oxide Nanoparticles." *The Journal of Physical Chemistry C* 115, no. 11 (2011): 4433-38.
43. Pons, Maria Antonieta Busolo, and Jose Maria Lagaron Cabello. "Cerium-Based Active Materials with Catalytic Capacity and Process for Obtaining Them." Google Patents, 2015.
 44. Seto, Hirokazu, Tamami Yoneda, Takato Morii, Yu Hoshino, Yoshiko Miura, and Tatsuya Murakami. "Membrane Reactor Immobilized with Palladium-Loaded Polymer Nanogel for Continuous-Flow Suzuki Coupling Reaction." *AIChE Journal* 61, no. 2 (2015): 582-89.
 45. Mittal, Garima, Kyong Y Rhee, Vesna Mišković-Stanković, and David Hui. "Reinforcements in Multi-Scale Polymer Composites: Processing, Properties, and Applications." *Composites Part B: Engineering* 138 (2018): 122-39.
 46. Wei, Haoran, Katia Rodriguez, Scott Renneckar, and Peter J Vikesland. "Environmental Science and Engineering Applications of Nanocellulose-Based Nanocomposites." *Environmental Science: Nano* 1, no. 4 (2014): 302-16.
 47. Cirtiu, Ciprian M, Alexandre F Dunlop-Briere, and Audrey Moores. "Cellulose Nanocrystallites as an Efficient Support for Nanoparticles of Palladium: Application for Catalytic Hydrogenation and Heck Coupling under Mild Conditions." *Green Chemistry* 13, no. 2 (2011): 288-91.
 48. Wu, Xiaodong, Canhui Lu, Wei Zhang, Guiping Yuan, Rui Xiong, and Xinxing Zhang. "A Novel Reagentless Approach for Synthesizing Cellulose Nanocrystal-Supported Palladium Nanoparticles with Enhanced Catalytic Performance." *Journal of Materials Chemistry A* 1, no. 30 (2013): 8645-52.
 49. Karimi, Babak, Abbas Biglari, James H Clark, and Vitaly Budarin. "Green, Transition-Metal-Free Aerobic Oxidation of Alcohols Using a Highly Durable Supported Organocatalyst." *Angewandte Chemie International Edition* 46, no. 38 (2007): 7210-13.
 50. Kaushik, Madhu, and Audrey Moores. "Nanocelluloses as Versatile Supports for Metal Nanoparticles and Their Applications in Catalysis." *Green Chemistry* 18, no. 3 (2016): 622-37.

51. Khwaldia, Khaoula, Elmira Arab-Tehrany, and Stephane Desobry. "Biopolymer Coatings on Paper Packaging Materials." *Comprehensive Reviews in Food Science and Food Safety* 9, no. 1 (2010): 82-91.
52. Song, Zhaoping, Jiebin Tang, Junrong Li, and Huining Xiao. "Plasma-Induced Polymerization for Enhancing Paper Hydrophobicity." *Carbohydrate polymers* 92, no. 1 (2013): 928-33.
53. CHAUHAN, OP, K CHITRAVATHI, and LAKSHMI E UNNI. "Bio-Based Packaging for Fresh Fruits and Vegetables." *Innovative Packaging of Fruits and Vegetables: Strategies for Safety and Quality Maintenance* (2018).
54. Andersson, Caisa. "New Ways to Enhance the Functionality of Paperboard by Surface Treatment—a Review." *Packaging Technology and Science: An International Journal* 21, no. 6 (2008): 339-73.
55. Lavoine, Nathalie, Isabelle Desloges, Bertine Khelifi, and Julien Bras. "Impact of Different Coating Processes of Microfibrillated Cellulose on the Mechanical and Barrier Properties of Paper." *Journal of Materials Science* 49, no. 7 (2014): 2879-93.
56. Barhoum, Ahmed, Pieter Samyn, Thomas Öhlund, and Alain Dufresne. "Review of Recent Research on Flexible Multifunctional Nanopapers." *Nanoscale* 9, no. 40 (2017): 15181-205.
57. Irkin, Reyhan, and Ozlem Kizilirmak Esmer. "Novel Food Packaging Systems with Natural Antimicrobial Agents." *Journal of food science and technology* 52, no. 10 (2015): 6095-111.
58. Guillaume, Carole, Jeremy Pinte, Nathalie Gontard, and Emmanuelle Gastaldi. "Wheat Gluten-Coated Papers for Bio-Based Food Packaging: Structure, Surface and Transfer Properties." *Food Research International* 43, no. 5 (2010): 1395-401.
59. Oymaci, Pelin, and Sacide Alsoy Altinkaya. "Improvement of Barrier and Mechanical Properties of Whey Protein Isolate Based Food Packaging Films by Incorporation of Zein Nanoparticles as a Novel Bionanocomposite." *Food Hydrocolloids* 54 (2016): 1-9.
60. Khwaldia, Khaoula, Altaf H Basta, Hajer Aloui, and Houssni El-Saied. "Chitosan–Caseinate Bilayer Coatings for Paper Packaging Materials." *Carbohydrate polymers* 99 (2014): 508-16.

61. Kopacic, Samir, Andrea Walzl, Armin Zankel, Erich Leitner, and Wolfgang Bauer. "Alginate and Chitosan as a Functional Barrier for Paper-Based Packaging Materials." *Coatings* 8, no. 7 (2018): 235.
62. Tyagi, Preeti, Martin A Hubbe, Lucian Lucia, and Lokendra Pal. "High Performance Nanocellulose-Based Composite Coatings for Oil and Grease Resistance." *Cellulose* 25, no. 6 (2018): 3377-91.
63. Basta, Altaf H, Khaoula Khwaldia, Hajer Aloui, and Houssni El-Saied. "Enhancing the Performance of Carboxymethyl Cellulose by Chitosan in Producing Barrier Coated Paper Sheets." *Nordic Pulp and Paper Research Journal* 30, no. 4 (2015): 617-25.
64. Mousavi, SM Mazhari, E Afra, M Tajvidi, DW Bousfield, and M Dehghani-Firouzabadi. "Cellulose Nanofiber/Carboxymethyl Cellulose Blends as an Efficient Coating to Improve the Structure and Barrier Properties of Paperboard." *Cellulose* 24, no. 7 (2017): 3001-14.
65. Hubbe, Martin A, Ana Ferrer, Preeti Tyagi, Yuanyuan Yin, Carlos Salas, Lokendra Pal, and Orlando J Rojas. "Nanocellulose in Thin Films, Coatings, and Plies for Packaging Applications: A Review." *BioResources* 12, no. 1 (2017): 2143-233.
66. Aulin, Christian, Mikael Gällstedt, and Tom Lindström. "Oxygen and Oil Barrier Properties of Microfibrillated Cellulose Films and Coatings." *Cellulose* 17, no. 3 (2010): 559-74.
67. Chinga-Carrasco, Gary, Nina Kuznetsova, Milyausha Garaeva, Ingebjørg Leirset, Guzaliya Galiullina, Anatoly Kostochko, and Kristin Syverud. "Bleached and Unbleached Mfc Nanobarriers: Properties and Hydrophobisation with Hexamethyldisilazane." *Journal of nanoparticle research* 14, no. 12 (2012): 1280.
68. Hult, Eva-Lena, Marco Iotti, and Marianne Lenes. "Efficient Approach to High Barrier Packaging Using Microfibrillar Cellulose and Shellac." *Cellulose* 17, no. 3 (2010): 575-86.
69. Österberg, Monika, Jari Vartiainen, Jessica Lucenius, Ulla Hippel, Jukka Seppälä, Ritva Serimaa, and Janne Laine. "A Fast Method to Produce Strong Nfc Films as a Platform for Barrier and Functional Materials." *ACS applied materials & interfaces* 5, no. 11 (2013): 4640-47.

70. Savadekar, NR, VS Karande, N Vigneshwaran, AK Bharimalla, and ST Mhaske. "Preparation of Nano Cellulose Fibers and Its Application in Kappa-Carrageenan Based Film." *International journal of biological macromolecules* 51, no. 5 (2012): 1008-13.
71. El-Wakil, Nahla A, Enas A Hassan, Ragab E Abou-Zeid, and Alain Dufresne. "Development of Wheat Gluten/Nanocellulose/Titanium Dioxide Nanocomposites for Active Food Packaging." *Carbohydrate polymers* 124 (2015): 337-46.
72. Wang, Hualin, Heng Zhang, Baicheng Niu, Suwei Jiang, Junfeng Cheng, and Shaotong Jiang. "Structure and Properties of the Poly (Vinyl Alcohol-Co-Ethylene)/Montmorillonite-Phosphorylated Soybean Protein Isolate Barrier Film." *RSC Advances* 6, no. 35 (2016): 29294-302.
73. Vartiainen, Jari, Yingfeng Shen, Timo Kaljunen, Tero Malm, Mika Vähä-Nissi, Matti Putkonen, and Ali Harlin. "Bio-Based Multilayer Barrier Films by Extrusion, Dispersion Coating and Atomic Layer Deposition." *Journal of Applied Polymer Science* 133, no. 2 (2016).
74. Pal, Akhilesh Kumar, and Vimal Katiyar. "Nanoamphiphilic Chitosan Dispersed Poly (Lactic Acid) Bionanocomposite Films with Improved Thermal, Mechanical, and Gas Barrier Properties." *Biomacromolecules* 17, no. 8 (2016): 2603-18.
75. Dai, Lei, Bin Wang, Zhu Long, Le Chen, Dan Zhang, and Shuai Guo. "Properties of Hydroxypropyl Guar/Tempo-Oxidized Cellulose Nanofibrils Composite Films." *Cellulose* 22, no. 5 (2015): 3117-26.
76. Puglia, D, F Luzi, IT Seoane, VP Cyras, LB Manfredi, and L Torre. "Study of Paperboard Material Layered with Plasticized Polyhydroxybutyrate/Nanocellulose Coatings for Packaging Application." Paper presented at the AIP Conference Proceedings 2018.
77. Cyras, Viviana P, Commisso Ma Soledad, and Vázquez Analía. "Biocomposites Based on Renewable Resource: Acetylated and Non Acetylated Cellulose Cardboard Coated with Polyhydroxybutyrate." *Polymer* 50, no. 26 (2009): 6274-80.

78. Rastogi, Vibhore Kumar, and Pieter Samyn. "Synthesis of Polyhydroxybutyrate Particles with Micro-to-Nanosized Structures and Application as Protective Coating for Packaging Papers." *Nanomaterials* 7, no. 1 (2016): 5.
79. Seoane, IT, LB Manfredi, and VP Cyras. "Bilayer Biocomposites Based on Coated Cellulose Paperboard with Films of Polyhydroxybutyrate/Cellulose Nanocrystals." *Cellulose* 25, no. 4 (2018): 2419-34.
80. Seoane, Irene T, Liliana B Manfredi, and Viviana P Cyras. "Properties and Processing Relationship of Polyhydroxybutyrate and Cellulose Biocomposites." *Procedia Materials Science* 8 (2015): 807-13.
81. Follain, Nadège, Corinne Chappéy, Eric Dargent, Frederic Chivrac, Raphaël Crétois, and Stephane Marais. "Structure and Barrier Properties of Biodegradable Polyhydroxyalkanoate Films." *The Journal of Physical Chemistry C* 118, no. 12 (2014): 6165-77.
82. Miguel, Oscar, and Juan José Iruin. "Evaluation of the Transport Properties of Poly (3-Hydroxybutyrate) and Its 3-Hydroxyvalerate Copolymers for Packaging Applications." Paper presented at the Macromolecular Symposia 1999.
83. Fabra, María José, Amparo Lopez-Rubio, and Jose M. Lagaron. "Nanostructured Interlayers of Zein to Improve the Barrier Properties of High Barrier Polyhydroxyalkanoates and Other Polyesters." *Journal of Food Engineering* 127 (2014): 1-9.
84. Arrieta, M. P., E. Fortunati, F. Dominici, J. López, and J. M. Kenny. "Bionanocomposite Films Based on Plasticized Pla-Phb/Cellulose Nanocrystal Blends." *Carbohydrate polymers* 121 (2015): 265-75.
85. Dilkes-Hoffman, Leela S, Steven Pratt, Paul A Lant, Ian Levett, and Bronwyn Laycock. "Polyhydroxyalkanoate Coatings Restrict Moisture Uptake and Associated Loss of Barrier Properties of Thermoplastic Starch Films." *Journal of Applied Polymer Science* 135, no. 25 (2018): 46379.
86. Martínez-Sanz, Marta, Marianna Villano, Catarina Oliveira, Maria GE Albuquerque, Mauro Majone, Maria Reis, Amparo Lopez-Rubio, and Jose M Lagaron. "Characterization of

- Polyhydroxyalkanoates Synthesized from Microbial Mixed Cultures and of Their Nanobiocomposites with Bacterial Cellulose Nanowhiskers." *New biotechnology* 31, no. 4 (2014): 364-76.
87. Martínez-Sanz, Marta, Amparo Lopez-Rubio, and Jose M Lagaron. "High-Barrier Coated Bacterial Cellulose Nanowhiskers Films with Reduced Moisture Sensitivity." *Carbohydrate polymers* 98, no. 1 (2013): 1072-82.
 88. Haider, Adnan, Sajjad Haider, and Inn-Kyu Kang. "A Comprehensive Review Summarizing the Effect of Electrospinning Parameters and Potential Applications of Nanofibers in Biomedical and Biotechnology." *Arabian Journal of Chemistry* 11, no. 8 (2018): 1165-88.
 89. Lee, Jeremy Kong Yoong, Nuan Chen, Shengjie Peng, Linlin Li, Lingling Tian, Nitish Thakor, and Seeram Ramakrishna. "Polymer-Based Composites by Electrospinning: Preparation & Functionalization with Nanocarbons." *Progress in Polymer Science* (2018).
 90. Moreira, Juliana Botelho, Michele Greque de Morais, Eteiele Greque de Morais, Bruna da Silva Vaz, and Jorge Alberto Vieira Costa. "Electrospun Polymeric Nanofibers in Food Packaging." In *Impact of Nanoscience in the Food Industry*, 387-417: Elsevier, 2018.
 91. da Silva Vaz, Bruna, Jorge Alberto Vieira Costa, and Michele Greque de Morais. "Innovative Nanofiber Technology to Improve Carbon Dioxide Biofixation in Microalgae Cultivation." *Bioresource technology* 273 (2019): 592-98.
 92. Gomes, Demetrius S, Ana NR da Silva, Nilton I Morimoto, Luiz TF Mendes, Rogerio Furlan, and Idalia Ramos. "Characterization of an Electrospinning Process Using Different Pan/Dmf Concentrations." *Polímeros* 17, no. 3 (2007): 206-11.
 93. Hasan, Anwarul, Adnan Memic, Nasim Annabi, Monowar Hossain, Arghya Paul, Mehmet R. Dokmeci, Fariba Dehghani, and Ali Khademhosseini. "Electrospun Scaffolds for Tissue Engineering of Vascular Grafts." *Acta Biomaterialia* 10, no. 1 (2014): 11-25.
 94. Muhamad, Farina. "Electrospun Scaffolds for Tissue Engineering." (2013).

95. Pugliese, Raffaele, Mahboubeh Maleki, Ronald N Zuckermann, and Fabrizio Gelain. "Self-Assembling Peptides Cross-Linked with Genipin: Resilient Hydrogels and Self-Standing Electrospun Scaffolds for Tissue Engineering Applications." *Biomaterials science* 7, no. 1 (2019): 76-91.
96. Ding, Bin, Moran Wang, Xianfeng Wang, Jianyong Yu, and Gang Sun. "Electrospun Nanomaterials for Ultrasensitive Sensors." *Materials Today* 13, no. 11 (2010): 16-27.
97. Ding, Bin, Moran Wang, Jianyong Yu, and Gang Sun. "Gas Sensors Based on Electrospun Nanofibers." *Sensors* 9, no. 3 (2009): 1609-24.
98. Moon, Jaehyun, Jin-Ah Park, Su-Jae Lee, Taehyoung Zyung, and Il-Doo Kim. "Pd-Doped Tio2 Nanofiber Networks for Gas Sensor Applications." *Sensors and Actuators B: Chemical* 149, no. 1 (2010): 301-05.
99. Gorji, M, Ali AA Jeddi, and AA Gharehaghaji. "Fabrication and Characterization of Polyurethane Electrospun Nanofiber Membranes for Protective Clothing Applications." *Journal of Applied Polymer Science* 125, no. 5 (2012): 4135-41.
100. Lee, Seungsin, and S Kay Obendorf. "Use of Electrospun Nanofiber Web for Protective Textile Materials as Barriers to Liquid Penetration." *Textile Research Journal* 77, no. 9 (2007): 696-702.
101. Gibson, Phillip, Heidi Schreuder-Gibson, and Donald Rivin. "Transport Properties of Porous Membranes Based on Electrospun Nanofibers." *Colloids and Surfaces A: Physicochemical and Engineering Aspects* 187 (2001): 469-81.
102. Gopal, Renuga, Satinderpal Kaur, Zuwei Ma, Casey Chan, Seeram Ramakrishna, and Takeshi Matsuura. "Electrospun Nanofibrous Filtration Membrane." *Journal of Membrane Science* 281, no. 1-2 (2006): 581-86.
103. Govinna, Nelaka, Papatya Kaner, Davette Ceasar, Anita Dhungana, Cody Moers, Katherine Son, Ayse Asatekin, and Peggy Cebe. "Electrospun Fiber Membranes from Blends of Poly (Vinylidene Fluoride) with Fouling-Resistant Zwitterionic Copolymers." *Polymer International* 68, no. 2 (2019): 231-39.

104. Guan, Xiaoyang, Guoqiang Zheng, Kun Dai, Chuntai Liu, Xingru Yan, Changyu Shen, and Zhanhu Guo. "Carbon Nanotubes-Adsorbed Electrospun Pa66 Nanofiber Bundles with Improved Conductivity and Robust Flexibility." *ACS applied materials & interfaces* 8, no. 22 (2016): 14150-59.
105. Sundaray, Bibekananda, V Subramanian, TS Natarajan, and K Krishnamurthy. "Electrical Conductivity of a Single Electrospun Fiber of Poly (Methyl Methacrylate) and Multiwalled Carbon Nanotube Nanocomposite." *Applied Physics Letters* 88, no. 14 (2006): 143114.
106. Cai, Jie, Jingyao Chen, Qian Zhang, Miao Lei, Jingren He, Anhong Xiao, Chengjie Ma, Sha Li, and Hanguo Xiong. "Well-Aligned Cellulose Nanofiber-Reinforced Polyvinyl Alcohol Composite Film: Mechanical and Optical Properties." *Carbohydrate polymers* 140 (2016): 238-45.
107. Neisiany, Rasoul Esmaeely, Saied Nouri Khorasani, Mohammadreza Naeimirad, Jeremy Kong Yoong Lee, and Seeram Ramakrishna. "Improving Mechanical Properties of Carbon/Epoxy Composite by Incorporating Functionalized Electrospun Polyacrylonitrile Nanofibers." *Macromolecular Materials and Engineering* 302, no. 5 (2017): 1600551.
108. Cerqueira, Miguel A, António A Vicente, and Lorenzo M Pastrana. "Nanotechnology in Food Packaging: Opportunities and Challenges." In *Nanomaterials for Food Packaging*, 1-11: Elsevier, 2018.
109. Kakoria, Ashish, and Sumit Sinha-Ray. "A Review on Biopolymer-Based Fibers Via Electrospinning and Solution Blowing and Their Applications." *Fibers* 6, no. 3 (2018): 45.
110. Vasile, Cornelia. "Polymeric Nanocomposites and Nanocoatings for Food Packaging: A Review." *Materials* 11, no. 10 (2018): 1834.
111. Zanjani, Jamal Seyyed Monfared, Oğuzhan Oğuz, Burcu Saner Okan, Mehmet Yildiz, and Yusuf Ziya Menciloğlu. "14 - Polymer Composites Containing Functionalized Nanoparticles and the Environment." In *Polymer Composites with Functionalized Nanoparticles*, edited by Krzysztof Pielichowski and Tomasz M. Majka, 437-66: Elsevier, 2019.

112. Mihindikulasuriya, Suramya DF, and Loong-Tak Lim. "Oxygen Detection Using Uv-Activated Electrospun Poly (Ethylene Oxide) Fibers Encapsulated with Tio₂ Nanoparticles." *Journal of Materials Science* 48, no. 16 (2013): 5489-98.
113. De Silva, RT, MMMGPG Mantilaka, KL Goh, SP Ratnayake, GAJ Amaratunga, and KM de Silva. "Magnesium Oxide Nanoparticles Reinforced Electrospun Alginate-Based Nanofibrous Scaffolds with Improved Physical Properties." *International journal of biomaterials* 2017 (2017).
114. Castro Mayorga, Jinneth Lorena, María José Fabra Rovira, Luis Cabedo Mas, Gloria Sánchez Moragas, and José María Lagarón Cabello. "Antimicrobial Nanocomposites and Electrospun Coatings Based on Poly (3-Hydroxybutyrate-Co-3-Hydroxyvalerate) and Copper Oxide Nanoparticles for Active Packaging and Coating Applications." *Journal of Applied Polymer Science* 135, no. 2 (2018): 45673.
115. Bhushani, J Anu, and Chinnaswamy Anandharamakrishnan. "Electrospinning and Electro spraying Techniques: Potential Food Based Applications." *Trends in Food Science & Technology* 38, no. 1 (2014): 21-33.
116. Arrieta, M. P., J. López, D. López, J. M. Kenny, and L. Peponi. "Development of Flexible Materials Based on Plasticized Electrospun Pla–Phb Blends: Structural, Thermal, Mechanical and Disintegration Properties." *European Polymer Journal* 73 (2015): 433-46.
117. — — —. "Biodegradable Electrospun Bionanocomposite Fibers Based on Plasticized Pla–Phb Blends Reinforced with Cellulose Nanocrystals." *Industrial Crops and Products* 93 (2016): 290-301.
118. Fabra, María José, Amparo López-Rubio, and Jose M. Lagaron. "On the Use of Different Hydrocolloids as Electrospun Adhesive Interlayers to Enhance the Barrier Properties of Polyhydroxyalkanoates of Interest in Fully Renewable Food Packaging Concepts." *Food Hydrocolloids* 39 (2014): 77-84.
119. Neo, Yun Ping, Simon Swift, Sudip Ray, Marija Gizdavic-Nikolaidis, Jianyong Jin, and Conrad O. Perera. "Evaluation of Gallic Acid Loaded Zein Sub-Micron Electrospun Fibre Mats as

- Novel Active Packaging Materials." *Food Chemistry* 141, no. 3 (2013): 3192-200.
120. Fabra, María José, María A Busolo, Amparo Lopez-Rubio, and Jose M Lagaron. "Nanostructured Biolayers in Food Packaging." *Trends in Food Science & Technology* 31, no. 1 (2013): 79-87.

2. General and specific objectives

2. General and specific objectives

Current strategies to solve environmental problems include the development of materials using biodegradable polymers obtained from renewable resources, so-called biopolymers, and the application of active nanotechnologies to tailor their properties. Biodegradable polymers are currently considered as an environmentally friendly substitute for the use of petroleum based plastic materials that are non-renewable and in general non-biodegradable. The frame of this PhD thesis was focused on the challenge of developing viable biodegradable high barrier paper based packaging strategies. Thus, the general and specific objectives of the work were:

- Development and characterization of biodegradable self-adhesive hydrophobic coatings and interlayers with active oxygen scavenging properties of potential application interest in fiber-based packaging.

In order to achieve this:

- First, we aimed at developing the proper conditions of processing and post-processing to obtain an electrospun fiber-based layer of PHB, so called biopaper.

-Secondly, apply the previously developed coating technology onto a conventional uncoated paper using different materials, one with oxygen barrier, PVOH, and others with water barrier such as PLA and PHB.

General and specific objectives

- Third, to apply the developed and optimized PHA water barrier coating technology to nanopapers made of cellulose microfibrils. Two types of nanopapers will be considered namely, with and without lignin content. The overall morphology, barrier and mechanical properties will be assessed.

- Fourth, to develop active oxygen scavenging films through the incorporation of palladium nanoparticles into PHA by the electrospinning technique. In order to improve the dispersion of the nanoparticles in the PHA matrix, food contact permitted surfactants will be used. The materials developed will be fully characterized.

- Fifth, to develop and apply an optimal active oxygen scavenging biopaper coating or coatings into conventional cellulose uncoated paper and characterize their morphology and properties. A lower oxygen and water barrier biodegradable polymer, i.e. PCL, will be assessed to boost the catalytic effect of Pd.

- Sixth, to develop an oxygen superbarrier nanocomposite layer by combining a high passive gas barrier polymer, i.e. EVOH, with CNC. CNC will be used to provide both an additional barrier reinforcing effect and a reducing support for the in-situ creation of the active oxygen scavenging PdNP. This layer is to be applied by the conventional casting method used by the paper making industry.

3. Results

Results

Different strategies in this thesis were directed towards achieving the development of monolayers and multilayers based on PHA, paper, nanopaper and PdNP with high barrier and active oxygen scavenging properties of application interest in coating fiber based food packaging.

Chapter I:

Cherpinski, A., Torres-Giner, S., Cabedo, L., & Lagaron, J. M. (2017). **Post-processing optimization of electrospun submicron poly (3-hydroxybutyrate) fibers to obtain continuous films of interest in food packaging applications.** *Food Additives & Contaminants: Part A*, 34(10), 1817-1830.

Chapter II:

Cherpinski, A., Torres-Giner, S., Cabedo, L., Méndez, J. A., & Lagaron, J. M. (2018). **Multilayer structures based on annealed electrospun biopolymer coatings of interest in water and aroma barrier fiber-based food packaging applications.** *Journal of Applied Polymer Science*, 135(24), 45501.

Chapter III:

Cherpinski, A., Torres-Giner, S., Vartiainen, J., Peresin, M. S., Lahtinen, P., & Lagaron, J. M. (2018). **Improving the water resistance of nanocellulose-based films with polyhydroxyalkanoates processed by the electrospinning coating technique.** *Cellulose*, 25(2), 1291-1307.

Chapter IV:

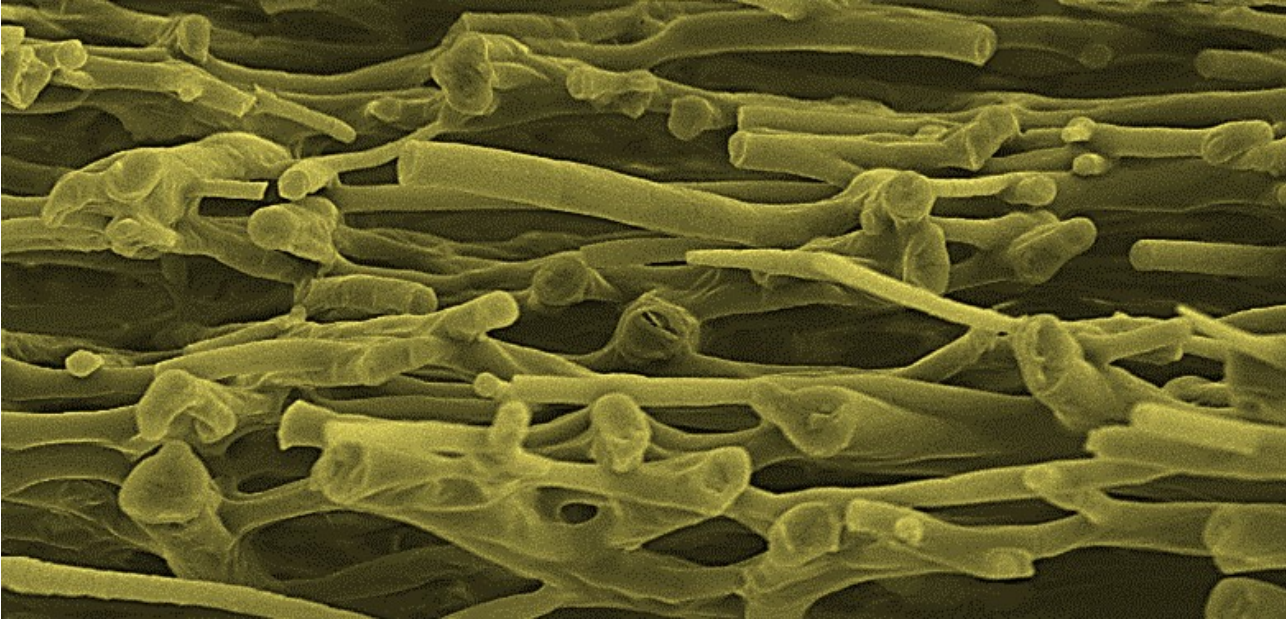
Cherpinski, A., Gozutok, M., Sasmazel, H., Torres-Giner, S., & Lagaron, J. (2018). **Electrospun oxygen scavenging films of poly (3-hydroxybutyrate) containing palladium nanoparticles for active packaging applications.** *Nanomaterials*, 8(7), 469.

Chapter V:

Adriane Cherpinski, Piotr K. Szewczyk, Adam Gruszczyński, Urszula Stachewicz and Jose M. Lagaron (2019). **Oxygen-Scavenging Multilayered Biopapers Containing Palladium Nanoparticles Obtained by the Electrospinning Coating Technique.** *Nanomaterials*, 9(2), 262.

Chapter VI:

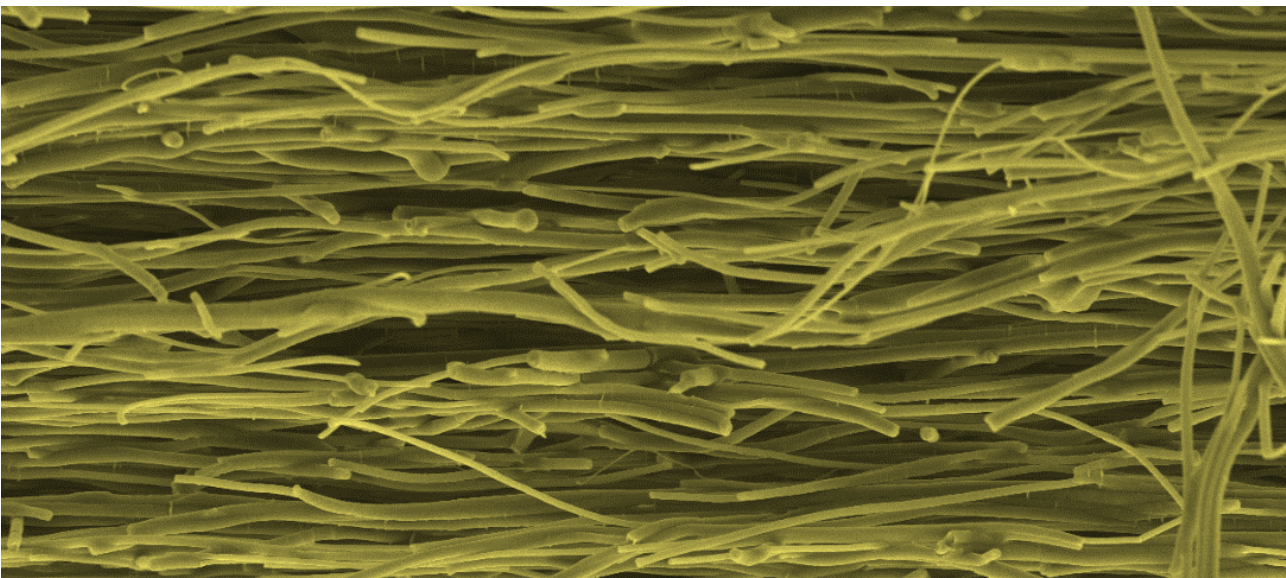
Adriane Cherpinski, Atanu Biswas, Jose M. Lagaron, Alain Dufresne, Sanghoon Kim, Megan Buttrum, Eduardo Espinosa and H. N. Cheng. **Preparation and evaluation of oxygen scavenging nanocomposite films incorporating poly(ethylene-co-vinyl alcohol), Pd nanoparticles, and cellulose nanocrystals.** *Submitted for publication.*



Chapter I

Post-processing Optimization of Electrospun Submicron Poly(3-hydroxybutyrate) Fibers to Obtain Continuous Films of Interest in Food Packaging Applications

Cherpinski, A., Torres-Giner, S., Cabedo, L., & Lagaron, J. M. (2017). Post-processing optimization of electrospun submicron poly (3-hydroxybutyrate) fibers to obtain continuous films of interest in food packaging applications. *Food Additives & Contaminants: Part A*, 34(10), 1817-1830.



Abstract

Polyhydroxyalkanoates (PHAs) are one of the most researched family of biodegradable polymers based on renewable materials due to their thermoplastic nature and moisture resistance. The present study was targeted to investigate the preparation and characterization of poly(3-hydroxybutyrate) (PHB) films obtained through the electrospinning technique. To convert them into continuous films and then to increase their application interest in packaging, the electrospun fiber mats were subsequently post-processed by different physical treatments. Thus, the effect of annealing time and cooling method on morphology, molecular order, thermal, optical, mechanical, and barrier properties of the electrospun submicron PHB fibers was studied. Annealing at 160°C, well below the homopolymer melting point, was found to be the minimum temperature at which homogeneous transparent films were produced. The film samples that were cooled slowly after annealing showed the lowest permeability to oxygen, water vapor, and limonene. The optimally post-processed electrospun PHB fibers exhibited similar rigidity to conventional compression-molded PHA films, but with enhanced elongation at break and toughness. Films made by this electrospinning technique have many potential applications, such as in the design of barrier layers, adhesive interlayers, and coatings for fiber- and plastic-based food packaging materials.

Keywords: Barrier properties, Coatings, Electrospinning, Packaging, Polyhydroxyalkanoates.

1. Introduction

The use of plastic materials in the food packaging area has been steadily increasing over the last decades due to a number of advantages (cost, versatility, lightness, etc.). However, their extensive use has brought up some serious challenges to the waste management treatment procedures. In this regard, the use of bio-based and biodegradable polymers has recently received increased attention because of their great potential as substitutes for petroleum-based polymers in a broad range of applications [1, 2]. The use of bio-based biodegradable and compostable polymers ('biopolymers') can lead to an improved management of the plastic residues, as well as a reduction in the dependency on fossil oil. However, one of the main disadvantages arising from the implementation of biopolymers based on renewable resources is that they present either low barrier performance or strong dependence of physical properties on moisture, which can potentially compromise both food quality and safety. Thus, depending on the application, different material characteristics are needed: for fresh produce, selective gas-permeable materials are essential, while high-barrier materials are needed for oxygen-sensitive products [3-5].

Among biopolymers, there has been particular interest in the use of polyhydroxyalkanoates (PHAs) [6]. However, the use of PHAs in the plastic industry has been limited by several drawbacks such as the high production costs, brittleness, and low thermal stability in the molten state. One of the most extensively studied biopolymers within the PHA family

is poly(3-hydroxybutyrate) (PHB). Its biocompatibility with the human body makes PHB also suitable for a number of biomedical applications (such as implants, surgical plasters, drug delivery systems, stents, etc.) [7-9]. However, PHB presents low thermal stability, a narrow processing window, a high degree of crystallinity, and high rigidity. PHB possesses an isotactic stereo-regularity that makes it viable to crystallize. However, the low nucleation density of PHB does not allow its efficient crystallization, resulting in the formation of large spherulites [10, 11]. To overcome these drawbacks, copolymerization of 3-hydroxybutyrate (3HB) units with 3-hydroxyvalerate (3HV) or 4-hydroxybutyrate (4HB) units to produce poly(3-hydroxybutyrate-co-3-hydroxyvalerate) (PHBV) or poly(3-hydroxybutyrate-co-4-hydroxybutyrate) (P(3HB-co-4HB)), respectively, has been proposed to improve the handling properties of the PHB films [12]. Other strategies such as blending with other biopolymers [13-15] or adding nucleating agents [14, 16] have also been suggested. More recently, melt-spinning and cold-drawing processing technologies have also been reported as strategies to improve, for instance, mechanical properties of PHB articles [17-19].

Electrohydrodynamic processing (EHDP), comprising both electrospinning and electrospraying techniques, is a broadly used and efficient technology for fiber or capsule formation that employs high electrical forces to product highly controlled materials [20, 21]. It has recently gained much attention not only due to its versatility in processing a wide range of polymer and biopolymer materials, but also because of

its ability to produce ultrathin structures of diameters within the submicron range that can not be achieved using other more conventional technologies [22]. In the literature, there are some reports on the use of electrospun PHA fibers with different purposes (*e.g.* filtration membranes and catalytic nanofibers) [22-24] as well as bioactive applications (*e.g.* encapsulation of food ingredients, antimicrobial coatings, and systems with sustained release capacity) [25].

In relation to PHB, composition-graded films (CGF) of fluoroapatite (FAP) and PHB with enhanced mechanical properties, such as tensile strength and extension rate compared to pure PHB, have been reported as an electrospinning scaffold material for tissue engineering [26]. Flexible polylactide (PLA)/PHB electrospun blends were also developed by means of electrospinning, where PLA was reported to slow down the disintegration process [27]. The properties of nanobiocomposites prepared by solvent casting made of PHBV and poly(ϵ -caprolactone) (PCL) containing carbon nanofibers or carbon nanotubes as fillers were also reported, where enhanced conductivity, thermal, mechanical, and barrier properties were found [28]. Another study reported on blends of starch/PHB where different parameters such as blend proportions, thermal, mechanical properties, and alike were discussed in detail [29].

In more direct relation to this study, multilayer systems containing electrospun fibers obtained from zein and pullulan with strong adhesive properties resulting from the high surface to volume ratios of the thin fibers obtained were reported to significantly contribute to improve the

barrier performance of compression-molded PHA films [30]. Multilayers containing post-processed PHA electrospun fibers were seen to exhibit improved barrier properties and strong interlayer adhesion for wheat gluten [30]. The gas and vapor barrier properties of the electrospun interlayers were mainly determined by the morphology, thickness, and inherent barrier of the materials but also by the thermal post-processing. Annealing below the melting point of the biopolymer leads to fibers coalescence and hence to a homogeneous and continuous film with virtually little or no porosity. However, the full impact of post-processing has never been studied in detail. Thus, to the best of our knowledge, there is no prior literature reporting on the characterization of PHB monolayer films obtained by electrospinning and more specifically on how annealing, cooling, and orientation of the fibers can affect the ultimate physico-chemical properties of the developed materials. Therefore, the main goal of this paper is to develop and characterize PHB films obtained by electrospinning and to evaluate how the morphology, molecular order, thermal, optical, mechanical, and barrier properties are influenced by the particular processing and post-processing conditions used.

2. Materials and Methods

2.1 Materials

Bacterial aliphatic homopolyester PHB was supplied by Biomer (Krailing Germany) as P226F. According to the manufacturer, this is certified both as compostable and food contact, presenting a density of 1.25 g/cm³ and a

melt flow rate (MFR) of 10 g/10 min at 180°C and 5 kg. The molecular weight (M_w) estimated by the manufacturer was 500 kDa and the polydispersity index of 2. 2,2,2-Trifluoroethanol (TFE) with 99 % purity and D-limonene with 98% purity were both purchased from Sigma–Aldrich (Madrid, Spain). All products were used as received without further purification.

2.2 Preparation of the films

The electrospinning solutions were prepared by dissolving PHB, under magnetic stirring, in TFE at 10% in weight (wt.-%). These conditions were found to be the most adequate for the formation of stable jets of the biopolymer. Other solvents were screened but did not provide better results.

The electrospinning device used was a Fluidnatek® LE10 lab line from Bioinicia S.L. (Valencia, Spain) with a scanning injector to obtain a homogeneous deposition of the fibers. Scanning has been rarely used by the scientific community in the past and is thought not only to provide a more homogeneous deposition of the fibers but also to generate a different more compact fiber mesh morphology as compared to conventional static injectors. To obtain the electrospun PHB layers, the biopolymer solution was transferred to a 30-mL plastic syringe and connected through polytetrafluorethylene (PTFE) tubes to a stainless-steel needle (diameter 0.9 mm). The solution was electrospun for 3 h under a steady flow-rate of 2 mL/h using a motorized injector, scanning horizontally towards a metallic grid or to a metallic rotating drum, which

were used as collectors. The distance between the injector and collector was optimal at 15 cm and the voltage was at 15 kV. All experiments were performed at room conditions, *i.e.* 23°C and 40% RH, in a controlled environmental chamber. As stated above, for fiber orientation, the electrospinning process was carried out in the same conditions but the fibers were deposited on a drum or mandrel collector rotating at 1000 rpm for 3 h. Although different rotating speeds were carried out, clear fiber orientation was only seen beyond 500 rpm and, additionally, at 1000 rpm a compromise between orientation and fiber collection was found optimal.

Of the different annealing temperatures used (140, 150, 160, and 170°C), 160°C was selected as it was the lowest suitable annealing temperature able to yield transparent continuous films. Thus, for the annealing steps, the films were subjected to a temperature of 160°C by compression-molding using a hydraulic press 4122-model from Carver, Inc. (Indiana, USA). Different annealing times and four cooling processes were used. These cooling treatments included: (i) air at room temperature (RT), (ii) water at 25°C, (iii) ice, and (iv) slow cooling without temperature within the hydraulic hot-press until reaching room temperature (25°C). The effect of annealing time was screened in samples cooled in air (0, 5, 10, 15, and 20 minutes), water (0 and 5 minutes), and ice (0 and 5 minutes). **Table 1** gathers the samples prepared and the coding used throughout the paper.

Table 1. Sample codification and description of the here-developed electrospun poly(3-hydroxybutyrate) (PHB) materials.

Sample Code	Processing time at 160°C (min)	Cooling method	Collector type
t ₀	0	Air at room temperature	Static
t ₅	5	Air at room temperature	Static
Drum w t ₀	0	Water	Drum
Ice t ₀	0	Ice	Static
Ice t ₅	5	Ice	Static
Water t ₀	0	Water	Static
Water t ₅	5	Water	Static
Hot-press	0	Cooled slowly inside the hot press	Static
PHB	-	Compression molding from pellets and cooled at room temperature	-
Fibers	-	-	Static

2.3. Characterization of the films

2.3.1 Film thickness

Film thickness was measured with a digital micrometer series S00014, having ± 0.001 mm accuracy, from Mitutoyo Corporation (Kawasaki, Japan) at three random positions. Average values were used for water vapor, oxygen, and D-limonene permeability determinations. The post-processed samples had a thickness of typically 30 ± 4 μm .

2.3.2 Water vapor permeability

The water vapor permeability (WVP) of the samples were determined, in triplicate, using the gravimetric method ASTM E96-95 [27, 31]. To this end, 5 mL of distilled water was placed inside a Payne permeability cup ($\varnothing=3.5$ cm) from Elcometer Sprl (Hermalle-sous-Argenteau, Belgium) to expose the film to 100% relative humidity (RH) on one side. The liquid was not in contact with the film. Once the films were secured with silicon rings, they were placed within a desiccator at 0% RH cabinet at 25°C. The dryness of the cabinet was held constant using dried silica gel. Cups with aluminum films were used as control samples to estimate solvent loss through the sealing. The cups were weighted periodically using an analytical balance with a ± 0.0001 g accuracy. Water vapor permeation was calculated from the steady-state permeation slopes obtained from the regression analysis of weight loss data *vs.* time, and the weight loss was calculated as the total loss minus the loss through the sealing. The permeability was obtained by multiplying the permeance by the film thickness [29, 32].

2.3.3 D-limonene permeability

Permeability to limonene vapor was measured as described above for WVP. For this, 5 mL of D-limonene was placed inside the Payne permeability cups. The cups containing the films were placed at controlled conditions, *i.e.* 25°C and 40% RH. Limonene vapor permeation rates were estimated from the steady-state permeation slopes and weight loss was calculated as the total cell loss minus the loss through the sealing.

The samples were measured in triplicate and limonene permeability rates were calculated taking into account the average film thickness in each case.

2.3.4 Oxygen permeability

The oxygen permeability coefficient was derived from oxygen transmission rate (OTR) measurements recorded, in duplicate, using an Oxygen Permeation Analyzer M8001 from Systech Illinois (Thame, UK) at 80% RH and 25°C. The samples were previously purged with nitrogen in the humidity equilibrated samples, before exposure to an oxygen flow of 10 mL/min. The exposure area during the test was 5 cm² for each sample. In order to obtain the oxygen permeability, film thickness and gas partial pressure were considered.

2.3.5 Scanning electron microscopy

A S-4800 microscope from Hitachi (Tokyo, Japan) was used to observe the morphology of the electrospun PHB films, cross-sections, and surfaces by scanning electron microscopy (SEM). Cross-sections of the samples were prepared by cryo-fracture of the electrospun PHB films using liquid nitrogen. Then, they were fixed to beveled holders using conductive double-sided adhesive tape, sputtered with a mixture of gold-palladium under vacuum, and observed using an accelerating voltage of 5 kV.

2.3.6 Differential scanning calorimetry

Thermal analyses of electrospun PHB fibers were carried out by differential scanning calorimetry (DSC) on a DSC 7 analyzer from

PerkinElmer, Inc (Waltham, MA, USA). A heating program from -20 to 200°C in a nitrogen atmosphere was used using a refrigerating cooling accessory Intracooler 2 also from PerkinElmer, Inc. The scanning rate was 10 °C/min in order to minimize the influence of this parameter in the thermal properties. An empty aluminum cup was used as a reference. Calibration was performed using an indium sample. All tests were carried out, at least, in triplicate.

2.3.7 Fourier Transform Infrared spectroscopy

Fourier transform infrared (FTIR) spectra were collected coupling the attenuated total reflection (ATR) accessory Golden Gate of Specac, Ltd. (Orpington, U.K.) to a Bruker Tensor 37 FTIR equipment (Rheinstetten, Germany). Single spectra were collected in the wavelength range from 4000 to 600 cm⁻¹ by averaging 20 scans at a resolution of 4 cm⁻¹.

2.3.8 Optical properties

The transparency of the films was determined through the surface reflectance spectra using a spectrophotometer CM-3600d from Minolta Co. (Tokyo, Japan) with a 10-mm illuminated sample area. Measurements were taken in triplicate for each sample by using both a white and a black background. Film transparency was evaluated through the internal transmittance (T_i) in a 0–1 theoretical range by applying the Kubelka–Munk theory for multiple scattering to the reflection, following Equation 1. In this equation, R_0 is the reflectance of the film on an ideal black background. Parameters a and b are calculated from the reflectance of the

sample (R) and the layer backed by a known reflectance (R_g) according to Equations 2 and 3, respectively [33].

$$T_i = \sqrt{(a - R_0)^2 - b^2} \quad (1)$$

$$a = \frac{1}{2} \left(R + \frac{R_0 - R + R_g}{R_0 R_g} \right) \quad (2)$$

$$b = \sqrt{(a^2 - 1)} \quad (3)$$

2.3.9 Mechanical Properties

Tensile tests were performed according to ASTM standard method D638 using an Instron 4400 universal testing instrument from Instron (Norwood, MA, USA). The tests were performed using 115 mm long and 16 mm wide stamped dumb-bell shaped specimens. The cross-head speed used in the tests was 10 mm/min. The experiments were performed at room conditions, *i.e.* 25°C and 40% RH. All the tests were recorded in quadruplicate.

2.4. Statistical Analysis.

The samples properties were evaluated through analysis of variance (ANOVA) using Statgraphics Plus for Windows 5.1 from Manugistics Corporation (Rockville, MD, U.S.A.). Fisher's least significant difference (LSD) was used at the 95% confidence level ($p < 0.05$). Mean values and standard deviations were also calculated.

3. Results and discussion

3.1. Morphology

The morphology of the electrospun fibers before and after the annealing and cooling processes was analyzed by SEM. As expected, significant changes can be discerned in the cross-sectional images before (**Figure 1**) and after (**Figures 2 and 3**) the post-processing treatment. Surface and cross-section micrographs gleaned similar information and clearly revealed different morphologies and arrangements. The diameter of the obtained electrospun PHB fibers was found to peak at around 210 nm. The morphology of the annealed PHB films indicates that the starting electrospun non-woven fibers mat morphology is lost due to ultrathin fiber coalescence during the annealing step, leading to a packing of the material into a continuous film with some varying levels of porosity.

For the samples cooled in air at room temperature, an increase in annealing time up to 5 min appeared to induce somewhat more compact or less porous structures as compared to its counterpart annealed but not isothermally treated (t_0). The differences between the non-isothermal treatment (sample t_0) and isothermal treatment for up to 5 minutes (t_5) at 160°C are, however, relatively small and relate mainly to somewhat lower porosity. Further annealing time also led to compact structures but with somewhat higher porosity, this is more noticeable in the SEM images taken at higher magnification of the samples annealed for 20 min. With increasing annealing time, some yellowing of the samples was also seen. Thus, longer annealing times seem suboptimal from a morphological and

stability viewpoint. In addition to this, due to the very fast film-making processes taking place in the plastics processing industry, long thermal treatments would strongly impair industrial application for this process.

For a given annealing time, no significant differences were neither encountered among the samples cooled under different conditions (see **Figure 3**), with the exception of the sample slowly cooled inside the hot-press, which was the one showing the highest compact structure since cooling occurred at a comparatively much slower pace. This sample also appears to exhibit the thinnest cross section, in accordance with its higher degree of compactness. Despite this, such slow cooling is not a process that could be industrially meaningful. The samples cooled in ice, are those with the highest expected cooling rate and, due to there was no isothermal treatment, they exhibit an apparent higher degree of porosity. In order of cooling rate, the samples were graded as follows: ice>water>RT>hot-press.

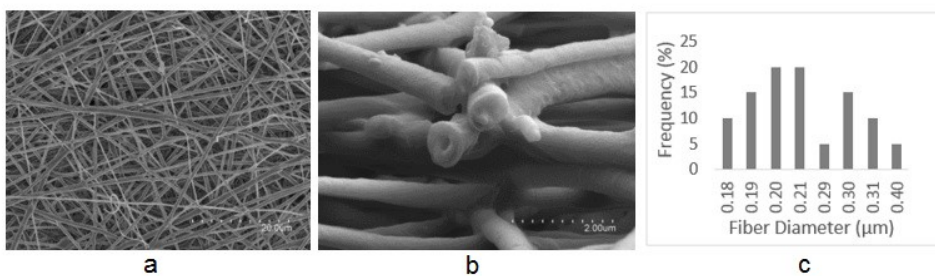


Figure1. Scanning electron microscopy (SEM) images of the electrospun poly(3-hydroxybutyrate) (PHB) fibers before the annealing process (160°C): (a) surface view, (b) cross-sectional view and (c) size distribution of fibers.

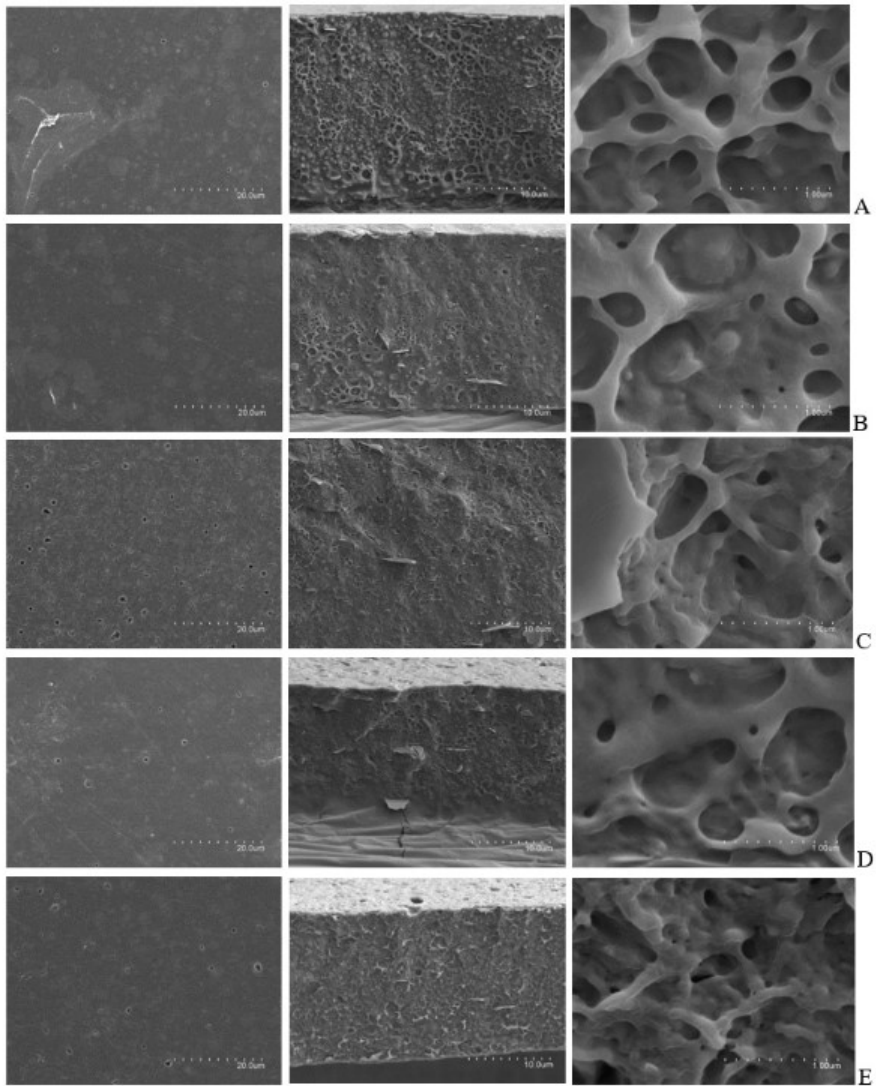


Figure 2. Scanning electron microscopy (SEM) images taken on surface of the electrospun poly(3-hydroxybutyrate) (PHB) fibers cooled at room temperature and isothermally post-processed at 160°C at different time intervals: (a) 0 minutes, (b) 5 minutes, (c) 10 minutes, (d) 15 minutes and (e) 20 minutes.

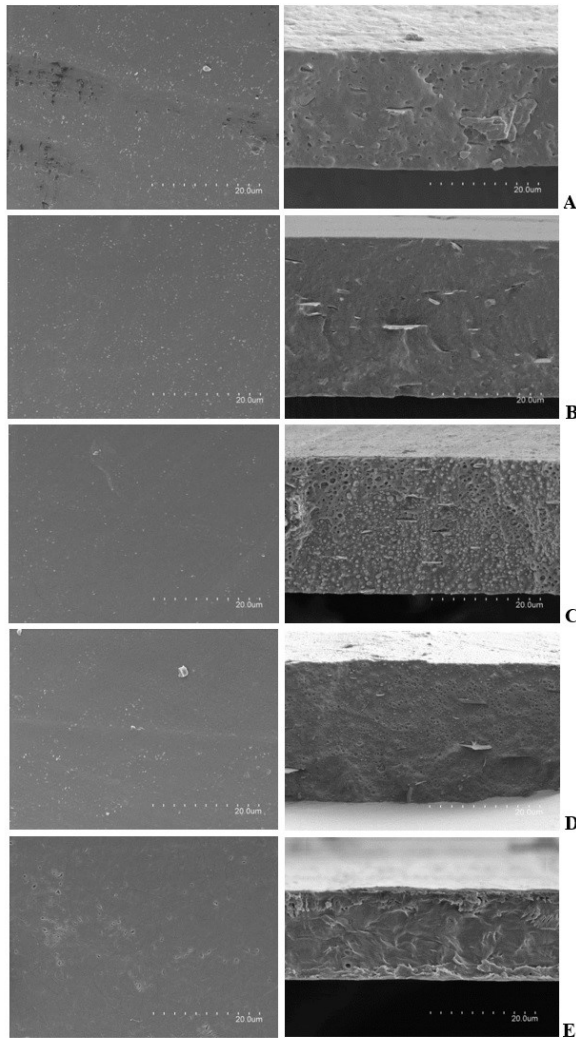


Figure 3. Scanning electron microscopy (SEM) images taken on surface and cross-section of the electrospun poly(3-hydroxybutyrate) (PHB) fibers isothermally post-processed at 160°C under different conditions: (A) 0 min of annealing and cooling in ice; (B) 5 min of annealing and cooling in ice (C); 0 min of annealing and cooling in water (D); 5 min of annealing and cooling in water; (E) 0 min of annealing and cooled in hot-press.

3.2. Chemical analysis

Generally, FTIR spectroscopy is sensitive to the conformational and local molecular environment of chemicals. Therefore, it has been extensively used as a convenient and powerful tool for investigating the chemical structure and conformational changes along the backbone of polymers. **Figure 4** shows the FTIR spectra of the samples annealed at different time intervals of between 0 and 20 min. In these spectra, the strong conformationally sensitive band at 1722 cm^{-1} assigned to C=O stretching vibration of the PHB is clearly visible [30]. Moreover, the C–O–C stretching vibration bands at 1228 cm^{-1} and 1278 cm^{-1} , with two small shoulder peaks at 1290 cm^{-1} and 1263 cm^{-1} , are also typical fingerprint vibrations of PHB [30]. From observation of the FTIR spectra as a function of time, there are no new features, band shift, or shape changes that could unambiguously suggest chemical alterations by annealing across time. These results are in accordance with the previous work reported by [34], which showed that despite the observed molar mass reduction and increase in melt index during polymer degradation, FTIR was not able to pick up significant band variations. However, closer inspection of **Figure 4** reveals that the carbonyl stretching band develops with annealing time an increasing high wavenumbers shoulder. This overall band widening with annealing time is here ascribed to changes in molecular order along the backbone and in turn to crystallinity.

In fact, FTIR has been previously used to estimate crystallinity in PHB. Mottin et al. [35] concluded that the ratio of the bands $A_{1230\text{cm}^{-1}}:A_{1453\text{cm}^{-1}}$ was indicative of changes in crystallinity in the sample. Xu et al. [36] heated a PHB film and collected the FTIR spectra *in situ* during the heating process, and found that the absorbance ratio of the crystalline band at 1230 cm^{-1} to the reference band at 1453 cm^{-1} was decreasing with decreasing crystallinity. They also found that the carbonyl stretching band was undergoing broadening with decreasing crystallinity. Porter and Yu [37] suggested that the ratio $A_{1184\text{cm}^{-1}}:A_{1382\text{ cm}^{-1}}$ was also providing an indication of crystallinity changes in PHB. According to their study, the absorption intensity at 1184 cm^{-1} decreases with increasing crystallinity while the 1382 cm^{-1} does not change. The band at 1186 cm^{-1} is assigned to the asymmetric stretching vibration of the C-O-C group, while the band at 1382 cm^{-1} is ascribed to the symmetric wagging of the CH_3 groups. Xu et al. [36] discussed that the latter band ratio was less reliable than the one of $A_{1230\text{cm}^{-1}}:A_{1453\text{cm}^{-1}}$, for that the band at 1382 cm^{-1} was seen to change during crystallization.

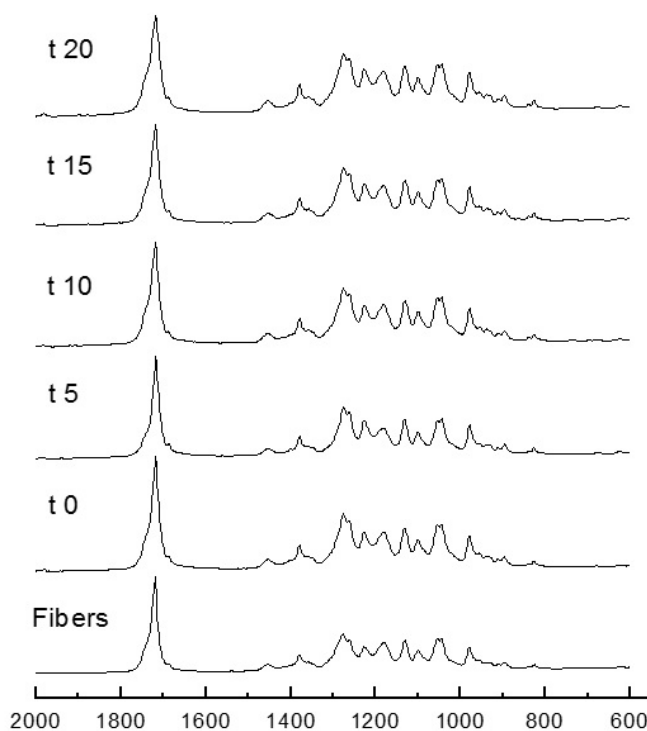


Figure 4. Fourier transform infrared spectroscopy (FTIR) spectra of the electrospun poly(3-hydroxybutyrate) (PHB) fibers mat and of the films annealed for up to 20 min.

Table 2 shows the full width at half maximum of the carbonyl band at *ca.* 1722 cm^{-1} and also the ratio $A_{1230\text{cm}^{-1}}:A_{1453\text{cm}^{-1}}$. From these indicators, it seems clear that annealing of the fibers leads to widening of the carbonyl band at 1722 cm^{-1} , which is associated with a decrease in crystallinity. Interestingly, the PHB fibers, when annealed at 160°C at t_0 , underwent a reproducible narrowing of the band, suggesting some increase in crystallinity, while crystallinity began to reduce with

increasing time of the isothermal treatment, especially beyond 10 min. Consistent with the overall behavior of the carbonyl band, the band ratio $A_{1230\text{cm}^{-1}}:A_{1453\text{cm}^{-1}}$ was seen to go up and then down.

Table 2. Fourier transform infrared spectroscopy (FTIR) crystallinity assessment from the full width at half maximum (FWHM) of the carbonyl band centered at $\sim 1722\text{ cm}^{-1}$ and the band area ratio $A_{1230\text{cm}^{-1}}/A_{1453\text{cm}^{-1}}$ for the electrospun poly(3-hydroxybutyrate) (PHB) samples processed with increasing annealing time and cooled in air at room temperature.

Sample	FWHM _{1722 cm⁻¹}	$A_{1230\text{cm}^{-1}}/A_{1453\text{cm}^{-1}}$
Fibers	17.50	3.53
t ₀	17.29	3.56
t ₅	19.71	3.36
t ₁₀	20.30	3.57
t ₁₅	25.44	3.01
t ₂₀	27.00	3.39

Table 3 summarizes the full width at half maximum of the carbonyl band at *ca.* 1722 cm^{-1} and also the band ratio $A_{1230\text{cm}^{-1}}:A_{1453\text{cm}^{-1}}$. From the first index, the samples cooled in the hot-press showed the lowest carbonyl band width suggesting the highest crystallinity and the fast-cooled samples at t₀ showed the largest values indicating lower crystallinity. During isothermal exposure for 5 minutes, crystallinity

seems to develop to some extent. A similar trend was provided by the $A_{1230\text{cm}^{-1}}:A_{1453\text{cm}^{-1}}$ ratio.

Table 3. Fourier transform infrared spectroscopy (FTIR) crystallinity estimation from the full width at half maximum (FWHM) of the carbonyl band centered at *ca.* 1722 cm^{-1} and the band area ratio $A_{1230\text{cm}^{-1}}/A_{1453\text{cm}^{-1}}$ for the electrospun poly(3-hydroxybutyrate) (PHB) samples processed with different cooling processes.

Sample	FWHM _{1722 cm⁻¹}	$A_{1230\text{cm}^{-1}}/A_{1453\text{cm}^{-1}}$
Hot-press	17.00	4.01
Ice t ₀	24.29	3.55
Ice t ₅	20.38	3.63
Water t ₀	22.90	3.28
Water t ₅	21.52	3.38

3.3. Thermal properties

It is clear from the DSC thermograms (**Figure 5**) that, while the PHB fibers showed two melting features, one at $\sim 50^\circ\text{C}$ related to the melting of a low molecular weight additive (typically a plasticizer and another one at $\sim 169^\circ\text{C}$ related to the melting of the PHB crystals), the annealed samples show a more complex melting behavior with multiple melting endotherms, which are ascribed in PHB to melting and recrystallization during the DSC runs. This makes it difficult to determine the actual sample crystallinity or a single melting point from the technique, since these develop over the run [38]. **Table 4** gathers the melting points, melting enthalpies, crystallization temperatures, and crystallization

Chapter I

enthalpies for the sample compression molded, for the fibers and for the annealed films at different times. From this, it seems that with increasing annealing time the crystallization temperature tends to decrease somewhat (especially in the samples processed with 15 and 20 min of annealing), as well as the crystallization enthalpy. This could indicate that these long-time annealed samples could develop some impairments for crystallization, perhaps due to partial degradation, consistent with the FTIR data and some light color development.

Since the samples annealed for times longer than 5 minutes did not yield a better morphology or even crystallinity and, furthermore, are not expected to meet current industrial processes, the rest of the characterization was carried out only on samples cooled under different conditions and annealed either at t_0 or at t_5 . Of these, the samples annealed at t_0 and cooled in air at RT are the ones that could show more potential applicability in the packaging industry since they could be applied to existing lamination and curing machinery.

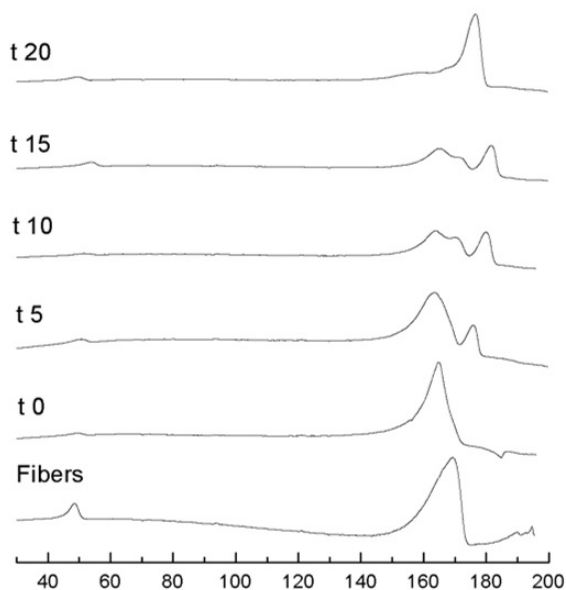


Figure 5. Differential scanning calorimetry (DSC) thermograms of the electrospun poly(3-hydroxybutyrate) (PHB) fibers and of the films with 0–20 min of annealing. DSC thermogram of the fibers and of the samples with 0-20 min of annealing.

Table 4. Thermal properties obtained from the differential scanning calorimetry (DSC) curves in terms of melting temperature of the plasticizer (T_{plast}), melting temperature (T_m), normalized melting enthalpy (ΔH_m), crystallization temperature (T_c), and crystallization enthalpies (ΔH_c) for the various poly(3-hydroxybutyrate) (PHB) samples.

Samples	T_{plast}	T_{m1} (°C)	T_{m2} (°C)	ΔH_m (J/g)	T_c (°C)	ΔH_c (J/g)
PHB	46.7 (0.7) ^{ab}	169.4 (0.2) ^a	-	76.8 (0.4) ^c	110.3 (0.3) ^a	64.0 (0.4) ^c
Fibers	47.5 (0.2) ^{ab}	169.3 (0.1) ^a	-	64.2 (1.6) ^a	110.4 (0.7) ^a	59.5 (0.5) ^{ab}

t 0	48.7 (0.7) ^{ab}	165.8 (1.3) ^b	-	71.9 (2.4) ^b	110.6 (0.7) ^c	61.1 (0.3) ^a
t 5	46.5 (0.6) ^{ab}	163.5 (0.2) ^{bc}	175.8 (1.2) ^a	81.2 (1.4) ^c	110.0 (0.3) ^c	60.0 (1.7) ^a
t 10	50.4 (1.2) ^a	162.2 (1.6) ^c	177.3 (0.3) ^a	78.4 (0.8) ^c	110.4 (1.0) ^a	60.8 (1.4) ^a
t 15	48.7 (0.3) ^{ab}	161.5 (1.0) ^c	176.9 (0.3) ^a	80.4 (1.9) ^c	109.6 (2.2) ^a	59.5 (1.7) ^a
t 20	47.0 (0.9) ^{ab}	176.5 (0.2) ^d	-	80.7 (0.6) ^c	109.7 (0.1) ^a	57.8 (0.6) ^b

Mean value (standard error).

a–d: Different superscripts within the same column indicate significant differences among samples ($p < 0.05$).

Table 5 summarizes the thermal data for the samples cooled using different methods, and for the sample collected on a rotating mandrel. These data demonstrate that the sample slowly cooled in the hot-press showed the highest melting temperature and enthalpy, as would be expected. These enhanced melting data could also correlate with a more pronounced melting recrystallization process during the DSC run, since the PHB sample was allowed to cool very slowly and so could also develop crystallinity more easily.

Table 5. Thermal properties obtained from the differential scanning calorimetry (DSC) curves in terms of melting temperature of the plasticizer (T_{plast}), melting temperature (T_m), normalized melting enthalpy (ΔH_m), crystallization temperature (T_c), and crystallization enthalpies (ΔH_c) for the electrospun poly(3-hydroxybutyrate) (PHB) samples cooled under different conditions.

Samples	T_{plast}	T_m (°C)	ΔH_m (J/g)	T_c (°C)	ΔH_c (J/g)
Ice t 0	44.1 (0.2) ^d	166.3 (0.3) ^{ab}	65.5 (1.1) ^a	110.9 (0.8) ^{ab}	60.5 (0.6) ^a

Water t 0	49.8 (0.1) ^a	166.8 (0.2) ^c	68.4 (0.6) ^c	111.6 (0.6) ^a	58.4 (0.3) ^c
Hot press t 0	50.3 (0.3) ^b	175.3 (0.7) ^d	78.6 (1.9) ^d	110.2 (0.1) ^a	61.3 (0.8) ^b
Drum t 0	49.0 (2.1) ^a	168.1 (1.4) ^b	61.7 (2.1) ^b	110.6 (1.1) ^a	61.1 (0.1) ^b

Mean value (standard error).

a–d: Different superscripts within the same column indicate significant differences among samples ($p < 0.05$).

3.4. Optical properties

The contact transparency images of the developed films prepared by annealing at the chosen temperature of 160°C and at two different time intervals are shown as an example in **Figure 6**. The samples annealed at t_0 and t_5 , A and B respectively, exhibit similar contact transparency. All the annealed materials for up to 5 minutes presented good contact transparency, which seemed not to be affected by annealing time, suggesting that PHB was not so strongly degraded after 5 minutes of the mild thermal treatment given to the electrospun fibers. By comparison to sample C, which is a compression-molded film of similar thickness, it clearly showed somewhat lower transparency, probably due to somewhat higher crystallinity (see crystallization enthalpy data in **Table 4**) but perhaps also due to the different sample preparation method where comparatively little thermal exposure is given to the samples. Sample D, which corresponds to the electrospun PHB fibers, was completely opaque as expected since the electrospun ultrathin fibers, close to the nano range, are known to refract the light very strongly.

Similarly, **Figure 7** shows the contact transparency for the annealed electrospun PHB fibers cooled at different cooling conditions such as cooled by direct immersion in water at room temperature, cooled by direct immersion in ice, and slow cooled in air. From the results, it is evident that all the samples remained highly transparent, which suggests that the different cooling conditions applied did not apparently alter the optical appearance of the post-processed PHB fibers. These results are further supported by the internal transmittance (T_i) data described below.



Figure 6. Contact transparency of the poly(3-hydroxybutyrate) (PHB) films prepared at various annealing times for up to 5 min and cooled in air at room temperature: (A) t_0 ; (B) t_5 ; (C). Compression molded PHB film; (D) Electrospun PHB fibers without heat treatment (opaque material, D letter underneath not discernible).



Figure 7. Contact transparency of the poly(3-hydroxybutyrate) (PHB) films prepared at different annealing times and cooled under different conditions. (A) Ice t_0 ; (B) Ice t_5 ; (C) Water t_0 ; (D) Water t_5 ; (E) Hot-press t_0 .

It is a well-established fact that post-processing strongly affects the optical behavior of electrospun fibrous materials [30]. In general, opacity can be quantitatively assessed in terms of internal transmittance (T_i). **Figure 8** describes the absorption properties of the short-time annealed PHB films. A higher value of T_i corresponds to a more transparent film, which indicates a more homogeneous refractive index. On the other hand, a lower T_i value indicates that PHB films are less transparent, due to their more heterogeneous morphology. As shown in **Figure 8**, the spectrograph indicates that both samples showed almost the same transmittance, both ranging from 79 to 84%, the sample at t_0 being slightly more transparent.

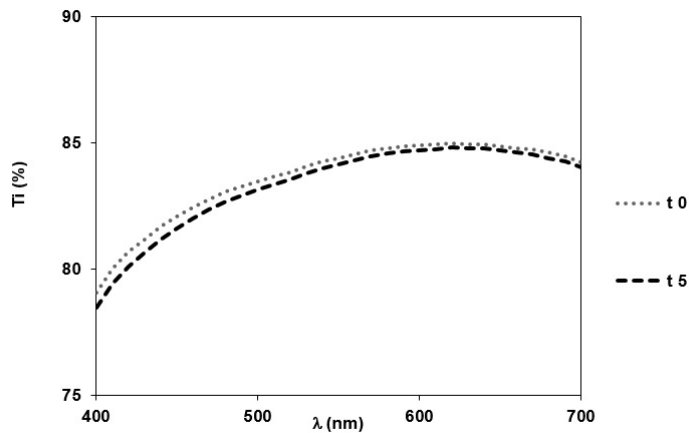


Figure 8. Spectral distribution of internal transmittance for the poly(3-hydroxybutyrate) (PHB) samples at t_0 and t_5 .

Figure 9 shows similar patterns also for all the post-processed PHB samples subjected to different cooling conditions. This indicates some differences in their transmittance values, which had a maximum range of 83-87%, again suggesting the highly transparent nature of the samples generated. It seems that the sample cooled in water showed a bit higher transparency. **Figure 9** also demonstrates that the PHB samples collected on the rotating drum showed somewhat higher transparency after post-processing, perhaps because the fibers deposited are aligned, thus generating a more homogeneous film after annealing.

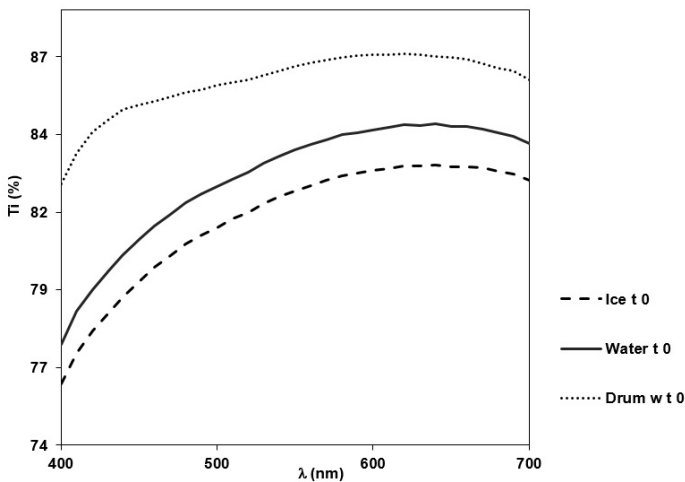


Figure 9. Spectral distribution of internal transmittance for the poly(3-hydroxybutyrate) (PHB) samples cooled in ice t0, water t0, and drum w t0.

3.5 Mechanical properties

Table 6 presents the results from the tensile tests carried out in some of the most relevant materials. Analysis of these data shows that the storage modulus and tensile strength were only somewhat higher for the oriented PHB sample as compared to the non-oriented fibers and the conventional compression-molding process. This indicates that alignment of the fibers during electrospinning does result in improved rigidity for the system, even when a similar post-processing annealing step was carried out. It is also relevant to observe that the annealed electrospun fibers exhibit an increased elongation at break, as well as toughness, compared with the PHB film. This is significant from an application viewpoint, because PHB is often considered a highly fragile material. By processing the material through electrospinning and post-processing in a controlled manner, a more balance mechanical performance is achieved whereby rigidity is retained but toughness is increased.

Table 6. Mechanical properties in terms of tensile modulus (E), tensile strength at break (σ_b), elongation at break (ϵ_b), and toughness (T), derived from tensile test of various electrospun poly(3-hydroxybutyrate) (PHB) samples.

Samples	E (MPa)	σ_b (MPa)	ϵ_b (%)	T (mJ/m ³)
PHB film	1104 (74) ^a	17.8 (1.8) ^b	2.9 (1.0) ^c	0.3 (0.1) ^b
to	1080 (145) ^a	17.3 (5.1) ^b	4.5 (1.0) ^a	0.6 (0.2) ^a
Water to	1135 (243) ^a	13.4(1.6) ^c	3.9 (2.0) ^b	0.4 (0.3) ^b
Drum w to	1171 (68) ^b	20.7 (4.7) ^a	3.8 (1.0) ^b	0.6 (0.2) ^a

Mean value (standard error).

a–c: Different superscripts within the same column indicate significant differences among samples ($p < 0.05$).

3.6 Barrier properties

To evaluate how the processing and post-processing parameters and, hence, the different molecular architecture of the samples affected the barrier properties of the developed PHB films, water, limonene, and oxygen permeability were finally measured in the most relevant samples. The barrier performance is, in fact, one of the main parameters of application interest in packaging. **Table 7** gathers the water vapor permeability values of the developed PHB films. The first observation is that the electrospun PHB films showed somewhat higher water vapor permeability values than a compressed-molded PHB film: $1.7 \cdot 10^{-15} \text{ kg}\cdot\text{m}/\text{s}\cdot\text{m}^2\cdot\text{Pa}$, as measured in our lab previously and reported by Sanchez-Garcia et al. [39]. This could be explained by the fibers network exhibiting some degree of porosity formed during the electrospinning process, but it may also be related to differences in molecular order. However, the samples with the lowest cooling rate, those cooled inside the hot-press or cooled at room temperature and annealed for 5 minutes, came closer to the reported value in a compression-molded PHB film. These observations suggest that by optimal post-processing of an electrospun fiber-based sample, the material goes from the very low permeability of the fibers mat to a barrier performance close to a film prepared in a conventional industrial process obtained by compression moulding [35,

39]. Thus, electrospun PHB films, which underwent slow cooling in the hot-press, showed the lowest values of WVP as stated above. **Table 7** also shows that higher annealing times after fast cooling resulted in a lower barrier, which is in line with the less favorable morphology and lower molecular order, i.e. lower free volume, observed in these samples.

Table 7. Values of water vapor permeability (WVP) of various electrospun poly(3-hydroxybutyrate) (PHB) samples.

Samples	Water vapor permeability $\times 10^{15}$ ($\text{kg}\cdot\text{m}\cdot\text{m}^{-2}\cdot\text{Pa}^{-1}\cdot\text{s}^{-1}$)
t₀	5.22 (0.40) ^a
t₅	2.01 (0.30) ^c
Ice t₀	8.96 (1.20) ^d
Ice t₅	2.39 (0.80) ^{bc}
Water t₀	6.92 (0.60) ^{bc}
Water t₅	3.46 (0.50) ^b
Hot-press w t₀	1.75 (0.50) ^c

Mean value (standard error).

a–d: Different superscripts within the same column indicate significant differences among samples ($p < 0.05$).

Tables 8 shows the D-limonene permeability values of the most relevant samples. Limonene transport properties are important because this component is usually used as a standard system to test aroma barrier. It is also relevant to note that limonene, as opposed to moisture, is a strong plasticizer for PHA materials [39]. **Table 8** indicates that no significant differences were observed between the samples probably due to

plasticization, although the sample prepared by slow cooling, *i.e.* hot-press, showed the lowest values of limonene permeability in line with the higher molecular order inferred for these samples. Sanchez-Garcia et al. reported that limonene permeability for a similar compression-molded PHB sample was at $8.8 \times 10^{-15} \text{ kg}\cdot\text{m}/\text{s}\cdot\text{m}^2\cdot\text{Pa}$ [39]. The latter result is somewhat higher than the ones measured in the present study, suggesting that plasticization may occur differently in the electrospun samples. Thus, post-processing interfiber coalescence may create lots of interphases between the ultrathin fibers and this could affect the mass transport along this material.

Table 8. Values of limonene permeability of various electrospun poly(3-hydroxybutyrate) (PHB) samples.

Samples	Limonene permeability $\times 10^{15} \text{ (kg}\cdot\text{m}\cdot\text{m}^{-2}\cdot\text{Pa}^{-1}\cdot\text{s}^{-1})$
t₀	3.20 (0.40) ^a
t₅	3.93 (0.30) ^e
Ice t₀	3.31 (1.30) ^b
Ice t₅	3.83 (0.70) ^d
Water t₀	4.18 (0.60) ^f
Water t₅	3.72 (1.20) ^c
Hot-press w t₀	1.95 (0.10) ^g

Mean value (standard error).

a–g: Different superscripts within the same column indicate significant differences among samples ($p < 0.05$).

Finally, **Table 9** shows the oxygen permeability measured for the PHB film and for the electrospun samples annealed and cooled in water. Oxygen is a non-condensable small gas molecule and, hence, it is more sensitive to the material free volume, defects and porosity. Thus, the lowest permeability was found for the continuous compression-molded PHB film. The sample annealed for a longer time of 5 min showed somewhat lower permeability as expected by the enhanced sample compactness and molecular order.

Table 9. Values of oxygen permeability of various poly(3-hydroxybutyrate) (PHB) samples.

Samples	Oxygen permeability $\times 10^{14}$ ($\text{m}^3 \cdot \text{m} \cdot \text{m}^2 \cdot \text{s}^{-1} \text{ Pa}^{-1}$)
PHB film	2.00 (0.10) ^c
Water t ₀	4.00 (0.30) ^a
Water t ₅	3.00 (0.30) ^b

Mean value (standard error).

a: Different superscripts within the same column indicate significant differences among samples ($p < 0.05$).

4. Conclusions

This study showed that novel films with variable properties can be obtained by optimizing the post-processing conditions of electrospun fibers of PHB, annealing temperature, isothermal time, and cooling rate. The electrospun films showed better optical properties than films of same thickness processed by conventional compression molding. In general, more compact morphologies and improved properties in terms of barrier

performance were found for samples where slow cooling occurred from the isothermal annealing post-processing step at 160°C. FTIR spectroscopy was found to be a non-dynamic adequate method, compared with the conventional dynamic DSC method, to assess molecular order in the materials and correlated fairly well with their barrier performance. The mechanical properties of this type of electrospun films resulted in higher elongation at break and toughness in comparison with their corresponding compression molded counterparts. Barrier properties were generally found to depend mostly on annealing time but, more importantly, on cooling rate. The results of this study show a very promising new plastic processing technology, the annealed electrospun fibers, to provide new valorizing forms of processing renewable polymers as interlayers or coatings with enhanced flexibility and transparency while potentially retaining the barrier performance to gases and vapours of the conventional compression molded films.

In addition, since these materials made of post-processed submicron electrospun fibers are known to exhibit self-adhesive properties, they offer potential as functional elements in packaging materials made of biopolymers. This is relevant since in the biopolymers field, there is a lack of functional bioadhesives that can help constitute fully biobased multilayers, by acting as tie layers, for use not only in packaging but also as hydrophobic coatings for fiber-based packaging. Finally, since these materials can easily incorporate active or/and bioactive packaging ingredients within the fibers structure, they can potentially be used in

active and bioactive packaging strategies requiring controlled release of the active/bioactive ingredients.

5. Acknowledgments

The authors would like to thank the Spanish Ministry of Economy and Competitiveness (MINECO) project AGL2015-63855-C2-1-R for financial support. A. Cherpinski also would like to thank the Brazilian Council for Scientific and Technological Development (CNPq) of Brazilian Government for her predoctoral grant (205955/2014-2).

6. References

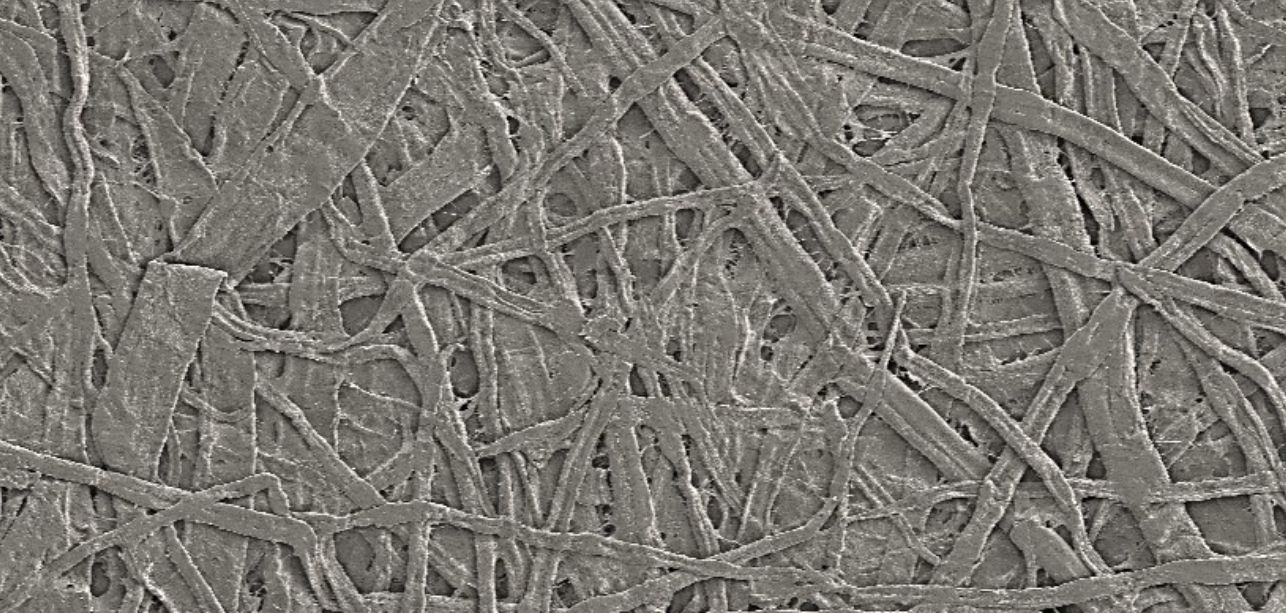
1. Shah, Aamer Ali, Satoshi Kato, Noboru Shintani, Numbi Ramudu Kamini, and Toshiaki Nakajima-Kambe. "Microbial Degradation of Aliphatic and Aliphatic-Aromatic Co-Polyesters." *Applied microbiology and biotechnology* 98, no. 8 (2014): 3437.
2. Tharanathan, RN. "Biodegradable Films and Composite Coatings: Past, Present and Future." *Trends in Food Science & Technology* 14, no. 3 (2003): 71-78.
3. Lagaron, JM. "Multifunctional and Nanoreinforced Polymers for Food Packaging. 2011." Elsevier, 2011.
4. Bhardwaj, Umesh, Prodyut Dhar, Amit Kumar, and Vimal Katiyar. "Polyhydroxyalkanoates (Pha)-Cellulose Based Nanobiocomposites for Food Packaging Applications." In *Food Additives and Packaging*, 275-314: ACS Publications, 2014.
5. Rujnić-Sokele, Maja, and Ana Pilipović. "Challenges and Opportunities of Biodegradable Plastics: A Mini Review." *Waste Management & Research* 35, no. 2 (2017): 132-40.
6. Plackett, David, and I Siro. "Polyhydroxyalkanoates (Phas) for Food Packaging." In *Multifunctional and Nanoreinforced Polymers for Food Packaging*, 498-526: Woodhead Publishing Ltd., 2011.

7. Doi, Y. "Microbial Polyesters, Vch, New York." *Google Scholar* (1990).
8. Hasirci, V. *Biodegradable Biomedical Polymers. Review of Degradation of and in Vivo Responses to Polylactides and Polyhydroxyalkanoates*: Marcel Dekker, New York, NY, 2000.
9. Lee, Sang Yup. "Bacterial Polyhydroxyalkanoates." *Biotechnology and bioengineering* 49, no. 1 (1996): 1-14.
10. El-Hadi, Ahmed, Rainer Schnabel, Ekkehard Straube, G Muller, and M Riemschneider. "Effect of Melt Processing on Crystallization Behavior and Rheology of Poly (3-Hydroxybutyrate)(Phb) and Its Blends." *Macromolecular Materials and Engineering* 287, no. 5 (2002): 363-72.
11. Weihua, Kai, Yong He, Naoki Asakawa, and Yoshio Inoue. "Effect of Lignin Particles as a Nucleating Agent on Crystallization of Poly (3-Hydroxybutyrate)." *Journal of applied polymer science* 94, no. 6 (2004): 2466-74.
12. Torres-Giner, S, N Montanes, T Boronat, L Quiles-Carrillo, and R Balart. "Melt Grafting of Sepiolite Nanoclay onto Poly (3-Hydroxybutyrate-Co-4-Hydroxybutyrate) by Reactive Extrusion with Multi-Functional Epoxy-Based Styrene-Acrylic Oligomer." *European Polymer Journal* 84 (2016): 693-707.
13. Avella, Maurizio, Ezio Martuscelli, and Pietro Greco. "Crystallization Behaviour of Poly(Ethylene Oxide) from Poly(3-Hydroxybutyrate)/Poly(Ethylene Oxide) Blends: Phase Structuring, Morphology and Thermal Behaviour." *Polymer* 32, no. 9 (1991): 1647-53.
14. Avella, Maurizio, Ezio Martuscelli, and Maria Raimo. "The Fractionated Crystallization Phenomenon in Poly(3-Hydroxybutyrate)/Poly(Ethylene Oxide) Blends." *Polymer* 34, no. 15 (1993): 3234-40.
15. Greco, Pietro, and Ezio Martuscelli. "Crystallization and Thermal Behaviour of Poly (D (-)-3-Hydroxybutyrate)-Based Blends." *Polymer* 30, no. 8 (1989): 1475-83.
16. Withey, RE, and JN Hay. "The Effect of Seeding on the Crystallisation of Poly (Hydroxybutyrate), and Co-Poly

- (Hydroxybutyrate-Co-Valerate)." *Polymer* 40, no. 18 (1999): 5147-52.
17. Furuhashi, Yukiko, Hiroshi Ito, Takeshi Kikutani, Takashi Yamamoto, Mitsugu Kimizu, and Mukerrem Cakmak. "Structural Analysis of Poly (3-Hydroxybutyrate-Co-3-Hydroxyvalerate) Fibers Prepared by Drawing and Annealing Processes." *Journal of Polymer Science Part B: Polymer Physics* 36, no. 14 (1998): 2471-82.
 18. Gordeyev, SA, and Yu P Nekrasov. "Processing and Mechanical Properties of Oriented Poly (B-Hydroxybutyrate) Fibers." *Journal of materials science letters* 18, no. 20 (1999): 1691-92.
 19. Yamamoto, T, M Kimizu, T Kikutani, Y Furuhashi, and M Cakmak. "The Effect of Drawing and Annealing Conditions on the Structure and Properties of Bacterial Poly (3-Hydroxybutyrate-Co-3 Hydroxyvalerate) Fibers." *International Polymer Processing* 12, no. 1 (1997): 29-37.
 20. Chronakis, Ioannis S. "Micro-/Nano-Fibers by Electrospinning Technology: Processing, Properties and Applications." *Micro-Manufacturing Engineering and Technology, William Andrew-ELSEVIER* (2010): 264-86.
 21. Echegoyen, Y, MJ Fabra, JL Castro-Mayorga, A Cherpinski, and JM Lagaron. "High Throughput Electro-Hydrodynamic Processing in Food Encapsulation and Food Packaging Applications." *Trends in Food Science & Technology* (2016).
 22. Subbiah, Thandavamoorthy, GS Bhat, RW Tock, S Parameswaran, and SS Ramkumar. "Electrospinning of Nanofibers." *Journal of applied polymer science* 96, no. 2 (2005): 557-69.
 23. Frenot, Audrey, and Ioannis S Chronakis. "Polymer Nanofibers Assembled by Electrospinning." *Current opinion in colloid & interface science* 8, no. 1 (2003): 64-75.
 24. Huang, Zheng-Ming, Y-Z Zhang, M Kotaki, and S Ramakrishna. "A Review on Polymer Nanofibers by Electrospinning and Their Applications in Nanocomposites." *Composites science and technology* 63, no. 15 (2003): 2223-53.
 25. Torres-Giner, Sergio, Rocío Pérez-Masiá, and Jose M Lagaron. "A Review on Electrospun Polymer Nanostructures as Advanced

- Bioactive Platforms." *Polymer Engineering & Science* 56, no. 5 (2016): 500-27.
26. Zhao, DM, YX Wang, RW Xu, G Wu, LQ Zhang, DS Yu, FZ Cui, DF Chen, and W Tian. "Composition-Graded Films of Fluoroapatite/Phb Fabricated Via Electrospinning for Tissue Engineering." *Journal of Bioactive and Compatible Polymers* 22, no. 4 (2007): 379-93.
 27. Arrieta, M. P., J. López, D. López, J. M. Kenny, and L. Peponi. "Development of Flexible Materials Based on Plasticized Electrospun Pla–Phb Blends: Structural, Thermal, Mechanical and Disintegration Properties." *European Polymer Journal* 73 (2015): 433-46.
 28. Sanchez-Garcia, MD, JM Lagaron, and SV Hoa. "Effect of Addition of Carbon Nanofibers and Carbon Nanotubes on Properties of Thermoplastic Biopolymers." *Composites science and technology* 70, no. 7 (2010): 1095-105.
 29. Lagaron, Jose M, and Amparo Lopez-Rubio. "Nanotechnology for Bioplastics: Opportunities, Challenges and Strategies." *Trends in Food Science & Technology* 22, no. 11 (2011): 611-17.
 30. Fabra, María José, Amparo Lopez-Rubio, and Jose M Lagaron. "High Barrier Polyhydroxyalcanoate Food Packaging Film by Means of Nanostructured Electrospun Interlayers of Zein." *Food Hydrocolloids* 32, no. 1 (2013): 106-14.
 31. Standard, ASTM. "Standard Test Methods for Water Vapor Transmission of Materials." *Annual book of ASTM standards. Designation E96-E80* (1989): 730-39.
 32. Sanchez-Garcia, MD, and JM Lagaron. "Novel Clay-Based Nanobiocomposites of Biopolyesters with Synergistic Barrier to Uv Light, Gas, and Vapour." *Journal of applied polymer science* 118, no. 1 (2010): 188-99.
 33. Hutchings, J.B. "Food and Colour Appearance. (2nd Ed.), Chapman and Hall Food Science Book, Aspen Publication, Gaithersburg, Md (1999)." (1999).
 34. Pachekoski, Wagner Maurício, Carla Dalmolin, and José Augusto Marcondes Agnelli. "The Influence of the Industrial Processing on

- the Degradation of Poly (Hidroxybutyrate)-Phb." *Materials Research* 16, no. 2 (2013): 237-332.
35. Mottin, Artur Caron, Eliane Ayres, Rodrigo Lambert Oréface, and Jairo José Drummond Câmara. "What Changes in Poly (3-Hydroxybutyrate)(Phb) When Processed as Electrospun Nanofibers or Thermo-Compression Molded Film?" *Materials Research* 19, no. 1 (2016): 57-66.
 36. Xu, Jun, Bao-Hua Guo, Rui Yang, Qiong Wu, Guo-Qiang Chen, and Zeng-Min Zhang. "In Situ Ftir Study on Melting and Crystallization of Polyhydroxyalkanoates." *Polymer* 43, no. 25 (2002): 6893-99.
 37. Porter, Michael, and Jian Yu. "Crystallization Kinetics of Poly (3-Hydroxybutyrate) Granules in Different Environmental Conditions." *Journal of Biomaterials and Nanobiotechnology* 2, no. 03 (2011): 301.
 38. Martínez-Abad, Antonio, Luis Cabedo, Catarina SS Oliveira, Loic Hilliou, Maria Reis, and José María Lagarón. "Characterization of Polyhydroxyalkanoate Blends Incorporating Unpurified Biosustainably Produced Poly (3-Hydroxybutyrate-Co-3-Hydroxyvalerate)." *Journal of applied polymer science* 133, no. 2 (2016).
 39. Sanchez-Garcia, MD, E Gimenez, and JM Lagaron. "Novel Pet Nanocomposites of Interest in Food Packaging Applications and Comparative Barrier Performance with Biopolyester Nanocomposites." *Journal of Plastic Film & Sheeting* 23, no. 2 (2007): 133-48.



Chapter II

Multilayer Structures Based on Annealed Electrospun Biopolymer Coatings of Interest in Water and Aroma Barrier Fiber-Based Food Packaging Applications

Cherpinski, A., Torres-Giner, S., Cabedo, L., Méndez, J. A., & Lagaron, J. M. (2018). Multilayer structures based on annealed electrospun biopolymer coatings of interest in water and aroma barrier fiber-based food packaging applications. *Journal of Applied Polymer Science*, 135(24), 45501.



Abstract

In this research work, for the first time, a fiber-based packaging material was coated by annealed electrospun ultrathin fibers of poly(3-hydroxybutyrate) (PHB), polyvinyl alcohol (PVOH), and polylactide (PLA). The resultant mono- and multilayer structures self-adhered to the paper substrate and were characterized in terms of morphology, optical, and barrier properties. Additionally, the use of a static flat plate and rotating mandrel collector as well as the application of different electrospinning deposition times were analyzed. The thermally treated electrospun biopolymers yielded totally transparent films while, due to the opaque nature of the uncoated paper substrate, the developed packaging materials were also opaque but with a glossier surface finish provided by the bioplastic coating. The annealed films obtained from random electrospun fibers, that is, the mats of ultrathin fibers collected on the static plate, presented higher transparency and thickness and also enhanced barrier performance. On the overall, the developed annealed electrospun biopolymer coatings resulted in a significant improvement of the paper barrier properties to water and limonene vapors, being the paper/PVOH/PHB film the best performing multilayer packaging structure.

Keywords: Biopolymers and renewable polymers; coatings; electrospinning; optical properties; packaging

1. Introduction

Lightweight, renewability, and recyclability represent the main advantages of fiber-based packaging, which is highly used in the food packaging industry. The concept of fiber-based packaging, habitually referred for simplicity as paper, includes different types of materials such as sulfite paper, Kraft paper, grease-free paper, paperboards, and laminated paper [1]. This material is mainly made of cellulosic pulp fibers that are derived from renewable resources, including wood and nonwood lignocellulosic materials [2]. After processing, the paper surface habitually remains rather rough and porous. Filling paper with a color-containing pigment is an excellent method to improve certain qualities, including weight, surface smoothness, opacity, gas permeability, and ink absorbency [3]. However, the porosity and hydrophilic nature of paper, which are intrinsically ascribed to the hydroxyl groups (O-H) of cellulose, creates some limitations for its use on food packaging applications. These are mainly related to the high permeation of moisture, organic vapors, and gases, and to the adsorption of oils. This certainly makes uncoated paper unable to retaining its proper shape, resulting in a loss of quality and organoleptic properties for the packaged products [4].

The limitations described above can be reduced by the application of plastic coatings to paper that can advantageously increase paper stiffness too. Nevertheless, these plastic materials are habitually based on polymers obtained from monomers derived from petroleum that

certainly limits intrinsic sustainability aspects of fiber-based packaging materials such as recyclability, biodegradability, carbon footprint, etc [5]. In contrast to traditional petroleum-based plastics, biopolymers certainly represent a promising alternative as paper coatings due to their environmentally friendly nature both in terms of natural origin and biodegradability [6]. Indeed, the association of biopolymers to paper provides interesting functionalities while maintaining the environmentally friendly characteristics of the packaging material [7]. In particular, biodegradable polymers can enhance compostability, recyclability, nontoxicity, and even biocompatibility of paper [8, 9]. Biodegradable polymers can be divided into four categories according to their origin: 1) Polymers directly extracted from biomass, including both polysaccharides (*e.g.* chitosan, starch, cellulose, etc.) and proteins (*e.g.* zein, whey protein, collagen, etc.); 2) Synthetic polymers based on petrochemical monomers such as poly(ϵ -caprolactone) (PCL), poly(butylene adipate-*co*-terephthalate) (PBAT), and polyvinyl alcohol (PVOH); 3) Synthetic polymers based on renewable monomers, for instance polylactide (PLA); 4) Natural polymers produced by microorganisms, typically polyhydroxyalkanoates (PHAs) such as poly(3-hydroxybutyrate) (PHB) and poly(3-hydroxybutyrate-*co*-3-valerate) (PHBV) [10, 11]. Among them, PLA is undoubtedly considered the front runner in the emerging bioplastics market since its basic building block, lactic acid, can be easily obtained from the fermentation of starch sources. In addition, PLA shows excellent processability, well-

balanced mechanical properties, and high transparency [12, 13]. More recently, PHAs, including PHB and its copolymers, are also receiving a great deal of attention in terms of production and characterization due to their excellent sustainable profile [14]. This is related to the fact that PHB-based materials are easily compostable, that is these can be enzymatically degraded in controlled compost soil, and fully bio-based, which allows achieving the so-called closed-loop sustainable model [15]. Additionally, in contrast to most biopolymers, because of its high crystallinity, PHB presents a relatively high gas and water vapor barrier so that it can replace polyolefins for a large number of food packaging applications [16-18].

The main objective for paper coatings based on bioplastics is currently to perform, in terms of both transparency and barrier properties, similarly as polyolefins and polyethylene terephthalate (PET) [19]. For this, the most challenging improvement of biopolyesters is related to reduce the water vapor and oxygen permeability [20]. While the study of both water vapor and oxygen barrier properties is of interest in food preservation, limonene transport properties are also important because this is usually used as a standard permeant to test aroma barrier. In this context, the barrier performance of biopolymers can be potentially enhanced through the application the electrohydrodynamic processing (EHDP) technology, including both electrospinning and electrospaying [21].

In particular, electrospun mats of biopolymer nanofibers can be applied as mono- and multilayers, layer-by-layer assemblies, and similar

structures in packaging materials [22]. Recent advances in this field have shown that multilayer systems containing electrospun ultrathin fibers, *i.e.* both submicron fibers and nanofibers, can significantly contribute to improve the barrier performance of biopolymers [23]. Additionally, more remarkably, the electrospinning technology provides novel routes to develop novel active and bioactive functionalities, for instance packaging materials with antimicrobial performance and control release capacity of health promoting functional ingredients [24].

In the first work, the oxygen barrier properties of PLA films made by wet casting were originally improved by electrospun ultrathin zein fibers laminated in a sandwich-type structure [25, 26]. Later on, interlayers of electrospun zein, pullulan, whey protein isolate (WPI) films were used to improve the barrier properties of compression-molded PHBV films [27, 28]. More recently, wheat gluten films were coated by post-processed electrospun PHB and PHBV fibers [29, 30]. Therefore, these previous research works have added a new insight into the potential of the so-called electrospinning coating technology to develop packaging structures of higher quality and safety, showing a high capacity to extend the shelf life of food products. In the case of the electrospun PHB films, interestingly, it was previously found that the storage time at dry conditions did not significantly modify the degree of crystallinity of the homopolyester [31]. In particular, the optical and barrier properties of PHB films stored for 3 months remained nearly constant.

This study describes, for the first time, the preparation of a fiber-based packaging material that is coated by films of different biopolymers, namely PHB, PVOH, and PLA, obtained by electrospinning. It further explores the influence of the electrospun coatings on the optical and barrier performance of the resultant paper-coated structures. To carry this out, different electrospun biopolymer mono- and multilayers were deposited on the paper substrate by means of two types of collectors, that is, a flat plate and a rotating drum, and the processing time during electrospinning was varied. Finally, the resultant multilayers were annealed in order to obtain transparent continuous electrospun films with improved adhesion to the paper substrate and enhanced barrier performance for their potential application in the field of fiber-based food packaging.

2. Experimental

2.1 Materials

Bacterial aliphatic homopolyester PHB was supplied by Biomer (Krailling Germany) as P226F. According to the manufacturer, this is certified both as compostable and food contact, presenting a density of 1.25 g/cm^3 and a melt flow rate (MFR) of 10 g/10 min at 180°C and 5 kg. Semi-crystalline PLA was Ingeo™ 2002D, which is an extrusion-grade resin produced by Natureworks (Minnesota, USA) with a D-isomer content of ~2%. This has a number-average molecular weight (M_N) of *ca.* 130000 g/mol and a weight-average molecular weight (M_W) of *ca.* 150000 g/mol. PVOH,

363065 grade, with M_w in the range of 146000-186000 g/mol and degree of hydrolysis of >99% was purchased from Sigma-Aldrich S.A. (Madrid, Spain). 2,2,2-trifluoroethanol (TFE) with 99% purity and D-limonene with 98% purity were obtained from Sigma-Aldrich S.A. too. N,N-dimethylformamide (DMF) and trichloromethane (TCM), both with 99% purity, were supplied by Panreac Quimica S.A. (Barcelona, Spain). All raw materials were used as received without further modification.

The fiber-based packaging substrate was prepared using commercial bleached Kraft eucalyptus pulp as raw material, which was kindly provided by Ence-Celulosas y Energía S.A. (Madrid, Spain). Briefly, the pulp was disintegrated in a pulp disintegrator for 1h at 3000 rpm to achieve a consistency of 1.5%. Paper sheets of 700 x 16 mm² with a final grammage of 75 g/m² were fabricated in an isotropic Rapid-Köthen sheet former and conditioned at 23°C and 50% of relative humidity (RH) according to ISO standard 187. The grammage and thickness were evaluated following ISO standards 536 and 534, respectively. Further details can be found in previous research [32].

2.2 Film Preparation

The biopolymers solutions for electrospinning were prepared by dissolving, under continuous stirring conditions, PHB and PLA in 2,2,2-trifluoroethanol and a trichloromethane/N,N-dimethylformamide mixture 85:15 (wt./wt.), respectively, at room temperature while PVOH

Chapter II

was dissolved in distilled water at 80°C. The weight content (wt.-%) of each biopolymer in the solutions is included in **Table I**.

Electrospinning was then performed using a Fluidnatek® LE10 lab line from Bioinicia S.L. (Valencia, Spain) with a variable high-voltage 0-30 kV power supply. This device was equipped with a motorized injector that was scanning horizontally towards a metallic collector, aiming to obtain a homogeneous electrospun deposition. The different biopolymer solutions were transferred to a 30-mL plastic syringe, which was coupled by means of a Teflon tube to a stainless-steel needle ($\varnothing=0.9$ mm) whereas the needle tip was connected to the power supply. The paper substrate was placed either on a flat plate collector or a rotating mandrel turning at 1000 rpm to achieve fiber orientation. The biopolymer solutions were electrospun in a controlled environmental chamber at room conditions, that is, 23°C and 40% RH, for a given processing time and in optimal conditions to achieve steady fiber formation. **Table I** also summarizes the parameters used during electrospinning.

Table I. Optimal electrospinning conditions for poly(3-hydroxybutyrate) (PHB), poly(vinyl alcohol) (PVOH), and polylactide (PLA).

Biopolymer	Solution content (wt.-%)	Voltage (kV)	Flow-rate (ml/h)	Tip-to-collector distance (cm)	Time (h)
PHB	10	15	6	15	1-4
PVOH	12	18	1		1
PLA	5	18	2		1

Finally, the obtained electrospun mats were subjected to annealing process using a hydraulic press 4122-model from Carver, Inc. (Indiana, USA). This was optimally performed at 160°C, without pressure, for 5 ± 1 s, based on a previous study [33]. The resultant films were air cooled at room temperature. **Figure 1** shows a scheme illustrating the prepared mono- and multilayer structures based on paper coated by different combinations of electrospun fibers and their annealed films. Prior to thermal treatment, the electrospun mats were equilibrated in desiccator at 25°C and 0% RH by using silica gel for at least 1 week.

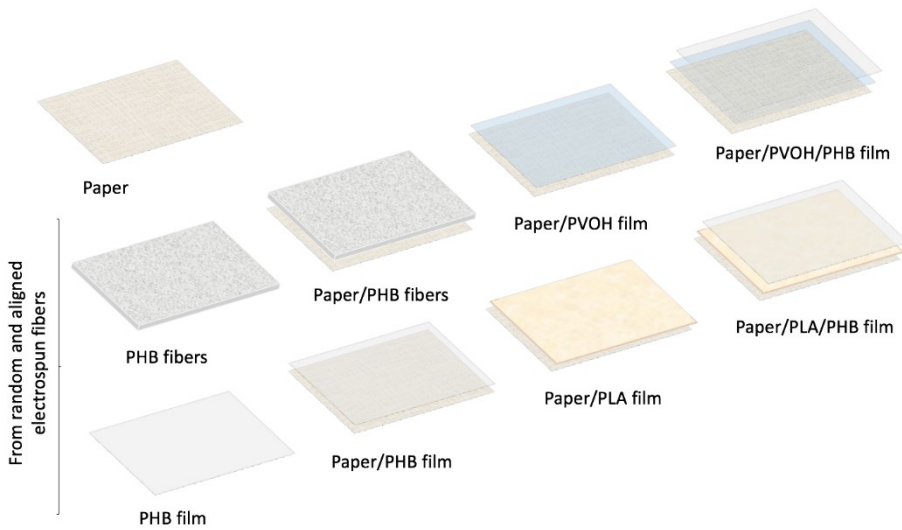


Figure 1. Scheme of the mono- and multilayer structures based on paper and annealed electrospun fibers of poly(3-hydroxybutyrate) (PHB), poly(vinyl alcohol) (PVOH), and polylactide (PLA).

2.3 Film thickness and conditioning

Before the tests, the whole thickness of all structures was measured using a digital micrometer series S00014, having ± 0.001 mm accuracy, from Mitutoyo Corporation (Kawasaki, Japan). Measurements were performed at three random positions and values were averaged. Films were stored in a desiccator at 25°C and 0% RH for 15 days before characterization.

2.4 Scanning electron microscopy

The morphology of the electrospun fibers and the fracture surfaces of the annealed films was observed by scanning electron microscopy (SEM) using an S-4800 from Hitachi (Tokyo, Japan). Cryo-fractures of the films

were obtained from the frozen samples using liquid nitrogen. Prior to examination, all samples were fixed to beveled holders using a conductive double-sided adhesive tape, sputtered with a mixture of gold-palladium under vacuum, and observed using an accelerating voltage of 5 kV. Fiber sizes and layer thicknesses were determined by means of the Aperture software from Apple (California, USA) using the SEM micrographs in their original magnification. At least 25 micrographs were used for the measurements.

2.5 Optical properties

Film transparency was evaluated through the surface reflectance spectra using a spectrophotometer CM-3600d from Minolta Co. (Tokyo, Japan). Film transparency was evaluated through the internal transmittance (T_i) in a 0–1 theoretical range by applying the Kubelka–Munk theory [34] for multiple scattering to the reflection, following **Equation 1**:

$$T_i = \sqrt{(a - R_0)^2 - b^2} \quad (1)$$

$$a = \frac{1}{2} \left(R + \frac{R_0 - R + R_g}{R_0 R_g} \right) \quad (2)$$

$$b = \sqrt{(a^2 - 1)} \quad (3)$$

where R_0 is the reflectance of the film on an ideal black background while a and b parameters are calculated from the reflectance of the sample (R) and the layer backed by a known reflectance (R_g) according to **Equations**

2 and 3, respectively. Measurements were taken, in triplicate, for each sample by using both a white and black background.

2.6 Water vapor permeability

The water vapor permeability (WVP) was determined using the ASTM 2011 gravimetric method. To this end, 5 mL of distilled water was placed inside a Payne permeability cup ($\varnothing=3.5$ cm) from Elcometer Sprl (Hermalle-sous-Argenteau, Belgium). The films were placed in the cups so that on one side they were exposed to 100% RH, avoiding direct contact with water. The cups containing the films were then secured with silicon rings and stored in a desiccator at 25°C and 0% RH. Identical cups with aluminum films were used as control samples to estimate water loss through the sealing. The cups were weighed periodically using an analytical balance of ± 0.0001 g accuracy. Water vapor permeation rate (WVRT), also called water permeance when corrected for permeant partial pressure, was determined from the steady-state permeation slope obtained from the regression analysis of weight loss data per unit area *vs.* time, in which the weight loss was calculated as the total cell loss minus the loss through the sealing. Permeability was obtained by correcting the permeance by the average film thicknesses. Measurements were performed in triplicate. In the case of multilayers, the coated layer was facing the permeant.

2.7 Limonene vapor permeability

Permeability to limonene vapor was measured as described above for WVP. For this, 5 mL of D-limonene was placed inside the Payne permeability cups. The cups containing the films were placed at controlled conditions, *i.e.* 25°C and 40% RH. Cups with aluminum films were used as control samples to estimate solvent loss through the sealing. Limonene permeation rates were obtained from the steady-state permeation slopes and weight loss was calculated as the total cell loss minus the loss through the sealing. Limonene permeability was calculated taking into account the average film thickness in each case. Three replicates per sample were measured. In the case of multilayers, the coated layer was facing the permeant.

2.8 Oxygen permeability

The oxygen permeability coefficient was derived from the oxygen transmission rate (OTR) measurements recorded, in duplicate, using an Oxygen Permeation Analyzer M8001 from Systech Illinois (Thame, UK) at 25°C and 60% RH. The samples were previously purged with nitrogen in the humidity equilibrated samples and then exposed to an oxygen flow of 10 mL/min. The exposure area during the test was 5 cm². In order to obtain the oxygen permeability, film thickness and gas partial pressure were considered.

3. Results and Discussion

3.1 Morphology

Tables II and **III** summarize the thicknesses of the here-obtained mono- and multilayer structures obtained from the random and aligned electrospun fibers of biopolymers, respectively. As it can be seen in **Figure 1**, these were based on different combinations of electrospun biopolymer fibers and their resultant annealed films, which were applied as coatings on paper. The tables include information about the mean thickness of each layer and of the whole structure.

The cross-sections of the fiber-based packaging structures are shown in the SEM images included in **Figures 2** to **4**. In particular, **Figure 2** shows the SEM images of the monolayer structures based on paper and electrospun PHB fibers and their annealed films. In **Figure 2 (a)** it can be observed that the neat paper was based on micro-sized fibers with a rough surface. These cellulosic fibers presented a mean diameter of $17 \pm 2 \mu\text{m}$, which clearly contribute to the high level of porosity of paper. In contrast, as shown in **Figure 2 (b)**, the electrospun PHB fibers collected on the plate were based on an ultrathin fiber morphology with a mean diameter of $220 \pm 20 \text{ nm}$. As expected, these nanofibers mostly presented a random orientation due to the use of a static flat collector. Alternatively, **Figure 2 (c)** shows the morphology of the electrospun PHB fibers mat for which the mandrel collector was employed. In this image, it can be clearly seen that the PHB nanofibers, with a mean diameter of $215 \pm 15 \text{ nm}$, were effectively aligned in the turning direction of the drum. Therefore, no

significant differences can be observed between the average fiber diameter in the randomly oriented electrospun fibers and in the aligned fibers, which is in agreement with a recent research work [35]. In any case, this confirms that through the use of a mandrel collector is possible to control locally the alignment pattern of the deposited fibers during electrospinning. A similar morphological effect has been previously reported [36-38]. However, visual comparison of both SEM micrographs, that is, random **Figure 2 (b)** and aligned **Figure 2 (c)** PHB nanofibers mats, suggests that the electrospun mat density increased for the same deposition time as a result of the fiber orientation process. As it can be seen in **Tables II** and **III**, while the layer thickness of the random PHB nanofibers was 258 μm , the thickness of the equivalent electrospun mat made of oriented nanofibers was 114 μm . In **Figure 2 (d)** it can be seen that the annealing process applied to the random PHB random nanofibers resulted in a film with a more continuous structure due to coalescence of nanofibers at the interphase [33]. The annealed film obtained from the aligned PHB fibers, shown in **Figure 2 (e)**, presented a similar cross-section. Additionally, it is also worthy to note that fiber orientation also had a similar effect on the annealed films thicknesses. In particular, film thickness was reduced from 38 μm , for the PHB film obtained from the random nanofibers **Figure 2 (d)**, to 26 μm , from the aligned nanofibers **Figure 2 (e)**.

Table II. Layer thickness of the mono- and multilayer structures based on paper, poly(3-hydroxybutyrate) (PHB), poly(vinyl alcohol) (PVOH), and polylactide (PLA).

Structure	Layer thickness (μm)				
	Paper	PVOH	PHB	PLA	Total
Paper	125 \pm 5				125 \pm 5
PHB fibers			258 \pm 7		258 \pm 7
PHB film			38 \pm 3		38 \pm 3
Paper/PHB fibers	125 \pm 5		269 \pm 7		394 \pm 6
Paper/PHB film	125 \pm 5		37 \pm 3		162 \pm 4
Paper/PVOH film	125 \pm 5	10 \pm 2			135 \pm 3
Paper/PLA film	125 \pm 5			7 \pm 2	132 \pm 3
Paper/PVOH/PHB film	125 \pm 5	48 \pm 3			173 \pm 4
Paper/PLA/PHB film	125 \pm 5		45 \pm 3		170 \pm 5

Annealed films were obtained from electrospun fibers collected on the plate.

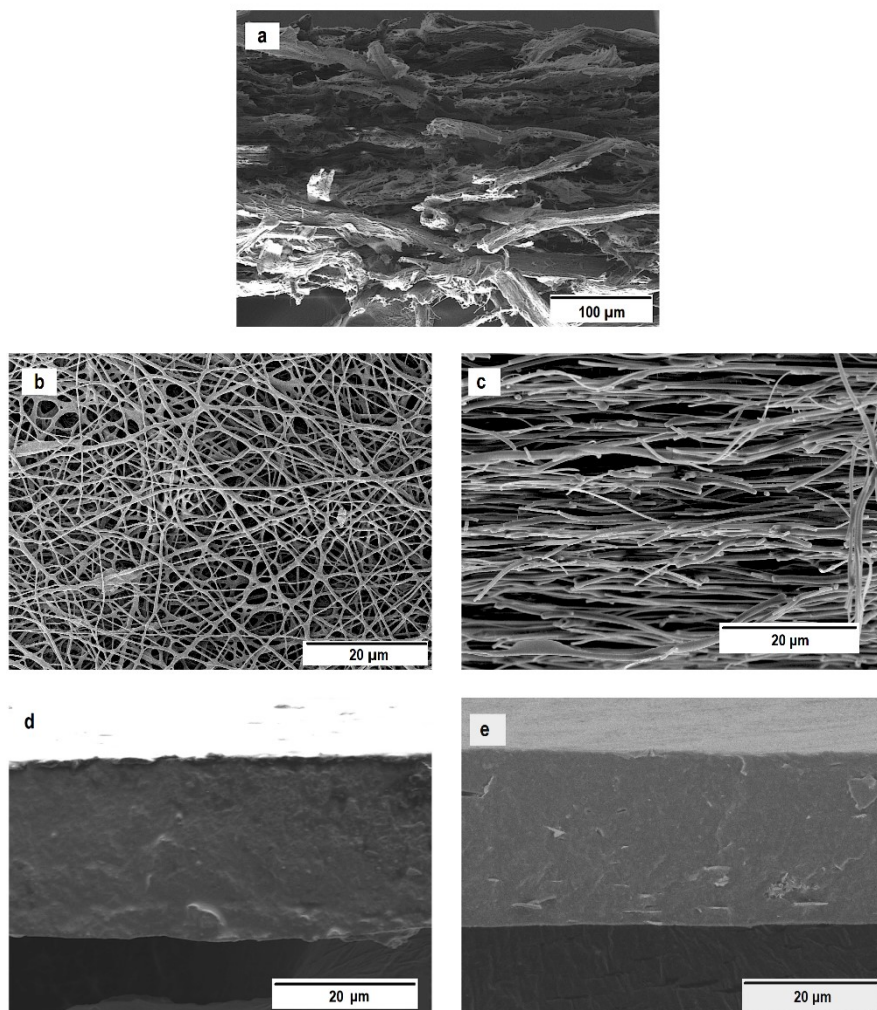


Figure 2. Scanning electron microscopy (SEM) images of monolayer structures of: a) paper; b) electrospun poly(3-hydroxybutyrate) (PHB) fibers collected on the plate; c) electrospun PHB fibers collected on the mandrel; d) annealed PHB film obtained from electrospun fibers collected on the plate; e) annealed PHB film obtained from electrospun fibers collected on the mandrel.

Figure 3 gathers the morphology of the multilayer structures obtained from the electrospun nanofibers using the plate-type collector. As it can be seen from **Table II**, for all these structures, the thickness of the paper layer was kept at 125 μm . **Figure 3 (a)** particularly shows the bilayer structure based on electrospun PHB nanofibers applied as a coating on the paper. This electrospun mat presented a mean thickness of 269 μm . Even though both layers were based on a fibrillar structure, the SEM micrograph clearly revealed that these presented morphologies with contrasting porosities. It can be also observed the large gap between the two layers, which resulted after cryo-fracture procedure, indicates that the electrospun mat may not be strongly adhered to the paper layer. **Figures 3 (b-d)** show the bilayer structures made of paper coated with annealed films of PHB, PVOH, and PLA. In these films one can observe that the PHB layer thickness **Figure 3 (b)** was considerably thicker than those of both PVOH **Figure 3 (c)** and PLA **Figure 3 (d)**, that is, 37 μm versus 10 and 7 μm , respectively. This can be directly related to the deposition time during the electrospinning process that was significantly lower for PVOH and PLA, which was 1h in both cases, than for PHB, that is, 2h. **Figure 3 (e,f)** shows the multilayer structures of paper/PVOH/PHB film and paper/PLA/PHB film, respectively. Both structures, based on three layers, presented a similar thickness than the bilayer structure of paper/PHB film, that is, around 160-180 μm . Interestingly, all biopolymer layers based on the annealed films presented good adhesion to the paper layer as expected from our previous works [6,27]. This observation

proved that, regardless of the chemistry of the contacting materials, the electrospun fibers coated very efficiently the paper substrate surface during annealing due to their large surface-to-volume ratio, resulting in a strong physical adhesion.

Table III. Layer thickness of the mono- and multilayer structures based on paper, poly(3-hydroxybutyrate) (PHB), poly(vinyl alcohol) (PVOH), and polylactide (PLA).

Structure	Layer thickness (μm)				
	Paper	PVOH	PHB	PLA	Total
Paper	125 \pm 5				125 \pm 5
PHB fibers			114 \pm 4		114 \pm 4
PHB film			26 \pm 3		26 \pm 3
Paper/PHB fibers	125 \pm 5		114 \pm 4		239 \pm 6
Paper/PHB film	125 \pm 5		26 \pm 3		151 \pm 5
Paper/PVOH film	125 \pm 5	6 \pm 2			131 \pm 4
Paper/PLA film	125 \pm 5			5 \pm 2	130 \pm 3
Paper/PVOH/PHB film	125 \pm 5	32 \pm 2			157 \pm 2
Paper/PLA/PHB film	125 \pm 5		31 \pm 3		156 \pm 2

Annealed films were obtained from electrospun fibers collected on the mandrel.

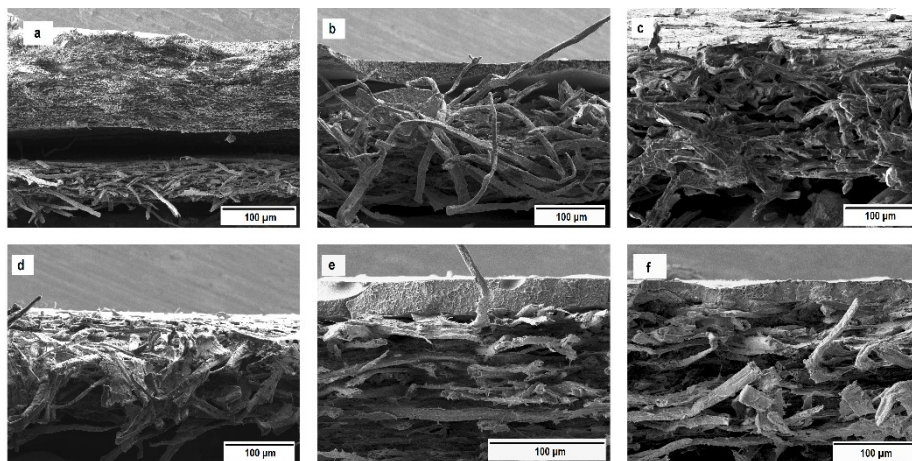


Figure 3. Scanning electron microscopy (SEM) images of multilayer structures of: a) paper/poly(3-hydroxybutyrate) (PHB) fibers; b) paper/PHB film; c) paper/polyvinyl alcohol (PVOH) film; d) paper/polylactide (PLA) film; e) paper/PHB/PVOH film; f) paper/PHB/PLA film. The electrospun fibers were collected on the plate.

Similar morphologies can be observed in **Figure 4** for the multilayer structures obtained from the aligned electrospun mats. However, interestingly, the electrospun mat of oriented PHB nanofibers appeared to be more adhered to the paper layer, as shown in **Figure 4 (a)**. In this sense, the rotating movement of the mandrel could favor the physical adhesion of both layers. In addition, all annealed multilayer films based on aligned electrospun fibers presented lower values of thickness than those films based on equivalent random fibers, which can be seen in **Table III**. This is related to the above-described higher density of the aligned electrospun fibers mats.

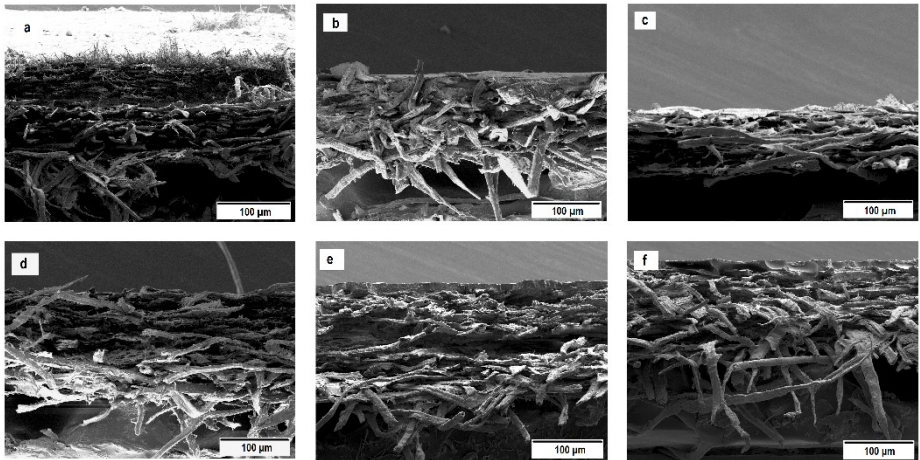


Figure 4. Scanning electron microscopy (SEM) images of multilayer structures of: a) paper/poly(3-hydroxybutyrate) (PHB) fibers; b) paper/PHB film; c) paper/polyvinyl alcohol (PVOH) film; d) paper/polylactide (PLA) film; e) paper/PHB/PVOH film; f) paper/PHB/PLA film. The electrospun fibers were collected on the mandrel.

3.2 Optical Appearance and Transparency Properties

Figure 5 shows the visual aspect of the mono- and multilayer structures. Simple naked eye examination of this figure indicates that the annealed films obtained from the electrospun PHB nanofibers produced highly transparent materials. Another general observation is that, as paper was opaque, the resulting multilayers were also opaque materials but with a glossier surface finish. Transparency was seen somewhat lower for the PHB film obtained from the oriented electrospun fibers. In particular,

these PHB films showed somewhat higher heterogeneity across the surface.

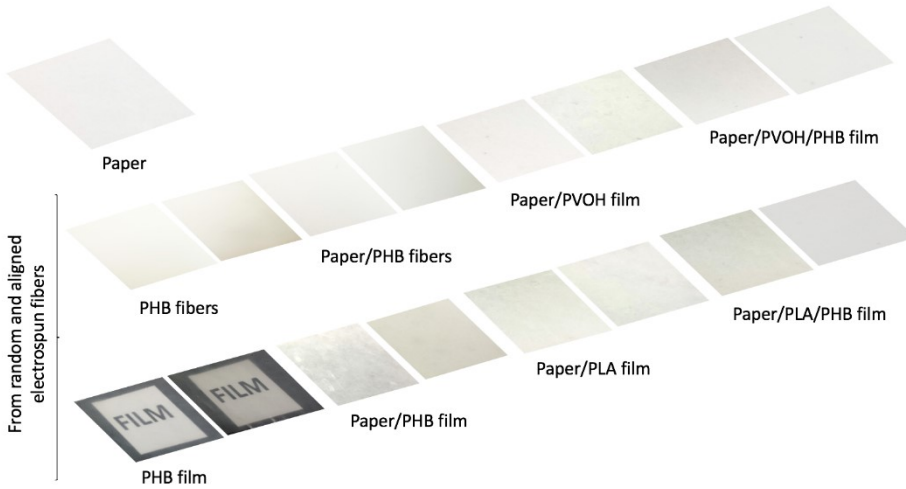


Figure 5. Contact transparency of the mono- and multilayer structures based on paper and electrospun fibers and annealed films of poly(3-hydroxybutyrate) (PHB), and poly(vinyl alcohol) (PVOH) and polylactide (PLA).

The opacity of the mono- and multilayer structures was measured in terms of T_i , which is proportionally related to the sample transparency. Samples spectra of T_i for the mono- and multilayer structures are given in **Figure 6**. These graphs show that, in general, the structures obtained from the electrospun fibers collected on the plate **Figure 6 (a)** presented similar transmittance behavior than those based on fibers collected on the drum **Figure 6 (b)**. However, as previously shown in **Tables II** and **III**, it is worthy to mention that the annealed films obtained from the random

electrospun fibers presented higher thicknesses. In particular, both PHB mono-layer films showed in the 75-85% range of T_i , indicating that these films present a single and relatively homogeneous refractive index. However, values of T_i were slightly higher for the annealed PHB film obtained from the random electrospun fibers. As expected, the PHB fibers presented the lowest transparency with T_i values in the range of 5-10% due to the high inherent porosity of the electrospun mat. In general, all multilayer structures showed poor transparency as a result of the opaque nature of paper, being in the 10-25% range of T_i . From these results, it is inferred that the here-prepared biopolymer coatings do not alter the transparency properties of paper due to both the intrinsically high opacity of paper and the high transparency achieved in the annealed electrospun films during thermal treatment [21]. In any case, it is apparent that a lower surface roughness can be anticipated for the biopolymer-coated paper materials. A full characterization of these samples in terms of typical paper industry characterization standards it is currently underway and will be published elsewhere.

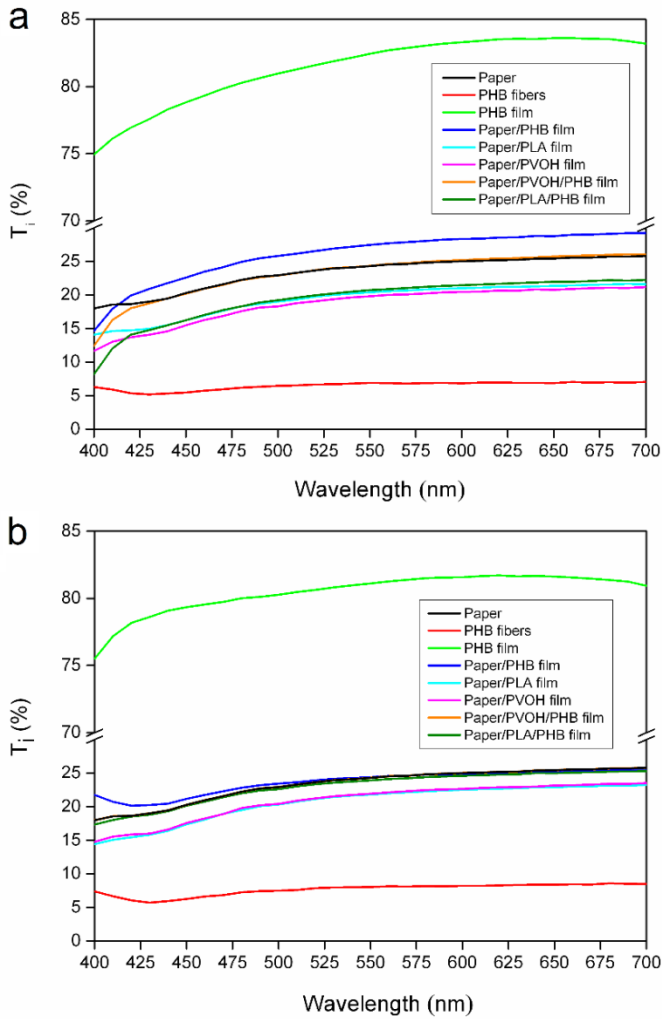


Figure 6. Spectral distribution of internal transmittance (T_i) at the range of 400-700 nm of the mono- and multilayer structures based on paper and annealed films of poly(3-hydroxybutyrate) (PHB), poly(vinyl alcohol) (PVOH) and polylactide (PLA) obtained from electrospun fibers collected on: a) plate; b) mandrel.

3.3 Barrier Properties

Initially, the effect of the nanofibers deposition time was related to the thickness of the PHB monolayer film, for a given flow-rate. As shown in **Figure 7**, higher processing times during electrospinning led to thicker electrospun mats that, in turn, resulted in annealed films with higher thickness. In particular, the increase of the electrospinning deposition time from 1h to 4h increased the PHB film thickness. This specifically increased from 29 μm to 50 μm and from 19 μm to 41 μm for the PHB films obtained from random and aligned electrospun fibers, respectively. Therefore, as expected, the resultant thicknesses of the PHB films can be successfully controlled by electrospinning deposition time. However, this did not follow a linear trend, suggesting that some nanofibers losses inside the electrospinning chamber occurred with deposition time.

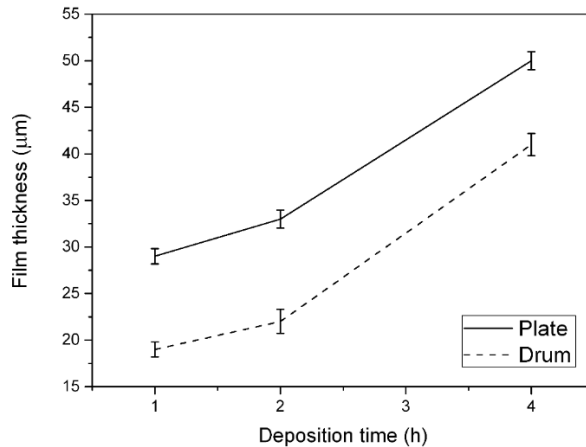


Figure 7. Resulting thickness values of films made from annealed electrospun poly(3-hydroxybutyrate) (PHB) fibers as a function of the electrospinning deposition time.

The barrier properties of the monolayer PHB films in relation to water and limonene vapors and also oxygen permeability are shown in **Figure 8**. Permeability is formally independent of samples thickness, however in practice, film thickness has usually an impact in permeability specially for very thin films or heterogeneous materials [39]. McHugh *et al.* also found relationships between film thickness and permeability properties for sodium caseinate films [40]. It was observed that, as film thickness increased, the film provided an increased resistance to mass transfer across it. Since the present materials were annealing-induced coalesced fiber mats, one can expect variations in permeability across thickness, especially for the smallest non-condensable permeants. As **Figure 8** shows, the permeability values were significantly affected by variances in the PHB film thickness. In particular, it can be observed that PHB films exhibited negative slope relationships between thickness and gas permeability. A lower permeability was seen for the films based on electrospun fibers collected on the static plate, which showed a tendency to *plateau* in thickness dependency beyond 30 μm for water but specially for limonene. It seems that, although alignment of the fibers in a rotating mandrel should in principle be expected to reduce porosity since the fibers are more efficiently packed, it probably also created some more heterogeneous materials in the current experiments. This is mostly likely

because the trapped remnant solvent cannot so easily evaporate from the strongly aligned fibers hence creating some more surface heterogeneities (see previous **Figure 5**).

In relation to WVP, which is shown in **Figure 8 (a)**, the annealed films obtained from the aligned electrospun PHB fibers presented higher WVP values than those obtained from the random fibers. Thus, as water sorption in the biopolymer is relatively low, that is, PHB is highly hydrophobic, WVP is known to be mainly diffusivity driven [41]. Therefore, it can be considered that heterogeneities within the PHB films do have, as expected, a strong effect on permeability. Interestingly, Sanchez-Garcia *et al.* reported in an earlier work carried out in our laboratory that compression-molded PHB films in the range of 100-700 μm presented a WVP value of $1.70 \times 10^{-15} \text{ kg m/s m}^2 \text{ Pa}$, which is just slightly lower than the one here obtained for 48 μm , that is, $2.05 \times 10^{-15} \text{ kg m/s m}^2 \text{ Pa}$ [42]. Interestingly, the WVP value of the present PHB films is in the same order of magnitude as PET films, that is, $2.30 \times 10^{-15} \text{ kg m/s m}^2 \text{ Pa}$, and approximately 10-12 times lower than commercial films made of polyamide 6 (PA6), that is, $2.06 \times 10^{-14} \text{ kg m/s m}^2 \text{ Pa}$, and ethylene-vinyl alcohol copolymer with 32-mol% ethylene, that is, $1.70 \times 10^{-14} \text{ kg m/s m}^2 \text{ Pa}$ [43].

Regarding limonene permeability, the type of deposition was less relevant, as it can be seen in **Figure 8 (b)**. Since limonene is a strong plasticizing component for the biopolymer, solubility plays a stronger

role in permeability than diffusion. For example, it has been previously reported that limonene uptake in PHBV films of around 100 μm prepared by solvent casting was 12.7 wt.-%, leading to a limonene permeability value of $1.99 \times 10^{-13} \text{ kg m/s m}^2 \text{ Pa}$ [44]. In another study, Fabra *et al.* recently reported the limonene permeability of PHB and PET films of approximately 75 μm prepared by compression-molding, showing values of $6.38 \times 10^{-15} \text{ kg m/s m}^2 \text{ Pa}$ and $6.43 \times 10^{-15} \text{ kg m/s m}^2 \text{ Pa}$, respectively [27]. These permeability values are higher than the here-obtained annealed PHB films above 35 μm , which presented a *plateau* at $3.89 \times 10^{-15} \text{ kg m/s m}^2 \text{ Pa}$. However, it is worthy to mention that the previously studied films were also plasticized with 5 wt.-% of polyethylene glycol.

A similar behavior to that observed above for WVP, but much more intense, was found for oxygen permeability. Since oxygen is a non-condensable small permeant, the degree of porosity and sample heterogeneities will serve as preferential passage ways, particularly for very small permeants. **Figure 8 (c)** shows that only thicker coatings, *that is*, beyond 80 μm , exhibited relatively low values of oxygen permeability. In particular, the oxygen permeability showed a value of $1.20 \times 10^{-18} \text{ m}^3 \text{ m/m}^2 \text{ s Pa}$ for a PHB film thickness of 142 μm . This is closer to the values typically reported for conventional 100- μm PHB films prepared by compression molding, that is, $2.24 \times 10^{-19} \text{ m}^3 \text{ m/m}^2 \text{ s Pa}$ [42]. In addition, to put these results into a more practical context for food packaging applications, these values are slightly higher than the oxygen permeability for PET films, that is, $1.35 \times 10^{-19} \text{ m}^3 \text{ m/m}^2 \text{ s Pa}$, but

considerably lower than those values for polyolefins such as polypropylene, that is, $6.75 \times 10^{-18} \text{ m}^3 \text{ m/m}^2 \text{ s Pa}$, and low-density polyethylene films, that is, $2.15 \times 10^{-17} \text{ m}^3 \text{ m/m}^2 \text{ s Pa}$ [43].

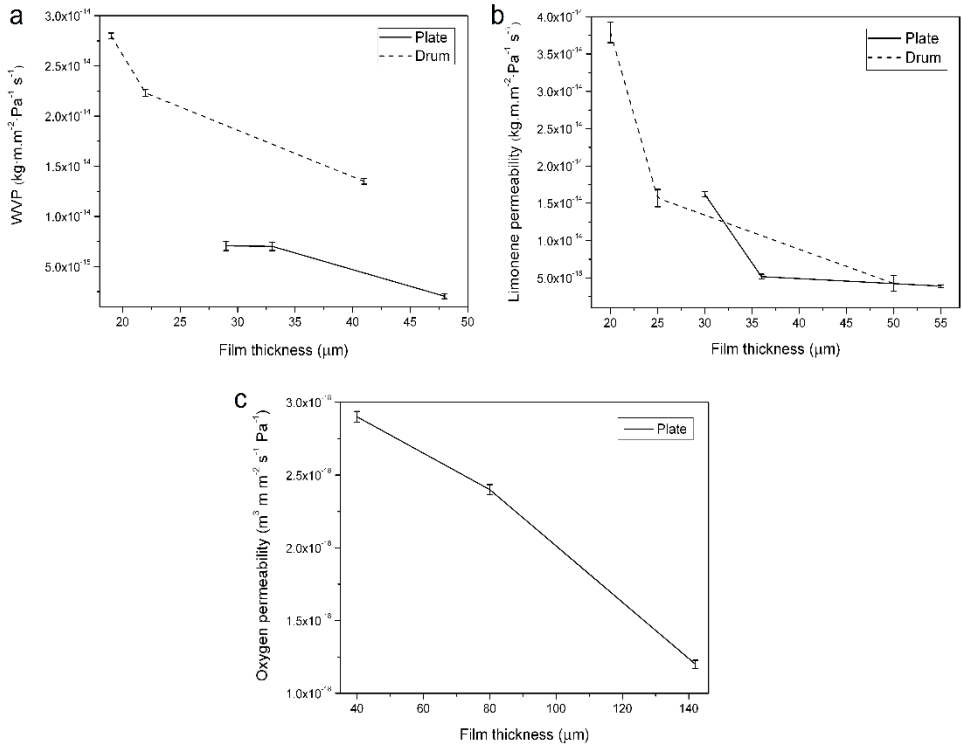


Figure 8. Effect of film thickness of annealed electrospun poly(3-hydroxybutyrate) (PHB) fibers on: a) water vapor permeability (WVP); b) limonene permeability; c) oxygen permeability.

Finally, **Figure 9** shows the values of permeance, since we deal with multicomponent materials, of water and limonene for the here-obtained mono- and multilayer structures. In both graphs, it can be observed that

the neat uncoated paper clearly showed the highest values of permeance. This confirms the inherent low barrier performance of uncoated paper for food packaging applications. Since to gain oxygen barrier, thicker and double side coatings were needed, we focused this preliminary study on achieving barrier to limonene and water vapor. Still oxygen permeability tests were attempted by measuring at 60% RH on the paper coated side and 0% RH on the paper uncoated side, but the multilayers yielded very high permeability values for the coating thicknesses used (results not shown).

Regarding water barrier, **Figure 9 (a)** indicates that all multi-layer structures showed significantly lower values of water vapor permeance than the uncoated paper. The lowest permeance values were observed for the multilayer films containing PHB. In particular, the multilayer structures of paper/PLA/PHB film and, more significantly, of paper/PVOH/PHB film presented the highest barrier performance. Regarding limonene, **Figure 9 (b)** shows that a significant decrease in aroma barrier can be also observed for the mono- and multilayer structures based on PHB films. The PHB films obtained from the electrospun fibers collected on the plate presented higher limonene barrier performance than the equivalent films based on aligned fibers. As previously described, this is based on the higher thickness achieved for the films obtained from random electrospun fibers and also to the more heterogeneity observed in the aligned ones. Surprisingly, PLA did not yield barrier performance to the aroma vapor, perhaps due to insufficient

coating thickness. Even more surprisingly, PVOH coatings, which are known to present high barrier to organic vapors when dry, also did not result in enhanced aroma barrier most likely because of insufficient sample thickness and plasticization by moisture during the test. On the other hand, the multilayer structures made of paper/PLA/PHB film but especially the paper/PVOH/PHB film showed the highest aroma barrier performance. Interestingly, a synergy between the PVOH and PHB coatings were, therefore, obtained for both permeants.

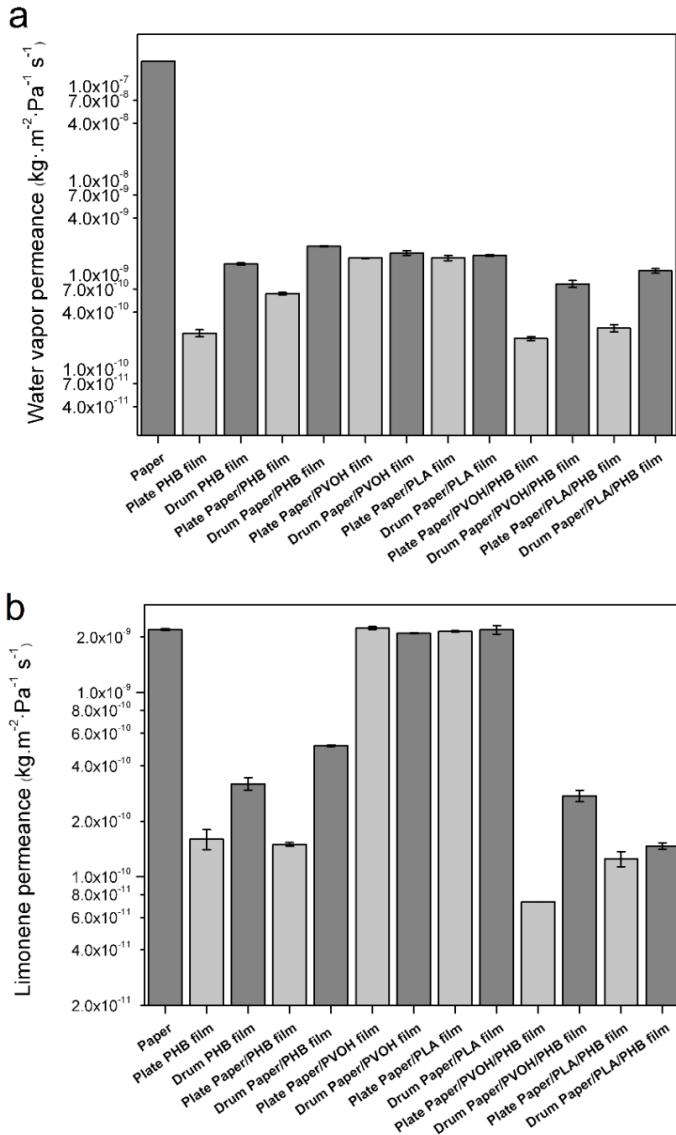


Figure 9. Permeance of the mono- and multilayer structures based on paper and electrospun fibers and annealed films of poly(3-hydroxybutyrate) (PHB), polylactide (PLA), and poly(vinyl) alcohol (PVOH) to: a) water vapor; b) limonene. The electrospun fibers were collected on the plate and mandrel.

4. Conclusions

Thermally post-processed electrospun biopolymer coatings over fiber-based packaging materials are very promising systems since they self-adhere during annealing as a result of the high surface-to-volume ratio of the fibers and do, furthermore, provide enhanced barrier to gases and vapors when built with sufficient thickness. It was observed that the minimal thickness of PHB coating required for high barrier to moisture and aroma was 30 μm while for oxygen it was 80 μm . These multilayer systems are also likely to provide potential environmental advantages over traditional paper coatings based on non-biodegradable petroleum-based materials.

5. Acknowledgments

The authors would like to thank the Spanish Ministry of Economy and Competitiveness (MINECO) project AGL2015-63855-C2-1-R for financial support. A. Cherpinski also wants to thank the Brazilian Council for Scientific and Technological Development (CNPq) of the Brazilian Government for her predoctoral grant (205955/2014-2).

6. References

1. Raheem, D. "Application of Plastics and Paper as Food Packaging Materials—an Overview." *Emirates Journal of Food and Agriculture* 25, no. 3 (2012): 177–88.
2. Hubbe, Martin A., and Cindy Bowden. *Handmade Paper: A Review of Its History, Craft, and Science*. Vol. 4, 2009, 2009.

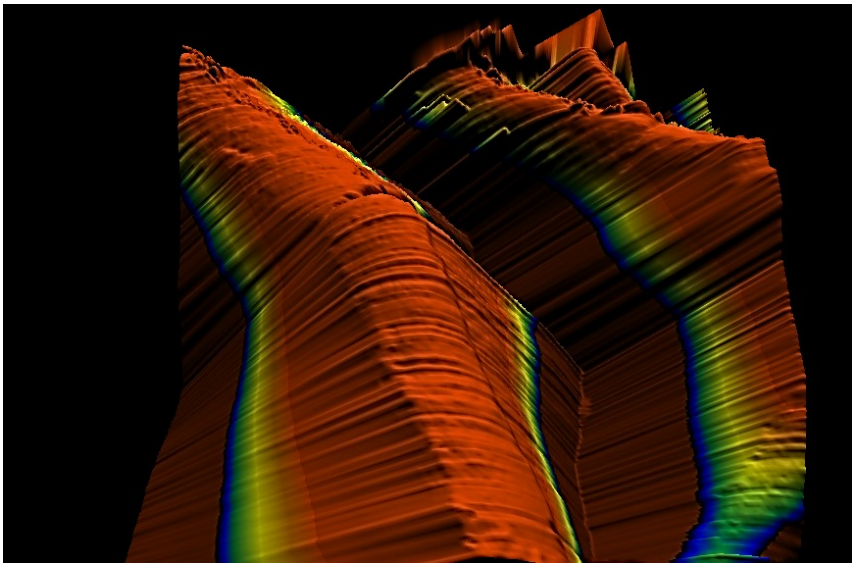
3. Barhoum, Ahmed, Hubert Rahier, Ragab Esmail Abou-Zaied, Mohamed Rehan, Thierry Dufour, Gavin Hill, and Alain Dufresne. "Effect of Cationic and Anionic Surfactants on the Application of Calcium Carbonate Nanoparticles in Paper Coating." *ACS Applied Materials & Interfaces* 6, no. 4 (2014): 2734-44.
4. Bandyopadhyay, A., B. V. Ramarao, and Shri Ramaswamy. "Transient Moisture Diffusion through Paperboard Materials." *Colloids and Surfaces A: Physicochemical and Engineering Aspects* 206, no. 1–3 (2002): 455-67.
5. Rastogi, Vibhore, and Pieter Samyn. "Bio-Based Coatings for Paper Applications." *Coatings* 5, no. 4 (2015): 887.
6. Fabra, María José, María A. Busolo, Amparo Lopez-Rubio, and Jose M. Lagaron. "Nanostructured Biolayers in Food Packaging." *Trends in Food Science & Technology* 31, no. 1 (2013): 79-87.
7. Khwaldia, Khaoula, Elmira Arab-Tehrany, and Stephane Desobry. "Biopolymer Coatings on Paper Packaging Materials." *Comprehensive Reviews in Food Science and Food Safety* 9, no. 1 (2010): 82-91.
8. Lück, E, and GW Lipinski. "Foods, 3." Food additives. In: Bellussi G, Bohnet M, Bus J, Drauz K, Greim H, Jäckel KP, Karst U, Kleemann A, Kreysa G, Laird T, Meier W, Ottow E, Röper M, Scholtz J, Sundmacher K, Ulber R, Wietelmann U, editors. *Ullmann's Encyclopedia of Industrial Chemistry*. Weinheim: Wiley-VCH (2000): 671-73.
9. Tang, X. Z., P. Kumar, S. Alavi, and K. P. Sandeep. "Recent Advances in Biopolymers and Biopolymer-Based Nanocomposites for Food Packaging Materials." *Crit Rev Food Sci Nutr* 52, no. 5 (2012): 426-42.
10. Martínez-Sanz, Marta, Amparo Lopez-Rubio, and Jose M. Lagaron. "Nanocomposites of Ethylene Vinyl Alcohol Copolymer with Thermally Resistant Cellulose Nanowhiskers by Melt Compounding (Ii): Water Barrier and Mechanical Properties." *Journal of Applied Polymer Science* 128, no. 3 (2013): 2197-207.
11. Busolo, Maria A., Patricia Fernandez, Maria J. Ocio, and Jose M. Lagaron. "Novel Silver-Based Nanoclay as an Antimicrobial in

- Poly(lactic acid) Food Packaging Coatings." *Food Additives & Contaminants: Part A* 27, no. 11 (2010): 1617-26.
12. Auras, R., L. T. Lim, S. E. M. Selke, and H. Tsuji. *Poly(Lactic Acid): Synthesis, Structures, Properties, Processing, and Applications*, *Poly(Lactic Acid): Synthesis, Structures, Properties, Processing, and Applications*, 2010.
 13. Chen, Bor-Kuan, Chien-Chang Shih, and Antonia F. Chen. "Ductile PLA Nanocomposites with Improved Thermal Stability." *Composites Part A: Applied Science and Manufacturing* 43, no. 12 (2012): 2289-95.
 14. Torres-Giner, S., N. Montanes, T. Boronat, L. Quiles-Carrillo, and R. Balart. "Melt Grafting of Sepiolite Nanoclay onto Poly(3-Hydroxybutyrate-Co-4-Hydroxybutyrate) by Reactive Extrusion with Multi-Functional Epoxy-Based Styrene-Acrylic Oligomer." *European Polymer Journal* 84 (2016): 693-707.
 15. Torres-Giner, S., N. Montanes, V. Fombuena, T. Boronat, and L. Sanchez-Nacher. "Preparation and Characterization of Compression-Molded Green Composite Sheets Made of Poly(3-Hydroxybutyrate) Reinforced with Long Pita Fibers." *Advances in Polymer Technology* (2016).
 16. Cyras, V. P., Ma S. Commisso, A. N. Mauri, and A. Vázquez. "Biodegradable Double-Layer Films Based on Biological Resources: Polyhydroxybutyrate and Cellulose." *Journal of Applied Polymer Science* 106, no. 2 (2007): 749-56.
 17. Bucci, D. Z., L. B. B. Tavares, and I. Sell. "Phb Packaging for the Storage of Food Products." *Polymer Testing* 24, no. 5 (2005): 564-71.
 18. Modi, S., K. Koelling, and Y. Vodovotz. "Assessment of Phb with Varying Hydroxyvalerate Content for Potential Packaging Applications." *European Polymer Journal* 47, no. 2 (2011): 179-86.
 19. Lagarón Cabello, José María; Martínez Sanz, Marta; López Rubio, Amparo. "<Procedimiento De Obtencion De Una Pelicula Multicapa Con Alta Barrera.Pdf>." (2013).
 20. Fabra, M.J., P. Talens, and A. Chiralt. "Water Sorption Isotherms and Phase Transitions of Sodium Caseinate-Lipid Films as

- Affected by Lipid Interactions." *Food Hydrocolloids* 2010 v.24 no.4, no. no. 4 (2010): pp. 384-91.
21. Fabra, María José, Amparo Lopez-Rubio, and Jose M. Lagaron. "High Barrier Polyhydroxyalkanoate Food Packaging Film by Means Of nanostructured Electrospun Interlayers of Zein." *Food Hydrocolloids* 32, no. 1 (2013): 106-14.
 22. Torres-Giner, S. "Electrospun Nanofibers for Food Packaging Applications." In *Multifunctional and Nanoreinforced Polymers for Food Packaging*, 108-25, 2011.
 23. Echegoyen, Y., M. J. Fabra, J. L. Castro Mayorga, A. Cherpinski, and J. M. Lagaron. "High Throughput Electro-Hydrodynamic Processing in Food Encapsulation and Food Packaging Applications: Viewpoint." *Trends in food science & technology* 60 (2017): 71-79.
 24. Torres-Giner, S., R. Páez-Masiá, and J. M. Lagaron. "A Review on Electrospun Polymer Nanostructures as Advanced Bioactive Platforms." *Polymer Engineering and Science* 56, no. 5 (2016): 500-27.
 25. Busolo, Maria A, Sergio Torres-Giner, and Jose M Lagaron. "Enhancing the Gas Barrier Properties of Polylactic Acid by Means of Electrospun Ultrathin Zein Fibers." Paper presented at the ANTEC, proceedings of the 67th annual technical conference, Chicago, IL 2009.
 26. Torres-Giner, S., A. Martinez-Abad, and J. M. Lagaron. "Zein-Based Ultrathin Fibers Containing Ceramic Nanofillers Obtained by Electrospinning. Ii. Mechanical Properties, Gas Barrier, and Sustained Release Capacity of Biocide Thymol in Multilayer Polylactide Films." *Journal of Applied Polymer Science* 131, no. 18 (2014): 9270-76.
 27. Fabra, María José, Amparo Lopez-Rubio, and Jose M. Lagaron. "Nanostructured Interlayers of Zein to Improve the Barrier Properties of High Barrier Polyhydroxyalkanoates and Other Polyesters." *Journal of Food Engineering* 127 (2014): 1-9.
 28. Fabra, María José, Amparo López-Rubio, and Jose M. Lagaron. "On the Use of Different Hydrocolloids as Electrospun Adhesive Interlayers to Enhance the Barrier Properties of

- Polyhydroxyalkanoates of Interest in Fully Renewable Food Packaging Concepts." *Food Hydrocolloids* 39 (2014): 77-84.
29. Fabra, María José, Amparo Lopez-Rubio, and Jose M Lagaron. "Effect of the Film-Processing Conditions, Relative Humidity and Ageing on Wheat Gluten Films Coated with Electrospun Polyhydroxyalkanoate." *Food Hydrocolloids* 44 (2015): 292-99.
 30. Fabra, María José, Amparo López-Rubio, and Jose M. Lagaron. "Three-Layer Films Based on Wheat Gluten and Electrospun Pha." *Food and Bioprocess Technology* 8, no. 11 (2015): 2330-40.
 31. Fabra, María José, Gloria Sánchez, Amparo López-Rubio, and José M. Lagaron. "Microbiological and Ageing Performance of Polyhydroxyalkanoate-Based Multilayer Structures of Interest in Food Packaging." *LWT - Food Science and Technology* 59, no. 2 (2014): 760-67.
 32. Tarrés, Q., M. Delgado-Aguilar, M. A. Pèlach, I. González, S. Boufi, and P. Mutjé. "Remarkable Increase of Paper Strength by Combining Enzymatic Cellulose Nanofibers in Bulk and Tempo-Oxidized Nanofibers as Coating." *Cellulose* 23, no. 6 (2016): 3939-50.
 33. Cherpinski, A.; Fabra, M.J.; Cabedo, L.; Lagaron, J.M. "Post-Processing Opimization of Electrospun Fibers of Polyhydroxybutyrate to Obtain Continous Films of Interest in Biopackaging Applications." *Food Additives & Contaminants. Part A* (2017).
 34. Hutchings, John B. *Food and Colour Appearance*. 2nd edition ed. Gaithersburg, USA: Chapman and Hall Food Science Book, Aspen Publication, , 1999.
 35. Neves, Nuno M, Rui Campos, AJ Pedro, José Cunha, Francisco Macedo, and Rui L Reis. "Patterning of Polymer Nanofiber Meshes by Electrospinning for Biomedical Applications." *International journal of nanomedicine* 2, no. 3 (2007): 433-48.
 36. El-hadi, Ahmed, and Fatma Al-Jabri. "Influence of Electrospinning Parameters on Fiber Diameter and Mechanical Properties of Poly(3-Hydroxybutyrate) (Phb) and Polyanilines (Pani) Blends." *Polymers* 8, no. 3 (2016): 97.

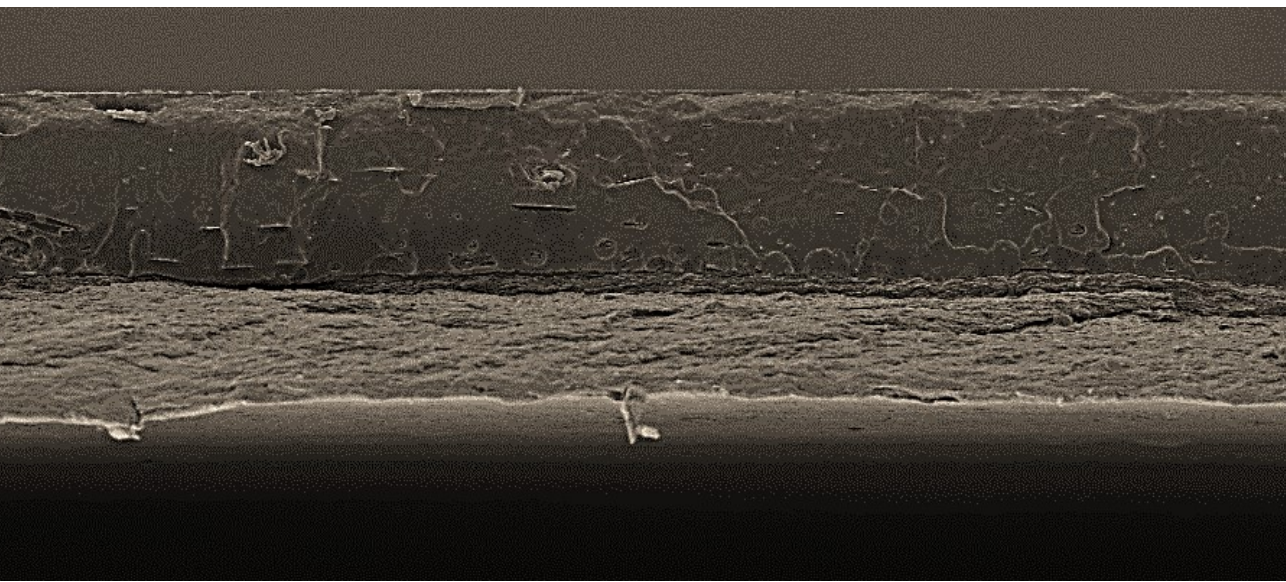
37. Torres-Giner, S., J. V. Gimeno-Alcañiz, M. J. Ocio, and J. M. Lagaron. "Optimization of Electrospun Polylactide-Based Ultrathin Fibers for Osteoconductive Bone Scaffolds." *Journal of Applied Polymer Science* 122, no. 2 (2011): 914-25.
38. Katta, P, M Alessandro, RD Ramsier, and GG Chase. "Continuous Electrospinning of Aligned Polymer Nanofibers onto a Wire Drum Collector." *Nano letters* 4, no. 11 (2004): 2215-18.
39. Patricia Miranda, S., Omar Garnica, Virginia Lara-Sagahon, and Galo Cárdenas. "Water Vapor Permeability and Mechanical Properties of Chitosan Composite Films." *Journal of the Chilean Chemical Society* 49 (2004): 173-78.
40. McHugh, T. Habig, R. Avena-Bustillos, and J. M. Krochta. "Hydrophilic Edible Films: Modified Procedure for Water Vapor Permeability and Explanation of Thickness Effects." *Journal of Food Science* 58, no. 4 (1993): 899-903.
41. Razumovskii, L. P., A. L. Iordanskii, G. E. Zaikov, E. D. Zagreba, and I. C. McNeill. "Sorption and Diffusion of Water and Organic Solvents in Poly(B-Hydroxybutyrate) Films." *Polymer Degradation and Stability* 44, no. 2 (1994): 171-75.
42. Sanchez-Garcia, M. D., E. Gimenez, and J. M. Lagaron. "Novel Pet Nanocomposites of Interest in Food Packaging Applications and Comparative Barrier Performance with Biopolyester Nanocomposites." *Journal of Plastic Film and Sheeting* 23, no. 2 (2007): 133-48.
43. Lagarón, J. M. "Multifunctional and Nanoreinforced Polymers for Food Packaging." In *Multifunctional and Nanoreinforced Polymers for Food Packaging*, 1-28, 2011.
44. Sanchez-Garcia, M. D., E. Gimenez, and J. M. Lagaron. "Morphology and Barrier Properties of Solvent Cast Composites of Thermoplastic Biopolymers and Purified Cellulose Fibers." *Carbohydrate Polymers* 71, no. 2 (2008): 235-44.



Chapter III

Improving the Water Resistance of Nanocellulose-Based Films with Polyhydroxyalkanoates Processed by the Electrospinning Coating Technique

Cherpinski, A., Torres-Giner, S., Vartiainen, J., Peresin, M. S., Lahtinen, P., & Lagaron, J. M. (2018). Improving the water resistance of nanocellulose-based films with polyhydroxyalkanoates processed by the electrospinning coating technique. *Cellulose*, 25(2), 1291-1307.



Abstract

Polyhydroxyalkanoates (PHAs) comprise a family of biodegradable aliphatic polyesters with enhanced sustainable profile and high water vapor barrier. As environmentally friendly materials, nanostructured cellulose-based films, also called nanopapers, such as films made of cellulose nanofibrils (CNFs) and lignocellulose nanofibrils (LCNFs), are also of growing interest due to their high mechanical strength and outstanding oxygen barrier properties at dry conditions. Unfortunately, nanopapers are highly hydrophilic, lacking of sufficient moisture resistance for uses in, for instance, food packaging. The present study reports, for the first time, on the effect of electrospun poly(3-hydroxybutyrate) (PHB) and poly(3-hydroxybutyrate-co-3-hydroxyvalerate) (PHBV) double side coatings on the morphology, mechanical properties, and barrier performance of CNF and LCNF films. The resultant multilayer structures showed significantly improved water contact resistance, more balanced mechanical properties, and higher barrier performance against water vapor in comparison to the neat nanopapers. Although the PHA-coated nanopapers presented slightly lower aroma barrier due to the intrinsic affinity of PHA for limonene uptake, these sustainable multilayer films further improved the oxygen performance of the nanopapers, showing significant potential as barrier materials even at high humidity conditions. As a result, the here-developed novel films, based on nanopapers double side coated with electrospun PHB and PHBV layers, appear as a very promising fully bio-based material concept for food packaging applications due to their outstanding water vapor and oxygen barrier performance.

Keywords: PHB; PHBV; nanopaper; nanocellulose; electrospinning; barrier packaging

1. Introduction

There is a remarkable trend in the packaging industry toward more sustainable packaging materials that are biodegradable, not interfering with the end-of-life or recovery schemes and helping to avoid plastic waste accumulation [1]. Simultaneously, there is a considerable interest in bio-based polymers, which can serve to develop sustainable polymer technologies from renewable resources [2, 3]. In this new bio-based scenario, owing to its own unique properties, nanocellulose can certainly play an important role as a novel sustainable material in future packaging applications [4]. Nanocelluloses naturally exist in plant cell walls and are mainly isolated from various wooden and non-wooden sources by different chemical and mechanical treatments [5]. Depending on the processing procedure, there exist two families of nanocelluloses, namely cellulose nanofibrils (CNFs), also called microfibrillated cellulose, and cellulose nanocrystals (CNCs), the so-called cellulose nanowhiskers [6]. CNFs are typically generated by mechanical grinding or high-pressure fluidization of vegetable fibers that are obtained from a large number of different natural sources such as banana, sugar beet, hemp, softwood, hardwood pulps, etc. [7]. The principle consists on the breakdown of the cell wall structure by the application of high shearing forces. Habitually, nanofibrils width is ~20 nm while length may exceed several microns, typically 5 μm , depending on the production methodology [8].

Although most recent studies apply different delignification methods to prepare lignin-free (bleached) fibers for CNFs production, unbleached

fibers containing residual lignin, hemicelluloses, and extractives represent an alternative raw material to produce lignocellulose nanofibrils (LCNFs). While the removal of non-cellulosic polymers such as lignin and hemicelluloses from pulps for nanocellulose production has been the procedure of choice, several research groups have focused on the benefits of using unbleached raw materials for CNF production [9-12]. These particularly present the benefits of high yield, reduced production costs, lower environmental impact, along with improvement in the barrier properties in the case of films [12]. In particular, lignin can be used to adjust the polarity and hydrophilicity of cellulose, which for some applications are challenges that certainly need to be addressed [10]. Therefore, depending on the process used in fiber production, LCNFs can be more hydrophobic than CNFs, allowing better dispersion in non-polar media. Additionally, residual lignin has proven to enhance the thermomechanical properties of CNFs, particularly in high-moisture environments [13].

In low concentrations, that is, <2% in weight (wt.-%), both CNFs and LCNFs lead to the formation of a gel-like transparent continuous material due to the inherent strength of the cellulose crystals combined with the interactions between the nanofibrils, which can be used for producing homogenous and dense films. These are habitually referred as “nanopapers” [14]. Nanopapers can be obtained when the water is removed from the gel that is, dewatering by several methods and through the use of a dynamic sheet former. For instance, CNF films produced by

vacuum filtration showed thicknesses in the range 60–80 μm [15]. Other CNF films were prepared using a solvent exchange process, which displayed various porosities and thicknesses, ranging from 70 to 90 μm [14]. Other nanopapers were also prepared by spraying [16] or by classical casting-evaporation technique from aqueous dispersions [12, 17]. However, the film formation using these approaches may take from several hours to days depending on the technique and kind of nanocellulose used. Recently, a new methodology has been developed that originally enables manufacturing of a wood-based plastic-like material at a large scale [18]. According to this, nanopapers can be manufactured by evenly coating fibril cellulose on surface-activated plastic films so that the spreading and adhesion on the plastic surface can be efficiently controlled.

As well as being completely renewable, biodegradable, and safe to use, the growing interest for nanopapers is due to its exceptional physical and chemical properties such as high-specific strength, enhanced hydrophilicity, and broad capacity for chemical modifications [19, 20]. In addition, these cellulose-based nanostructures also show excellent oxygen barrier properties at dry conditions [21]. However, nanopapers are highly hydrophilic due to the presence of a large number of hydroxyl groups ($-\text{OH}$) on the cellulose surface. Therefore, the strength and barrier properties of both CNF- and LCNF-based films are highly dependent on the environmental humidity conditions [22]. In particular, at high relative humidity (RH), these tend to swell as a result of moisture sorption [23,

24]. Unfortunately, most practical packaging applications demand that the film withstands high humidity conditions. In addition to this, once dried, nanopapers are not easy to handle, which can also limit their applications.

A few attempts have been made in an effort to study and enhance the barrier properties of nanopapers at elevated humidity conditions. For instance, Spence *et al.* [12] found that the lignin present in the LCNF increases the water vapor transmission rate (WVTR) through the film, which was ascribed to an increase of porosity. Similarly, acetylation of cellulose nanofibrils prior to film formation enhanced the barrier properties only at very low degrees of substitution while had a deteriorating effect at higher levels of substitution [25]. Multilayer systems have been additionally tested in previous works, in which the outer layers consist on cost-effective and water-barrier polymers with stronger mechanical properties such as polyolefins and/or polyethylene terephthalate (PET) [26, 27]. However, one of the most important problems facing these multilayer films is that these plastic materials are habitually based on polymers derived from petroleum, which are not biodegradable. This certainly limits the intrinsic sustainability of nanopapers.

Polyhydroxyalkanoates (PHAs) are considered the most promising bio-based and biodegradable polymers to replace polyolefins in the packaging industry. PHAs are aliphatic, semi-crystalline, thermoplastic

biopolyesters. These biopolymers are efficiently biosynthesized within bacteria that produce and store them as energy-reserve inclusions in the cytoplasm when exposed to excess carbon sources, typically under specific nutrient-deficient conditions [28]. Poly(3-hydroxybutyrate) (PHB) is the most commonly synthesized PHA, which is highly crystalline and relatively comparable in certain physical properties to isotactic polypropylene (iPP) and polystyrene (PS) [29]. However, the application of this homopolymer in packaging and other industrial sectors is currently limited due to its high cost, narrow thermal processing window, low impact strength, and excessive brittleness [30]. In this sense, the use of green composites [31] has been shown to improve the mechanical strength and processability of PHB while its copolymers such as poly(3-hydroxybutyrate)-*co*-poly(3-hydroxyvalerate) (PHBV) [32] and, more recently, poly(3-hydroxybutyrate)-*co*-4-hydroxybutyrate) P(3HB-*co*-4HB) [31] can decrease its inherent stiffness and increase both impact strength and ductility. In addition, the processing window is also broadened with increasing the comonomer content [33].

An innovative route based on the incorporation of electrospun coatings and intermediate layers by electrohydrodynamic processing (EHDP) has been recently developed in our research group, in which different layers of biopolymers can be properly assembled [34]. The formation of ultrathin fibers by EHDP, generally referred to as electrospinning, is achieved by subjecting the biopolymer solution to high electric fields. Thus, the resultant electrospun nanostructures can be applied for a wide range of

applications, including food packaging [35, 36]. In particular, this technology has been successfully applied to develop mono- and multilayers, layer-by-layer assemblies, and similar structures [37, 38]. Interestingly, recent works have shown that multilayer systems based on electrospun coatings of PHAs can significantly contribute to improve the barrier performance of the same or other biopolymers and even of fiber-based packaging [39, 40], which can certainly open the door to its advantageous application to nanopapers as well. Therefore, the current work originally explores the use of the electrospinning coating technique by PHA layers to improve the water resistance of nanopapers.

2. Materials and methods

2.1. Materials

A plasticized homopolyester PHB was supplied by Biomer (Krailing Germany) as P226F. This is certified by the manufacturer both as compostable and food contact, presenting a density of 1.25 g/cm³ and a melt flow rate (MFR) of 10 g/10 min at 180°C and 5 kg. A non-additivated copolyester PHBV was obtained from Tianan Biological Materials Company (Zhejiang, China) under the trade name ENMAT™ Y1000P. According to the manufacturer, this contains 2–3 mol.-% hydroxyvalerate (HV) and presents a density of 1.25 g/cm³. Both bacterial aliphatic polyesters were supplied in a pelletized form.

D-sorbitol with 99% purity, 2,2,2-trifluoroethanol (TFE) with 99% purity, and D-limonene with 98% purity were all purchased from Sigma-Aldrich

(Madrid, Spain). Diaf dissolver 100WH was provided by Pilvad Diaf A/S (Fredensborg, Denmark). All products were used as received without further purification.

Native once-dried bleached birch Kraft pulp was provided by a local industrial pulp mill. Industrial liner paper made of 100% virgin softwood fibers obtained from *Pinus elliottii* and *Pinus taeda* was supplied by Papel Misionero S.A. (Puerto Mineral, Argentina). Lignin content of bleached pulp was <1 wt.-%, according to the manufacturer. For the softwood fibers, lignin content was 12–13 wt.-% as determined according to the National Renewable Energy Laboratory (NREL)/TP 510-42618, following the analytical procedure described in [41].

2.2. Production of nanocellulose films

Preparation of both CNF and LCNF suspensions consisted of two main steps: Mechanical pre-treatment and high-shear disintegration *via* microfluidization. First step was performed on a MKZA10-15J Supermasscolloider friction grinder from Masuko Sangyo Co., Ltd (Kawaguchi, Japan). Second step was carried out using a Microfluidics M-7115-30 Microfluidizer® from Microfluidics Corp. (Newton, MA, USA). In the case of CNF, the bleached cellulosic fibers were first soaked at 1.7% consistency in water and the resultant slurry was dispersed using a high-shear Diaf dissolver 100 WH for 10 min at 700 rpm. The suspension was pre-refined in the friction grinder at 1500 rpm with a gap width of 0.15–0.17 mm. The obtained suspension was then microfluidized in which the

first pass was through chambers having a diameter of 500 μm and 200 μm while the next six passes were through chambers of 500 μm and 100 μm . The operating pressure was 1800 bar. The fiber slurry became a viscous gel after the homogenization treatment with a final solid content of 1.6 wt.-% [18]. For LCNF, the unbleached cellulosic fibers were mechanically processed, three times, using the friction grinder. This was followed by disintegration, performing 20 passes, by means of the microfluidizer. The resulting LCNF suspension had a consistency of 1.6%. It was sonicated and then centrifuged at 8800 rpm for 2 h. Colloidal nanofibrils were then collected from supernatant.

Both nanopapers, *that is*, CNF and LCNF films, were produced using their respective above-prepared suspension according to the patented SutCo-concept [42]. For this, each dispersion, including 30 wt.-% of sorbitol, was first carefully pre-homogenized by mixing with Diaf dissolver for 30 min and 300 rpm, and then processed in a SpeedMixer™ DAC 110.1 VAC-P from Hauschild & Co KG (Hamm, Germany) for 2 min at 1500 rpm under vacuum to prevent formation of air bubbles. Resultant dispersions were thereafter cast onto a plastic substrate using a specific feeding head to form an even and uniform wet layers. Spreading and adhesion between the substrate and the aqueous cellulosic dispersions were carefully controlled by physical plasma-activation. A Corona-Plus type TF-415 (CP1C MKII 2.0 kW) from Vetaphone A/S (Kolding, Denmark) equipped with argon/nitrogen plasma-unit was used for increasing the surface energy of the plastic substrate. After drying overnight at ambient

conditions, the CNF and LCNF films, both presenting a thickness of approximately 30 μm , were finally delaminated from the support and cut into A4-sized sheets.

2.3. Electrospinning

The PHB and PHBV solutions were prepared by dissolving 10 wt.-% of each biopolymer in TFE under magnetic stirring conditions at room temperature. The electrospinning device used was a Fluidnatek® LE10 benchtop equipment from Bioinicia S.L. (Valencia, Spain) with a variable high-voltage 0–30 kV power supply and a motorized scanning injector. To obtain the electrospun PHA mats, each biopolymer solution was transferred to a 30-mL plastic syringe and coupled by a Teflon tube to a stainless-steel needle ($\varnothing = 0.9$ mm) that was connected to the power supply. The nanopapers were then placed on a flat metallic collector and each PHA solution was electrospun on their surface at room temperature, *that is*, 25°C, for 2 hours under a steady flow-rate of 6 mL/h, scanning horizontally toward the collector. A distance between the injector and collector was optimal at 15 cm and the applied voltage was 16 kV. Neat electrospun PHA mats were also produced in the same conditions.

The resultant neat electrospun PHA mats and coated nanopapers were subjected to annealing process at 160°C, below the biopolymer melting point, using a hydraulic press 4122-model from Carver, Inc. (Wabash, IN, USA). The post-processing thermal treatment was applied for 5 s, without pressure, and the resultant films were air cooled at room temperature.

These conditions were selected based on previous research [36]. **Table 1** summarizes the here-prepared mono- and multilayer films.

Table 1. Film samples description.

Sample	Description
CNF	Monolayer film made of cellulose nanofibrils (CNFs)
LCNF	Monolayer film made of lignocellulose nanofibrils (LCNFs)
PHB	Monolayer film made of annealed electrospun poly(3-hydroxybutyrate) (PHB)
PHBV	Monolayer film made of annealed electrospun poly(3-hydroxybutyrate-co-3-hydroxyvalerate) (PHBV)
PHB/CNF/PHB	Multilayer film made of CNF double side coated by PHB
PHB/LCNF/PHB	Multilayer film made of LCNF double side coated by PHB
PHBV/CNF/PHBV	Multilayer film made of CNF double side coated by PHBV
PHBV/LCNF/PHBV	Multilayer film made of LCNF double side coated by PHBV

2.4. Film thickness and conditioning

Prior to characterization, the whole thickness of all films was measured using a digital micrometer series S00014, from Mitutoyo Corporation (Kawasaki, Japan), having ± 0.001 mm accuracy. Measurements were performed at three random positions and values were averaged. All samples were equilibrated, before evaluation, in a desiccator at 0% RH containing dried silica gel at a constant temperature of 25°C for 1 week.

2.5. Electron microscopy

The morphologies of the NFC and LCNF films were determined by transmission electron microscopy (TEM). This was performed using a JEOL 1010 from JEOL USA, Inc. (Peabody, MA, USA) equipped with a digital image acquisition system from Bioscan (Edmonds, WA, USA). The fracture surfaces of the mono- and multilayer structures were observed by scanning electron microscopy (SEM) using an S-4800 from Hitachi (Tokyo, Japan). Cryofractures of the films were obtained from the frozen samples using liquid nitrogen. Prior to examination, all samples were fixed to beveled holders using a conductive double-sided adhesive tape, sputtered with a mixture of gold-palladium under vacuum, and observed using an accelerating voltage of 5 kV. Fibril sizes and layer thicknesses were determined by means of the Aperture software from Apple (Cupertino, CA, USA) using the SEM and TEM micrographs in their original magnification. At least 25 micrographs of each sample were used for the measurements.

2.6. Atomic force microscopy

For the characterization of the film topographies, atomic force microscopy (AFM) imaging in air was applied. A NanoScope® MultiMode™ scanning probe microscope V6.13 R1 from Digital Instruments Inc. (Santa Barbara, CA, USA) was used. Silicon cantilevers with aluminum coating (HQ:NSC15/Al BS) from MikroMasch Europe (Tallinn, Estonia) and with nominal resonance frequencies of 265–410 kHz were used for imaging in

tapping mode under ambient conditions. At least three sample areas of $5 \times 5 \mu\text{m}^2$ for each sample were scanned. The values of average roughness (R_a) and root mean square roughness (R_q) were calculated from the parallel surface AFM images. Images were not processed by any other means except flattening.

2.7. Contact angle measurements

The contact angle of water on the films was determined by the sessile drop method employing a fully computer-controlled contact angle meter from KSV Instruments Ltd. (Helsinki, Finland) equipped with CAM 200 video camera. For each measurement, a drop volume of $\sim 4.5 \mu\text{L}$ was placed on the surface of the film sample and images were recorded every second for 1 min. Tests were performed at 23°C and 50% RH using pure water. The contact angle of each sample was measured at 3–5 different positions by triplicate.

2.8. Tensile tests

Mechanical properties were determined on the film samples using a LS5 Series Universal Testing Machine from Lloyd Instruments Ltd (Bognor Regis, England). Tensile tests were performed according to the modified SCAN P 38:80 Paper and board - Determination of tensile properties - standard using uniform film strips with dimensions of $50 \times 5 \text{ mm}^2$. The grip distance was 20 mm, the cell load was 100 N, and the cross-head speed was 2 mm/min. The samples were conditioned in a controlled

atmosphere at 23°C and 50% RH for at least two days prior to testing. A minimum of least six samples of each material were tested.

2.9. Water vapor permeance

For multilayer systems permeance is the most appropriate mass transport parameter to assess barrier performance. The water vapor permeance was determined using the ASTM 2011 gravimetric method. To this end, 5 mL of distilled water was placed inside a Payne permeability cup ($\varnothing=3.5$ cm) from Elcometer Sprl (Hermalle-sous-Argenteau, Belgium). The films were placed in the cups so that on one side they were exposed to 100% RH, avoiding direct contact with water. The cups containing the films were then secured with silicon rings and stored in a desiccator at 0% RH using dried silica gel at 25°C. Identical cups with aluminum films were used as control samples to estimate water loss through the sealing. The cups were weighed periodically using an analytical balance of ± 0.0001 g accuracy. WVRT, also called water vapor permeance when corrected for permeant partial pressure, was determined from the steady-state permeation slope obtained from the regression analysis of weight loss data per unit area *vs.* time, in which the weight loss was calculated as the total cell loss minus the loss through the sealing. Measurements were performed in triplicate.

2.10. Limonene vapor permeance

Permeance to limonene vapor was measured as described above for water vapor permeance. For this, 5 mL of D-limonene were placed inside the Payne permeability cups and the cups containing the films were placed at

controlled conditions of 25°C and 40% RH. Cups with aluminum films were used as control samples to estimate solvent loss through the sealing. Limonene permeation rates (LPRs) were obtained from the steady-state permeation slopes and weight loss was calculated as the total cell loss minus the loss through the sealing. Three replicates per sample were taken into account.

2.11. Oxygen permeance

The oxygen permeance was derived from the oxygen transmission rate (OTR) measurements, which were recorded, in duplicate, using an Oxygen Permeation Analyzer M8001 from Systech Illinois (Thame, UK) at 60% RH and 25°C. The samples were previously purged with nitrogen in the humidity equilibrated samples and then exposed to an oxygen flow of 10 mL/min. The exposure area during the test was 5 cm². In order to obtain the oxygen permeance, OTR was corrected with the gas partial pressure.

2.12. Statistical Analysis

The contact angle and tensile test data were evaluated through analysis of variance (ANOVA) using Statgraphics Plus for Windows 5.1 from Manugistics Corporation (Rockville, MD, USA). Fisher's least significant difference (LSD) was used at the 95% confidence level ($p < 0.05$). Mean values and standard deviations were also calculated.

3. Results and discussion

3.1. Morphology

The detailed morphology of the nanopapers and the sizes of the cellulosic fibrils are shown in the TEM images of **Figure 1**. Fibrils with an average diameter of approximately 20 nm were observed in **Figure 1a** for the fully bleached CNF film. TEM image of the LCNF film, included in **Figure 1b**, shows that the mean diameter of the lignin-containing fibrils was reduced to ~12 nm. This reduction in fibril diameter is related to lignin's ability to promote fibrillation, which stabilizes cellulosic mechano-radicals formed during the microfluidization [11]. It is also worthy to mention that, in addition to the fibrils, some globular-shaped nanoparticles were also observed in the LCNF film. These nanoparticles were predominantly located between the nanofibrils, forming complex composite nanostructures, which have been ascribed to lignin [10]. This is consistent with the role of lignin in the native wood cell wall, where it exists as a stiff phase between cellulosic fibers.

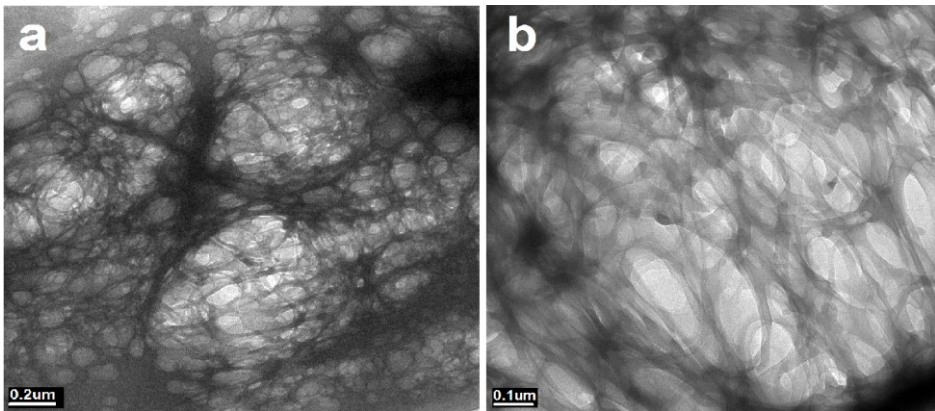


Figure 1. Transmission electron microscopy (TEM) images of: a) Cellulose nanofibril (CNF) film; b) Lignocellulose nanofibril (LCNF) film. Scale markers of 0.2 and 0.1 μm .

Figure 2 presents the SEM images of both nanopapers, i.e. the CNF and LCNF films, the PHB and PHBV monolayers, and the multilayer structures. In **Table 2**, the thickness of each layer and of the whole structure, obtained from the SEM images, is included. As it can be observed in the SEM cross-section images of the CNF (**Figure 2a**) and LCNF (**Figure 2b**) films, both materials formed layered structures made of nanofibrils. It is also worthy to mention that the laminar structure seems to be more consistent in the LCNF film, which can be related to the presence of lignin. In this sense, lignin is known to act as “cementing material” between the nanofibrils, reducing their interlayer distance [9]. It was previously observed that nanopapers with high lignin contents were primarily organized with their principal axis in the plane of the film

to yield an improved layered structure [10]. In this sense, [9] also reported that the layer spacing was less in nanopapers containing more residual lignin.

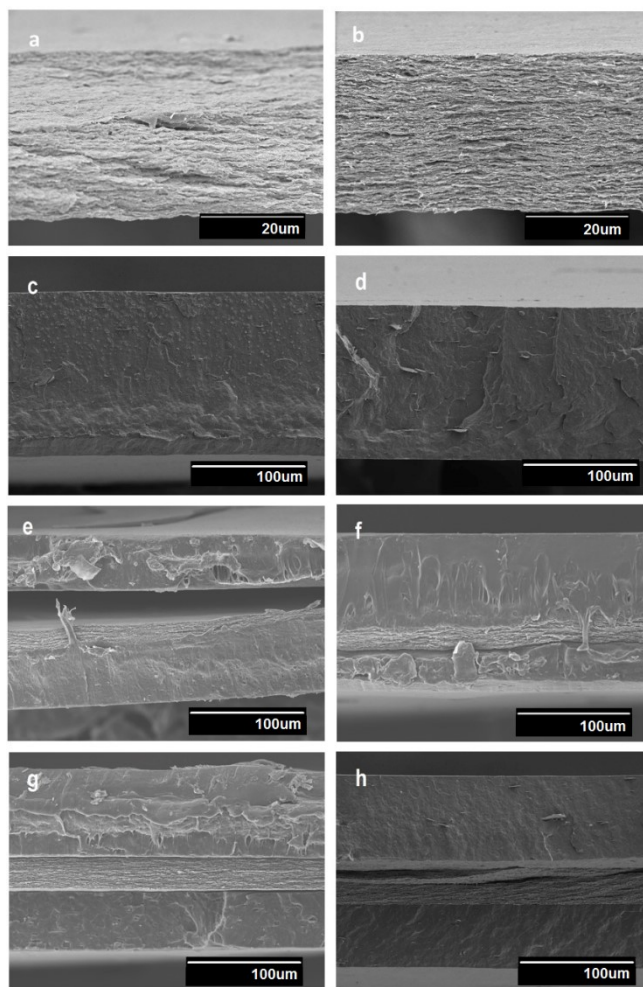


Figure 2. Scanning electron microscopy (SEM) images of: a) Cellulose nanofibril (CNF) film; b) Lignocellulose nanofibril (LCNF) film; c) Annealed electrospun poly(3-hydroxybutyrate) (PHB) film; d) Annealed

electrospun poly(3-hydroxybutyrate-*co*-3-hydroxyvalerate) (PHBV) film; e) PHB/CNF/PHB multilayer film; f) PHB/LCNF/PHB multilayer film; g) PHBV/CNF/PHBV multilayer film; h) PHBV/LCNF/PHBV multilayer film. Scale markers of 20 μm and 100 μm .

Table 2. Layers thickness of the mono- and multilayer films based on layers of cellulose nanofibrils (CNFs), lignocellulose nanofibrils (LCNFs), and electrospun poly(3-hydroxybutyrate) (PHB) and poly(3-hydroxybutyrate-*co*-3-hydroxyvalerate) (PHBV).

Sample	Layer thickness (μm)				
	CNF	LCNF	PHB	PHBV	Total
CNF	29.2 \pm 3.0	-	-	-	29.2 \pm 3.0
LCNF	-	30.1 \pm 3.0	-	-	30.1 \pm 3.0
PHB	-	-	108 \pm 3.0	-	108 \pm 3.0
PHBV	-	-	-	98.2 \pm 4.0	98.2 \pm 4.0
PHB/CNF/PHB	29.2 \pm 2.0	-	45.4/46.1 \pm 3.0	-	120.7 \pm 3.0
PHB/LCNF/PHB	-	30.1 \pm 3.0	46.4/45.2 \pm 4.0	-	121.7 \pm 4.0
PHBV/CNF/PHBV	29.2 \pm 3.0	-	-	55.1/53.9 \pm 4.0	138.2 \pm 4.0
PHBV/LCNF/PHBV	-	30.1 \pm 3.0	-	56.5/54.9 \pm 4.0	141.5 \pm 5.0

The cross-sections of the mono- and multilayer structures based on annealed electrospun PHA films are shown in the SEM images displayed in **Figures 1c-h**. Regarding the neat annealed electrospun films of PHB and PHBV, shown in **Figure 1c** and **1d**, respectively, one can observe that both materials present a similar continuous structure. This is known to take place as a result of nanofibers coalescence at the fiber interphase [36]. In the case of the multilayer structures, both CNF and LCNF films can be discerned as the inner layers, showing a thickness of approximately 30 μm and being coated by two external layers of PHA of 50–55 μm . The SEM image of the PHB/CNF/PHB film, included in **Figure 1e**, shows that some of the samples can undergo delamination during sample preparation for microscopy observation. In general, the samples showed strong interlayer adhesion, even after the cryofracture process, in agreement with previous studies carried out in the group with other biopolymer matrices [36]. It is relevant to point out that a significant interlayer adhesion is attained by the high surface-to-volume ratio of the ultrathin fibers, which promotes strong physical adhesion, especially after the annealing post-processing [36]. For the multilayer films based on LCNF, interlayer adhesion may be even enhanced provided by a potential binding effect of lignin during the hot-pressing treatment. This can be related to the fact that the softening temperature for softwood lignin is $\sim 135^\circ\text{C}$ [43], which is below the temperature applied to post-process the here-described multilayer films. At this processing temperature, lignin is able to fill the voids between the cellulosic nanofibrils and potentially also

at the interphase with the electrospun ultrathin biopolymer fibers, according to the previous model proposed by [10].

The surface topography and roughness of the films were evaluated by AFM. **Figure 3** shows the representative tridimensional (3D) plane views and **Table 3** includes the R_a and R_q values. The AFM images of the CNF and LCNF films, respectively included in **Figure 3a** and **3b**, revealed that both materials present a similar in-plane structural characteristics. In general, both nanopapers showed a relatively rough surface, though the LCNF film was smoother as indicated by its lower R_a and R_q values. This change in roughness can be related to both the diameter of the fibrils and the degree of consolidation on the surface upon drying, as discussed above by TEM and SEM, respectively. A previous study focused on nanopapers with different lignin content indicated that nanopapers with higher residual lignin content presented smaller widths and then formed smoother surfaces [10]. In addition, the binding effect provided by lignin to the nanofibrils also contributed to reduce roughness of the LCNF film surface.

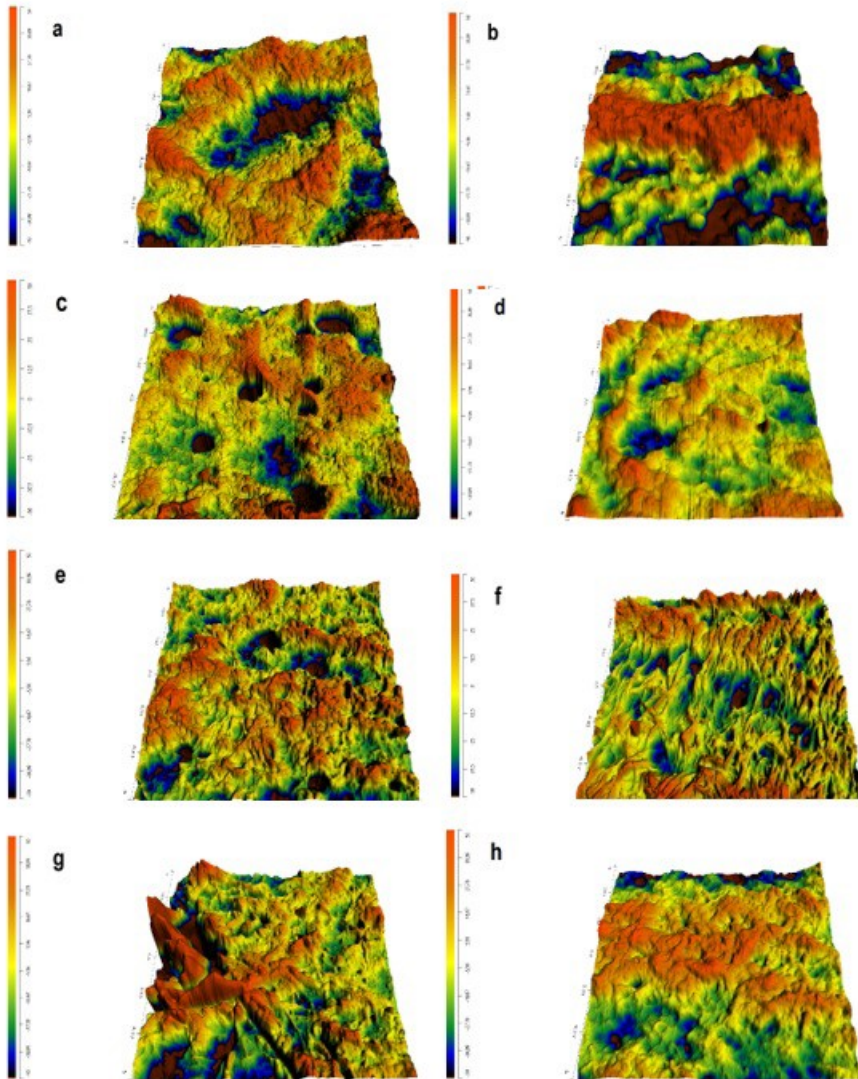


Figure 3. Atomic force microscopy (AFM) images taken on 4- μm^2 areas of: a) Cellulose nanofibril (CNF) film; b) Lignocellulose nanofibril (LCNF) film; c) Electrospun poly(3-hydroxybutyrate) (PHB) film; d) Electrospun

poly(3-hydroxybutyrate-*co*-3-hydroxyvalerate) (PHBV) film; e) PHB/CNF/PHB film; f) PHB/LCNF/PHB film; g) PHBV/CNF/PHBV film; h) PHBV/LCNF/PHBV film. The sample height is presented in the left column.

Table 3. Mean average roughness (R_a) and root mean square roughness (R_q) obtained from the atomic force microscopy (AFM) images of the mono- and multi-layer films based on layers of cellulose nanofibrils (CNFs), lignocellulose nanofibrils (LCNFs), and electrospun poly(3-hydroxybutyrate) (PHB) and poly(3-hydroxybutyrate-*co*-3-hydroxyvalerate).

Sample	R_a (nm)	R_q (nm)
CNF	61.5	75.0
LCNF	39.4	49.9
PHB	15.8	20.8
PHBV	17.4	22.4
PHB/CNF/PHB	18.6	24.2
PHB/LCNF/PHB	17.7	22.5
PHBV/CNF/PHBV	29.4	36.5
PHBV/LCNF/PHBV	24.3	36.4

Standard deviations were within the typical errors of the measurement (<10 %).

In relation to the AFM images of the monolayer electrospun films of PHB and PHBV, shown in **Figure 3c** and **3d**, respectively, one can observe that both surfaces showed topographies with similar roughness. These surfaces were significantly smoother and glossier than in the case of the both nanopapers. Comparison of both neat electrospun films indicates that the PHB film surface was slightly smoother than that of PHBV, leading to the film sample with the highest smoothness. In relation to the multilayer films, gathered in **Figure 3e** to **3h**, these mostly presented an intermediate topography between the neat electrospun films and the nanopapers. Higher values of roughness were observed in the case of the multilayer films based on the electrospun PHBV coatings. This effect can be ascribed to the intrinsic lower softening characteristics of the copolyester by which the rougher topography of the inner nanopapers layers can be more easily transfer to the film surface during the post-processing thermal treatment.

3.2. Water contact angle

Figure 4 shows the water contact angle images for all film samples, including the mean values and standard deviations in the insets. Contact angle relates to the degree of affinity for water of each film surface. As expected, results clearly indicate that the uncoated nanopapers presented the highest hydrophilicity, *that is*, lower contact angles, than the ones coated with electrospun PHA films. In particular, angles of $\sim 39^\circ$ and 47° were observed for CNF and LCNF films, respectively. This difference can be also related to the presence of lignin since the hydrophobic character

of the nanopapers was found to increase with the presence of lignin [10]. This previous study also indicated that certain hydrophobicity is probably a desirable attribute for enhancing compatibility with hydrophobic polymer materials, which is the case of the present study and it would explain the higher adhesion of both PHA to LCNF than to CNF. As expected, the electrospun PHA coatings applied to the nanopapers considerably increased the contact angle values, *that is*, values in the 75-85° range. This is a very positive observation for potential uses in applications such as packaging in which water resistance is required.

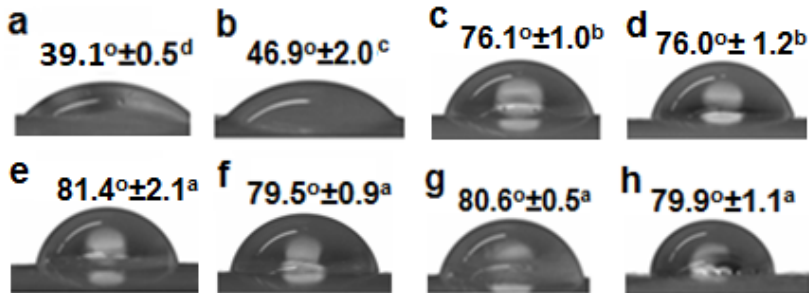


Figure 4. Contact angle of water for: a) Cellulose nanofibril (CNF) film; b) Lignocellulose nanofibril (LCNF) film; c) Electrospun poly(3-hydroxybutyrate) (PHB) film; d) Electrospun poly(3-hydroxybutyrate-co-3-hydroxyvalerate) (PHBV) film; e) PHB/CNF/PHB film; f) PHB/LCNF/PHB film; g) PHBV/CNF/PHBV film; h) PHBV/LCNF/PHBV film. Images and values were determined after 1 min of drop deposition.

Mean value (standard error). a–d: Different superscripts within the same column indicate significant differences among samples ($p < 0.05$).

3.3. Mechanical properties

The tensile stress-strain curves of the uncoated and coated films are gathered in **Figure 5**, with the exception of the multilayer sample PHB/LCNC/PHB, which specimens failed by delamination during testing and showed very large variations in mechanical performance among the samples. The corresponding values for each film of Young modulus (E), tensile strength at yield (σ_y) and at break (σ_b), and elongation at break (ϵ_b) are displayed in **Table 4**. As one can observe, CNF and LCNF films differed greatly from each other. The highest mechanical performance was observed for the lignin-free nanopaper that showed approximately a tensile modulus of 4.5 GPa, a tensile strength at break close to 138 MPa, and an elongation at break of 18%. In the case of the lignin-containing nanopaper, these values were of ~ 3 GPa, 99 MPa, and 14%, respectively.

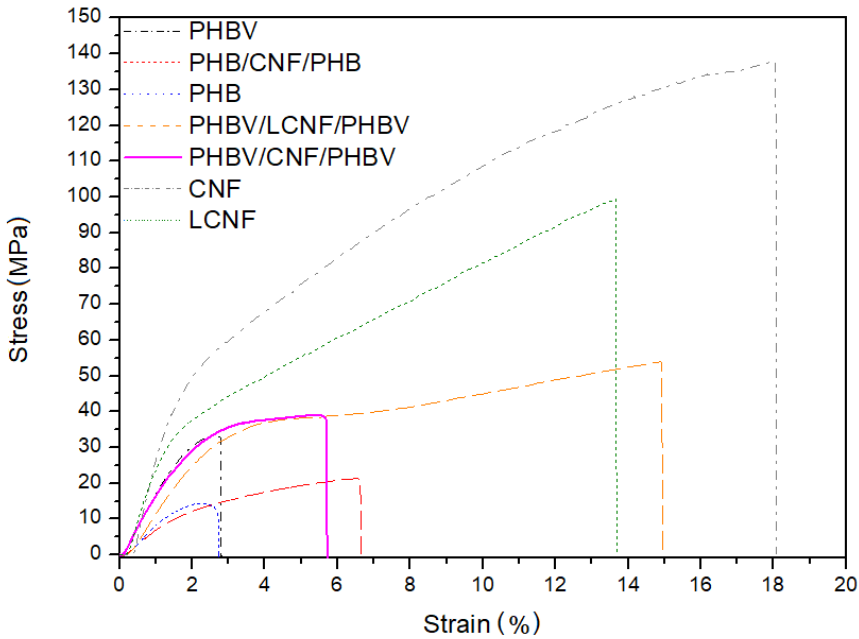


Figure 5. Tensile stress-strain curves of the mono- and multilayer films based on layers of cellulose nanofibrils (CNFs), lignocellulose nanofibril (LCNFs), and electrospun poly(3-hydroxybutyrate) (PHB) and poly(3-hydroxybutyrate-*co*-3-hydroxyvalerate) (PHBV).

Table 4. Mechanical properties of the mono- and multilayer films based on layers of cellulose nanofibrils (CNFs), lignocellulose nanofibrils (LCNFs), and electrospun poly(3-hydroxybutyrate) (PHB) and poly(3-hydroxybutyrate-*co*-3-hydroxyvalerate) (PHBV) in terms of tensile modulus (E), tensile strength at yield (σ_y), tensile strength at break (σ_b), and elongation at break (ϵ_b). Superscript letters within the same column

indicate significant differences ($p < 0.05$) among the samples for each mechanical property.

Sample	E (MPa)	σ_y (MPa)	σ_b (MPa)	ϵ_b (%)
CNF	4504.2 \pm 105 ^a	48.4 \pm 4.5 ^a	137.7 \pm 9.3 ^a	18.1 \pm 2.2 ^a
LCNF	2991.4 \pm 184 ^b	32.3 \pm 2.0 ^b	99.3 \pm 10.2 ^b	13.7 \pm 0.5 ^b
PHB	981.9 \pm 69 ^f	13.8 \pm 1.4 ^f	14.5 \pm 0.6 ^g	2.8 \pm 0.2 ^d
PHBV	2014.9 \pm 155 ^d	28.0 \pm 3.2 ^e	33.0 \pm 4.8 ^e	2.8 \pm 0.1 ^d
PHB/CNF/PHB	869.5 \pm 81 ^g	18.0 \pm 1.3 ^e	22.5 \pm 0.4 ^f	6.6 \pm 0.1 ^c
PHB/LCNF/PHB	-	-	-	-
PHBV/CNF/PHBV	2056.7 \pm 78 ^c	21.0 \pm 1.8 ^d	37.7 \pm 0.6 ^d	5.9 \pm 0.6 ^c
PHBV/LCNF/PHBV	1486.9 \pm 38 ^e	30.5 \pm 2.7 ^{bc}	53.8 \pm 0.6 ^e	14.9 \pm 0.4 ^b

In relation to the mechanical properties of nanopapers, some previous studies in literature have reported values of elastic modulus, tensile strength, and elongation at break within the ranges 2–18 GPa, 75–250 MPa, and 1–10%, respectively [44]. Most of these correspond to nanopapers based on fully bleached CNF obtained from softwood, hardwood, and non-wood resources. In general, the presence of lignin is known to reduce both mechanical strength and ductility when compared to lignin-depleted CNF films. In particular, LCNF films with lignin contents from 1.7 to 13.5 wt.-% were 10.5–14.3 GPa for tensile modulus, 116–164 MPa for tensile strength, and 1.7–3.5% for elongation at break

[10]. This reduction in mechanical strength with increasing the lignin content has been ascribed to the molecular restriction imposed by the lignin fraction. Additionally, ductility impairment typically occurs due to a lower fibrils dispersion as a result of the faster filtration process during the manufacture of the lignin-containing nanopapers [10].

Incorporation of the electrospun PHA coatings reduced the mechanical stiffness of the coated nanopapers. In general, PHAs, and particularly unplasticized PHB, suffer from excessive rigidity, hence exhibiting a relatively low plastic deformation during tensile efforts. For the neat annealed electrospun PHB and PHBV films, the mechanical values were in the range of 1–2 GPa of tensile modulus, 14–28 MPa of tensile strength, and approximately 3% of elongation at break. Similar mechanical values were recently reported for neat PHB sheets [31] and PHBV films [45], both obtained by compression molding, though the tensile modulus was relatively lower in the case of the homopolyester. More recently, it was observed that annealed electrospun films of PHB exhibited higher ductility and toughness than compression-molded PHB films [36], it can be particularly significant from an application viewpoint due to the excessive rigidity reported for conventional melt-compounded PHB. Additionally, in the present results, the mechanical strength of PHBV was seen higher than that of PHB, which can be related to the fact that the latter material was a plasticized grade.

The resultant multilayer structures presented values within the range of the mechanical strength of the neat PHA films. Indeed, the reduction observed for the mechanical strength can be related to a delamination failure during breakage, which is typically observed for multilayer structures. Interestingly, the here-developed multilayers presented higher elongation-at-break values than the neat PHA films as a result of the good adhesion of the electrospun film layers to the nanopapers. Among the multilayers, the highest ductility was observed for the PHBV/LCNF/PHBV, which failed at a deformation of $\sim 15\%$, *that is*, in the same range of the neat nanopapers. As compared to commercial sustainable packaging materials, the here-developed multilayer structures are still significantly less deformable but more elastic than polyolefins. For instance, bio-based high-density polyethylene (bio-HDPE) has been reported to present elongation-at-break values slightly above of 500%, while the tensile modulus and strength was around 375 and 19.5 MPa, respectively [40].

Thus, while the biopolymer coating is advantageous in terms of surface hydrophobization and hence water resistance, the overall mechanical performance of the resulting nanopapers are, to some extent, compromised. This loss in mechanical properties could limit certain engineering applications where high mechanical strength is required. However, from a point a view of flexible packaging, this loss of rigidity can contribute to obtain more flexible and better handling materials. In particular, this can result beneficial in fiber-based packaging applications

in which certain flexibility is certainly demanded. Of particular interest seem to be the multilayer structures based on PHBV coatings since the developed sustainable multilayer packaging structures reduced the tensile strength but also retained ductility to a significant high extent.

3.4. Barrier properties

The permeance values of the nanopapers and some of their multilayer structures based on PHA coatings are shown in **Figure 6**. These were evaluated in terms of water vapor, limonene, and oxygen permeance. The barrier performance is, in fact, one of the main parameters of application interest for a packaging material, especially for shelf life extension of foodstuff.

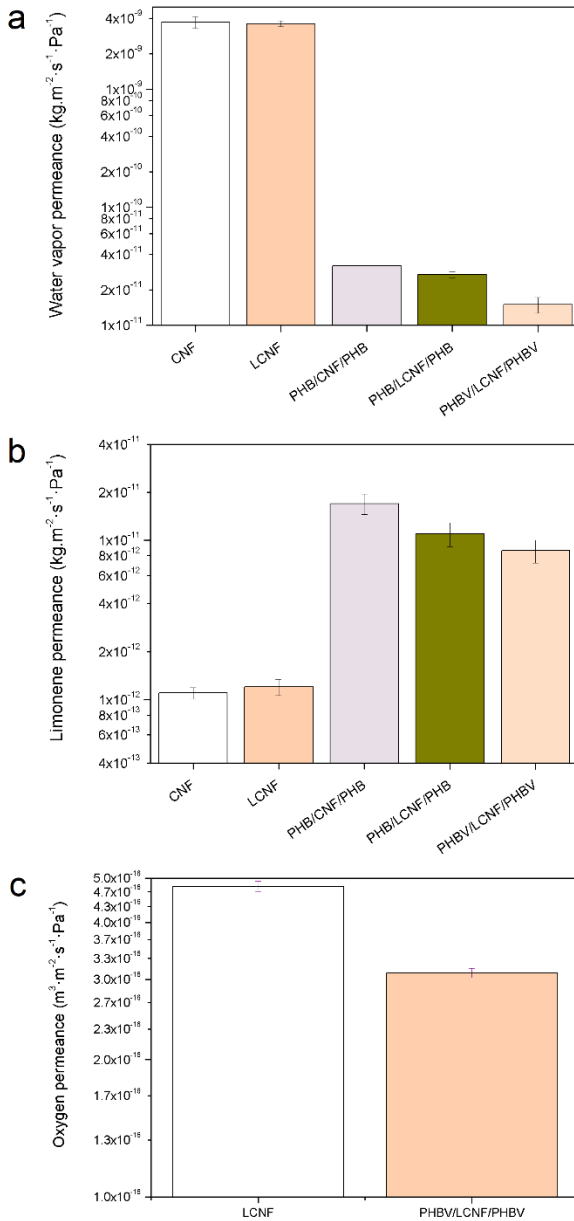


Figure 6. Permeance of the mono- and multilayer films based on layers of cellulose nanofibrils (CNFs), lignocellulose nanofibril (LCNFs), and

electrospun poly(3-hydroxybutyrate) (PHB) and poly(3-hydroxybutyrate-co-3-hydroxyvalerate) (PHBV) to: a) water vapor; b) limonene; c) oxygen.

In relation to water vapor transport properties, **Figure 6a** shows that both nanopapers, having similar thicknesses, that is, 30 μm , presented similar permeance values. In particular, these were 3.7×10^{-9} and $3.6 \times 10^{-9} \text{ kg/m}^2\cdot\text{s}^{-1}\cdot\text{Pa}^{-1}$ for the CNF film and LCNF film, respectively. This correlates well with a previous study where lignin content proved to have a small effect on water vapor permeability [10]. This has been previously related to the fact that, even when lignin is in principle more hydrophobic than cellulose in its native state, the residual lignin in fibers after pulping can be also hydrophilic depending on the digestion process and cellulose source used. Nevertheless, since the water contact angle was seen somewhat lower for the unbleached nanopaper, there must be a morphological factor involved. Interestingly, the nanopapers double side coated with electrospun PHB films had significantly lower water vapor permeance, with values in the range of $2.5\text{--}3.5 \times 10^{-11} \text{ kg/m}^2\cdot\text{s}^{-1}\cdot\text{Pa}^{-1}$. This particularly represents a permeance drop by a factor of *ca.* 115 and 133 for the CNF- and LCNF-coated films, respectively, as compared to the neat nanopapers. The permeance drop was even higher for the lignin-containing nanopaper coated with PHBV, i.e. $1.5 \times 10^{-11} \text{ kg/m}^2\cdot\text{s}^{-1}\cdot\text{Pa}^{-1}$, since the water permeability is higher for the unplasticized PHBV as compared to the plasticized PHB [36, 39]. Therefore, the application of electrospun PHA outer layers seems to be a very effective strategy to

protect nanopapers from environmental moisture penetration and hence material barrier properties plasticization.

Figure 6b shows the limonene permeance of the neat nanopapers and those double side coated with PHB. Limonene transport properties are important because this component is usually used as a standard system to test aroma barrier. The first clear observation is that the permeance of limonene was also very similar between the CNF film, i.e. 1.1×10^{-12} $\text{kg/m}^2\cdot\text{s}^{-1}\cdot\text{Pa}^{-1}$, and the LCNF film, i.e. 1.2×10^{-12} $\text{kg/m}^2\cdot\text{s}^{-1}\cdot\text{Pa}^{-1}$. The presence of the PHB electrospun coatings, however, increased the permeance to limonene by around one order of magnitude, in particular to 1.7×10^{-11} and 1.1×10^{-11} $\text{kg/m}^2\cdot\text{s}^{-1}\cdot\text{Pa}^{-1}$ for the PHB/CNF/PHB and PHB/LCNF/PHB films, respectively. This can be ascribed to the fact that limonene, as opposed to moisture, is a strong plasticizer for PHA materials [46]. Indeed, it has been previously reported that PHBV films obtained by solvent casting were able to uptake limonene by up to 12.7 wt.-% [47]. Thus, the outer PHA layers will act as a continuous reservoir of limonene uptake, increasing the overall limonene solubility and diffusion throughout the multilayer. A plausible strategy to address this challenge is, for instance, surface modification of the PHA films [48].

Oxygen, is also a very challenging permeant in packaging applications since it is a major source of shelf life shortening by oxidation in many products. It is also a difficult permeant to test in thin non-industrial films because small defects and/or sample brittleness can provide great

variations in the measurements. In the current samples, after many tests with large variations (often overrange) in permeance among the samples, it was decided to focus the test on the film samples that exhibited repeated OTR values with more reproducible readings, i.e. LCNF and PHBV/LCNF/PHBV. Regarding oxygen permeance, the LCNF film showed a high barrier performance, as it can be seen in **Figure 6c**. For a *ca.* 30- μm thick LCNF film, this was $4.8 \times 10^{-16} \text{ m}^3/\text{m}^2\cdot\text{s}^{-1}\cdot\text{Pa}^{-1}$, which results in a permeability of $1.4 \times 10^{-20} \text{ m}^3\cdot\text{m}/\text{m}^2\cdot\text{s}^{-1}\cdot\text{Pa}^{-1}$. If this value is compared with those reported for synthetic polymer materials commonly used in the food packaging industry, it is slightly less permeable than high-barrier polyvinyl alcohol (PVOH), i.e. $1.7 \times 10^{-20} \text{ m}^3\cdot\text{m}/\text{m}^2\cdot\text{s}^{-1}\cdot\text{Pa}^{-1}$, and about 5 times more barrier than ethylene-vinyl alcohol copolymer (EVOH), i.e. $7.7 \times 10^{-20} \text{ m}^3\cdot\text{m}/\text{m}^2\cdot\text{s}^{-1}\cdot\text{Pa}^{-1}$, being the later one of the main oxygen barrier films used in flexible packaging [49]. This can be certainly related to the crystalline components of the cellulose fibrils, which can also be further improved due to the ability of the nanofibers to form a dense network by strong inter-fibrillar bonds [51]. The present results show lower values of oxygen permeability than previous studies describing the barrier performance of nanopapers. For instance, it was observed that the oxygen permeability of CNF films was 3–6 times higher than that of EVOH films and approximately 2.5–7.5 lower than films of polyesters, *e.g.* polyethylene terephthalate (PET) [52]. The here-observed high oxygen barrier of the lignin-containing nanopaper implies that the samples selected for permeation had lower defects or even fragility through the

whole cross-section of the LNFC film, being permeability only dependent on the dissolution of oxygen and its rate of diffusion. It is very important and well known in high barrier materials to have homogeneous industrial films to test oxygen permeability with high level of confidence. So reducing sample testing area, as it has been done here, reduces the likelihood of incorporating defects in the characterization of non-industrial materials. However, it should be also noted that oxygen permeability of cellulose-based materials is strongly influenced by moisture sorption from the environment. For example, it was observed that the oxygen permeability of cellophane increased by about 20 times when RH increased from 0 to 50% [53]. In this particular study, the measurements were performed at 60% RH, which suggests a good barrier performance of the nanopaper at room conditions. In comparison to the neat nanopaper, the PHBV/LCNF/PHBV multilayer film additionally reduced the oxygen permeance by *ca.* 35%. This enhanced gas barrier performance is attributed to the PHA coatings that result in a reduced moisture sorption for the materials and hence in a reduced moisture sorption induced plasticization for the oxygen permeation process in the multilayer.

4. Conclusions

The multilayer technology is known to be the most efficient technological approach to improve the physicochemical properties, mainly barrier, of hydrophilic materials such as those based on cellulose. In this study, for

the first time, annealed electrospun layers of PHAs were used to create multilayers with enhanced moisture resistance for nanopapers. The results in this study point out that the incorporation of double side coatings of PHAs by the so-called electrospinning coating technique considerably reduced nanopapers hydrophilicity and provided a more balanced mechanical performance. In addition, and as expected, a reduced water vapor permeance of both lignin-free and -containing nanopapers was observed while the aroma barrier tested by direct permeation of limonene was seen slightly higher due to PHAs being strong organic aroma sorbers. Interestingly, in the case of oxygen barrier, the electrospun PHBV coating further improved the oxygen barrier of the nanopaper at medium high humidity conditions, i.e. 60% RH, which better simulate real application conditions. The overall results suggest that coating nanopapers by PHAs using the electrospinning coating technique provides a promising alternative technology to other conventional technologies, such as lamination extrusion, where high temperatures are required that, in turn, could compromise the stability of biopolymers and of potential active additives, such as antimicrobials. Further investigations are currently underway to optimize processing and post-processing parameters to reduce the coating thickness while guaranteeing a strong interlayer adhesion and enhanced physicochemical properties. Therefore, future research works will be also aimed to assess the impact of scalability of both nanopapers manufacturing and coating on performance.

5. Acknowledgments

The authors would like to thank the Spanish Ministry of Economy and Competitiveness (MINECO) project AGL2015-63855-C2-1-R for financial support. A. Cherpinski also acknowledges the European Cooperation in Science and Technology (COST) Action FP1405 for funding through a Short Term Scientific Mission (STSM) and the Brazilian Council for Scientific and Technological Development (CNPq) of the Brazilian Government for her predoctoral scholarship (205955/2014-2).

6. References

1. Babu, Ramesh P., Kevin O'Connor, and Ramakrishna Seeram. "Current Progress on Bio-Based Polymers and Their Future Trends." *Progress in Biomaterials* 2 (2013): 8.
2. Quiles-Carrillo, L., N. Montanes, T. Boronat, R. Balart, and S. Torres-Giner. "Evaluation of the Engineering Performance of Different Bio-Based Aliphatic Homopolyamide Tubes Prepared by Profile Extrusion." *Polymer Testing* 61 (2017): 421-29.
3. Torres-Giner, Sergio, Ana Torres, Marcela Ferrándiz, Vicent Fombuena, and Rafael Balart. "Antimicrobial Activity of Metal Cation-Exchanged Zeolites and Their Evaluation on Injection-Molded Pieces of Bio-Based High-Density Polyethylene." *Journal of Food Safety* 37, no. 4 (2017): e12348-n/a.
4. Vartiainen, J., M. Vähä-Nissi, and A. Harlin. "Biopolymer Films and Coatings in Packaging Applications - a Review of Recent Developments." *Mater. Sci. Appl.* 5, no. 10 (2014): 708-18.
5. Dufresne, A. *Natural Polymers: Volume 2 Nanocomposites*. London, UK: The Royal Society of Chemistry, 2012.
6. Kim, Joo-Hyung, Bong Sup Shim, Heung Soo Kim, Young-Jun Lee, Seung-Ki Min, Daseul Jang, Zafar Abas, and Jaehwan Kim. "Review of Nanocellulose for Sustainable Future Materials."

- International Journal of Precision Engineering and Manufacturing-Green Technology 2, no. 2 (2015): 197-213.
7. Moon, Robert J., Ashlie Martini, John Nairn, John Simonsen, and Jeff Youngblood. "Cellulose Nanomaterials Review: Structure, Properties and Nanocomposites." *Chemical Society Reviews* 40, no. 7 (2011): 3941-94.
 8. Österberg, Monika, Jari Vartiainen, Jessica Lucenius, Ulla Hippi, Jukka Seppälä, Ritva Serimaa, and Janne Laine. "A Fast Method to Produce Strong Nfc Films as a Platform for Barrier and Functional Materials." *ACS Applied Materials & Interfaces* 5, no. 11 (2013): 4640-47.
 9. Ferrer, Ana, Elisabet Quintana, Ilari Filpponen, Iina Solala, Teresa Vidal, Alejandro Rodríguez, Janne Laine, and Orlando J. Rojas. "Effect of Residual Lignin and Heteropolysaccharides in Nanofibrillar Cellulose and Nanopaper from Wood Fibers." *Cellulose* 19, no. 6 (2012): 2179-93.
 10. Rojo, Ester, Maria Soledad Peresin, William W. Sampson, Ingrid C. Hoeger, Jari Vartiainen, Janne Laine, and Orlando J. Rojas. "Comprehensive Elucidation of the Effect of Residual Lignin on the Physical, Barrier, Mechanical and Surface Properties of Nanocellulose Films." *Green Chemistry* 17, no. 3 (2015): 1853-66.
 11. Solala, Iina, Aleksander Volperts, Anna Andersone, Tatiana Dizhbite, Nina Mironova-Ulmane, Annikki Vehniäinen, Jaakko Pere, and Tapani Vuorinen. "Mechanoradical Formation and Its Effects on Birch Kraft Pulp During the Preparation of Nanofibrillated Cellulose with Masuko Refining." In *Holzforschung*, 477, 2012.
 12. Spence, Kelley L., Richard A. Venditti, Orlando J. Rojas, Youssef Habibi, and Joel J. Pawlak. "The Effect of Chemical Composition on Microfibrillar Cellulose Films from Wood Pulps: Water Interactions and Physical Properties for Packaging Applications." *Cellulose* 17, no. 4 (2010): 835-48.
 13. Nair, Sandeep S., and Ning Yan. "Effect of High Residual Lignin on the Thermal Stability of Nanofibrils and Its Enhanced Mechanical Performance in Aqueous Environments." *Cellulose* 22, no. 5 (2015): 3137-50.

14. Henriksson, Marielle, Lars A. Berglund, Per Isaksson, Tom Lindström, and Takashi Nishino. "Cellulose Nanopaper Structures of High Toughness." *Biomacromolecules* 9, no. 6 (2008): 1579-85.
15. Sehaqui, H., A. Liu, Q. Zhou, and L. A. Berglund. "Fast Preparation Procedure for Large, Flat Cellulose and Cellulose/Inorganic Nanopaper Structures." *Biomacromolecules* 11, no. 9 (2010): 2195-98.
16. Wågberg, L., G. Decher, M. Norgren, T. Lindström, M. Ankerfors, and K. Axnäs. "The Build-up of Polyelectrolyte Multilayers of Microfibrillated Cellulose and Cationic Polyelectrolytes." *Langmuir* 24, no. 3 (2008): 784-95.
17. Aulin, C., M. Gällstedt, and T. Lindström. "Oxygen and Oil Barrier Properties of Microfibrillated Cellulose Films and Coatings." *Cellulose* 17, no. 3 (2010): 559-74.
18. Vartiainen, J., J. Pelto, T. Kaljunen, and E. Kenttä. "Hydrophobization of Cellophane and Cellulose Nano-Fibrils Films by Supercritical State Carbon Dioxide Impregnation with Walnut Oil." *Nordic Pulp and Paper Research Journal* 31, no. 4 (2016): 541-47.
19. Vartiainen, J., T. Pöhler, K. Sirola, L. Pykkänen, H. Alenius, J. Hokkinen, U. Tapper, P. Lahtinen, A. Kapanen, K. Putkisto, P. Hiekkataipale, P. Eronen, J. Ruokolainen, and A. Laukkanen. "Health and Environmental Safety Aspects of Friction Grinding and Spray Drying of Microfibrillated Cellulose." *Cellulose* 18, no. 3 (2011): 775-86.
20. Vikman, M., J. Vartiainen, I. Tsitko, and P. Korhonen. "Biodegradability and Compostability of Nanofibrillar Cellulose-Based Products." *Journal of Polymers and the Environment* 23, no. 2 (2015): 206-15.
21. Lavoine, Nathalie, Isabelle Desloges, Alain Dufresne, and Julien Bras. "Microfibrillated Cellulose – Its Barrier Properties and Applications in Cellulosic Materials: A Review." *Carbohydrate Polymers* 90, no. 2 (2012): 735-64.

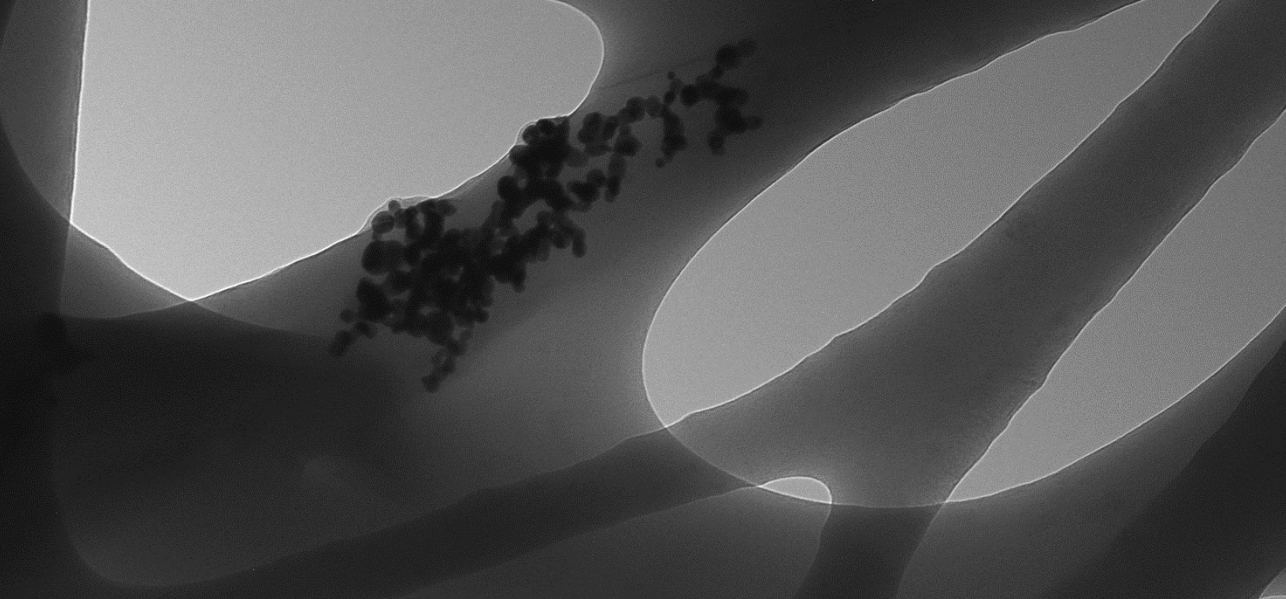
22. Barhoum, Ahmed, Pieter Samyn, Thomas Öhlund, and Alain Dufresne. "Review of Recent Research on Flexible Multifunctional Nanopapers." *Nanoscale* 9, no. 40 (2017): 15181-205.
23. Kadla, J. F., and R. D. Gilbert. "Cellulose Structure: A Review." *Cellulose Chemistry and Technology* 34, no. 3-4 (2000): 197-216.
24. Wei, L., and A. G. McDonald. "A Review on Grafting of Biofibers for Biocomposites." *Materials* 9, no. 4 (2016).
25. Rodionova, Galina, Marianne Lenes, Øyvind Eriksen, and Øyvind Gregersen. "Surface Chemical Modification of Microfibrillated Cellulose: Improvement of Barrier Properties for Packaging Applications." *Cellulose* 18, no. 1 (2011): 127-34.
26. Vähä-Nissi, Mika, Hanna M. Koivula, Heidi M. Räisänen, Jari Vartiainen, Pietro Ragni, Eija Kenttä, Timo Kaljunen, Tero Malm, Hannu Minkkinen, and Ali Harlin. "Cellulose Nanofibrils in Biobased Multilayer Films for Food Packaging." *Journal of Applied Polymer Science* 134, no. 19 (2017): n/a-n/a.
27. Vartiainen, Jari, Yingfeng Shen, Timo Kaljunen, Tero Malm, Mika Vähä-Nissi, Matti Putkonen, and Ali Harlin. "Bio-Based Multilayer Barrier Films by Extrusion, Dispersion Coating and Atomic Layer Deposition." *Journal of Applied Polymer Science* 133, no. 2 (2016): n/a-n/a.
28. Anderson, A. J., and E. A. Dawes. "Occurrence, Metabolism, Metabolic Role, and Industrial Uses of Bacterial Polyhydroxyalkanoates." *Microbiological Reviews* 54, no. 4 (1990): 450-72.
29. Savenkova, L., Z. Gercberga, V. Nikolaeva, A. Dzene, I. Bibers, and M. Kalnin. "Mechanical Properties and Biodegradation Characteristics of Phb-Based Films." *Process Biochemistry* 35, no. 6 (2000): 573-79.
30. Avella, M., E. Martuscelli, and M. Raimo. "Review Properties of Blends and Composites Based on Poly(3-Hydroxy)Butyrate (Phb) and Poly(3-Hydroxybutyrate-Hydroxyvalerate) (Phbv) Copolymers." *Journal of Materials Science* 35, no. 3 (2000): 523-45.
31. Torres-Giner, Sergio, Nestor Montanes, Vicent Fombuena, Teodomiro Boronat, and Lourdes Sanchez-Nacher. "Preparation and Characterization of Compression-Molded Green Composite

- Sheets Made of Poly(3-Hydroxybutyrate) Reinforced with Long Pita Fibers." *Advances in Polymer Technology* (2016): n/a-n/a.
32. Reinsch, Veronika E., and Stephen S. Kelley. "Crystallization of Poly(Hydroxybutyrate-Co-Hydroxyvalerate) in Wood Fiber-Reinforced Composites." *Journal of Applied Polymer Science* 64, no. 9 (1997): 1785-96.
 33. Thellen, Christopher, Sarah Cheney, and Jo Ann Ratto. "Melt Processing and Characterization of Polyvinyl Alcohol and Polyhydroxyalkanoate Multilayer Films." *Journal of Applied Polymer Science* 127, no. 3 (2013): 2314-24.
 34. Fabra, María José, Amparo Lopez-Rubio, and Jose M. Lagaron. "High Barrier Polyhydroxyalkanoate Food Packaging Film by Means Of nanostructured Electrospun Interlayers of Zein." *Food Hydrocolloids* 32, no. 1 (2013): 106-14.
 35. Torres-Giner, S., A. Chiva-Flor, and J. L. Feijoo. "Injection-Molded Parts of Polypropylene/Multi-Wall Carbon Nanotubes Composites with an Electrically Conductive Tridimensional Network." *Polymer Composites* 37, no. 2 (2016): 488-96.
 36. Echegoyen, Y., M. J. Fabra, J. L. Castro Mayorga, A. Cherpinski, and J. M. Lagaron. "High Throughput Electro-Hydrodynamic Processing in Food Encapsulation and Food Packaging Applications: Viewpoint." *Trends in food science & technology* 60 (2017): 71-79.
 37. Torres-Giner, S. "Electrospun Nanofibers for Food Packaging Applications." In *Multifunctional and Nanoreinforced Polymers for Food Packaging*, edited by J. M. Lagaron, 108-25. Cambridge, UK: Woodhead Publishing Limited, 2011.
 38. Busolo, M. A., S. Torres-Giner, and J. M. Lagaron. "Enhancing the Gas Barrier Properties of Polylactic Acid by Means of Electrospun Ultrathin Zein Fibers." Paper presented at the Annual Technical Conference - ANTEC, Conference Proceedings 2009.
 39. Castro-Mayorga, Jinneth Lorena, Maria Jose Fabra, Luis Cabedo, and Jose Maria Lagaron. "On the Use of the Electrospinning Coating Technique to Produce Antimicrobial Polyhydroxyalkanoate Materials Containing in Situ-Stabilized Silver Nanoparticles." *Nanomaterials* 7, no. 1 (2017): 4.

40. Cherpinski, Adriane, Sergio Torres-Giner, Luis Cabedo, Jose Alberto Méndez, and Jose M. Lagaron. "Multilayer Structures Based on Annealed Electrospun Biopolymer Coatings of Interest in Water and Aroma Barrier Fiber-Based Food Packaging Applications." *Journal of Applied Polymer Science* (2017): 45501-n/a.
41. Galván, M. V., P. Mocchiutti, L. M. Cornaglia, and M. A. Zanuttini. "Dual-Polyelectrolyte Adsorption of Poly(Allylamine Hydrochloride) and Xylan onto Recycled Unbleached Kraft Pulps." *BioResources* 7, no. 2 (2012): 2075-89.
42. Tammelin, Tekla, Ulla Hippinen, and Arto Salminen. "Method for the Preparation of Nfc Films on Supports." 2013.
43. Sixta, H. *Handbook of Pulp*. Weinheim, Germany: Wiley-VCH, 2006.
44. González, I, M Alcalà, Gary Chinga-Carrasco, F Vilaseca, S Boufi, and P Mutjé. "From Paper to Nanopaper: Evolution of Mechanical and Physical Properties." *Cellulose* 21, no. 4 (2014): 2599-609.
45. Martínez-Abad, Antonio, Luis Cabedo, Catarina S. S. Oliveira, Loic Hilliou, Maria Reis, and José María Lagarón. "Characterization of Polyhydroxyalkanoate Blends Incorporating Unpurified Biosustainably Produced Poly(3-Hydroxybutyrate-Co-3-Hydroxyvalerate)." *Journal of Applied Polymer Science* 133, no. 2 (2016): n/a-n/a.
46. Sanchez-Garcia, M. D., E. Gimenez, and J. M. Lagaron. "Novel Pet Nanocomposites of Interest in Food Packaging Applications and Comparative Barrier Performance with Biopolyester Nanocomposites." *Journal of Plastic Film and Sheeting* 23, no. 2 (2007): 133-48.
47. — — —. "Morphology and Barrier Properties of Solvent Cast Composites of Thermoplastic Biopolymers and Purified Cellulose Fibers." *Carbohydrate Polymers* 71, no. 2 (2008): 235-44.
48. Kang, I. K., S. H. Choi, D. S. Shin, and S. C. Yoon. "Surface Modification of Polyhydroxyalkanoate Films and Their Interaction with Human Fibroblasts." *International Journal of Biological Macromolecules* 28, no. 3 (2001): 205-12.

Chapter III

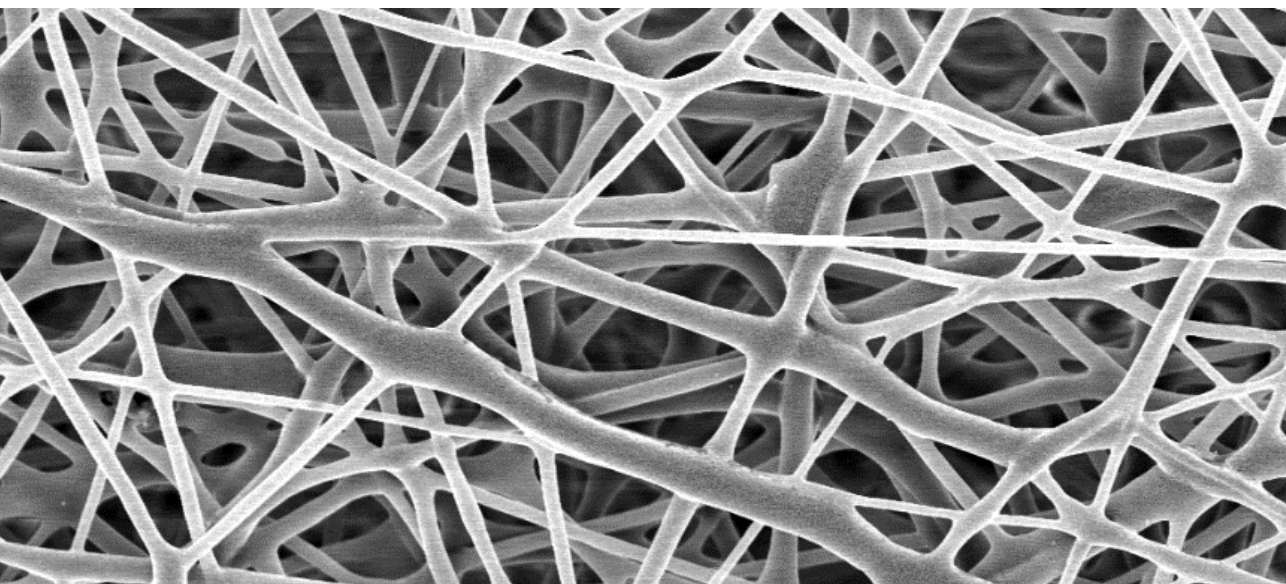
49. Lagaron, J. M. "Multifunctional and Nanoreinforced Polymers for Food Packaging." In *Multifunctional and Nanoreinforced Polymers for Food Packaging*, 1-28, 2011.
50. "Structural Characteristics Defining High Barrier Properties in Polymeric Materials." *Materials Science and Technology* 20, no. 1 (2004): 1-7.
51. Lagaron, J. M., R. Catalá, and R. Gavara. "Structural Characteristics Defining High Barrier Properties in Polymeric Materials." *Materials Science and Technology* 20, no. 1 (2004): 1-7.
52. Syverud, Kristin, and Per Stenius. "Strength and Barrier Properties of Mfc Films." *Cellulose* 16, no. 1 (2008): 75.
53. Krochta, J.M., E.A. Baldwin, and M.O. Nisperos-Carriedo. *Edible Coatings and Films to Improve Food Quality*. Lancaster, USA: Technomic Publishing Co Inc, 1994.



Chapter IV

Electrospun Oxygen Scavenging Films of Poly(3-hydroxybutyrate) Containing Palladium Nanoparticles for Active Packaging Applications

Cherpinski, A., Gozutok, M., Sasmazel, H., Torres-Giner, S., & Lagaron, J. (2018). Electrospun oxygen scavenging films of poly (3-hydroxybutyrate) containing palladium nanoparticles for active packaging applications. *Nanomaterials*, 8(7), 469.



Abstract

This paper reports on the development and characterization of oxygen scavenging films made of poly(3-hydroxybutyrate) (PHB) containing palladium nanoparticles (PdNP) prepared by electrospinning followed by annealing treatment at 160 °C. The PdNP were modified with the intention to optimize their dispersion and distribution in PHB by means of two different surfactants permitted for food contact applications, that is,, hexadecyltrimethylammonium bromide (CTAB) and tetraethyl orthosilicate (TEOS). Analysis of the morphology and characterization of the chemical, thermal, mechanical, and water and limonene vapor barrier properties and the oxygen scavenging capacity of the various PHB materials were carried out. From the results, it was seen that a better dispersion and distribution was obtained using CTAB as the dispersing aid. As a result, the PHB/PdNP nanocomposites containing CTAB provided also the best oxygen scavenging performance. These films offer a significant potential as new active coating or interlayer systems for application in the design of novel active food packaging structures.

Keywords: polyhydroxyalkanoates; palladium nanoparticles; packaging; electrospinning

1. Introduction

An important increasing quantity of plastic waste is being generated yearly for which the precise needed time for its biodegradation is certainly unknown. This environmental awareness has driven the development and improvement of new biodegradable polymers, especially for single-use plastic items [1]. In this sense, polyhydroxyalkanoates (PHAs) are well-known biopolymers that can be produced microbially by a variety of microorganisms as an energy storage mechanism. They exhibit similar performance in terms of mechanical, thermal, and barrier properties than petroleum-derived polymers and, thus, they can potentially replace conventional thermoplastics (e.g., polyolefins) in a wide range of applications [2]. In particular, barrier properties are of fundamental importance for food packaging applications. For instance, there are many food products that are very sensitive to oxidation and, to overcome this issue, packages with reduced oxygen permeability are desirable. Additionally, the water resistance is also important, particularly for plastic materials intended for direct contact with high moisture foodstuff as well as materials to be applied in high humidity conditions during storage and/or transport [3].

Poly(3-hydroxybutyrate) (PHB) is currently the most common representative of PHAs and this biopolymer has been proposed for short-term food applications [4]. However, PHB is a brittle polymer, as its enzymatic polymerization leads to the formation of macromolecules with highly ordered stereochemical structures, resulting in a large degree of

crystallinity [5]. One of the great advantages of PHB over many other biodegradable polymers is its biodegradability under aerobic as well as anaerobic conditions [6]. For this reason, PHB and their blends with other biopolymers, for instance polylactide (PLA), have been extensively investigated for food packaging applications [7-9]. One of the potential application fields of these materials is the development of films for packaging applications. As an example, Zhang et al. [10] studied PHB/PLA blends in different ratios and concluded that by blending PLA with 25 wt. % of PHB some interactions between both biopolymer matrices can be achieved. Furthermore, their results also showed improved mechanical properties.

Palladium nanoparticles (PdNP) are well known by their ability to dissociate hydrogen molecules to single atoms. This fact is further enhanced due to its nano-sized form and resultant high surface-to-volume ratio [11]. It has been demonstrated that the oxygen scavenging activity of palladium-based oxygen scavenging films is strongly dependent on the coating substrate as well as on the palladium deposition thickness. Optimization of these parameters can result in active scavenging films where the residual headspace oxygen of packaged foods can be scavenged very quickly [10]. There is a drive to find ways to incorporate active packaging technologies directly into the package walls. In spite of the advantages that they offer in maintaining quality and extending shelf life, such systems are still little used. The reason stems from the additional cost involved, the potential toxicity of the added

scavenger in the food contact layer, and even more so because of the lack of sufficient technical information on their performance and the lack of understanding of how to apply them effectively [12].

Electrospinning is a fiber production method that employs high electric forces to draw charged threads of polymer solutions or melts up to fiber diameters below 100 nm. It is a low startup cost process in which a wide variety of both polymer and non-polymer materials have been used to form mats composed of nanofibers with a high surface area-to-volume ratio [13]. The electrospinning process has a wide variety of applications such as medical, filtration, tissue engineering, food engineering, packaging, etc. [14-16]. Until now, this processing technology remained to a laboratory scale. However, recent developments in instrumentation and process aid design have allowed this process to be scaled to achieve the production volumes required in certain industrial commodity applications such as fortified foods and active packaging [17].

In active packaging, nanotechnology has a significant potential because nanostructures display a high surface-to-volume ratio and specific surface properties. Considering the high surface energy of nanoparticles, which tend to agglomerate and to prevent this aggregation, either polar polymers or surfactants can be used as protective agents and stabilizers of the nanoparticles. This is extremely necessary to obtain mono-dispersed uniform particles and to be, thereafter, used in various application purposes [18-20]. The objective of the present study was to

prepare and characterize, for the first time, PHB films by the electrospinning process incorporating PdNP. In order to improve the dispersion of the PdNP in the PHB matrix, different surfactants were tested.

2. Materials and Methods

2.1. Materials

Bacterial aliphatic homopolyester PHB was supplied by Biomer (Krailling, Germany) as P226F. According to the manufacturer, this is certified both as compostable and food contact grade, presenting a density of 1.25 g/cm³ and a melt flow rate (MFR) of 10 g/10 min at 180 °C and 5 kg. The weight-average molecular weight (M_w) estimated by the manufacturer was 500 kDa and the polydispersity index (PDI) was 2.

2,2,2-trifluoroethanol (TFE) with 99% purity and D-limonene with 98% purity were both purchased from Sigma-Aldrich S.A. (Madrid, Spain). The two tested surfactants, hexadecyltrimethylammonium bromide (CTAB), with 99% purity, and tetraethyl orthosilicate (TEOS), with 98% purity, as well as palladium (Pd) nano-powder, <25 nm particle size measured by transmission electronic microscopy (TEM) and $\geq 99.5\%$ trace metals basis, were also purchased from Sigma-Aldrich S.A. All products were used as received without further purification.

2.2. Electrospinning

A PHB solution for electrospinning was prepared by dissolving the biopolymer at 10 wt. %. The PdNP were added at 1 wt. % in relation to PHB to the solution. To improve the dispersion of the PdNP, CTAB and TEOS were also added as dispersing aids at 0.5 wt. % with the PHB and PdNP mixture.

Electrospinning was performed using a Fluidnatek® LE50 benchtop line from Bioinicia S.L. (Valencia, Spain) with a variable high-voltage 0–30 kV power supply. This device was equipped with a motorized injector that was scanning towards a metallic collector, aiming to obtain a homogeneous electrospun deposition. The different biopolymers solutions were transferred to a 30-mL plastic syringe and the syringe was connected through polytetrafluoroethylene (PTFE) tubes to a stainless-steel needle ($\varnothing = 0.9$ mm) whereas the needle tip was connected to the power supply. The solution was electrospun for 2 h under a steady flow-rate of 6 mL/h using a motorized injector, scanning horizontally towards a metallic grid. The distance between the injector and collector was optimal at 15 cm and the voltage was set at 15 kV. The biopolymer solutions were electrospun in a controlled environmental chamber at 23 °C and 40% relative humidity (RH), for a given processing time and in optimal conditions to achieve steady fiber formation. The processing and solution characterization parameters for the optimal electrospinning of this PHA grade were determined and optimized in a previous work [21].

Finally, the obtained electrospun mats were subjected to an annealing step below the biopolymer's melting point without applying pressure using a hydraulic press 4122-model from Carver, Inc. (Wabash, IN, USA). The annealing was found optimal at 160 °C, without pressure, for 5 ± 1 s, based on our previous study [21]. The resultant films were air cooled at room temperature. Prior to thermal treatment, the electrospun mats were equilibrated in a desiccator at 25 °C and 0% RH by using silica gel for at least 1 week.

2.3. *Characterization*

2.3.1. Film Thickness

Film thickness was measured with a digital micrometer series S00014, having ± 0.001 mm accuracy, from Mitutoyo Corporation (Kawasaki, Japan) at three random positions. The post-processed samples had a thickness of typically 55 ± 4 μm .

2.3.2. Scanning Electron Microscopy

A S-4800 microscope from Hitachi (Tokyo, Japan) was used to observe by scanning electron microscopy (SEM) the morphology of the electrospun PHB fibers and the film cross-sections and surfaces. Cross-sections of the samples were prepared by cryo-fracture of the electrospun PHB films using liquid nitrogen. Then, they were fixed to beveled holders using conductive double-sided adhesive tape, sputtered with a mixture of gold-palladium under vacuum, and observed using an accelerating

voltage of 5 kV. Image J Launcher v 1.41 software was used to determine the average fiber diameter and standard deviation by measuring the diameter of at least 100 fibers.

2.3.3. Transmission Electronic Microscopy

The morphology and distribution of the PdNP was studied using a JEOL 1010 from JEOL USA, Inc. (Peabody, MA, USA) by TEM using an accelerating voltage of 80 kV.

2.3.4. Differential Scanning Calorimetry

Thermal properties of the neat electrospun PHB fibers and films and of the multilayer systems were evaluated by differential scanning calorimetry (DSC) using a Perkin-Elmer DSC 8000 (Waltham, MA, USA) thermal analysis system under nitrogen atmosphere. The measurement was carried out on ~3 mg of each sample using a two-step program from 0 to 200 °C followed by a subsequent cooling down to -50 °C, both at a heating rate of 10 °C/min. The DSC equipment was previously calibrated with indium as a standard and the slope of the thermograms was corrected by subtracting similar scans of an empty pan. Tests were done, at least, in triplicate.

2.3.5. Thermogravimetric Analysis

Thermogravimetric analysis (TGA) was performed in a TG-STDA Mettler-Toledo model TGA/STDA851e/LF/1600 analyzer from Mettler-Toledo, LLC (Columbus, OH, USA). The samples, with an initial weight

typically about 15 mg, were heated from 50 to 500 °C at a heating rate of 10 °C/min under nitrogen/air flow.

2.3.6. Infrared Spectroscopy

Fourier transform infrared spectroscopy (FTIR) spectra were collected coupling the attenuated total reflection (ATR) accessory Golden Gate of Specac, Ltd. (Orpington, UK) to Bruker Tensor 37 FTIR equipment (Rheinstetten, Germany). Single spectra were collected in the wavelength range from 4000 to 600 cm^{-1} by averaging 20 scans at a resolution of 4 cm^{-1} .

2.3.7. Mechanical Tests

Dumbbell-shaped specimens were die-cut from the electrospun films and conditioned to ambient conditions, that is,, 25 °C and 50% RH, for 24 h prior to tensile testing. Tests were carried out at room temperature in a universal mechanical testing machine AGS-X 500N from Shimadzu Corp. (Kyoto, Japan) in accordance with ASTM D638 (Type IV) standard. This was equipped with a 1-kN load cell and the cross-head speed was set at 10 mm/min. A minimum of six specimens was measured for each sample and the average results with standard deviation were reported.

2.3.8. Water Vapor Permeability

The water vapor permeability (WVP) of the samples was determined, in triplicate, using the gravimetric method ASTM E96-95. To this end, 5 mL of distilled water was placed inside a Payne permeability cup ($\varnothing = 3.5$ cm) from Elcometer Sprl (Hermalle-sous-Argenteau, Belgium) to expose

the film to 100% RH on one side. The liquid was not in contact with the film. Once the films were secured with silicon rings, they were placed within a desiccator at 0% RH cabinet at 25 °C. The dryness of the cabinet was held constant using dried silica gel. Cups with aluminum films were used as control samples to estimate solvent loss through the sealing. The cups were weighted periodically using an analytical balance with a ± 0.0001 g accuracy. Water vapor permeation was calculated from the steady-state permeation slopes obtained from the regression analysis of weight loss data vs. time, and the weight loss was calculated as the total loss minus the loss through the sealing.

2.3.9. D-Limonene Permeability

Permeability to limonene vapor was measured as described above for WVP. For this, 5 mL of D-limonene was placed inside the Payne permeability cups. The cups containing the films were placed at controlled environmental conditions, that is,, 23 °C and 40% RH. Limonene vapor permeation rates were estimated from the steady-state permeation slopes and the weight loss was calculated as the total cell loss minus the loss through the sealing. The samples were measured in triplicate and the limonene permeability (LP) values were calculated taking into account the average film thickness in each case.

2.3.10. Oxygen Scavenging Activity

Round-bottom Schlenk flasks from VidraFoc S.A. (Barcelona, Spain) with a PTFE stopcock and a headspace volume of 50 cm³ were used for the oxygen scavenging measurements. The flasks contained a valve for gas flushing in and a O₂-sensitive sensor spot (PSt3, detection limit 15 ppb, 0–100% oxygen) from PreSens (Regensburg, Germany) was glued onto the inner side of the flasks for measuring oxygen depletion. The electrospun fibers and films were cut (5 × 5 cm²) and placed into the flasks. The flask was subsequently flushed for 30 s at 1 bar with a gas mixture containing 1 vol. % oxygen, 4 vol. % hydrogen, and 95 vol. % nitrogen, which was provided by Abelló Linde, S.A. (Barcelona, Spain). The oxygen concentration in the cell was monitored by a non-destructive measurement method using the OXY-4 mini (PreSens) multi-channel fiber optic oxygen meter for simultaneous read-out of up to 4 oxygen sensors, used with sensors based on a 2 mm optical fiber. Oxygen concentrations over time were measured by linking the light-emitting (600–660 nm) optical fibers to the flasks inner sensing spots. The sensor emits a certain amount of luminescence depending on the oxygen concentration in the cell that was calibrated to yield concentration by the equipment. All measurements were carried out at 23 °C and at 50% and 100% RH.

2.4. Statistical Analysis

The test data were evaluated through analysis of variance (ANOVA) using STATGRAPHICS Centurion XVI v 16.1.03 from StatPoint

Technologies, Inc. (Warrenton, VA, USA). Fisher's least significant difference (LSD) was used at the 95% confidence level ($p < 0.05$). Mean values and standard deviations were also calculated.

3. Results and Discussion

3.1. Morphology and Optical Properties

3.1.1. Optical Appearance

Figure 1 shows the contact transparency pictures of the electrospun PHB fibers, Figure 1a–c, as well as of their respective annealed films, Figure 1d–f. From these pictures, it can be observed that all the electrospun fiber mats were completely opaque due to the ultrathin size of the fibers that generate a significant level of porosity and hence refract the light very strongly [21]. On the other hand, the annealed films presented an improved contact transparency, specially the sample with CTAB. Due to the presence of the PdNP, the films developed an expected dark color.

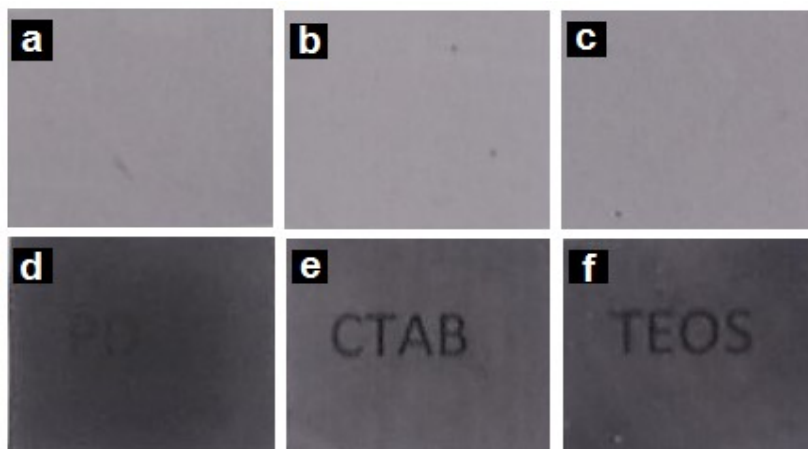


Figure 1. Contact transparency pictures of the electrospun poly(3-hydroxybutyrate) (PHB) fibers containing palladium nanoparticles (PdNP) and their respective annealed films: (a) PHB/PdNP fibers; (b) PHB/PdNP/hexadecyltrimethylammonium bromide (CTAB) fibers; (c) PHB/PdNP/tetraethyl orthosilicate (TEOS) fibers; (d) PHB/PdNP film, (e) PHB/PdNP/CTAB film, (f) PHB/PdNP/TEOS film.

3.1.2. Morphology of Electrospun PHB Materials

The morphology of the electrospun fibers and their annealed films were studied by SEM. Representative images of all the electrospun samples are gathered in Figure 2. The images were taken from the surface and cross-sections of the obtained fibers and films. As shown in Figure 2a, the diameter of the neat electrospun PHB fibers was distributed primarily in the range of 200–600 nm, presenting a smooth and bead-free morphology. In particular, the mean diameter was found to be at 350 ± 147 nm. One can observe that the presence of the PdNP led to a fraction

with increased fiber diameter and also resulted in a spindle-type beads formation. This effect can be observed in Figure 2d,g, corresponding to the electrospun PHB/PdNP and CTAB-containing PHB/PdNP fibers, respectively. This observation may suggest that, in some fibrillar regions, partial agglomeration of the PdNP may occur. Indeed, some degree of agglomeration is a common phenomenon in composites due to the large surface area and high total surface energy associated with nanoparticles incorporated into polymer matrices that makes them amenable to clustering [22]. The nanofibers diameter was previously reported to decrease when the surfactant concentration increased in the electrospinning solution [23]. Interestingly, the TEOS-containing PHB/PdNP fibers, shown in Figure 2j, presented a significant fraction of the fibers with reduced fiber diameter. This effect has been previously described for other electrospun materials and it has been particularly attributed to both the expected decrease in surface tension and an increase in conductivity, which in turn produce an increase in the stretching forces in the jet and consequently decreases the fiber diameter [24-26].

From the SEM images of the fibers cross-sections, one can observe that Figure 2b,e, corresponding to the neat PHB and PHB/PdNP fibers, respectively, showed similar morphologies. In particular, both electrospun mats presented cross-sections with relatively high porosity and low compaction. Alternatively, the cross-section of the surfactant-containing PHB/PdNP fibers, included in Figure 2h,k, were seen to be more compacted since the adhesion among the fibers in the layered

structure was higher. For all layers, it was also possible to perceive some particles aggregation that may not be necessarily related to the presence of the PdNP but, more probably, to additives such as the nucleating agent boron nitride, originally included in the biopolymer by the manufacturer.

In the SEM images of the films cross-sections, shown in Figure 2c, f, i, l, it can be observed that the electrospun fibers fused and interconnected among each other after the annealing treatment at 160 °C, successfully leading to the packing of the fiber mat into a continuous film. Among the here-prepared films, the neat PHB film showed a more uniform, smooth, and homogeneous surface. After the addition of the PdNP and surfactants, the films became more heterogeneous, rougher, and also presented some cavities. This morphology change can be then related to the presence of the PdNP, which more likely interfered in the fibers coalescence process.

3.1.3. Dispersion of PdNP

In order to provide a more resolved information about the dispersion of the PdNP into the PHB biopolymer matrix, TEM was performed on the nanocomposite fibers and films. The distribution of the PdNP inside the electrospun fibers are illustrated in the TEM images included in Figure 3d, 3g. From the TEM image included in Figure 3a, one can clearly discern that the PdNP were mainly agglomerated in certain regions of the submicron PHB fibers. One can also observe that the addition of both surfactants, that is,, CTAB and TEOS, as respectively shown in Figure 3d

and 3g, successfully improved the PdNP dispersion in the PHB fibers. Dispersion and distribution was, however, seen higher in the CTAB-containing sample.

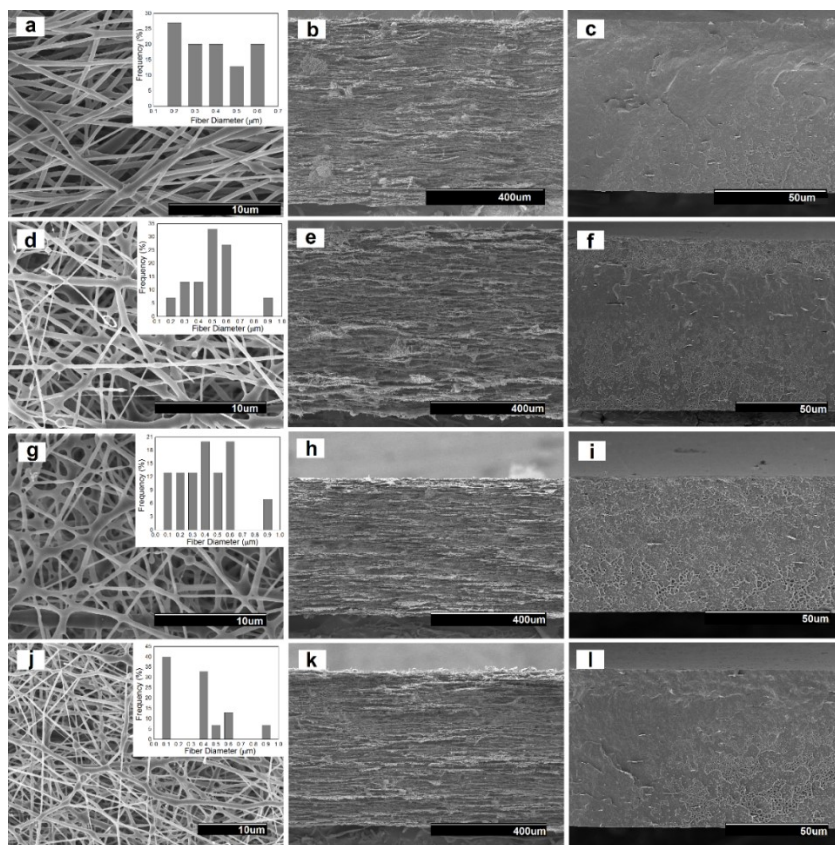


Figure 2. Scanning electron microscopy (SEM) images taken on the surface views and cross-sections of the electrospun poly(3-hydroxybutyrate) (PHB) fibers containing palladium nanoparticles (PdNP) and their respective annealed films: (a) Surface view of the neat PHB fibers; (b) Cross-section of the neat PHB fibers; (c) Cross-section of the neat PHB film; (d) Surface view of the PHB/PdNP fibers; (e) Cross-section of the PHB/PdNP fibers; (f) Cross-section of

the PHB/PdNP film; (g) Surface view of the PHB/PdNP/hexadecyltrimethylammonium bromide (CTAB) fibers; (h) Cross-section of the PHB/PdNP/CTAB fibers; (i) Cross-section of the PHB/PdNP/CTAB film; (j) Surface view of the PHB/PdNP/tetraethyl orthosilicate (TEOS) fibers; (k) Cross-section of the PHB/PdNP/TEOS fibers; (l) Cross-section of the PHB/PdNP/TEOS film.

In relation to the annealed films, the PHB/PdNP film without surfactant, shown in Figure 3b,c, still presented a clear aggregation of the particles. As opposite, Figure 3e,f, for the CTAB-containing film sample, and Figure 3,i, for the TEOS-containing film sample, clearly showed that the PdNP were evenly and relatively well distributed in the PHB films without forming agglomerates. In the case of the TEOS-containing film sample, the nanoparticle dispersion was less uniform when compared to the sample prepared with CTAB surfactant due to the absence of large grey dark areas. In both PHB films, very small nanoparticles of approximately 5 ± 2 nm can be seen, being homogeneously dispersed along the biopolymer matrix. The present results are in agreement with the results showed by Shaukat et al., where PdNP were incorporated into polyamide 6 (PA6)/clay nanocomposites and the nanoparticles were largely separated from each other and oriented in all possible directions in the polymer matrix [27]. However, due to the absence of surfactant, some particles still agglomerated into clusters of bigger sizes that increased at the PA6 interfaces with the nanoclays.

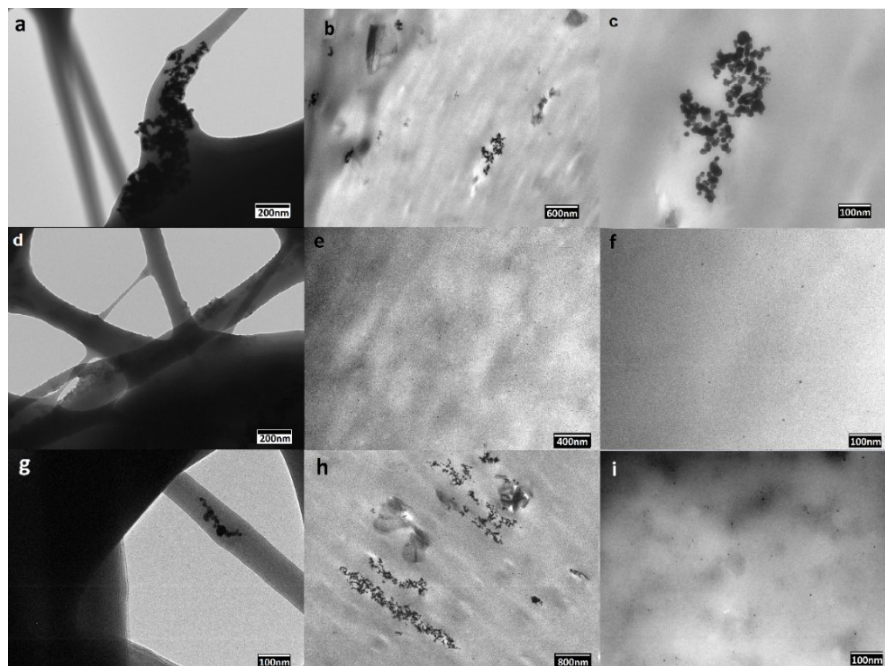


Figure 3. Transmission electron microscopy (TEM) images of the electrospun poly(3-hydroxybutyrate) (PHB) fibers containing palladium nanoparticles (PdNP) and their respective annealed films: (a) PHB/PdNP fibers; (b,c) PHB/PdNP film; (d) PHB/PdNP/hexadecyltrimethylammonium bromide (CTAB) fibers; (e,f) PHB/PdNP/CTAB film; (g) PHB/PdNP/tetraethyl orthosilicate (TEOS) fibers; (h,i) PHB/PdNP/TEOS film.

3.2. Thermal Properties

3.2.1. Melting Profile

The thermal properties of the electrospun PHB fibers and films containing the PdNP nanoparticles were firstly investigated by DSC analysis. Table 1 gathers the melting temperatures (T_{m1} and T_{m2}) and

enthalpies (ΔH_m) obtained from the first heating run. Likewise, the crystallization temperature (T_c) was also obtained from the cooling run. One can observe that when thermal annealing was applied to the fibers, the melting profile of the PHB materials, both temperature and enthalpy, slightly decreased. In particular, the T_m values of the neat PHB-based fibers varied in the 168–170 °C range, melting in a single peak, whereas these values were around 3 °C lower in their counterpart film samples. In addition, the incorporation of the PdNP into PHB induced a slight decrease in both the melting temperature and enthalpy as well as resulted in the formation of multiple melting peaks. This observation may suggest that the nanoparticles interfered with the crystallization process of the homopolyester, producing more imperfect crystals composed of thinner lamellae that melted over a wider range at lower temperatures and with lower enthalpies [28]. This effect was more intense in the case of the surfactant-containing film samples, which suggests that the PdNP were better dispersed then highly influencing the packing process of the PHB chains during cooling. In relation to the crystallization from the melt, the PHB film samples incorporating the PdNP also showed slightly lower values of T_c than the fibers, which confirms that the nanoparticles provided an anti-nucleating effect on PHB during the film formation. In any case, given that PHB is known to exhibit cold crystallization during the dynamic DSC runs, it becomes difficult to discuss with certainty potential changes in crystallinity and crystalline morphology [21, 26].

Table 1. Thermal properties obtained from the differential scanning calorimetry (DSC) curves in terms of melting temperature (T_m), normalized melting enthalpy (ΔH_m), crystallization temperature (T_c), and normalized crystallization enthalpy (ΔH_c) for the various poly(3-hydroxybutyrate) (PHB) and palladium nanoparticles (PdNP) fibers and films with and without hexadecyltrimethylammonium bromide (CTAB) and tetraethyl orthosilicate (TEOS).

Sample	T_{m1} (°C)	T_{m2} (°C)	ΔH_m (J/g)	T_c (J/g)	ΔH_c (J/g)
PHB Fibers	-	169.1 ± 0.9 ^a	64.1 ± 1.1 ^a	110.2 ± 0.9 ^a	59.3 ± 2.0 ^{b,c}
PHB Film	-	168.4 ± 1.3 ^a	71.8 ± 1.3 ^e	110.5 ± 1.2 ^a	61.1 ± 0.4 ^{a,b}
PHB/PdNP Fibers	156.4 ± 2.1 ^{a,b}	168.3 ± 1.1 ^{a,b}	59.4 ± 0.9 ^{c,d}	108.4 ± 0.5 ^{a,b}	63.1 ± 1.5 ^a
PHB/PdNP Film	155.0 ± 1.2 ^a	168.4 ± 1.2 ^{a,b}	58.5 ± 0.8 ^d	109.5 ± 2.1 ^a	56.3 ± 1.0 ^{c,d}
PHB/PdNP/CTAB Fibers	156.7 ± 0.5 ^{a,b}	167.7 ± 0.9 ^{a,b}	62.2 ± 1.4 ^b	109.1 ± 0.9 ^{a,b}	60.3 ± 0.8 ^{a,b}
PHB/PdNP/CTAB Film	158.6 ± 1.4 ^c	165.1 ± 1.4 ^b	60.3 ± 1.5 ^c	106.8 ± 0.3 ^b	55.1 ± 0.7 ^d
PHB/PdNP/TEOS Fibers	155.2 ± 0.7 ^a	169.9 ± 0.5 ^a	59.7 ± 0.9 ^d	110.8 ± 1.0 ^a	60.1 ± 1.1 ^{a,b}
PHB/PdNP/TEOS Film	159.4 ± 1.9 ^c	165.5 ± 1.2 ^b	62.9 ± 0.8 ^{a,b}	110.0 ± 2.3 ^a	51.4 ± 1.8 ^c

a–e: Different superscripts within the same column indicate significant differences among the samples ($p < 0.05$).

3.2.2. Thermal Stability

Figure 4 shows the evolution of the mass loss as a function of temperature for the PHB samples, including the curves of the first derivative analysis (blue lines). As shown in Table 2, it can be seen that the neat PHB initiated degradation at 207 °C while the biopolymer fully decomposed in two steps, seen at 262 °C and 348 °C, providing a residual mass of approximately 3%. Thermal degradation of the PHB films

containing the PdNP and the surfactants also occurred in two stages with a slight increase in thermal stability. In particular, the onset degradation took place in the 220–230 °C range that continued to the first degradation stage at 270–275 °C and, at a slower rate, to over 360–380 °C, remaining a residue of 3–4% of the initial mass of the sample. In this sense, Díez-Pascual et al. [29] demonstrated that the incorporation of zinc oxide (ZnO) improved the heat resistance of PHB, which was ascribed to the barrier effect of the nanoparticles that effectively hindered the diffusion of decomposition products during thermal degradation. Therefore, the PdNP probably also functioned as a thermal barrier, absorbing heat, thus also resulting in an enhanced thermal stability.

It is also worthy to note the slight increase observed in the thermal stability of the PHB/PdNP films with the incorporation of both surfactants, especially in the case of CTAB. This suggests that the surfactant increased the matrix–nanoparticle interaction, inducing a positive delay in thermal degradation. Taking into account that the ammonium salts degrade at the temperature range of 150–460 °C, the surfactants could successfully provide a bonding effect between both components of the nanocomposite and, eventually, enhance the whole thermal stability of PHAs.

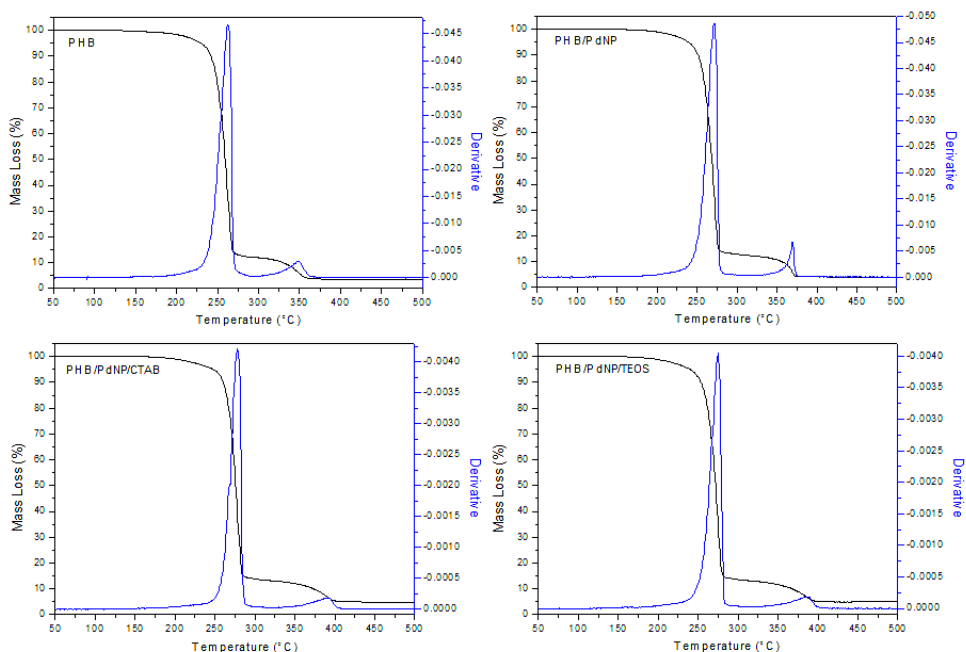


Figure 4. Thermogravimetric analysis (TGA) curves of the electrospun poly(3-hydroxybutyrate) (PHB) and palladium nanoparticles (PdNP) films with and without hexadecyltrimethylammonium bromide (CTAB) and tetraethyl orthosilicate (TEOS) surfactants.

Table 2. Mean values of thermal stability obtained from the thermogravimetric analysis (TGA) curves of the electrospun poly(3-hydroxybutyrate) (PHB) and palladium nanoparticles (PdNP) films with and without hexadecyltrimethylammonium bromide (CTAB) and tetraethyl orthosilicate (TEOS) in terms of degradation temperature at 5% of mass loss ($T_{5\%}$), degradation temperature (T_{deg}), and residual mass at 500 °C (R_{500}).

Film sample	$T_{5\%}$ (°C)	T_{deg1} (°C)	T_{deg2} (°C)	R_{500} (%)
PHB	207.0 ± 4.4	262.0 ± 3.8	348.0 ± 6.4	3.08 ± 0.04
PHB/PdNP	224.1 ± 3.6	271.3 ± 2.6	368.2 ± 3.8	3.17 ± 0.03
PHB/PdNP/CTAB	220.0 ± 8.1	278.1 ± 3.4	392.2 ± 5.4	3.81 ± 0.04
PHB/PdNP/TEOS	230.2 ± 2.5	275.2 ± 4.1	386.1 ± 2.3	4.44 ± 0.04

3.3. FTIR Analysis

FTIR is a powerful tool, which is very sensitive to the molecular environment, to investigate the structural changes that occur in the material during any chemical or physical process. In Figure 5, the FTIR spectra are presented for the above-mentioned PHB-based fibers and films. From the given spectra of the PHB materials, the band centered at 1722 cm^{-1} is an indicative of the C=O stretching vibration for the biopolyester molecule. The absorption bands in the $1200\text{--}1300\text{ cm}^{-1}$ range were previously related to the presence of the C–O–C stretching vibrations whereas the band centered at approximately 980 cm^{-1} has been ascribed to stretching bands of the carbon–carbon single bond (C–C) in PHAs [21, 30]. In the spectra of the pure surfactants, it is interesting to be noted that the bands at 2873 cm^{-1} and 2977 cm^{-1} correspond to the anti-symmetric C–H stretching of CTAB while the bands located at 1168 cm^{-1} , 1103 cm^{-1} , and 1080 cm^{-1} have been assigned to the CH_3 rocking and C–O asymmetric stretching of TEOS, respectively [19,31]. For the surfactant-containing PHB films, the above surfactant bands or others could not be

detected most likely due to the low concentration in which these additives are present in the composite.

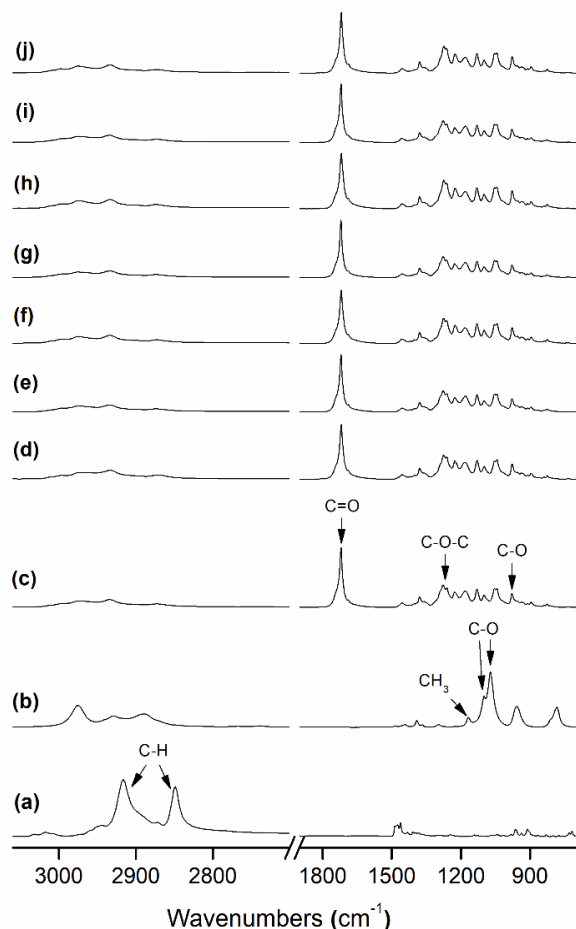


Figure 5. Fourier transform infrared (FTIR) spectra of: (a) Hexadecyltrimethylammonium bromide (CTAB); (b) Tetraethyl orthosilicate (TEOS); (c) Poly(3-hydroxybutyrate) (PHB) fibers; (d) PHB film; (e) PHB/palladium nanoparticles (PdNP) fibers; (f) PHB/PdNP film; (g) PHB/PdNP/CTAB fibers; (h) PHB/PdNP/CTAB film; (i) PHB/PdNP/TEOS fibers; (j) PHB/PdNP/TEOS film. Arrows indicate the chemical bonds and/or groups discussed in the text.

Table 3 gathers the band area ratio A1230:A1453 and the 1722 cm⁻¹ carbonyl band width at half maximum, which have been recently associated with crystallinity content in electrospun PHB materials [21]. Both a 1722 cm⁻¹ band broadening and reduction in the A1230:A1453 band area ratio have been previously connected with a reduction in molecular order and, hence, in crystallinity. Figure 5 and also Table 3 indicate that the band at 1722 cm⁻¹ tended to broaden somehow in the case of the film samples as compared to their respective fibers, which can be indicative of a phenomenon of molecular disorder due to thermal treatment in the material. The band ratio seems to be less sensitive, as previously discussed, than the carbonyl band [21]. These results may be in close agreement with those previously reported by Pachekoski et al., in which it was indicated that band widening with annealing correlates with the changes in molecular backbone stability and, hence, crystallinity in PHB [32]. Similarly, Mottin et al. also reported a change in crystallinity in PHB by annealing process [33].

Table 3. Full width at half maximum (FWHM) of the carbonyl band centered at $\sim 1722\text{ cm}^{-1}$ and the band area ratio $A_{1230}:A_{1453}$ for the electrospun poly(3-hydroxybutyrate) (PHB) and palladium nanoparticles (PdNP) films with and without hexadecyltrimethylammonium bromide (CTAB) and tetraethyl orthosilicate (TEOS).

Sample	FWHM ₁₇₂₂ (cm ⁻¹)	A ₁₂₃₀ :A ₁₄₅₃
PHB Fibers	16.20	4.28
PHB Film	16.35	4.03
PHB/PdNP Fibers	15.10	4.24
PHB/PdNP Film	15.60	4.86
PHB/PdNP/CTAB Fibers	14.44	3.58
PHB/PdNP/CTAB Film	14.23	4.28
PHB/PdNP/TEOS Fibers	15.89	4.25
PHB/PdNP/TEOS Film	16.00	4.28

3.4. Mechanical Properties

Table 4 presents the mechanical properties, obtained from the tensile tests, of the electrospun PHB films. The incorporation of the PdNP into PHB caused an increase in both the modulus of elasticity and tensile strength, therefore increasing the elastic deformation and stiffness of the PHB film. The enhancement in mechanical resistance attained in the nanocomposite films can be attributed to the combination of fairly good nanoparticle dispersion and strong interfacial adhesion between both phases through interactions via H-bonding of PHB [29]. In relation to

elongation at break, all films presented values of around 3%, which confirms the intrinsic brittleness of PHB. In any case, the presence of the PdNP did not alter the film ductility and toughness characteristics of PHB while the effect of the surfactants addition on their mechanical performance was also not statistically significant.

Table 4. Mechanical properties in terms of elastic modulus (E), tensile strength at break (σ_b), elongation at break ($\% \epsilon_b$), and toughness (T) of the electrospun poly(3-hydroxybutyrate) (PHB) and palladium nanoparticles (PdNP) films with and without hexadecyltrimethylammonium bromide (CTAB) and tetraethyl orthosilicate (TEOS).

Sample	E (MPa)	σ_b (MPa)	ϵ_b (%)	T (mJ/m ³)
PHB film *	1104 ± 74 ^a	17.8 ± 1.8 ^a	2.9 ± 1.0 ^a	0.3 ± 0.1 ^a
PHB/PdNP	1255 ± 15 ^b	22.5 ± 4.2 ^b	3.1 ± 1.0 ^a	0.4 ± 0.1 ^a
PHB/PdNP/CTAB	1262 ± 14 ^b	23.3 ± 1.4 ^c	3.0 ± 0.1 ^a	0.4 ± 0.1 ^a
PHB/PdNP/TEOS	1288 ± 230 ^c	21.7 ± 4.1 ^b	2.7 ± 1.0 ^a	0.3 ± 0.2 ^a

a–c: Different superscripts within the same column indicate significant differences among the samples ($p < 0.05$). * Obtained in previous work [21].

3.5. Barrier Properties

3.5.1. Water Vapor Permeability

Measuring the loss or gain in water content is a common method to estimate the WVP of film samples. The WVP values of the electrospun PHB films are gathered in Figure 6. It can be observed that the neat PHB film showed a higher barrier performance to water vapor than their respective nanocomposites with the PdNP. In particular, while the neat PHB film showed a WVP value of $5.2 \times 10^{-15} \text{ kg}\cdot\text{m}\cdot\text{m}^{-2}\cdot\text{Pa}^{-1}\cdot\text{s}^{-1}$, this value was $1.2 \times 10^{-14} \text{ kg}\cdot\text{m}\cdot\text{m}^{-2}\cdot\text{Pa}^{-1}\cdot\text{s}^{-1}$ for the PHB/PdNP film. The observed permeability increase in the nanocomposite films can be related to the existence of not bonded interfacial regions acting as preferential paths, especially in the vicinity of agglomerates. These preferential pathways could accelerate the diffusion of gas molecules, thus increasing the diffusion coefficient [34]. Interestingly, the WVP values of the PHB/PdNP films was lower in the case of the CTAB-containing film, i.e, $8.0 \times 10^{-15} \text{ kg}\cdot\text{m}\cdot\text{m}^{-2}\cdot\text{Pa}^{-1}\cdot\text{s}^{-1}$, and considerably higher for the film with TEOS, that is,, $6.6 \times 10^{-14} \text{ kg}\cdot\text{m}\cdot\text{m}^{-2}\cdot\text{Pa}^{-1}\cdot\text{s}^{-1}$. This result suggests that the dispersion in the PHB/PdNP/CTAB film was higher and, then, the sizes of such unbonded interfacial regions were lower. In addition, the high WPV value observed for the PHB/PdNP/TEOS film suggests that this film sample could be also plasticized by the surfactant, increasing the free volume of the film and favoring the diffusion of water vapor molecules through the film sample [35, 36].

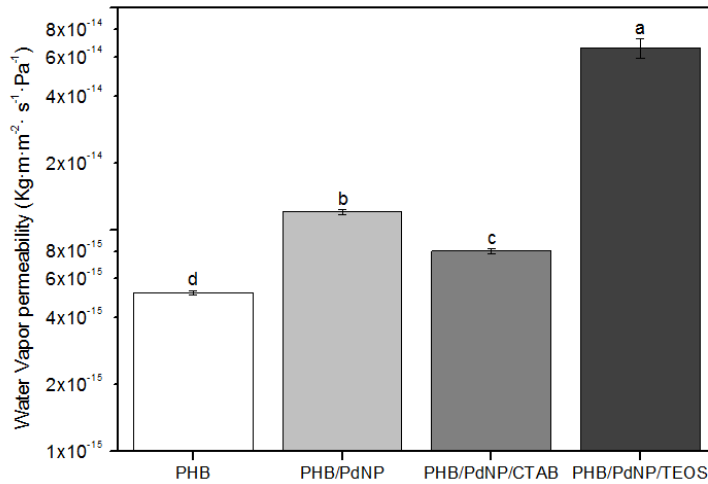


Figure 6. Values of water vapor permeability (WVP) of the electrospun poly(3-hydroxybutyrate) (PHB) and palladium nanoparticles (PdNP) films with and without hexadecyltrimethylammonium bromide (CTAB) and tetraethyl orthosilicate (TEOS) surfactants. Different letters indicate significant differences among the samples ($p < 0.05$).

3.5.2. D-Limonene Permeability

To test the barrier performance for volatile compounds such as aromas, D-limonene is commonly used. Figure 7 shows the values of LP, where one can observe that the neat PHB film presented the lowest permeability for D-limonene with a value of $3.2 \times 10^{-15} \text{ kg}\cdot\text{m}\cdot\text{m}^{-2}\cdot\text{Pa}^{-1}\cdot\text{s}^{-1}$. In the case of the nanocomposite films, the LP values increased from $4.7 \times 10^{-15} \text{ kg}\cdot\text{m}\cdot\text{m}^{-2}\cdot\text{Pa}^{-1}\cdot\text{s}^{-1}$, for the PHB/PdNP film, to 9.6×10^{-15} and $9.0 \times 10^{-15} \text{ kg}\cdot\text{m}\cdot\text{m}^{-2}\cdot\text{Pa}^{-1}\cdot\text{s}^{-1}$, for the CTAB- and TEOS-containing PHB/PdNP films, respectively. As discussed above, the presence of the PdNP and their agglomerates may result in the creation of preferential paths for sorption

and diffusion of the aroma molecules hence resulting in a reduced barrier performance. The here-obtained results are showing opposite behavior as the ones reported earlier by Busolo and co-workers who dispersed silver nanoparticles (nAg) in PLA, yielding nanocomposites with enhanced barrier properties [37]. Similarly, Rhim et al. reported agar/nAg composites where they confirmed a substantial improvement in barrier properties of the composite [38]. In the case of the surfactants-containing PHB/PdNP films, it should be also taken into account that permeability of α -limonene in PHB is mainly controlled by a solubilization mechanism due to the capacity of PHAs to uptake large amounts of this organic compound [39]. This supports the fact that plasticized PHB materials present increased values of aroma permeability.

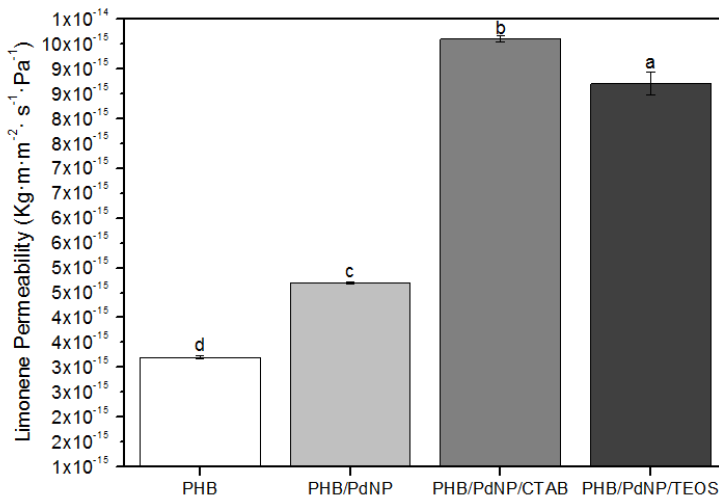


Figure 7. Values of α -limonene permeability (LP) of the electrospun poly(3-hydroxybutyrate) (PHB) and palladium nanoparticles (PdNP) films with and without hexadecyltrimethylammonium bromide

(CTAB) and tetraethyl orthosilicate (TEOS) surfactants. Different letters indicate significant differences among the samples ($p < 0.05$).

3.5.3. Oxygen Scavenging Activity

The oxygen scavenging activity of the here-prepared electrospun fibers and films containing the PdNP was determined by measuring the oxygen scavenging rate (OSR). In relation to the electrospun fibers, Figure 8 shows the decay or depletion of the oxygen concentration as a function of time, for a span time of 800 min, at both 50% and 100% RH. From observation of the graph it can be seen that, while the neat PHB fibers were unable to reduce the amount of oxygen in the cell, comparatively, the free PdNP in powder form were able to reduce all available headspace oxygen in an extremely short time. The incorporation of the PdNP into the PHB fibers by electrospinning generated mat samples with intermediate oxygen scavenging activity. However, as it can also be observed in the graph, the performance of the developed nanocomposite fibers was strongly dependent on the RH conditions. All electrospun mats presented a significantly lower oxygen scavenging activity at 50% than at 100% RH. For instance, at the end of the experiment carried out at 50% RH, oxygen depletion varied from almost 40%, for the PHB/PdNP/CTAB fibers, to only ca. 10%, for the PHB/PdNP/TEOS fibers. However, at 100% RH, the electrospun PHB/PdNP mat reached a reduction in the oxygen volume of approximately 85% while both surfactant-containing PHB/PdNP fibers were able to fully consume the whole amount of oxygen after 800 min. It is also worthy to mention that the depletion rate was

faster in the case of the PHB/PdNP/CTAB mat, which further confirmed the higher dispersion achieved for the nanoparticles with this surfactant. In relation to the effect of humidity, it is known that moisture favors the catalytic activity of the PdNP, which can be mainly related to the fact that water can be associatively adsorbed directly on the PdNP surface and thereby interact with the adsorbed hydrogen and oxygen [10]. A possible mechanism is that the adsorbed atomic oxygen and hydrogen forms an OH intermediate that reacts with an adsorbed hydrogen atom or another OH molecule. Another possible explanation is the reaction of adsorbed oxygen with gas-phase hydrogen or with some kind of dihydrogen species weakly adsorbed on the surface. Finally, a concerted reaction of two adsorbed hydrogen atoms and an adsorbed oxygen atom has been also considered [40].

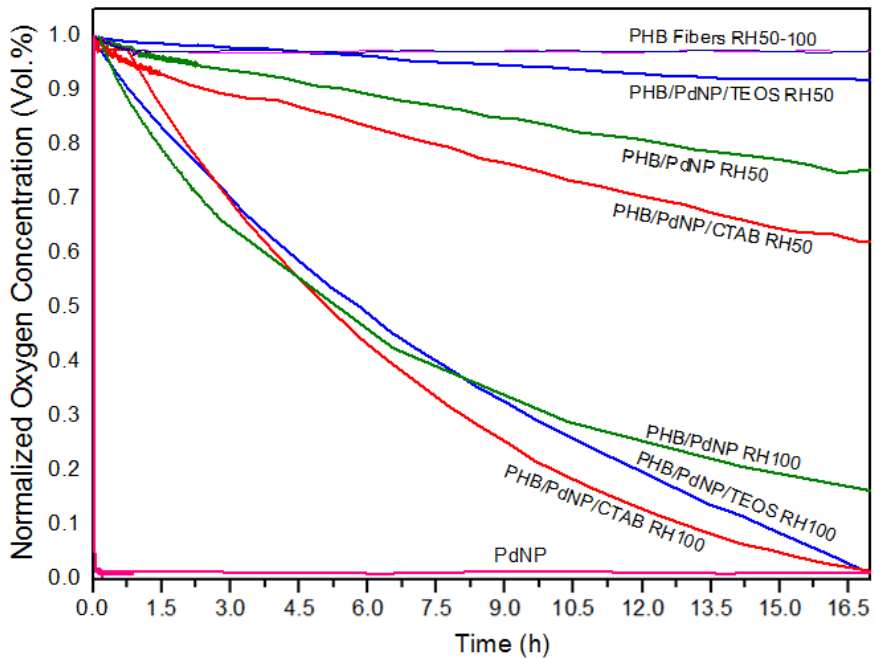


Figure 8. Oxygen depletion of the electrospun poly(3-hydroxybutyrate) (PHB) and palladium nanoparticles (PdNP) fibers with and without hexadecyltrimethylammonium bromide (CTAB) and tetraethyl orthosilicate (TEOS) surfactants. Values were measured at 50% and 100% relative humidity (RH).

In Figure 9, the oxygen volume depletion obtained with the electrospun films at 100% RH are shown. Comparison between Figures 8 and 9 revealed that the oxygen scavenging effect of the films was considerably lower than that of the same material in the fiber form. This reduction in the OSR is related to the higher surface-to-volume ratio of the electrospun fibers than the films, since the fibers mats present an extremely high porosity. In any case, all PHB/PdNP films still presented

significant oxygen scavenging capacity and, among the samples tested, the CTAB-containing films showed the highest performance as expected in view of all the above observations. This result can be explained by the better dispersion of the PdNP achieved in the PHB matrix using CTAB. In agreement with the data reported here, Ahalawat and co-workers evaluated the simultaneous effects of cationic surfactants on the textural and structural properties of silica nanoparticles [41]. It was observed that the silica nanoparticles displayed better dispersion and lower size than those prepared with other two cationic surfactants using an aqueous TEOS precursor solution with CTAB. In relation to this, it has also been reported that an SiO_x matrix between a coating of palladium and the substrate presents higher values of OSR than the palladium coated directly onto PET films [42]. These findings were later confirmed on PLA [10].

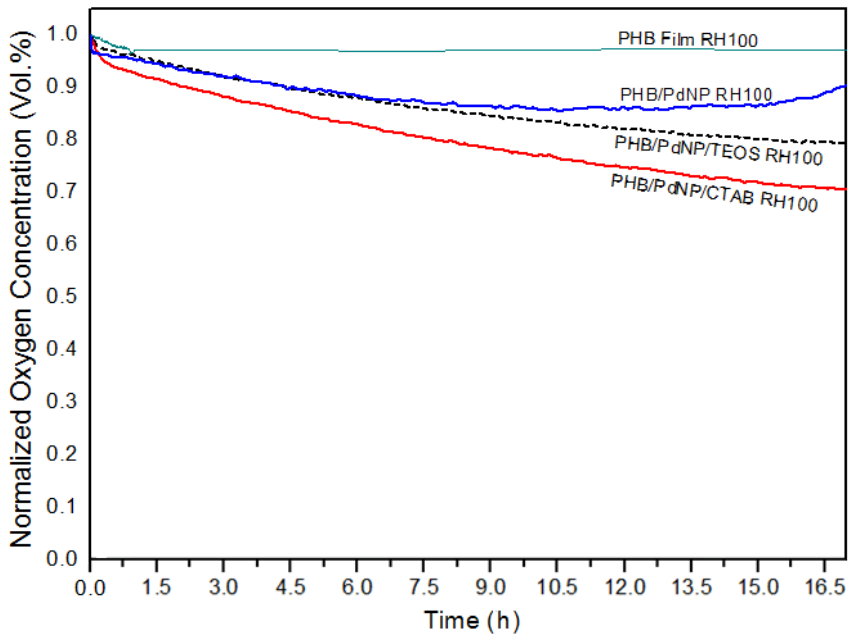


Figure 9. Oxygen depletion of the electrospun poly(3-hydroxybutyrate) (PHB) and palladium nanoparticles (PdNP) films with and without hexadecyltrimethylammonium bromide (CTAB) and tetraethyl orthosilicate (TEOS) surfactants. Values were measured at 100% relative humidity (RH).

4. Conclusions

In this study, PdNP were mixed with CTAB and TEOS surfactants to have better dispersion in electrospun PHB fibers. The resultant fibers were annealed at 160 °C to form continuous PHB films of direct application interest. Morphological analysis carried out by SEM and TEM showed that a better dispersion was achieved for the electrospun

PHB/PdNP/CTAB film. DSC indicated that the presence of the PdNP reduced both the melting point and the degree of crystallinity of PHB, thus acting as an anti-nucleating agent, which was further confirmed by FTIR analysis. WVP and LP measurements indicated that the nanocomposite films, including those modified with surfactants, presented lower barrier performance than the neat PHB film. These results were ascribed to the reduced crystallinity degree and to existence of unbonded interfacial regions and/or voids between the biopolymer matrix and the inorganic nanoparticles that may serve as preferential ways for the diffusion of gas molecules. Finally, the oxygen scavenging activity of the PHB materials was evaluated at different RHs. Although the electrospun films presented lower capacity to absorb oxygen than their counterpart fibers, these still presented significant activity at 100% RH. The here-developed and characterized electrospun PHB films are suitable potential candidates as coatings or interlayer systems for active food packaging applications and the followed methodology represents a new route to prepare these films due to the relative high dispersion achieved of the PdNP.

5. Acknowledgments

A.C. and S.T.-G. would like to thank the Brazilian Council for Scientific and Technological Development (CNPq) for her predoctoral grant (205955/2014-2) and his Juan de la Cierva contract (IJCI-2016-29675), respectively. This research has received funding from the Spanish

Ministry of Economy and Competitiveness (MINECO, project AGL2015-63855-C2-1-R) and the EU H2020 project YPACK (reference number 773872).

6. References

1. Puglia, D, E Fortunati, David Alberto D'amico, Liliana Beatriz Manfredi, Viviana Paola Cyras, and JM Kenny. "Influence of Organically Modified Clays on the Properties and Disintegrability in Compost of Solution Cast Poly (3-Hydroxybutyrate) Films." *Polymer Degradation and Stability* 99 (2014): 127-35.
2. Ma, P, P Xu, M Chen, W Dong, X Cai, Pauline Schmit, AB Spoelstra, and PJ Lemstra. "Structure–Property Relationships of Reactively Compatibilized Phb/Eva/Starch Blends." *Carbohydrate polymers* 108 (2014): 299-306.
3. Molinaro, Stefano, Malco Cruz Romero, Marta Boaro, Alessandro Sensidoni, Corrado Lagazio, Michael Morris, and Joe Kerry. "Effect of Nanoclay-Type and Pla Optical Purity on the Characteristics of Pla-Based Nanocomposite Films." *Journal of Food Engineering* 117, no. 1 (2013): 113-23.
4. Imre, Balázs, and Béla Pukánszky. "Compatibilization in Bio-Based and Biodegradable Polymer Blends." *European Polymer Journal* 49, no. 6 (2013): 1215-33.
5. Bittmann, Birgit, Rebeca Bouza, Luis Barral, Javier Diez, and Carmen Ramirez. "Poly (3a, Luis Barral, Javier Diezezo-Based and Biodegradable Polymer Blends." *ris*, and Joe Kerry. *actively CompatiPolymer Composites* 34, no. 7 (2013): 1033-40.
6. Castro-Mayorga, JL, MJ Fabra, and JM Lagaron. "Stabilized Nanosilver Based Antimicrobial Poly (3-Hydroxybutyrate-Co-3-Hydroxyvalerate) Nanocomposites of Interest in Active Food Packaging." *Innovative Food Science & Emerging Technologies* 33 (2016): 524-33.
7. Bartzak, Zbigniew, Andrzej Galeski, Marek Kowalczyk, Michal Sobota, and Rafal Malinowski. "Tough Blends of Poly (Lactide)

- and Amorphous Poly ([R, S]-3-Hydroxy Butyrate)–Morphology and Properties." *European Polymer Journal* 49, no. 11 (2013): 3630-41.
8. Furukawa, Tsuyoshi, Harumi Sato, Rumi Murakami, Jianming Zhang, Yong-Xin Duan, Isao Noda, Shukichi Ochiai, and Yukihiro Ozaki. "Structure, Dispersibility, and Crystallinity of Poly (Hydroxybutyrate)/Poly (L-Lactic Acid) Blends Studied by Ft-Ir Microspectroscopy and Differential Scanning Calorimetry." *Macromolecules* 38, no. 15 (2005): 6445-54.
 9. Zhang, Min, and Noreen L Thomas. "Blending Polylactic Acid with Polyhydroxybutyrate: The Effect on Thermal, Mechanical, and Biodegradation Properties." *Advances in Polymer Technology* 30, no. 2 (2011): 67-79.
 10. Yildirim, Selçuk, Bettina Röcker, Nadine Rüegg, and Wolfgang Lohwasser. "Development of Palladium-Based Oxygen Scavenger: Optimization of Substrate and Palladium Layer Thickness." *Packaging Technology and Science* 28, no. 8 (2015): 710-18.
 11. Cernohorsky, Ondrej, Karel Zdansky, Jiri Zavadil, Pavel Kacerovsky, and Katerina Piksova. "Palladium Nanoparticles on Inp for Hydrogen Detection." *Nanoscale research letters* 6, no. 1 (2011): 410.
 12. Damaj, Ziad, Catherine Joly, and Emmanuel Guillon. "Toward New Polymeric Oxygen Scavenging Systems: Formation of Poly (Vinyl Alcohol) Oxygen Scavenger Film." *Packaging Technology and Science* 28, no. 4 (2015): 293-302.
 13. Wendorff, J. H., S. Agarwal, and A. Greiner. *Electrospinning: Materials, Processing, and Applications*, Electrospinning: Materials, Processing, and Applications, 2012.
 14. Uyar, T., and E. Kny. *Electrospun Materials for Tissue Engineering and Biomedical Applications: Research, Design and Commercialization*, *Electrospun Materials for Tissue Engineering and Biomedical Applications: Research, Design and Commercialization*, 2017.
 15. Torres-Giner, S., R. Pérez-Masiá, and J. M. Lagaron. "A Review on Electrospun Polymer Nanostructures as Advanced Bioactive

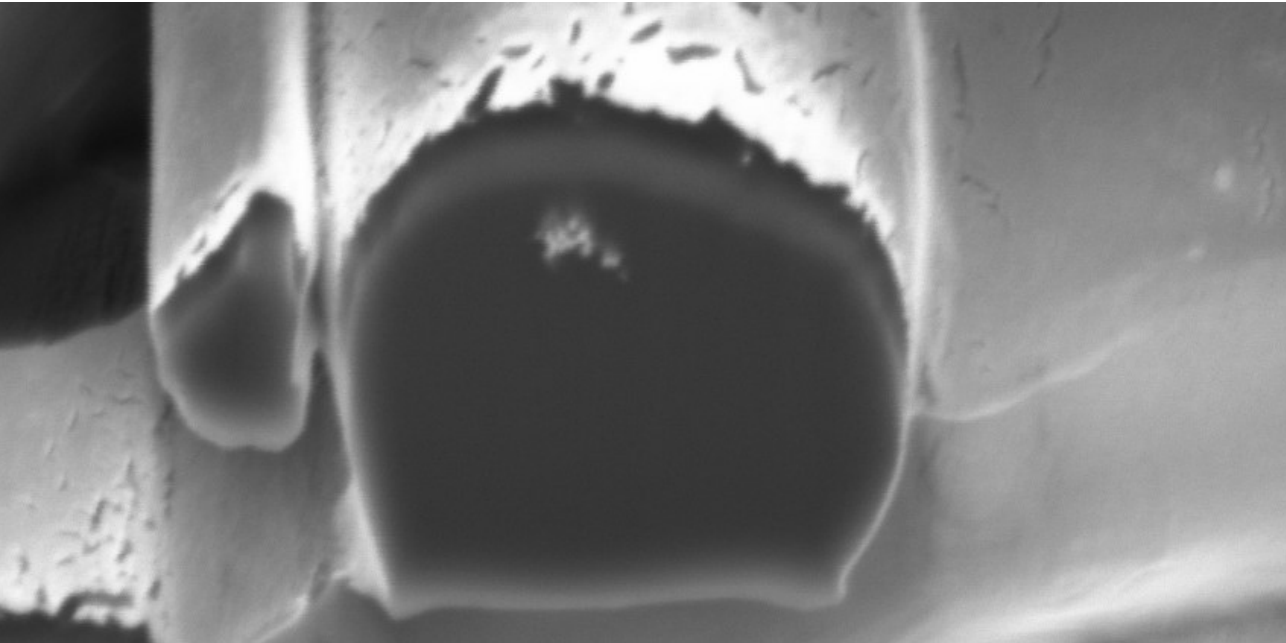
- Platforms." *Polymer Engineering and Science* 56, no. 5 (2016): 500-27.
16. Torres-Giner, S. "Electrospun Nanofibers for Food Packaging Applications." In *Multifunctional and Nanoreinforced Polymers for Food Packaging*, 108-25, 2011.
 17. Echegoyen, Y., M. J. Fabra, J. L. Castro-Mayorga, A. Cherpinski, and J. M. Lagaron. "High Throughput Electro-Hydrodynamic Processing in Food Encapsulation and Food Packaging Applications: Viewpoint." *Trends in Food Science and Technology* 60 (2017): 71-79.
 18. Dainelli, Dario, Nathalie Gontard, Dimitrios Spyropoulos, Esther Zondervan-van den Beuken, and Paul Tobback. "Active and Intelligent Food Packaging: Legal Aspects and Safety Concerns." *Trends in Food Science & Technology* 19 (2008): S103-S12.
 19. Kundu, Subrata. "A New Route for the Formation of Au Nanowires and Application of Shape-Selective Au Nanoparticles in SERS Studies." *Journal of Materials Chemistry C* 1, no. 4 (2013): 831-42.
 20. Mayer, A, and M Antonietti. "Investigation of Polymer-Protected Noble Metal Nanoparticles by Transmission Electron Microscopy: Control of Particle Morphology and Shape." *Colloid & Polymer Science* 276, no. 9 (1998): 769-79.
 21. Cherpinski, Adriane, Sergio Torres-Giner, Luis Cabedo, and Jose M. Lagaron. "Post-Processing Optimization of Electrospun Submicron Poly(3-Hydroxybutyrate) Fibers to Obtain Continuous Films of Interest in Food Packaging Applications." *Food Additives & Contaminants: Part A* 34, no. 10 (2017): 1817-30.
 22. Tekmen, C, Y Tsunekawa, and H Nakanishi. "Electrospinning of Carbon Nanofiber Supported Fe/Co/Ni Ternary Alloy Nanoparticles." *Journal of Materials Processing Technology* 210, no. 3 (2010): 451-55.
 23. Sainudeen, Shijina S, Lakshmi B Asok, Anitta Varghese, A Sreekumaran Nair, and Gopi Krishnan. "Surfactant-Driven Direct Synthesis of a Hierarchical Hollow Mgo Nanofiber-Nanoparticle Composite by Electrospinning." *RSC Advances* 7, no. 56 (2017): 35160-68.

24. Sakai, Shinji, Koei Kawakami, and Masahito Taya. "Controlling the Diameters of Silica Nanofibers Obtained by Sol-Gel/Electrospinning Methods." *Journal of chemical engineering of Japan* 45, no. 6 (2012): 436-40.
25. Castro-Mayorga, Jinneth Lorena, Maria Jose Fabra, Luis Cabedo, and Jose Maria Lagaron. "On the Use of the Electrospinning Coating Technique to Produce Antimicrobial Polyhydroxyalkanoate Materials Containing in Situ-Stabilized Silver Nanoparticles." *Nanomaterials* 7, no. 1 (2016): 4.
26. Martínez-Abad, A, G Sanchez, JM Lagaron, and MJ Ocio. "Influence of Speciation in the Release Profiles and Antimicrobial Performance of Electrospun Ethylene Vinyl Alcohol Copolymer (EvoH) Fibers Containing Ionic Silver Ions and Silver Nanoparticles." *Colloid and Polymer Science* 291, no. 6 (2013): 1381-92.
27. Shaukat, Muhammad Sajjad, Sonia Zulfiqar, and Muhammad Ilyas Sarwar. "Incorporation of Palladium Nanoparticles into Aromatic Polyamide/Clay Nanocomposites through Facile Dry Route." *Polymer Science Series B* 57, no. 4 (2015): 380-86.
28. Yeo, SY, WL Tan, M Abu Bakar, and J Ismail. "Silver Sulfide/Poly (3-Hydroxybutyrate) Nanocomposites: Thermal Stability and Kinetic Analysis of Thermal Degradation." *Polymer Degradation and Stability* 95, no. 8 (2010): 1299-304.
29. Díez-Pascual, Ana M, and Angel L Díez-Vicente. "Poly (3-Hydroxybutyrate)/Zno Bionanocomposites with Improved Mechanical, Barrier and Antibacterial Properties." *International journal of molecular sciences* 15, no. 6 (2014): 10950-73.
30. Torres-Giner, S., N. Montanes, T. Boronat, L. Quiles-Carrillo, and R. Balart. "Melt Grafting of Sepiolite Nanoclay onto Poly(3-Hydroxybutyrate-Co-4-Hydroxybutyrate) by Reactive Extrusion with Multi-Functional Epoxy-Based Styrene-Acrylic Oligomer." *European Polymer Journal* 84 (2016): 693-707.
31. Primeau, N., C. Vautey, and M. Langlet. "The Effect of Thermal Annealing on Aerosol-Gel Deposited SiO₂ Films: A Ftir Deconvolution Study." *Thin Solid Films* 310, no. 1 (1997): 47-56.

32. Pachekoski, Wagner Maurício, Carla Dalmolin, and José Augusto Marcondes Agnelli. "The Influence of the Industrial Processing on the Degradation of Poly(Hidroxybutyrate) - Phb." *Materials Research* 16 (2013): 237-332.
33. Mottin, Artur Caron, Eliane Ayres, Rodrigo Lambert Oréface, and Jairo José Drummond Câmara. "What Changes in Poly(3-Hydroxybutyrate) (Phb) When Processed as Electrospun Nanofibers or Thermo-Compression Molded Film?" *Materials Research* 19 (2016): 57-66.
34. Choudalakis, G., and A. D. Gotsis. "Permeability of Polymer/Clay Nanocomposites: A Review." *European Polymer Journal* 45, no. 4 (2009): 967-84.
35. Terada, Mikio, and R. H. Marchessault. "Determination of Solubility Parameters for Poly(3-Hydroxyalkanoates)." *International Journal of Biological Macromolecules* 25, no. 1 (1999): 207-15.
36. Tan, B., and N. L. Thomas. "A Review of the Water Barrier Properties of Polymer/Clay and Polymer/Graphene Nanocomposites." *Journal of Membrane Science* 514 (2016): 595-612.
37. Busolo, Maria A, Patricia Fernandez, Maria J Ocio, and Jose M Lagaron. "Novel Silver-Based Nanoclay as an Antimicrobial in Polylactic Acid Food Packaging Coatings." *Food Additives and Contaminants* 27, no. 11 (2010): 1617-26.
38. Rhim, JW, LF Wang, and SI Hong. "Preparation and Characterization of Agar/Silver Nanoparticles Composite Films with Antimicrobial Activity." *Food Hydrocolloids* 33, no. 2 (2013): 327-35.
39. Sanchez-Garcia, M. D., E. Gimenez, and J. M. Lagaron. "Morphology and Barrier Properties of Solvent Cast Composites of Thermoplastic Biopolymers and Purified Cellulose Fibers." *Carbohydrate polymers* 71, no. 2 (2008): 235-44.
40. Nyberg, C, and CG Tengstål. "Adsorption and Reaction of Water, Oxygen, and Hydrogen on Pd (100): Identification of Adsorbed Hydroxyl and Implications for the Catalytic H₂-O₂ Reaction." *The Journal of chemical physics* 80, no. 7 (1984): 3463-68.

Chapter IV

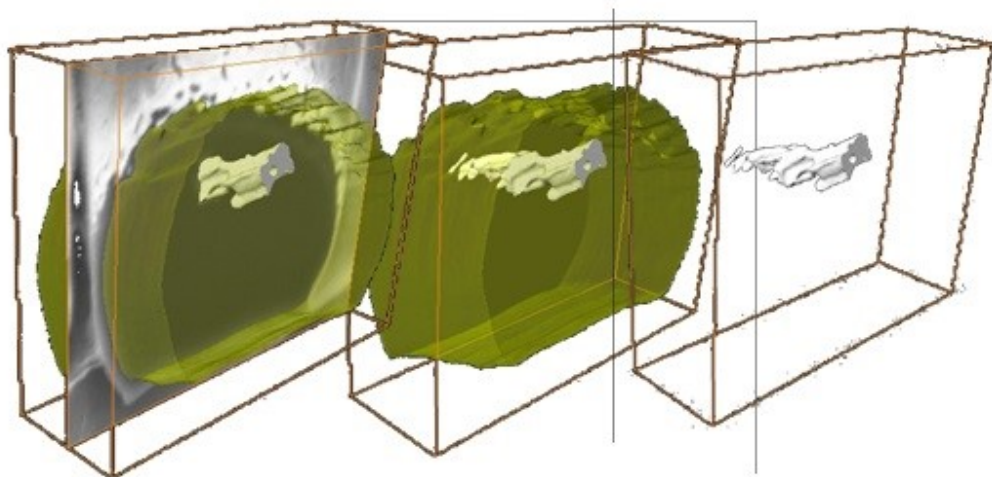
41. Singh, L. P., S. K. Bhattacharyya, G. Mishra, and S. Ahalawat. "Functional Role of Cationic Surfactant to Control the Nano Size of Silica Powder." *Applied Nanoscience* 1, no. 3 (2011): 117-22.
42. Nestorson, A., K. G. Neoh, E. T. Kang, L. Järnström, and A. Leufvén. "Enzyme Immobilization in Latex Dispersion Coatings for Active Food Packaging." *Packaging Technology and Science* 21, no. 4 (2008): 193-205.



Chapter V

Oxygen-Scavenging Multilayered Biopapers Containing Palladium Nanoparticles Obtained by the Electrospinning Coating Technique

Adriane Cherpinski, Piotr K. Szewczyk, Adam Gruszczyński, Urszula Stachewicz and Jose M. Lagaron. Oxygen-Scavenging Multilayered Biopapers Containing Palladium Nanoparticles Obtained by the Electrospinning Coating Technique. *Nanomaterials* 2019, 9(2), 262



Abstract

The main goal of this study was to obtain, for the first time, highly efficient water barrier and oxygen-scavenging multilayered electrospun biopaper coatings of biodegradable polymers over conventional cellulose paper, using the electrospinning coating technique. In order to do so, poly(3-hydroxybutyrate) (PHB) and polycaprolactone (PCL) polymer-containing palladium nanoparticles (PdNP) were electrospun over paper, and the morphology, thermal properties, water vapor barrier, and oxygen absorption properties of nanocomposites and multilayers were investigated. In order to reduce the porosity, and to enhance the barrier properties and interlayer adhesion, the biopapers were annealed after electrospinning. A previous study showed that electrospun PHB-containing PdNP did show significant oxygen scavenging capacity, but this was strongly reduced after annealing, a process that is necessary to form a continuous film with the water barrier. The results in the current work indicate that the PdNP were better dispersed and distributed in the PCL matrix, as suggested by focus ion beam-scanning electron microscopy (FIB-SEM) experiments, and that the Pd enhanced, to some extent, the onset of PCL degradation. More importantly, the PCL/PdNP nanobiopaper exhibited much higher oxygen scavenging capacity than the homologous PHB/PdNP, due to most likely, the higher oxygen permeability of the PCL polymer and the somewhat higher dispersion of the Pd. The passive and active multilayered biopapers developed here may be of significant relevance to put forward the next generation of fully biodegradable barrier papers of interest in, for instance, food packaging.

Keywords: Polyhydroxyalkanoates; Polycaprolactone; Biopapers; Palladium nanoparticles; Oxygen scavengers; Electrospinning; Fiber based packaging

1. Introduction

Active technologies, when applied to packaging refer to the incorporation of certain additives into the packaging structure. These additives may be loose as sachets within the design, attached to the inside part or, more recently, dispersed as an additive within the packaging materials, in order to maintain or even extend product quality and shelf-life [1].

Permeated or head space oxygen in packaged foods, beverages, and pharmaceuticals can promote a range of oxidative degradation reactions and support microbial growth, ultimately impacting on product quality and shelf-life. Oxygen-scavenging active packaging systems have therefore been explored, to control headspace oxygen content [2].

The application of oxygen scavengers is one of the most important active packaging technologies, which aim to remove any residual oxygen that is present in the food packaging. In some cases, the residual levels of oxygen in the package can be reduced to < 0.01 vol %, and actively controlled, which is not possible with other packaging systems [3].

Oxygen scavengers are by far the most commercially important sub-categories of active packaging, and the market has been growing steadily over the last few years. Almost all oxygen scavenger sachets used commercially are based on the principle of iron oxidation. On the other hand, oxygen-scavenging film is a more promising emerging packaging technology, because it contains the active material within the film, and consumers are not in favor of having foreign objects such as sachets in the

lining of their product packaging. With oxygen scavenger films, the consumer cannot physically see the oxygen scavenger materials, yet are able to experience its benefits [4–6].

The incorporation of scavengers into packaging films is a better way of resolving sachet-related problems. Scavengers may either be imbedded into a solid, dispersed in the plastic, or introduced into various layers of the package, including adhesive, lacquer, or enamel layers. Multi-layer oxygen scavengers more effectively absorb oxygen than single-layer scavenging systems [7].

Several new oxygen-scavenging technologies have been developed over the last decade, incorporating active substances and metals directly into packaging films or containers [8]. However, only a few of them have been successfully implemented in real food systems, due to, for instance, in the case of metals that function by chemical reduction, low reaction capacities and the need for triggering mechanisms, among other factors. Consequently, real application studies demonstrating the benefits of alternative oxygen-scavenging systems to particular food products are rather rare [9].

Recently, Hutter et al. [10] developed an oxygen scavenging film based on a catalytic system with palladium (CSP), which is able to reduce residual headspace oxygen very quickly. Palladium, in very low dosages, catalyzes the oxidation of hydrogen into water, and thus can remove the residual oxygen in the headspace of a modified atmosphere package containing hydrogen. Catalytic systems based on palladium have also

been reported to have other interesting applications, such as the construction of complex molecules [11–14].

The main difficulties of this approach are the dispersion of the scavenger in the matrix, the accessibility of the scavenger to oxygen, and the necessity of an activation system for the oxygen absorption reaction. Without an activation system, the oxygen-scavenging capacity of the active film would be consumed during storage, before the packaging is used [15].

In addition, consumer trends for better quality, fresh-like, and convenient food products have intensified over the last decade. Therefore, a variety of active packaging technologies have been developed to provide better quality, wholesome, and safe foods, and also to limit package-related environmental pollution and disposal problems.

Recently, the environmental impact of persistent plastic packaging wastes is raising general global concern, since disposal methods are limited. Biopolymers have been considered as a potential environmentally-friendly substitute for the use of non-biodegradable and non-renewable plastic packaging materials [16].

Polycaprolactone (PCL) is petroleum-based, but it can be degraded by microorganisms, and the polyhydroxyalkanoate (PHA) homopolymer called poly(hydroxybutyrate) (PHB) is produced from biomass or renewable resources, and it is readily biodegradable [17]. The aim of this emerging and developing field is to change the nature of polymer products and to minimize the environmental impact. Various approaches

are currently being investigated for possible polymers that may be utilized to design adequate environmentally friendly packaging [18].

Electrospinning is a feasible, efficient, and convenient technique for obtaining biopolymer-active nanofibers of interest in many application fields, such as active packaging, and since recently, it has also been scaled up for mass production [19–23]. Many factors influence fiber morphology and diameter, including solid concentrations, types of solvent, surface tension, additivation, solution viscosity, polymer molecular weight, flow rate, injector design, spinneret diameter, solution conductivity, injector to collector distance, and applied voltage. Of the many parameters discussed, concentration/solution viscosity, surface tension, and conductivity are probably the most important factors affecting the final fiber morphology and diameter [24–26]. A previous study [15] dealt with the development of a monolayer of oxygen-scavenging electrospun PHB containing palladium nanoparticles (PdNP). This monolayer demonstrated oxygen scavenging, but after annealing of the fibers to reduce porosity and to generate a water barrier, the material reduced the oxygen scavenging capacity to a significant extent.

The present work focuses, for the first time, on the preparation of significantly enhanced oxygen-scavenging bilayered coatings of PHB and PCL electrospun fibers, so-called biopapers, containing PdNP, so-called nanobiopapers, deposited on a cellulose paper, to derive an optimized passive and active coating of interest in biodegradable fiber-based packaging.

2. Materials and Methods

2.1. Materials

The microbial homobiopolyester PHB, P226F grade, was obtained from Biomer (Krailling Germany). This grade is certified as both compostable and food contact. It has a density of 1.25 g/cm³ and a melt flow rate (MFR) of 10 g/10 min when tested at 180 °C using a 5 kg load.

Polycaprolactone (PCL) (Mw: Mn 80 kDa), 2,2,2-trifluoroethanol (TFE) with 99% purity and D-limonene with 98% purity were purchased from Sigma-Aldrich S.A. (Madrid, Spain). Hexadecyltrimethylammonium bromide (CTAB) with 99% purity and palladium (Pd) nano-powder, <25 nm particle size measured by transmission electronic microscopy (TEM) and ≥ 99.5% trace metals basis, were also purchased from Sigma-Aldrich S.A. Chloroform (≥ 99%) and 1-butanol (99.5%) were purchased from AppliChem. All products were used as received without further purification. CTAB was selected as surfactant for PHB, because it is currently permitted for food contact applications by FDA and EFSA.

The conventional cellulose fiber-based packaging substrate was prepared using commercial bleached Kraft eucalyptus pulp as raw material, which was kindly provided by Ence-Celulosas y Energia S.A. (Madrid, Spain). Briefly, the pulp was disintegrated in a pulp disintegrator for 1 h at 3000 rpm to achieve a consistency of 1.5%. Paper sheets of 700 × 16 mm² with a final grammage of 75 g/m² were fabricated

in an isotropic Rapid-Köthen sheet former and conditioned at 23 °C and 50% of relative humidity (RH) according to ISO standard 187. The grammage and thickness were evaluated following ISO standards 536 and 534, respectively. Further details can be found in previous research [22,27].

2.2. Preparation of the Films

Before electrospinning, the PHB solution was prepared by dissolving 10 wt % in TFE under magnetic stirring conditions at 50 °C. The PHB/PdNP suspension was prepared by adding CTAB (0.25 wt.-% in the fibers) surfactant and PdNP (1 wt.-% in the fibers) to the PHB solution.

PCL was prepared by dissolving 10 wt % in butanol:chloroform (25:75) under magnetic stirring conditions at room temperature. To prepare the solution of PCL/PdNP, PdNP were added (1 wt % in the fibers) in the previous solution and dissolved while magnetically stirring.

The electrospinning device used was a high throughput Fluidnatek® LE-500, used in lab mode with temperature and relative humidity control pilot plant equipment from Bioinicia S.L. (Valencia, Spain), a variable 0–60 kV dual polarizer high-voltage power supply, and a scanning injector, to obtain a homogeneous deposition of fibers. To obtain the electrospun PHB layers, the biopolymer solution was transferred to a 30 mL plastic syringe and coupled by a Teflon tube to a stainless-steel needle ($\varnothing = 0.9$ mm) that was connected to the power supply. PHB and PCL solutions were electrospun at 25 °C and 30% RH on a flat metallic collector, for 2

and 1 hours under a steady flow-rate of 6 mL/hr and 2 mL/hr, respectively, using a motorized injector, scanning vertically toward a metallic grid collector. A distance between the injector and collector was both optimal at 15 cm, and the applied voltage was 16 kV and 12 kV.

The electrospun PHB and PCL coatings were subjected to an annealing post-processing step below the polymers' melting points, at temperatures of 160 °C and 50 °C, respectively using a hydraulic press 4122-model from Carver, Inc. (Indiana, IN, USA). This post-processing thermal treatment was applied for 5 s without pressure, to ensure the coalescence of the fibers mat into a continuous film. The conditions were selected based on the research conducted in previous works [21,28,29].

2.3. Characterization of the Films

2.3.1. Film Thickness

Prior to characterization, the whole thickness of all of the structures was measured by using a digital micrometer (Series S00014, having ± 0.001 mm accuracy, from Mitutoyo Corporation (Kawasaki, Japan)). Measurements were performed at three random positions, and values were averaged. All samples were stored before evaluation, in desiccators containing dried silica gel at 25 °C.

2.3.2. Focus Ion Beam Scanning Electron Microscopy (FIB-SEM)

Electrospun samples were prepared for microscopy evaluation by fixing nanofibers deposited on aluminum foil with carbon tape, and they

were gold coated with a 5 nm layer, using a rotary-pump sputter coater (Q150RS, Quorum Technologies, UK). The samples were imaged with a scanning electron microscope (SEM), using an accelerating voltage of 3 kV, 0.15 nA current and a working distance of 5 mm. 3D tomography of nanofibers with nanoparticles was achieved by using a dual beam system (NEON CrossBeam 40EsB, Zeiss, Germany) integrating a SEM with a focused ion beam (FIB). The sample stage was tilted at 54° so that the sample surface was perpendicular to the FIB direction [30], as demonstrated in previous research [31]. The 12–14 nm thick cross-sectional slices were milled by using FIB from the nanofiber sample at 30 kV and a beam current of 0.5 nA. [32,33]. The collected SEM images during FIB sectioning were filtered and reconstructed in 3D using Avizo Fire (version 6.3—FEI Edition, U.S.A.). To obtain the 3D reconstructions of the PCL fibers, 50 images and 108 images, respectively, for fiber 1 and 2 were used, maintaining the voxel size ($5 \times 5 \times 14$ nm). In the case of the PHB fibers, 50 images and a voxel size of $4 \times 4 \times 12$ nm were used. Additionally, Avizo Fire was used to calculate the Pd nanoparticle concentration in the investigated pieces of electrospun fibers from the 3D reconstructions already obtained.

2.3.3. Scanning Electron Microscopy

An S-4800 SEM microscope from Hitachi (Tokyo, Japan) was further used to observe the morphology of the electrospun PHB films, and their cross-sections and surfaces. Cross-sections of the samples were prepared

by cryo-fracture of the electrospun PHB films in liquid nitrogen. Then, they were fixed to beveled holders by using conductive double-sided adhesive tape, sputtered with a mixture of gold-palladium under a vacuum, and observed using an accelerating voltage of 5 kV.

2.3.4. Transmission Electronic Microscopy

The morphology and distribution of Pd nanoparticles were studied in electrospun fibers directly deposited onto clamping holders, and in the case of the films, on ultrathin microtomed sections as described in reference [15], using a Jeol 1010 (Hitachi, Tokyo, Japan) transmission electronic microscope, at an accelerating voltage of 80 kV.

2.3.5. Differential Scanning Calorimetry (DSC)

Thermal properties of neat PCL and Pd containing PCL electrospun fibers and films were evaluated by differential scanning calorimetry (DSC) using a Perkin-Elmer DSC 8000 (Waltham, MA, USA) thermal analysis system under a nitrogen atmosphere. The analysis was carried out on ~3 mg of each sample at a heating rate of 10 °C/min, from -25 °C to 125 °C, with subsequent cooling to -25°C. The DSC equipment was calibrated with indium as a standard, and the slope of the thermograms was corrected by subtracting similar scans of an empty pan. Tests were done at least in triplicate.

2.3.6. Thermogravimetric Analysis (TGA)

The TGA was performed in a TG-STDA Mettler Toledo model TGA/STDA851e/LF/1600 analyzer. The samples with an initial weight of typically about 15 mg were heated from 50 to 1300 °C at a heating rate of 10 °C/min under nitrogen/air flow.

2.3.7. Infrared Spectroscopy

Fourier transform infrared spectroscopy (FTIR) spectra were collected coupling the attenuated total reflection (ATR) accessory Golden Gate of Specac, Ltd. (Orpington, UK) to Bruker Tensor 37 FTIR equipment (Rheinstetten, Germany). Single spectra were collected in the wavelength range from 4000 to 600 cm^{-1} by averaging 20 scans at a resolution of 4 cm^{-1} .

2.3.8. Water Vapor Permeance

The water vapor permeance was determined by using the ASTM 2011 gravimetric method. To this end, 5 mL of distilled water was placed inside a Payne permeability cup ($\text{Ø} = 3.5 \text{ cm}$) from Elcometer Sprl (Hermalle-sous-Argenteau, Belgium). The films were placed in the cups so that on one side, they were exposed to 100% RH on the coated side, avoiding direct contact with water. The cups containing the films were then secured with silicon rings and stored in a desiccator at 0% RH using dried silica gel, at 25 °C. Identical cups with aluminum films were used as control samples to estimate water loss through the sealing. The cups were

weighed periodically using an analytical balance of ± 0.0001 g accuracy. The water vapor transmission rate (WVTR), also called water vapor permeance when corrected for permeant partial pressure, was determined from the steady-state permeation slope obtained from the regression analysis of weight loss data per unit area versus time, in which the weight loss was calculated as the total cell loss minus the loss through the sealing. Measurements were performed in triplicate.

2.3.9. Measurement of Oxygen Scavenging Activity

Round-bottom flasks (to Schlenk) from VidraFoc S.A. (Barcelona, Spain) with a polytetrafluoroethylene (PTFE) stopcock and a headspace volume of 50 cm^3 was used for the oxygen scavenging measurements. The flasks contained a valve for flushing gas in, and an O_2 -sensitive sensor spot (PSt3, detection limit 15 ppb, 0–100 % oxygen) from PreSens (Regensburg, Germany) was glued onto the inner side of the flasks for the oxygen depletion measurements. Electrospun fibers and multilayers containing electrospun fibers with same sample areas were cut ($5 \times 5 \text{ cm}^2$) and placed into the flasks. The flask was subsequently flushed for 30 s at 1 bar with a gas mixture containing 1 vol % oxygen, 4 vol % hydrogen, and 95 vol % nitrogen, which was provided by Abelló Linde, S.A. (Barcelona, Spain). The oxygen concentration in the cell was monitored by a non-destructive measurement method, using the OXY-4 mini (PreSens) multi-channel fiber optic oxygen meter for simultaneous read-outs of up to four oxygen sensors, and used with sensors based on a 2 mm

optical fiber. Oxygen concentrations over time were measured by linking the light-emitting (600–660 nm) optical fibers to the flasks' inner sensing spots. The sensor emits a certain amount of luminescence, depending on the oxygen concentration in the cell that is calibrated to yield the concentration by the equipment. All measurements were carried out at 23 °C and 50 % RH, simulating typical ambient conditions.

2.4. Statistical Analysis

The test data were evaluated through analysis of variance (ANOVA) using STATGRAPHICS Centurion XVI v 16.1.03 from StatPoint Technologies, Inc. (Warrenton, VA, USA). Fisher's least significant difference (LSD) was used at the 95% confidence level ($p < 0.05$). Mean values and standard deviations were also calculated.

3. Results and Discussion

3.1. Morphology of the Electrospun PCL Fibers and Films

As it can be seen from the observation of Figure 1 a,b, a narrow distribution of fiber diameter with an average at 2.75 ± 0.4 μm in PCL fibers, and 2.25 ± 0.7 μm in PCL/PdNP fibers was observed. The surface of the formed fibers was seen to be smooth and without beaded regions. The diameters of the fibers produced by electrospinning primarily depended on the spinning parameters, the most crucial being the solution concentration [34]. The smaller average diameter of the PCL/PdNP fibers can be attributed to an expected increase in conductivity, in agreement

with previous works making use of metallic nanoparticles. Thus, in the case of nanoparticles of ZnO, the authors hypothesized that the solution was seen to have a larger charge capacity, and then to be driven by a stronger electric force along the fibers; therefore, smaller fiber diameters were obtained [35].

The SEM images of the films' cross-sections, shown in Figure 1 c,d, indicated the presence of compact structures that resulted from the annealing post-processing step, which was in good agreement with previous works [20–22].

Additionally, FIB-SEM was used to cross-section the internal structure of the electrospun fibers. The detailed examples of the FIB-SEM images of PCL /PdNP fibers collected during FIB sectioning are presented in Figure 2, showing that Pd particles are incorporated in the two fibers. The cross-sectional images enabled the visualization of the PCL/PdNP fibers in 3D, as shown in Figure 3. The Pd nanoparticles were seen to be distributed along the PCL fibers, forming small agglomerates at different parts within the fiber cross-sections. Finally, the concentration of particles was also estimated per the given volume of the piece of fiber analyzed, and for the PCL fiber 1, this was 1.1 %, and for PCL fiber 2, this was 0.9 %. These observations suggest that the PdNP are better dispersed and distributed across the PCL fibers, and that the agglomerates may account for most of the Pd in the nanocomposites.

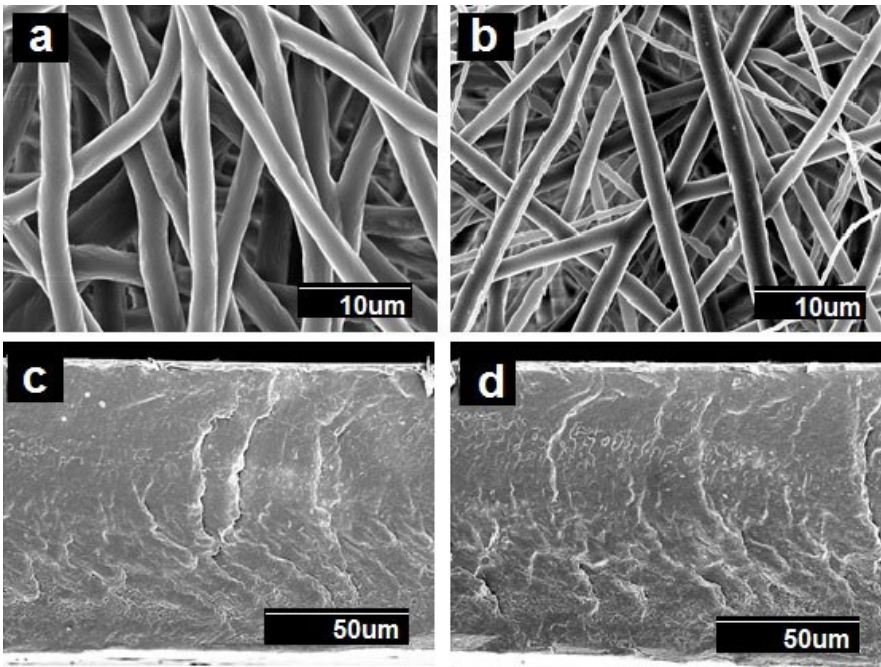


Figure 1. Scanning electron microscopy (SEM) images of the surface view and the cross-section of the polycaprolactone (PCL) fibers, with and without palladium nanoparticles (PdNP), and their respective annealed films: (a) Surface view of the neat PCL fibers; (b) Surface view of the PCL/PdNP fibers; (c) Cross-section of the neat PCL film; (d) Cross-section of the PCL/PdNP film.

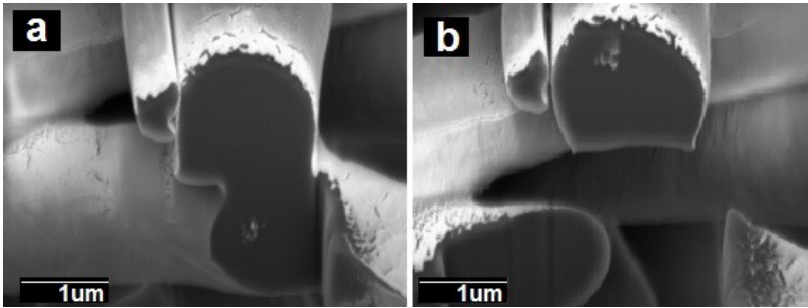


Figure 2. The cross-sectional SEM image of two PCL fibers with Pd nanoparticles after (FIB-SEM) sectioning. (a) PCL fiber 1 at the bottom with visible bright nanoparticles and (b) PCL fiber 2 at the top of the image with visible bright nanoparticles.

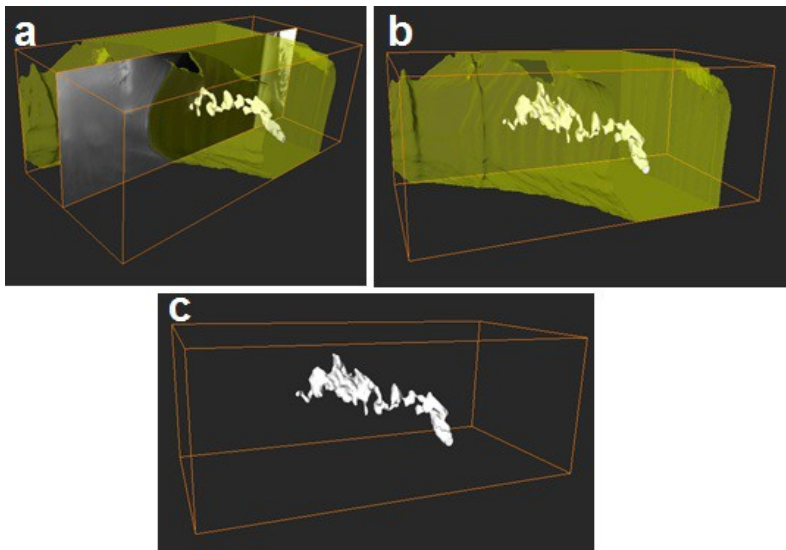


Figure 3. (a) The side view of 3D reconstructions of PCL fiber 1 (in semi-transparent yellow) and Pd nanoparticles (in white), including the SEM image (obtained from FIB sectioning) in the middle of the reconstruction, (b) 3D reconstruction of PCL fiber 1 with Pd

nanoparticles inside, (c) 3D reconstruction of particles only inside of PCL fiber 1. The binding box size for this reconstruction had the following dimensions $3.105 \times 1.185 \times 1.526$ μm .

In spite of the very revealing FIB-SEM results, the SEM technique is thought to be inadequate for resolving highly dispersed Pd nanoparticles within the polymer matrix [36]. In order to check for this, additional TEM experiments were conducted on the samples.

The additional TEM experiments displayed in Figure 4 indicate that the Pd nanoparticles, in agreement with the FIB-SEM experiments, exhibit a significant degree of aggregation within the fiber. Due to attractive forces (Van der Waals and others), particles tend to agglomerate, even in suspension, unless stabilized by equivalent repulsive forces such as surface charge or steric effects. Thus, the smaller the particle size, the greater the relative attractive forces per unit mass. This means that it becomes progressively more difficult to disperse nanoscale materials as the size decreases [37]. In any case, TEM also revealed the presence of some highly dispersed and distributed nanoparticles within the cross-section of the biopaper film. The smallest particles were seen to have diameters of $\text{ca. } 6 \pm 2$ nm, and they seemed evenly distributed throughout the fibers/film. Our prior studies of PHB/PdNP electrospun fibers, also showed a similar dispersion of Pd nanoparticles, with some clear agglomeration zones within the fibers [20].

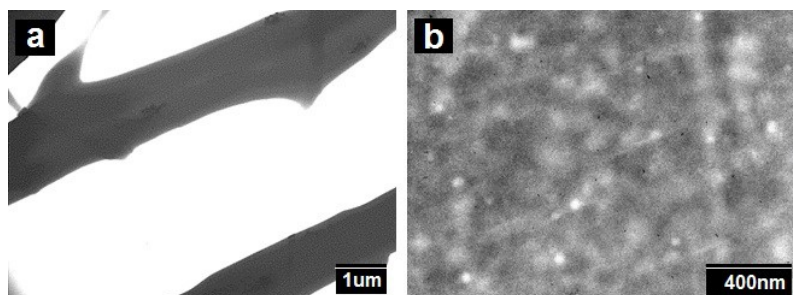


Figure 4. Scanning electron microscopy (TEM) images taken (a) directly on electrospun polycaprolactone (PCL) fibers containing palladium nanoparticles (PdNP) and on (b) microtomed sections of their corresponding annealed film.

3.2. FTIR Analysis of the PCL Electrospun Fibers and Films

The FTIR spectra of the electrospun neat PCL fibers and film, and the PCL/PdNP fibers and film are shown in Figure 5.

The PCL spectrum displays the characteristic peaks of C=O stretching vibrations at 1726 cm^{-1} , CH₂ bending modes at 1361 , 1397 , and 1473 cm^{-1} , and CH₂ asymmetric stretching at 2942 and symmetric stretching at 2862 cm^{-1} . The C-O-C stretching vibrations yield peaks at 1042 , 1107 and 1233 cm^{-1} . The bands at 1160 and 1290 cm^{-1} are assigned to C-O and C-C stretching in the amorphous and crystalline phases, respectively [38–40].

The overall PCL spectrum, including the main bands ascribed to PCL, such as the peaks at 2949 and 2865 cm^{-1} from methylene (CH₂) groups, and the strong carbonyl (C=O) peak centered at 1720 cm^{-1} , were not seen

to be affected either by incorporating PdNP, nor by the post-processing step, suggesting a lack of changes across the polymer molecular backbone.

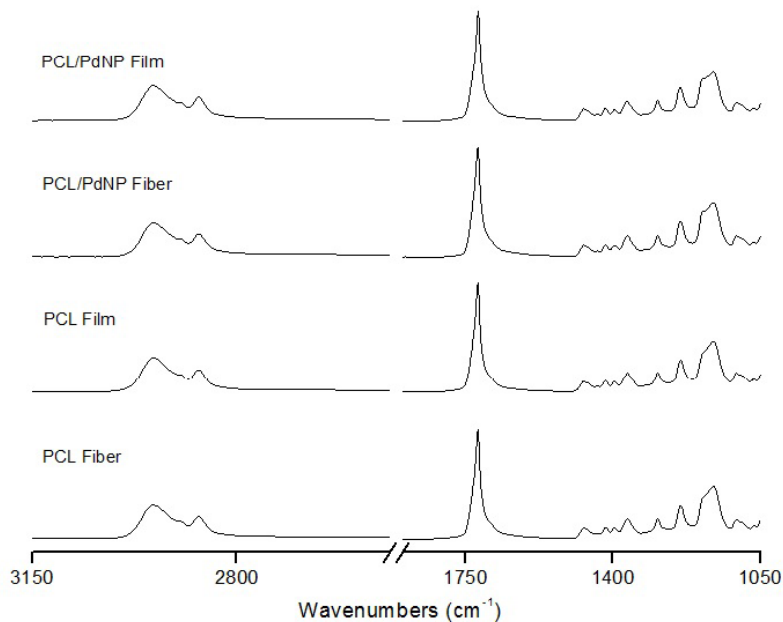


Figure 5. ATR-FTIR spectra of the electrospun PCL and the PCL/PdNP fiber mats and annealed films.

3.3. Thermal Properties of the PCL Electrospun Fibers

Table 1 shows the thermal properties, melting and crystallization points and enthalpies, in the first heating run and the subsequent crystallization run from the melt for the PCL and PCL/PdNP fibers mats. With the exception of the melting point, the rest of the thermal features

were very similar for the neat PCL and nanocomposite fibers. The melting temperature for pure PCL is typically reported at 60 °C, and the glass transition temperature is -60°C. As discussed, in the melting point, there was an increase of ca. 5 °C in comparison with the mean PCL, which must be explained by the addition of PdNP to the polymer. This may be due to the interaction of the polymer chains with the surface of the particles, which can change the chain kinetics in the region immediately surrounding the nanoparticles [41]. Similar results were reported by Bajsić et.al, where the melting point of the PCL/TiO₂ composites was found to increase slightly with an increasing load of TiO₂ micro- and nanoparticles [42].

Table 1. Thermal properties obtained by DSC in terms of melting temperature (T_m), normalized melting enthalpy (ΔH_m), crystallization temperature (T_c), and crystallization enthalpies (ΔH_c) for PCL and PCL/PdNP fibers.

Sample	T_m (°C)	ΔH_m (J/g)	T_c (J/g)	ΔH_c (J/g)
PCL Fibers	59.7 ± 1.2 ^a	33.8 ± 2.0 ^b	32.6 ± 0.9 ^b	41.4 ± 2.1 ^b
PCL/PdNP Fibers	64.7 ± 0.7 ^b	27.8 ± 1.5 ^a	31.2 ± 1.2 ^a	38.2 ± 0.9 ^a

Thermogravimetric analysis (TGA) was carried out to evaluate the degradation temperature of the PCL and PCL/PdNP fibers, including the curves of the first derivative analysis (blue lines) (see Figure 6), and the results are summarized in Table 2.

From Figure 6, it can be observed that PCL and PCL/PdNP initiated degradation at 342 and 355 °C, respectively, exhibiting two transition peaks: The first transition peaks were at 388 and 391 °C, and the second transition peaks were at 449 and 447 °C, respectively. The residual material of PCL and PCL/PdNP had a slight difference of ca. 0.8%, which is ascribed to the Pd that is present in the sample.

The data in the work reported here indicate that adding 1 wt % PdNP resulted in a slightly higher degree of thermal stability for the composite. Previous studies showed that other metallic nanofillers can impact the degradation temperature of PCL in different ways. Thus, Wang et al. demonstrated that the thermal stability of PCL was depressed by the incorporation of Fe₃O₄/GO nanoparticles, most likely due to the filler acting as a catalyst for polymer degradation [43]. Castro-Mayorga et al. also observed that the degradation temperature of poly(3-hydroxybutyrate-co-3-hydroxyvalerate) (PHBVs containing ZnO nanoparticles) showed lower degradation temperatures than that of pure PHBV3. This was attributed to the high thermal conductivity and catalytic properties of the ZnO nanoparticles [19]. Other studies suggest that a temperature drop can also be explained by the fact that nanoparticles can weaken to some extent the interactive force of polymer inter-chains, and hence assist the thermal decomposition of the nanocomposite [44]. However, in the current work, it was observed that the nanofiller induced a somewhat improved degree of thermal stabilization, which may be ascribed to a better adhesion between the nanoparticles and the polymer

matrix, resulting in both a hindered diffusion of volatile decomposition products, and/or the sorption of these over the filler surface, for the nanocomposites. Thus, the effect of a filler in thermal stability is in fact thought to depend on the type, content, interfacial interaction, and the degree of dispersion and distribution of this into the polymer matrix [45]. Thus, Ag [45], Fe, and Zn nanoparticles [46,47] have also been previously reported to enhance the thermal stability of PHA, supporting the current results for PCL.

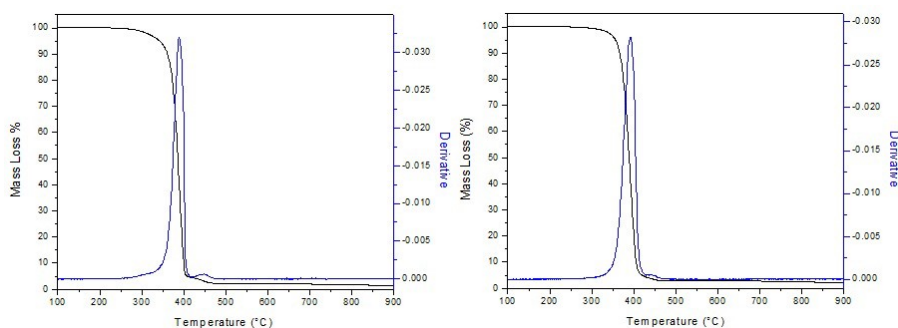


Figure 6. Thermogravimetric analysis (TGA) curves of the electrospun PCL (**left**) and PCL-containing palladium nanoparticles (PdNP) fibers (**right**).

Table 2. Values of thermal stability obtained from the thermogravimetric analysis (TGA) curves of the electrospun PCL and PCL/PdNP electrospun fibers in terms of degradation temperature at 5% of mass loss ($T_5\%$), maximum degradation temperature of the two degradation peaks (T_{d1} , T_{d2}), and residual mass at 900 °C (R_{900}).

Sample	T5% (°C)	Td1 (°C)	Td2 (°C)	R900 (%)
PCL	342.5 ± 4.1	388.0 ± 5.3	449.3 ± 4.2	1.3 ± 0.05
PCL/PdNP	355.1 ± 4.5	391.7 ± 3.6	447.8 ± 5.3	2.1 ± 0.03

3.4. PHB Electrospun Fiber Morphology

Similarly to the FIB-SEM investigation of PCL fibers, the sectioning of PHB mats was also carried out, and it is displayed in Figure 7. The SEM images in Figure 7 indicate that the PHB fibers morphology is similar to the one reported in earlier work, with the fiber cross-section ranging between 200 and 400 nm, and showing a smooth and beads-free fiber morphology [20–22].

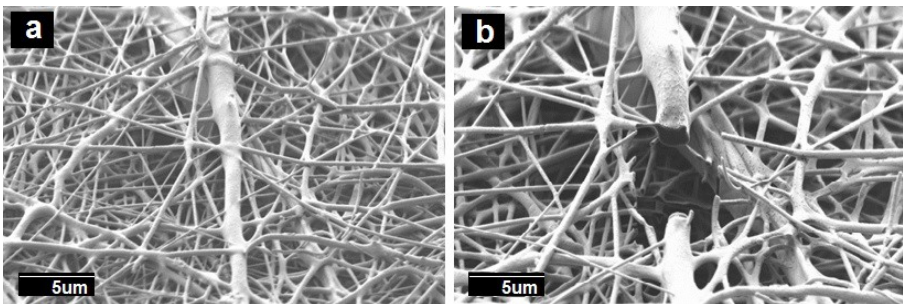


Figure 7. SEM images of the PHB sample. (a) Overview of PHB nanofibers, (b) PHB fibers after FIB sectioning.

The cross-section of the individual PHB fiber shown in Figure 8 revealed that the PdNP agglomerated even more strongly than seen in PCL at the core of fiber, even with a surfactant, which was also visualized

with the 3D reconstructions present in Figure 9. The 3D tomography allowed us to verify the presence of PdNP in the individual PHB fiber section scanned, similarly to the PCL data shown in Figure 3. The estimation of the Pd nanoparticle concentration of the fiber section analyzed yielded a concentration of 3%, suggesting that Pd is not as well-distributed as in PCL. This is a relevant finding that suggests that even when a surfactant was added to the PHB to improve filler distribution, as suggested by our earlier work [20], the distribution was still seen lower than for PCL without a surfactant. The reason for this could be explained by the different chemistry, but also by the fact that PHB is known to be a more rigid polymer that crystallizes to a greater extent into thick spherulites than PCL, which has more available free volume in the amorphous phase for dispersion.

Figure 10 shows the TEM analysis of the fibers and the corresponding film, which are in agreement with the FIB-SEM results, in which some Pd agglomerations could be observed but also the presence of some Pd nanoparticles dispersed and distributed across the material matrix. These results are also in agreement with previous findings for PHB [20].

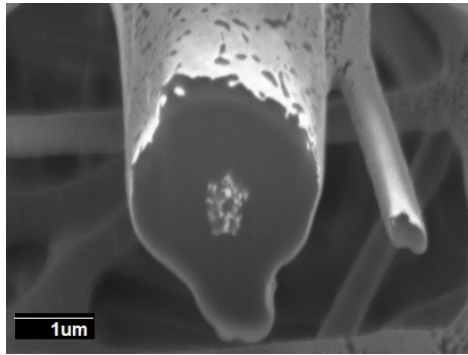


Figure 8. The cross-sectional SEM image of two PHB fibers with Pd nanoparticles after FIB sectioning.

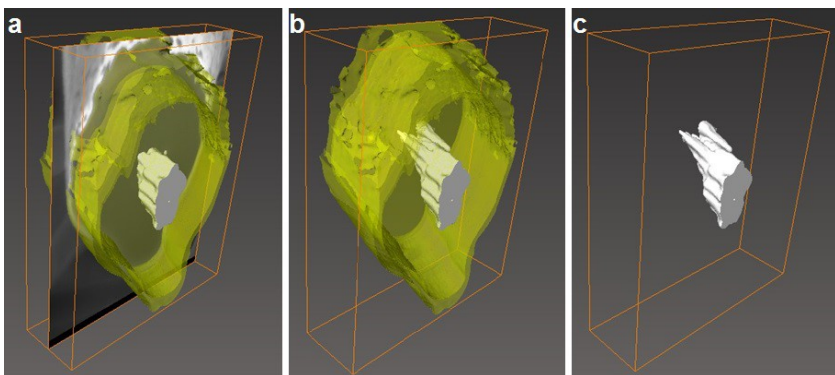


Figure 9. (a) The side view of the 3D reconstruction of the PHB fiber (in semi-transparent yellow) and Pd nanoparticles (in white), including the SEM image (obtained from FIB sectioning) in the middle of the reconstruction, (b) 3D reconstruction of the PHB fiber with Pd nanoparticles inside (c) 3D reconstruction of particles only from the inside of PHB fiber 2. The binding box size for this reconstruction had the following dimensions: $1.996 \times 2.464 \times 0.612$ nm.

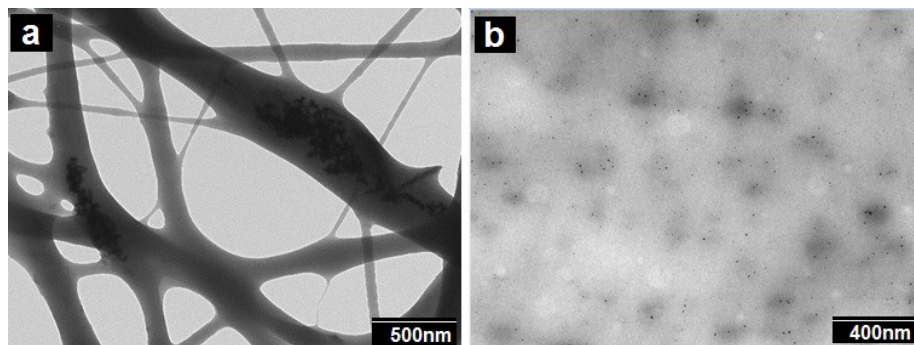


Figure 10. TEM images of (a) the PHB/PdNP fibers and (b) the PHB/PdNP film.

3.5. Morphology of the Multilayers

Figure 11 shows the SEM images of the multilayer structures obtained, which contain a paper substrate, and electrospun PHB/PCL fibers containing PdNP and their annealed films. In all cases, the amount of PCL deposited (1 hr coating time) was lower than the amount of PHB (2 hr coating time) because PHB is a better water barrier than PCL. In a previous paper, PHB containing Pd nanoparticles showed a significant decrease in oxygen absorption after annealing; hence, in this work we intended to explore the feasibility of using some PCL in the coating, in the hope of enhancing the oxygen scavenging effect of Pd. As a result, the PCL layer has a lower thickness, and it was set as the top layer. After annealing, there is an additional packing of the fibers, resulting in an even lower layer thickness, as can be seen in Figure 11.

The thickness of the paper layer was 117 μm and, of course, the fiber mean cross section of the paper was found to be higher, $18.37 \pm 2.45 \mu\text{m}$,

compared to the electrospun fibers. Figure 11 (b) shows that the surface of the electrospun neat PCL fibers exhibit significant fiber interconnections suggesting either remnant solvent induced coalescence and/or coarser fibers due to a drop in electric field as a result of deposition over other insulating materials as compared to direct deposition over the metallic collector (compare with Figure 1a).

The multilayers presented in Figure 11 c-f indicate the coalescence of fibers during the annealing step as expected, leading to a much less porous continuous film. Even though the samples had similar morphologies, it seems that sample (c) showed somewhat greater porosity, and sample (f) showed the least porosity. This was surely the effect of annealing in both coatings, leading to a higher level of packing structure.

In agreement with previous studies carried out on coatings with electrospun fibers over paper or polymer substrates, it is seen that the adhesion achieved after annealing between layers was very strong, due to the high surface-to-volume ratio of the electrospun fibers [22,48].

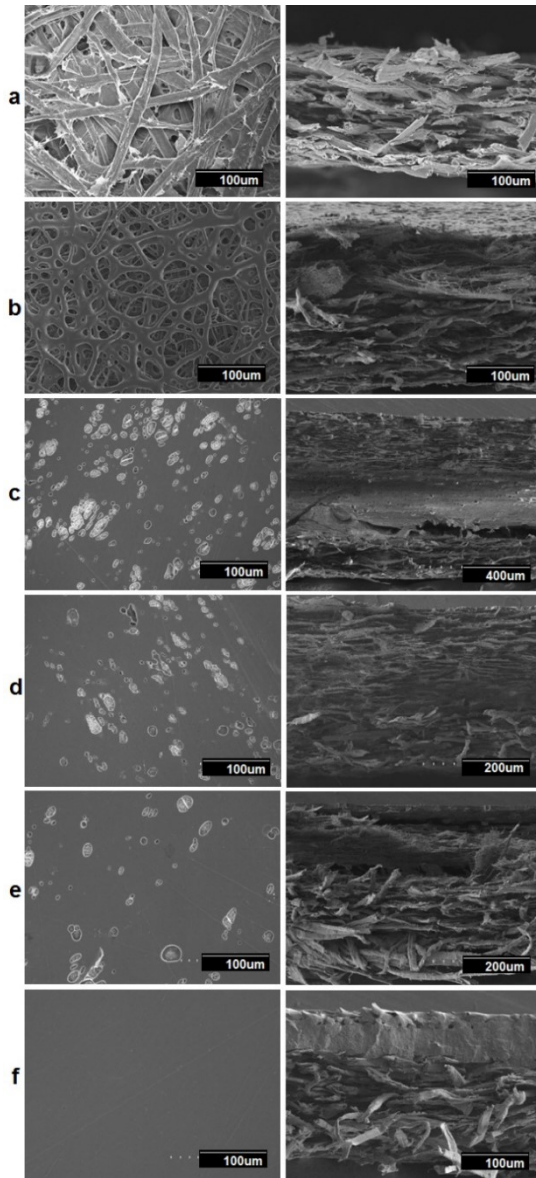


Figure 11. SEM images of the top view, and the cross section of (a) paper; (b) paper/PHB fibers/PCL fibers; (c) paper/PHB fibers/PCL-PdNP film; (d) Paper/PHB-PdNP fibers/PCL film; (e) Paper/PHB-PdNP fiber/PCL-PdNP film; (f) paper/PHB film/PCL-PdNP film.

3.6. *Passive and Active Barrier Properties of the Multilayers*

3.6.1. Water Vapor Passive Permeance

In general, the barrier properties of materials depend on the solubility and diffusion of the permeants, and hence, they depend on the permeant size, shape, and polarity; but also on the crystallinity, degree of cross-linking, and polymer chain segmental motion of the polymer matrix, among other factors [49,50].

The diffusion coefficient of water in an amorphous or semi-crystalline polymer is related to the particular molecular dynamics or segmental motions within the amorphous regions of the polymer. In addition, in semi-crystalline materials, a low crystallinity index and the formation of crystals of inferior quality confer a high degree of mobility to the macromolecular chains, resulting in lower barrier performance [51]. It is known that PHA is a better barrier material than PCL [52]. However, for fiber-based materials such as the paper/PHB fibers/PCL fibers multilayer generated here, the barrier performance was expected to be as low as paper, due to the existing porosity between the adjacent fibers.

The water permeance data of the multilayer samples are gathered in Figure 12. From this figure, it can be clearly seen that the samples that contained fibers and that had porosity at the surface did not significantly enhance the barrier of the multilayers compared to neat paper. However, it can also be seen that when the two electrospun coatings underwent

annealing, this led to a porosity reduction and stronger adhesion, and the water barrier performance was significantly increased.

The higher water barrier of the sample paper/PHB film/PCLPdNP film is then explained by a reduction in sample porosity, and also by the expected improvement in the crystalline morphology that occurs in the sample after annealing, which is known to be both impermeable to the diffusion of sorbed water molecules, and impose restraints to the mobility of the amorphous phase [53]. The barrier data gathered for this sample ($4.3 \times 10^{-11} \text{ kg/m}^2\cdot\text{s}^{-1}\cdot\text{Pa}^{-1}$) is in the same order of magnitude as the results obtained in a previous work for PHB ($9.6 \times 10^{-11} \text{ kg/m}^2\cdot\text{s}^{-1}\cdot\text{Pa}^{-1}$) [20].

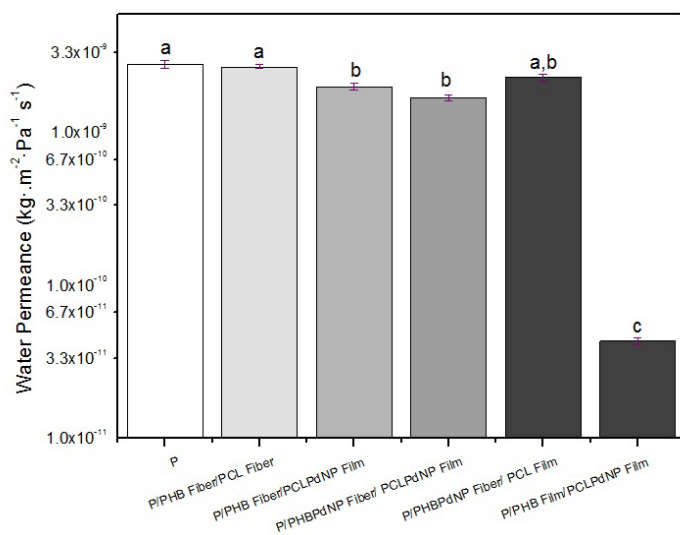


Figure 12. Water vapor permeance (WVP) of paper and Paper/PHB/PCL multilayers with and without palladium nanoparticles (PdNP). Different letters indicate significant differences among samples ($p < 0.05$).

3.6.2. Active Oxygen Scavenging Performance

Figure 13 shows the oxygen scavenging rate (OSR) of the PCL and PHB fibers, and the prepared paper based multilayers. The oxygen absorption of the fibers and resulting multilayers was investigated at 23 °C, with an initial oxygen concentration of 1.0 % in the headspace of the measuring flasks, and at an RH of 50 %. As reported earlier, due to the higher barrier of the material against water and oxygen compared to PCL, the PHB-PdNP fibers are not very efficient as oxygen scavengers at low or intermediate relative humidity, and even at high relative humidity as a film. However, PCL fibers and films are extremely quick at removing oxygen from the head space, suggesting that PCL is more adequate for hosting PdNP for oxygen scavenging purposes. The higher fractional free volume of the PCL polymer allows for moisture and oxygen to reach the catalyst quickly, and hence oxygen removal is more efficient. The greater reduction in the OSR of the fibers is, of course, related to the high surface-to-volume ratio of the electrospun fibers as compared to the annealed films. The dissociation rate of the hydrogen molecules into hydrogen atoms over the Pd surface in the films depends on the available surface area that is presented by the PdNP within the film.

As mentioned above, another important factor to be considered is that oxygen depletion is dependent on the RH conditions applied, and oxygen scavenging decreases when the RH increases [15,54]. In this work, we intended to conduct testing at medium relative humidities to simulate an intermedium case study. Figure 13 clearly indicates that, as expected,

neither the paper nor the neat PCL polymer had any oxygen scavenging capacity.

Figure 13 also indicates that the best performing multilayer materials, in terms of OSR were, as expected, paper/PHB fibers/PCL-PdNP film and paper/PHB-PdNP fibers/PCL-PdNP film. In the cases where the intermediate layer is a PHB film or where the PdNP are not at the surface, the performance is reduced, since oxygen and moisture will possess slower kinetics of diffusion.

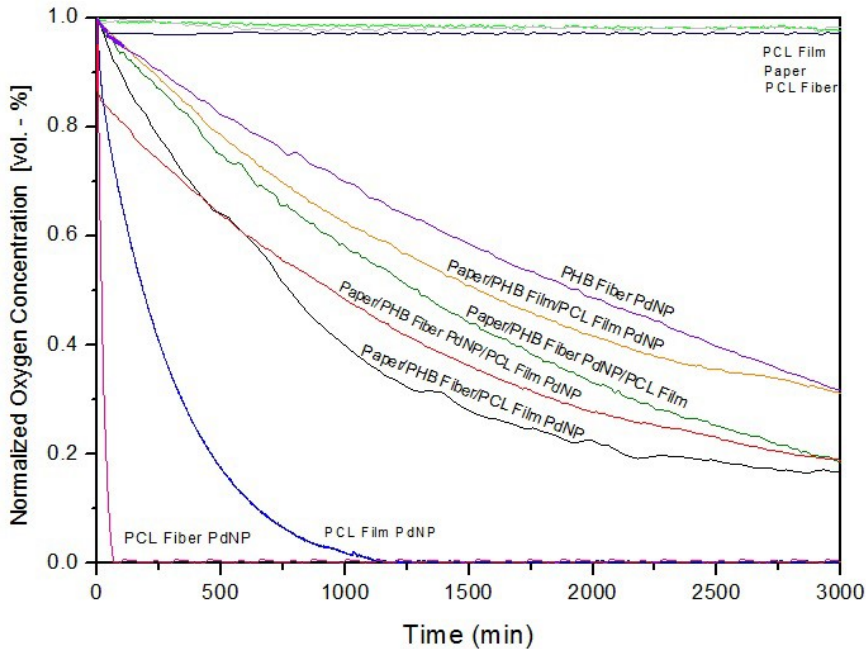


Figure 13. Oxygen depletion of PCL and PHB fibers, and paper/PHB/PCL multilayers and films with and without palladium nanoparticles (PdNP). Values were measured at 50% relative humidity (RH).

4. Conclusions

Electrospun nanobiopaper bilayer coatings of water barrier PCL and PHB biopolymers containing PdNP were here developed for the first time over conventional cellulose paper. Some of the materials were post-processed by annealing, to achieve both better adhesion among layers, and to form a continuous structure to improve the barrier properties to water. SEM and FIB-SEM results indicated that the PdNP agglomerated in certain areas of the fiber cross-section, but TEM results also indicated that some of the PdNP were dispersed and distributed within the biopolymer matrix. Better distribution of the PdNP was inferred for the PCL matrix. FIB-SEM 3D reconstruction was a very powerful tool for visualizing composites beyond the conventional SEM results, and it seen to exhibit good correspondence with TEM results. However, TEM was further able to resolve better at the nanoscale, and it showed that some of the PdNP were highly dispersed and distributed within the fibers. The water barrier was enhanced, as expected, after annealing of the fiber-based materials, but the annealing process also decreased the oxygen absorption capacity. A previous work indicated that with electrospun PHB fibers containing PdNP, the oxygen scavenging capacity of the films reduced to a significant extent after annealing, compared to the non-heated highly porous electrospun fibers. In this more advanced study on the topic, the oxygen scavenging of the PdNP was largely enhanced, even after annealing, by incorporating these within PCL, a more oxygen permeable material that is still biodegradable.

The fully biodegradable fiber-based multilayered materials developed here show their tremendous potential for becoming the next generation of barrier papers, with demonstrated water barrier and oxygen scavenging capacity that are of interest in, for instance, food packaging applications.

5. Acknowledgements:

A. Cherpinski would like to thank the Brazilian Council for Scientific and Technological Development (CNPq) of the Brazilian Government for her predoctoral grant (205955/2014-2). U. Stachewicz thanks the National Science Centre in Poland for the Sonata Bis 5 project, No 2015/18/E/ST5/00230 allowing this study, and a PhD scholarship for P.K. Szewczyk. The 3D imaging was supported by the infrastructure at the International Centre of Electron Microscopy for Materials Science (IC-EM) at AGH University of Science and Technology. This research was funded by the Spanish Ministry of Economy and Competitiveness (MINECO) project AGL2015-63855-C2-1-R, the H2020 EU YPACK (reference number 773872) and ResUrbis (Reference number 730349).

6. References

1. Kerry, J.P.; O'Grady, M.N.; Hogan, S.A. Past, Current and Potential Utilisation of Active and Intelligent Packaging Systems for Meat and Muscle-Based Products: A Review. *Meat Sci.* **2006**, *74*, 113–130.

2. Wong, D.E.; Andler, S.M.; Lincoln, C.; Goddard, J.M.; Talbert, J.N. Oxygen Scavenging Polymer Coating Prepared by Hydrophobic Modification of Glucose Oxidase. *J. Coat. Technol. Res.* **2017**, *14*, 489–495.
3. Yildirim, S.; Röcker, B.; Rüegg, N.; Lohwasser, W. Development of Palladium-Based Oxygen Scavenger: Optimization of Substrate and Palladium Layer Thickness. *Packag. Technol. Sci.* **2015**, *28*, 710–718.
4. Brody, A.L.; Strupinsky, E.P.; Kline, L.R. *Active Packaging for Food Applications*; CRC Press: Boca Raton, FL, USA, 2001.
5. Dobrucka, R.; Cierpiszewski, R. Active and Intelligent Packaging Food-Research and Development—A Review. *Pol. J. Food Nutr. Sci.* **2014**, *64*, 7–15.
6. Kaufman, J.; Lacoste, A.; Schulok, J.; Shehady, E.; Yam, K. An Overview of Oxygen Scavenging Packaging and Applications, 2000. Available online: <https://www.bakeryonline.com/doc/an-overview-of-oxygen-scavenging-packaging-an-0002>. (accessed on 08-10-17).
7. Ozdemir, M.; Floros, J.D. Active Food Packaging Technologies. *Crit. Rev. Food Sci. Nutr.* **2004**, *44*, 185–193.
8. Solovyov, S.E. Oxygen Scavengers. In *Kirk-Othmer Encyclopedia of Chemical Technology*; John Wiley and Sons; New York, NY, USA, 2000; pp. 1–31.
9. Yildirim, S.; Röcker, B.; Pettersen, M.K.; Nilsen-Nygaard, J.; Ayhan, Z.; Rutkaite, R.; Radusin, T.; Suminska, P.; Marcos, B.; Coma, V. Active Packaging Applications for Food. *Compr. Rev. Food Sci. Food Saf.* **2018**, *17*, 165–199.
10. Hutter, S.; Rüegg, N.; Yildirim, S. Use of Palladium Based Oxygen Scavenger to Prevent Discoloration of Ham. *Food Packag. Shelf Life* **2016**, *8*, 56–62.
11. Li, M.; Posevins, D.; Gustafson, K.P.J.; Tai, C.; Shchukarev, A.; Qiu, Y.; Bäckvall, J. Diastereoselective Cyclobutenol Synthesis: A

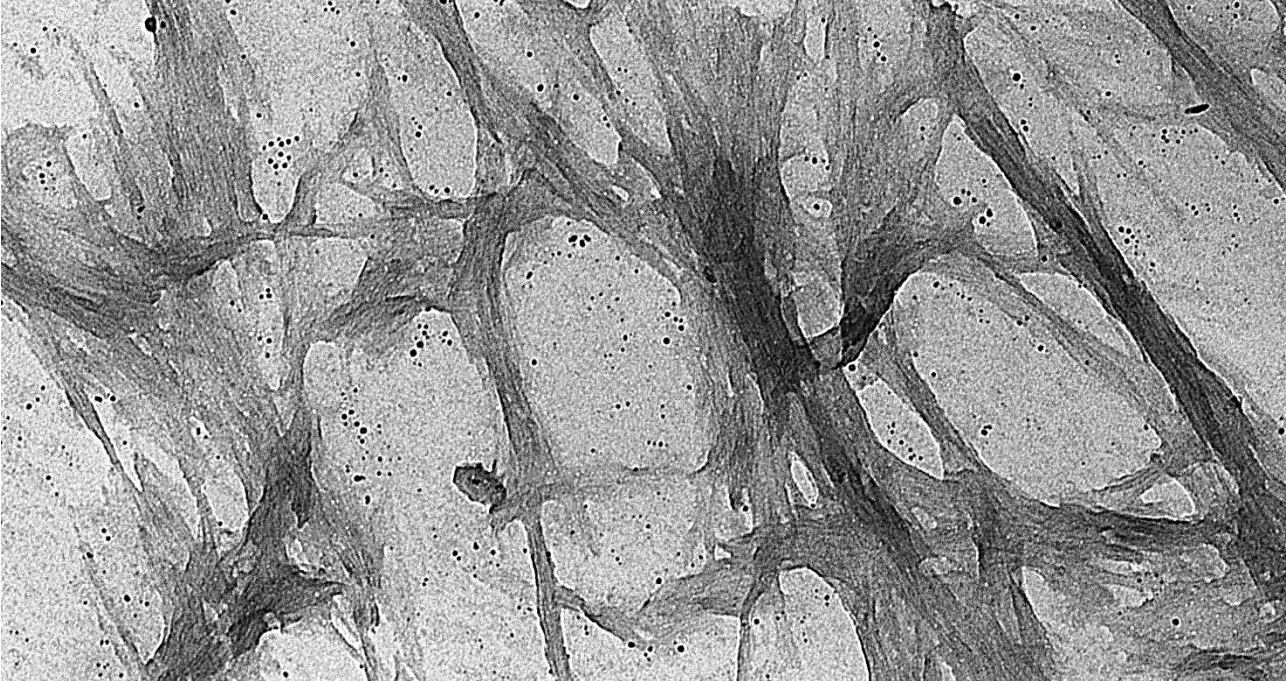
- Heterogeneous Palladium-Catalyzed Oxidative Carbocyclization-Borylation of Enallenols. *Chem. Eur. J.* **2019**, *25*, 210–215.
12. Li, M.; Inge, A.K.; Posevins, D.; Gustafson, K.P.J.; Qiu, Y.; Backvall, J. Chemodivergent and Diastereoselective Synthesis of Γ -Lactones and Γ -Lactams: A Heterogeneous Palladium-Catalyzed Oxidative Tandem Process. *J. Am. Chem. Soc.* **2018**, *140*, 14604–14608.
 13. Zhu, C.; Yang, B.; Backvall, J. Highly Selective Cascade C–C Bond Formation Via Palladium-Catalyzed Oxidative Carbonylation–Carbocyclization–Carbonylation–Alkynylation of Enallenes. *J. Am. Chem. Soc.* **2015**, *137*, 11868–11871.
 14. Zhu, C.; Yang, B.; Jiang, T.; Bäckvall, J. Olefin-Directed Palladium-Catalyzed Regio- and Stereoselective Oxidative Arylation of Allenes. *Angew. Chem. Int. Ed.* **2015**, *54*, 9066–9069.
 15. Mahieu, A.; Terrié, C.; Youssef, B. Thermoplastic Starch Films and Thermoplastic Starch/Polycaprolactone Blends with Oxygen-Scavenging Properties: Influence of Water Content. *Ind. Crop Prod.* **2015**, *72*, 192–199.
 16. Rhim, J.; Park, H.; Ha, C. Bio-Nanocomposites for Food Packaging Applications. *Prog. Polym. Sci.* **2013**, *38*, 1629–1652.
 17. Tokiwa, Y.; Calabia, B.P.; Ugwu, C.U.; Aiba, S. Biodegradability of Plastics. *Int. J. Mol. Sci.* **2009**, *10*, 3722–3742.
 18. Pan, Y.; Farmahini-Farahani, M.; O’Hearn, P.; Xiao, H.; Ocampo, H. An Overview of Bio-Based Polymers for Packaging Materials. *J. Bioresour. Bioprod.* **2016**, *1*, 106–113.
 19. Castro-Mayorga, Jinneth Lorena, et al. "The impact of zinc oxide particle morphology as an antimicrobial and when incorporated in poly (3-hydroxybutyrate-co-3-hydroxyvalerate) films for food packaging and food contact surfaces applications." *Food and Bioproducts Processing* 101 (2017): 32-44.
 20. Cherpinski, A.; Gozutok, M.; Sasmazel, H.; Torres-Giner, S.; Lagaron, J. Electrospun Oxygen Scavenging Films of Poly(3-Hydroxybutyrate)

- Containing Palladium Nanoparticles for Active Packaging Applications. *Nanomaterials* **2018**, *8*, 469.
21. Cherpinski, A.; Torres-Giner, S.; Cabedo, L.; Lagaron, J.M. Post-Processing Optimization of Electrospun Sub-Micron Poly(3-Hydroxybutyrate) Fibers to Obtain Continuous Films of Interest in Food Packaging Applications. *Food Addit. Contam. Part A* **2017**, *34*, 1817–1830.
 22. Cherpinski, A.; Torres-Giner, S.; Cabedo, L.; Méndez, J.A.; Lagaron, J.M. Multilayer Structures Based on Annealed Electrospun Biopolymer Coatings of Interest in Water and Aroma Barrier Fiber-Based Food Packaging Applications. *J. Appl. Polym. Sci.* **2018**, *135*, 45501.
 23. Hu, M.; Li, C.; Li, X.; Zhou, M.; Sun, J.; Sheng, F.; Shi, S.; Lu, L. Zinc Oxide/Silver Bimetallic Nanoencapsulated in Pvp/Pcl Nanofibres for Improved Antibacterial Activity. *Artif. Cells Nanomed. Biotechnol.* **2018**, *46*, 1248–1257.
 24. Deitzel, J.M.; Kleinmeyer, J.; Harris, D.E.A.; Tan, N.C.B. The Effect of Processing Variables on the Morphology of Electrospun Nanofibers and Textiles. *Polymer* **2001**, *42*, 261–272.
 25. Theron, S.A.; Zussman, E.; Yarin, A.L. Experimental Investigation of the Governing Parameters in the Electrospinning of Polymer Solutions. *Polymer* **2004**, *45*, 2017–2030.
 26. Zander, N.E. Hierarchically Structured Electrospun Fibers. *Polymers* **2013**, *5*, 19–44.
 27. Tarrés, Q.; Delgado-Aguilar, M.; Pèlach, M.A.; González, I.; Boufi, S.; Mutjé, P. Remarkable Increase of Paper Strength by Combining Enzymatic Cellulose Nanofibers in Bulk and Tempo-Oxidized Nanofibers as Coating. *Cellulose* **2016**, *23*, 3939–3950.
 28. Figueroa-Lopez, K.J.; Castro-Mayorga, J.L.; Andrade-Mahecha, M.M.; Cabedo, L.; Lagaron, J.M. Antibacterial and Barrier Properties of Gelatin Coated by Electrospun Polycaprolactone Ultrathin Fibers

- Containing Black Pepper Oleoresin of Interest in Active Food Biopackaging Applications. *Nanomaterials* **2018**, *8*, 199.
29. Lasprilla-Botero, J.; Storres-Giner, E.; Pardo-Figueroa, M.; Álvarez-Láinez, M.; Lagaron, J.M. Superhydrophobic Bilayer Coating Based on Annealed Electrospun Ultrathin Poly (E-Caprolactone) Fibers and Electrospayed Nanostructured Silica Microparticles for Easy Emptying Packaging Applications. *Coatings* **2018**, *8*, 173.
 30. Stachewicz, U.; Modaresifar, F.; Bailey, R.J.; Peijs, T.; Barber, A.H. Manufacture of Void-Free Electrospun Polymer Nanofiber Composites with Optimized Mechanical Properties. *ACS Appl. Mater. Interfaces* **2012**, *4*, 2577–2582.
 31. Stachewicz, U.; Qiao, T.; Rawlinson, S.C.F.; Almeida, F.V.; Li, W.; Cattell, M.; Barber, A.H. 3d Imaging of Cell Interactions with Electrospun Plga Nanofiber Membranes for Bone Regeneration. *Acta Biomater.* **2015**, *27*, 88–100.
 32. Bailey, R.J.; Geurts, R.; Stokes, D.J.; de Jong, F.; Barber, A.H. Evaluating Focused Ion Beam Induced Damage in Soft Materials. *Micron* **2013**, *50*, 51–56.
 33. Stachewicz, U.; Bailey, R.J.; Zhang, H.; Stone, C.A.; Willis, C.R.; Barber, A.H. Wetting Hierarchy in Oleophobic 3d Electrospun Nanofiber Networks. *ACS Appl. Mater. Interfaces* **2015**, *7*, 16645–16652.
 34. Garg, K.; Bowlin, G.L. Electrospinning Jets and Nanofibrous Structures. *Biomicrofluidics* **2011**, *5*, 013403.
 35. Yu, W.; Lan, C.; Wang, S.; Fang, P.; Sun, Y. Influence of Zinc Oxide Nanoparticles on the Crystallization Behavior of Electrospun Poly(3-Hydroxybutyrate-Co-3-Hydroxyvalerate) Nanofibers. *Polymer* **2010**, *51*, 2403–2409.
 36. Kane, M. Investigation and Characterization of the Dispersion of Nanoparticles in a Polymer Matrix by Scattering Techniques. Ph.D. Thesis, University of Florida, Gainesville, FL, USA, 2007.

37. Powers, K.W.; Palazuelos, M.; Moudgil, B.M.; Roberts, S.M. Characterization of the Size, Shape, and State of Dispersion of Nanoparticles for Toxicological Studies. *Nanotoxicology* **2007**, *1*, 42–51.
38. Abdelrazek, E.M.; Hezma, A.M.; El-khodary, A.; Elzayat, A.M. Spectroscopic Studies and Thermal Properties of Pcl/Pmma Biopolymer Blend. *Egypt. J. Basic Appl. Sci.* **2016**, *3*, 10–15.
39. Liverani, L.; Lacina, J.; Roether, J.A.; Boccardi, E.; Killian, M.S.; Schmuki, P.; Schubert, D.W.; Boccaccini, A.R. Incorporation of Bioactive Glass Nanoparticles in Electrospun Pcl/Chitosan Fibers by Using Benign Solvents. *Bioact. Mater.* **2018**, *3*, 55–63.
40. Mohamed, A.; Finkenstadt, V.L.; Gordon, S.H.; Biresaw, G.; Palmquist, D.E.; Rayas-Duarte, P. Thermal Properties of Pcl/Gluten Bioblends Characterized by Tga, Dsc, Sem, and Infrared-Pas. *J. Appl. Polym. Sci.* **2008**, *110*, 3256–3266.
41. Aliah, N.N.; Ansari, M.N.M. Thermal Analysis on Characterization of Polycaprolactone (Pcl) E Chitosan Scaffold for Tissue Engineering. *Int. J. Sci. Res. Eng. Technol.* **2017**, *6*, 2278–2882.
42. Bajsić, E.G.; Bulatović, V.O.; Slouf, M.; Šitum, A. Characterization of Biodegradable Polycaprolactone Containing Titanium Dioxide Micro and Nanoparticles. *Int. J. Chem. Nucl. Met. Mater. Eng.* **2014**, *8*, 572–576.
43. Wang, G.; Yang, S.; Wei, Z.; Dong, X.; Wang, H.; Qi, M. Facile Preparation of Poly(E-Caprolactone)/Fe₃O₄@Graphene Oxide Superparamagnetic Nanocomposites. *Polym. Bull.* **2013**, *70*, 2359–2371.
44. Hong, R.Y.; Qian, J.Z.; Cao, J.X. Synthesis and Characterization of Pmma Grafted Zno Nanoparticles. *Powder Technol.* **2006**, *163*, 160–168.
45. Castro-Mayorga, J.L.; Fabra, M.J.; Lagaron, J.M. Stabilized Nanosilver Based Antimicrobial Poly (3-Hydroxybutyrate-Co-3-

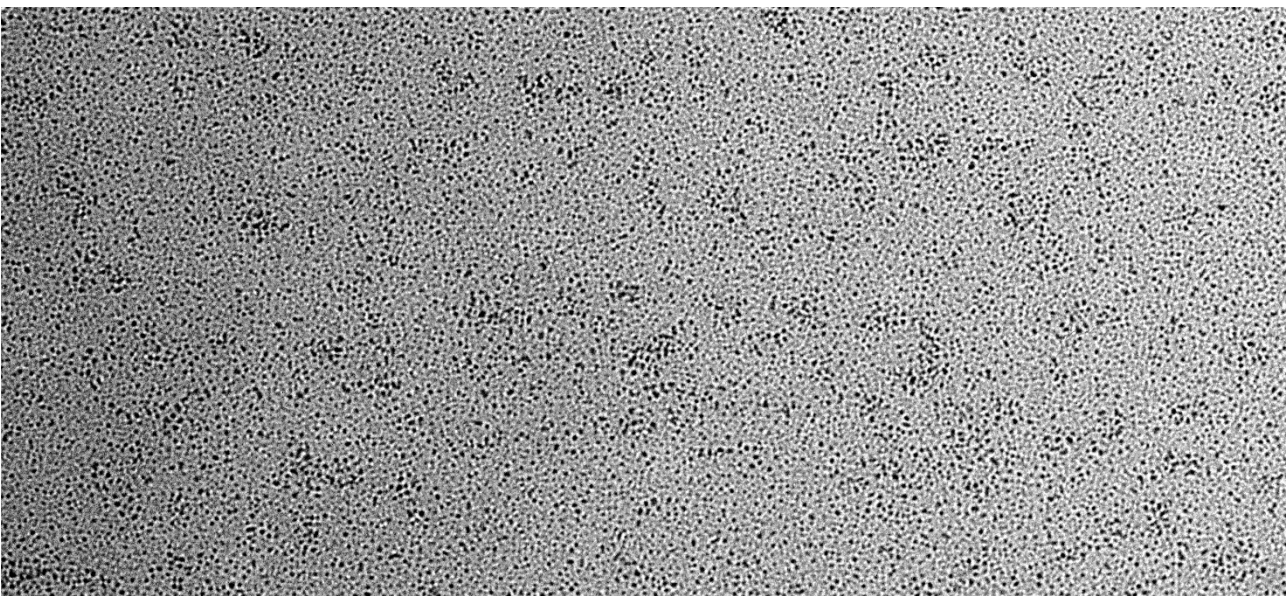
- Hydroxyvalerate) Nanocomposites of Interest in Active Food Packaging. *Innov. Food Sci. Emerg. Technol.* **2016**, *33*, 524–533.
46. Díez-Pascual, A.M.; Díez-Vicente, A.L. Poly (3-Hydroxybutyrate)/Zno Bionanocomposites with Improved Mechanical, Barrier and Antibacterial Properties. *Int. J. Mol. Sci.* **2014**, *15*, 10950–10973.
47. Panaitescu, D.M.; Ionita, E.R.; Nicolae, Cr.; Gabor, A.R.; Ionita, M.D.; Trusca, R.; Lixandru, Br.; Codita, I.; Dinescu, G. Poly (3-Hydroxybutyrate) Modified by Nanocellulose and Plasma Treatment for Packaging Applications. *Polymers* **2018**, *10*, 1249.
48. Cherpinski, A.; Torres-Giner, S.; Vartiainen, J.; Peresin, M.S.; Lahtinen, P.; Lagaron, J.M. Improving the Water Resistance of Nanocellulose-Based Films with Polyhydroxyalkanoates Processed by the Electrospinning Coating Technique. *Cellulose* **2018**, *25*, 1291–1307.
49. Siracusa, V. Food Packaging Permeability Behaviour: A Report. *Int. J. Polym. Sci.* **2012**, doi:10.1155/2012/302029.
50. Zeman, S.; Kubík, L. Permeability of Polymeric Packaging Materials. *Tech. Sci.* **2007**, *10*, 26–34.
51. Cavalcante, M.; Rodrigues, E.; Tavares, M.I. Avaliação Da Cristalinidade De Blendas De Polihidróxibutirato E Policaprolactona. In Proceedings of the 13th Congresso Brasileiro de Polímeros, Natal-RN, Brazil; 18-10-2015.
52. Sanchez-Garcia, M.D.; Gimenez, E.; Lagaron, J.M. Morphology and Barrier Properties of Nanobiocomposites of Poly (3-Hydroxybutyrate) and Layered Silicates. *J. Appl. Polym. Sci.* **2008**, *108*, 2787–2801.
53. Shogren, R. Water Vapor Permeability of Biodegradable Polymers. *J. Environ. Polym. Degrad.* **1997**, *5*, 91–95.
54. Gibis, D.; Rieblinger, K. Oxygen Scavenging Films for Food Application. *Procedia Food Sci.* **2011**, *1*, 229–234.



Chapter VI

Preparation and Evaluation of Oxygen Scavenging Nanocomposite Films Incorporating Poly(ethylene-co-vinyl alcohol), Pd Nanoparticles, and Cellulose Nanocrystals

Adriane Cherpinski, Atanu Biswas, Jose M. Lagaron, Alain Dufresne, Sanghoon Kim, Megan Buttrum, Eduardo Espinosa and H. N. Cheng .
Submitted for publication.



ABSTRACT

There is current interest in active packaging, where the packaging material exhibits desirable functions in addition to containment of product. One of these functions is to reduce the oxygen content in the package in order to minimize product oxidation and spoilage, and prolong product shelf-life. In this work, we have developed novel nanocomposites, comprising poly(ethylene-co-vinyl alcohol) (EVOH), Pd nanoparticles, and cellulose nanocrystals. The nanocellulose reduces Pd precursor to Pd metal and also enhances the physical properties of the EVOH film. Pd nanoparticles react with oxygen to serve as oxygen scavenger. The cellulose nanocrystals have also been optionally oxidized, which exhibit improved oxygen absorption. These features make the nanocomposites promising candidates as active packaging materials. Included in this work are the preparation and the characterization of these materials.

Keywords: active packaging, cellulose nanocrystals, ethylene-vinyl alcohol copolymer, polymer films, nanocomposite, oxygen scavenging, palladium nanoparticles

1. Introduction

A current trend in polymer research is active packaging, which aims to impart active functionalities to packaging beyond simple containment or protection of the product. Active packaging has the capability of maintaining product quality, extending the product shelf life (thereby minimizing price reductions), and enhancing cost-effectiveness of the product [1]. One of the common features of active packaging is to control the atmosphere inside the packaging, such as oxygen and moisture [2, 3].

Additionally, consumer acceptance of advanced food packaging techniques has increased as a result of the improvement in the quality of the product (such as color, flavor and freshness). Reduction of oxygen and moisture can decrease the possibility of product oxidation, spoilage, and corrosion; different methods are being used, including antioxidants, oxygen absorbers, desiccants, and corrosion inhibitors [4]. Amongst active packaging techniques, oxygen scavenging films have been recently developed.

Currently available oxygen scavengers are often inserted in the package in the form of a sachet. A problem of an oxygen scavenging film is the tendency of oxygen scavengers in the film to agglomerate, which can reduce not only the mechanical and thermal properties but also the oxygen absorbing capacity (Shin et al., 2011). A technical challenge is to design oxygen scavenging multilayer films without any agglomeration of the active ingredients.

Nanotechnology is a promising tool for active packaging because the nanomaterials have high surface-to-volume ratio and can enhance the functions of active substances utilized in the packaging. However, a polar polymer or surfactant is needed preferably to minimize aggregation of the nanoparticles in order to mitigate the high surface energy of nanoparticles [5-7].

Another recent development is the increasing use of agro-based materials and their derivatives as possible replacements for the synthetic polymers (Cheng et al., 2018). Such materials have the advantage of being easily available, cost competitive, nontoxic, ecofriendly and biodegradable. Some of the earlier attempts have involved the blends of synthetic polymers with biodegradable or biobased polymers [8]. Additional approaches have been developed involving entirely biobased materials and their derivatives (e.g., Biswas et al., 2018). Current trends suggest that biobased or biodegradable materials will be increasingly adopted in response to public awareness of plastic wastes and societal and legislative pressure.

As a nanomaterial and a biobased substance, nanocellulose has often been formulated into packaging films, particularly for food-related applications, and many review articles have appeared [9, 10]. Cellulose nanocrystals (CNCs) are often obtained from wood pulp or cellulose fibers by an acid hydrolysis, giving rise to highly crystalline and rigid nanoparticles [11]. Chemical modifications can be performed on the surface hydroxyl groups of CNCs, in order to impart hydrophilic or

hydrophobic character to the nanoparticle surface that can enhance the compatibility between CNC and the continuous matrix and improve the properties of the resulting nanocomposite. Examples of chemical modifications on nanocellulose include oxidation, esterification, etherification, silylation, and polymer grafting [8, 12, 13].

In addition to nanocellulose, a number of metal-based nanoparticles (NPs) have been incorporated into biobased materials, e.g., starch, cellulose, and chitosan [14]. The approach of producing a CNC-supported palladium NPs can obviate the need for chemical reductants and also improve the stability and catalytic activity of Pd NPs. Whereas the mechanism of nanocellulose-metal NP binding is still not fully understood, the combined CNC-Pd NP system has several advantages. Certainly, cellulose (and CNC) are available, biodegradable, and sustainable, and they should be attractive materials for commercial development [15]. The reaction of cellulose with 2,2,6,6-tetramethylpiperidine-1-oxyl (TEMPO) is well known to convert C6 hydroxyl on the anhydrous glucose unit of cellulose, which provide enhanced functionality and hydrophilicity for cellulose [16]. Nanocellulose surface is hydrophilic due to the hydroxyl groups present. Because most of the conventional CNCs are produced via sulfuric acid digestion, some sulfate esters likely reside at the surface. When the surface is further oxidized with TEMPO, aldehydes and carboxyls are formed, and all these functionalities may serve to effectively stabilize metal centers via the formation of dative bonds [17].

Among the most efficient methods, the combined organic-inorganic nanocomposite technique (i.e., polymers embedded with metal nanoparticles) proved to be highly effective [18]. A possible bugbear is the tendency of the nanoparticles to self-agglomerate. Thus, a useful preparative strategy in order to achieve improved dispersion in an aqueous medium or a polymer matrix is to minimize the attractive interactions between the nanoparticles by modifying the surface of the particles or the use of additives such as polymeric surfactants [19]. The properties of the resulting nanocomposite depend on the specific features of the nanoparticles, including their particle size, aspect ratio, specific surface area, volume fraction, polymer-particle compatibility, and dispersibility [20].

Poly(ethylene-co-vinyl alcohol) (EVOH) is commercially available, biodegradable, and attractive as a polymeric matrix for the design of nanocomposite films because the OH groups in the polymer can enhance compatibility with the nanoparticles [21]. EVOH is often used as a barrier for oxygen, CO₂, or organic vapor in food and beverage packages. Despite the fact that it is a synthetic polymer, EVOH is recyclable in the polyolefin regrind using existing infrastructure [22]. As EVOH is hydrophilic, it is often fabricated as part of a multilayer film between water-resistance polymer layers [23].

In this work, we have combined some of the techniques previously described in order to produce novel and workable films that can scavenge oxygen and have acceptable properties in active packaging. These

materials were based on CNCs and Pd NPs embedded in EVOH. The CNCs were also optionally oxidized, which permitted improved oxygen absorption of the resultant film. The nanocomposite films were characterized with various analytical techniques and their effectiveness in oxygen absorption was demonstrated.

2. Materials and methods

2.1. Materials

Ethylene-vinyl alcohol copolymer (containing 32 mol% of ethylene), sodium hydroxide (NaOH 97%), and poly(N,N-diallyldimethylammonium chloride) (poly-DADMAC) were acquired from Sigma-Aldrich (St Louis, MO, USA). The following chemicals were purchased from Fisher Scientific (Pittsburgh, PA, USA): palladium chloride ($\text{PdCl}_2 >95\%$), ethanol 100%, sodium hypochlorite (NaClO , 10–15 % available), sodium bromide (NaBr 99%), hydrochloric acid (HCl 37.5%), TEMPO (2,2,6,6-tetramethylpiperidine 1-oxyl, 98%) and 2-propanol (99.9%). Dialysis membrane Spectra/Por® (MW cut-off = 3.5 kD) was purchased from Spectrum Chemical (New Brunswick, NJ, USA). Cellulose nanocrystals (CNC aqueous slurry ~12% and CNC freeze dried ~98%) were purchased from the University of Maine (Orono, ME, USA). Millipore de-ionized water (Burlington, MA, USA) was used for all the experiments.

2.2. Methods

2.2.1. Preparation of TEMPO-oxidized CNC (TOCNC)

Oxidation experiments were carried out as previously reported [24-27]. The CNCs (1 g) were suspended in water (100 mL) containing TEMPO (TO, 0.016 g, 0.1 mmol) and sodium bromide (0.1 g, 1 mmol). A solution of NaOCl was added continuously with stirring at 500 rpm at room temperature in order to start the oxidation. The reaction was continued until the desired amount of NaClO (1.3-5.0 mmol NaClO per gram of cellulose) was dispensed. Throughout the process, 0.5 N NaOH was added to the reaction with a pH-stat in order to keep the pH at 10 until no NaOH consumption was observed. After oxidation, the reaction was quenched by the ethanol addition (ca. 1 mL), and 0.5 N HCl was added to increase the pH to 7. The resulting suspension of oxidized CNC (TOCNC) was washed and centrifuged three times with water, dialyzed, and then freeze-dried to yield a powder product. In this work the CNCs both in slurry and in powder form were subjected to TEMPO-oxidation to obtain samples called TOCNC-SP and TOCNC-PP, respectively.

2.2.2. Preparation of nano-sized cellulose/palladium (CNCs/PdNP)

The CNCs (0.3, 0.6 and 1 wt.%) were added to water (5 mL), and PdCl₂ (0.3, 0.6 and 1 wt.%) was added to water (5 mL). The pH was adjusted to 1 with HCl (37.5%). A mixture of PdCl₂ aqueous solution and CNC suspension was prepared and stirred for 20 min at room temperature in a 10–20 mL Biotage vial, similar to the method previously

reported [15]. The mixture was then placed in the Biotage microwave reactor (Biotage Initiator Microwave Synthesis Systems, Biotage AB, Uppsala, Sweden), which was programmed for 1 min pre-stirring and 2-h heating at 120 °C. After the reaction mixture was cooled to room temperature for the next procedure, the solution turned from pale brown to pale yellow color.

2.2.3. Preparation of EVOH solution and EVOH/CNCs/PdNP

For the preparation of EVOH solution, the polymer (10 wt %) was dissolved in a solvent mixture containing 2-propanol/water (70:30 v/v) and stirred at 100°C for 1 h. The EVOH solution was mixed with the previous CNC/Pd NP solutions and cooled for the next procedure.

2.2.4. Film-Casting Procedure

For film casting, the EVOH/CNC/PdNP solution was spread on a K 101 Control Coater apparatus (RK Print-Coat Instruments Ltd., Royston, UK) with a speed setting of 2. A closely wound meter bar kept the filmogenic solutions at a controlled thickness such that the dried film had a thickness of 10 ± 2 μm . After spreading, the films were dried under laminar air flow for 15 min at room temperature.

2.3. Characterization of CNCs

2.3.1. X-ray diffraction analysis (XRD)

X-ray diffraction analysis of the CNC powder samples, TOCNC-SP and TOCNC-PP, was carried out on a Bruker D8 Discover instrument (Karlsruhe, Germany). A monochromatic source $\text{CuK}\alpha 1$ was used over an angular range of $5\text{-}50^\circ$ at a scan speed of $1.56^\circ/\text{min}$. The Crystallinity Index (CI) of each CNC was computed with the use of the Segal Method [28].

2.3.2. Optical Transmittance

The optical transmittance of 0.1 wt.% solution was determined in a quartz cuvette using a Lambda 25 UV-Spectrometer (Perkin Elmer, Branford, CT, USA) from 400 to 800 nm. As reference, a spectrum of distilled water was obtained.

2.3.3. Cationic Demand

Each of the CNC samples (unmodified CNC, TOCNC-SP and TOCNC-PP), at 0.04 g dried weight, was diluted in 1 L distilled water and dispersed with a pulp disintegrator for 10 min at 3000 rpm. Then, 10 mL of the suspension was added with magnetic stirring to 25 mL of the cationic polymer, poly-DADMAC, for 5 min. The mixture was then centrifuged for 90 min at 4000 rpm in a Model 6K unit (Sigma Laborzentrifugen GmbH, Osterode am Harz, Germany). Thereafter, 10 mL of the supernatant were taken to a polyelectrolyte titrator (Mütek PCD

03, Herrsching, Germany), and an anionic polymer (sodium polyethylene sulphate) was added until the reading gave 0 mV. The amount of the anionic polymer consumed allowed the cationic demand to be calculated, according to the methodology described by Espinosa et al. (2017).

2.3.4. Carboxyl Content

The carboxyl content of CNCs was determined by conductometric titration following the methodology previously published by Besbes et al. (2011).

2.4. Characterization of films

2.4.1. Film thickness and conditioning

Before evaluation, all samples were equilibrated in desiccators containing dried silica gel at a constant temperature of 25°C for 1 week. The thickness of the films was measured with a Mitutoyo digital micrometer S00014 (Kawasaki, Japan). Three measurements at random positions of the film were made. Each reported value consisted of the average and the standard deviation. The accuracy was ± 0.001 mm.

2.4.2. Scanning electron microscopy (SEM)

The morphology of the EVOH films were evaluated via both cross-sections and surfaces on a Hitachi scanning electron microscope, S-4800 (Tokyo, Japan). The film cross-section was prepared by cryo-fracture of the EVOH films using liquid nitrogen. Each film was attached to beveled holders with conductive double-sided adhesive tape. A thin coating of gold and palladium was sputtered onto the specimen under vacuum. The

specimen was then observed on the SEM using an accelerating voltage of 5 kV.

2.4.3. *Transmission electronic microscopy (TEM)*

The Pd nanoparticles in the CNCs/PdNP solution were directly deposited onto clamping holders. The morphology and distribution of the Pd NPs were observed on a Jeol 1010 transmission electronic microscope (Hitachi, Tokyo, Japan) at an accelerating voltage of 80 kV.

2.4.4. *Fourier transform infrared (FTIR) spectroscopy*

FTIR spectra were acquired on the attenuated total reflection (ATR) accessory (Golden Gate of Specac, Ltd., Orpington, U.K.), which was coupled to a Bruker Tensor 37 FTIR instrument (Rheinstetten, Germany). A typical spectrum was collected in the 4000 to 600 cm^{-1} range by averaging 20 scans at a resolution of 4 cm^{-1} .

2.4.5. *Differential scanning calorimetry (DSC)*

Thermal properties of neat EVOH, EVOH/CNC/PdNP, and EVOH/TOCNC/PdNP films were evaluated by DSC using a Q2000 MDSC instrument (TA Instruments, New Castle, DE, USA) under nitrogen atmosphere. A small piece of each film (5mm x 5mm) was cut and weighed (~1mg) into a Tzero hermetic aluminum pan and sealed. The sample was equilibrated to 10 °C and then heated to 200 °C under nitrogen at a rate of 10 °C/min. The sample was then cooled at the same rate to 10 °C, and this heat-cool process was repeated. The equipment was

Chapter VI

calibrated with indium standard. Each sample was run in triplicate. Signal processing was achieved with the TA Instruments Universal Analysis 2000 software (version 4.5A).

2.4.6. Thermogravimetric analysis (TGA)

TGA was conducted on a Q500 TGA instrument (TA Instruments, New Castle, DE, USA). Typically, a square piece of film (about 10mm x 10mm) was cut and placed on a tared, open platinum TGA pan. The sample was heated from room temperature up to 800 °C under nitrogen at a rate of 10 °C/min. Along with weight loss data, the differential thermogravimetric weight loss (DTG, %/°C) was recorded as well. Each sample was run in triplicate.

2.4.7. Water Vapor Permeability (WVP)

The WVP value was determined gravimetrically according to the ASTM E96-95 method. A small sample of the film was placed at the top of a Payne permeability cup ($\varnothing = 3.5$ cm) from Elcometer Sprl (Hermalle-sous-Argenteau, Belgium) that contained 5 mL distilled water. One side of the film was exposed to 100% RH, but not in direct contact with water. The cup and the film were then sealed with silicon rings and placed in a desiccator containing dried silica at 24 °C and 47% RH. An identical setup with aluminum films served as a control sample to estimate water loss through the seal. The cups were weighed periodically over a 24-h period with ± 0.0001 g accuracy. The water vapor transmission rate (WVTR),

which could be converted to WVP when corrected for permeant partial pressure, was determined from the steady-state permeation slope obtained from the regression analysis of weight loss data per unit area versus time, from which the weight loss was calculated as the total cell loss minus the loss through the seal. Measurements were performed in triplicate.

2.4.8. Measurement of oxygen scavenging activity

The same method as reported earlier (Cherpinski et al., 2018) was used for the oxygen scavenging experiment. This involved round-bottom flasks (Schlenk) from VidraFoc S.A. (Barcelona, Spain) with a PTFE stopcock and a headspace volume of 50 cm³. The flasks contained a valve for gas flushing, and O₂-sensitive sensor spot (PSt3, detection limit 15 ppb, 0 – 100 % oxygen) from PreSens (Regensburg, Germany) was glued onto the inner side of the flasks for the oxygen depletion measurements. The sample films of same thickness were cut (4 × 4 cm²) and placed in the flasks. The flask was subsequently flushed for 30 s at 1 bar with a gas mixture containing 1 vol.% oxygen, 4 vol.% hydrogen, and 95 vol.% nitrogen, which was provided by Abelló Linde, S.A. (Barcelona, Spain). The oxygen concentration in the cell was monitored by a non-destructive measurement method using the OXY-4 mini (PreSens) multi-channel fiber optic oxygen meter for simultaneous read-out of up to 4 oxygen sensors, used with sensors based on a 2-mm optical fiber. Oxygen concentrations over time were measured by linking the light-emitting (600–660 nm)

optical fibers to the flask's inner sensing spots. The sensor emitted a certain amount of luminescence depending on the oxygen concentration in the cell that was calibrated to yield the concentration by the equipment. All measurements were carried out at 23 °C and 100 % RH.

2.5. Statistical analysis

The test data were evaluated through analysis of variance (ANOVA) using STATGRAPHICS Centurion XVI v 16.1.03 from StatPoint Technologies, Inc. (Warrenton, VA, USA). Fisher's least significant difference (LSD) was used at the 95% confidence level ($p < 0.05$). Mean values and standard deviations were also calculated.

3. Results and discussion

3.1. Cationic demand, carboxyl content and optical transmittance

The stability of CNC suspension depends on the fiber surface charge. In order to study the stability of the different samples used in this work, the cationic demand and the carboxyl content were analyzed (Table 1). The cationic demand increases when CNC is subjected to TEMPO oxidation due in part to the increase in the carboxyl groups by the selective oxidation of the C6 primary hydroxyl groups of cellulose. These carboxyl functionalities increase the anionic charge on the cellulose surface, thereby enhancing repulsion and decreasing agglomeration among the fibers. A reduction in aggregated fibers result in greater surface area and expose more surface hydroxy groups. The hydrophilicity of the fibers is also enhanced [29]. Moreover, these carboxyl groups on

cellulose can directly interact with metal ions, thus obviating the use of anchoring molecules [30].

The optical transmittance of the CNC suspensions is associated with the content of nanofibrillated material, being more transparent when the size of cellulose nanocrystals is smaller (Table 1, column 4). The oxidized CNC samples present lower transparency values due to the presence of aggregates that correspond presumably to a higher specific surface area and stronger hydrogen bonding between the nanocrystals [31].

3. Results and Discussion

3.1. Cationic demand, carboxyl content and optical transmittance

The stability of CNC suspension depends on the fiber surface charge. In order to study the stability of the different samples used in this work, the cationic demand and the carboxyl content were analyzed (Table 1). The cationic demand increases when CNC is subjected to TEMPO oxidation due in part to the increase in the carboxyl groups by the selective oxidation of the C6 primary hydroxyl groups of cellulose to C6 sodium carboxylate groups. Carboxyl groups on the cellulose surface increase the overall surface's negative charge, which generates repulsion between fibers. More individualized fibers translate into a larger specific surface area, which exposes more of the hydroxyl groups on the surface of the cellulose fiber. The hydrophilicity of the fibers is also enhanced [30]. Moreover, the formation of carboxyl sites in cellulose structure permits

the direct coordination of metal ions in its structure, thus obviating the use of anchoring molecules for that purpose [31].

The optical transmittance of the CNC suspensions is associated with the content of nanofibrillated material, being more transparent when the size of cellulose nanocrystals is smaller (Table 1, column 4). The oxidized CNC samples present lower transparency values due to the presence of aggregates that correspond presumably to a higher specific surface area and a stronger hydrogen bonding between the nanocrystals [32].

Table 1. Characterization of unmodified CNC powder and TEMPO-oxidized powder samples, TOCNC-SP and TOCNC-PP.

Sample	Cationic Demand ($\mu\text{eq/g}$)	Carboxyl Content ($\mu\text{mol COOH/g}$)	T_{800} (%)
CNC powder	448.44 ± 38.44	64.88 ± 40.59	97.22
TOCNC-SP	$1,284.89 \pm 9.19$	482.05 ± 58.43	57.38
TOCNC-PP	$1,314.30 \pm 0$	418.94 ± 37.88	40.97

3.2. X-ray Diffraction (XRD) Analysis

The XRD patterns for CNCs are shown in Figure 1. The diffraction peaks of CNCs at $2\theta = 15.0, 16.5, 22.3$ and 34.4 are assigned to the $(\mathbf{1}\bar{\mathbf{1}}\mathbf{0})$, (110) , (200) and (004) planes, respectively, which represent the crystalline structure of cellulose I [32]. Cellulose II presents diffraction peaks at 12.1 and 20.1° associated with the $(\mathbf{1}\bar{\mathbf{1}}\mathbf{0})$ and (110) planes [33]. TOCNC-SP presents only cellulose I contribution; however, TOCNC-PP and CNC powder contain both cellulose I and cellulose II polymorphs. Cellulose II

usually ensues from cellulose I by two distinct routes, i.e., mercerization (alkali treatment), and regeneration (solubilization and recrystallization) or acid hydrolysis of mercerized cellulose, but the detailed mechanism of this phenomenon for nanocellulose is still being studied [34, 35]. All samples present a crystallinity index around 70% due to the removal of most parts of amorphous regions; however, 30% of CNC composition is still composed of residual amorphous cellulose.

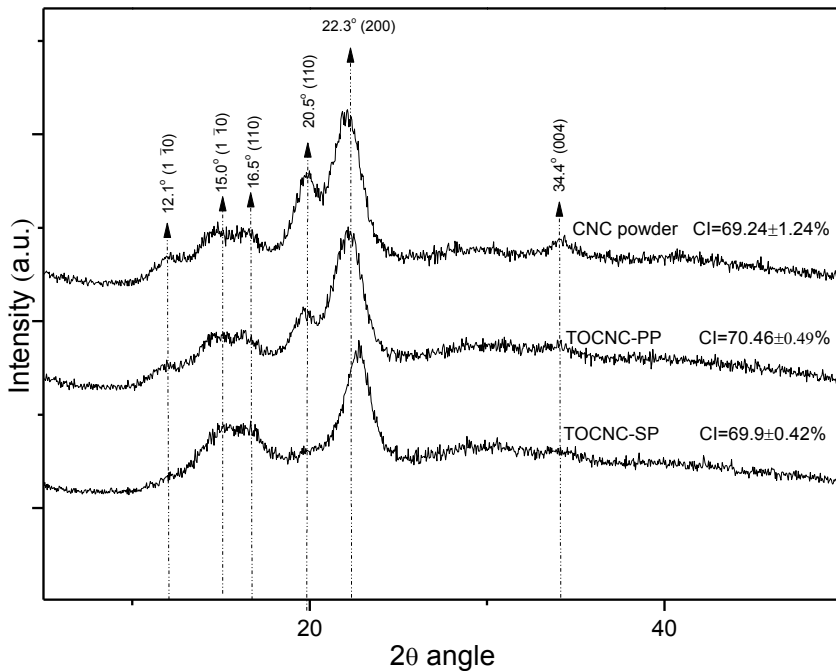


Fig. 1. XRD patterns of CNCs, the samples from top to bottom being unmodified CNC powder, TOCNC-PP, and TOCNC-SP

3.3. Morphology of nanocomposite Films

The contact transparency of neat EVOH film and EVOH with different concentrations of CNCs/Pd is shown in Figure 2. All the films were found to exhibit similar contact transparency and significantly different from that of the neat EVOH film. Thus, a good dispersion of the PdNP must have been achieved. However, samples C, D and E with 0.6 and 1 wt. % of PdNP showed a yellow color probably due to the presence of the Pd nanoparticles.



Fig. 2. Photographs of films containing: (A) neat EVOH 10%; (B) EVOH/CNC (0.3% wt.-%)/ PdNP (0.3 wt.-%); (C) EVOH/CNC (0.6 wt.-%)/PdNP (0.6 wt.-%); (D) EVOH/CNC (1 wt.-%)/PdNP (1 wt.-%); (E) EVOH/TOCNC (1 wt.-%)/PdNP (1 wt.-%).

3.4. Scanning electron microscopy (SEM)

The morphology of the materials was analyzed by SEM. As observed in Figure 3, the film surface (Figure 3b and 3c) was altered by adding CNCs/PdNP and revealed roughness when compared with the neat EVOH film (Figure 3a) that exhibited a relatively smoother surface. The photomicrographs of the cross-sections obtained presented a similar morphology that verified the presence of spherical domains dispersed in a matrix for samples with CNCs/PdNP, without agglomerates, and this

confirmed the efficient dispersion of the nanoparticles. This observation was in agreement with contact transparency data, which suggested that CNCs/PdNP particles were highly dispersed into the EVOH polymeric matrix.

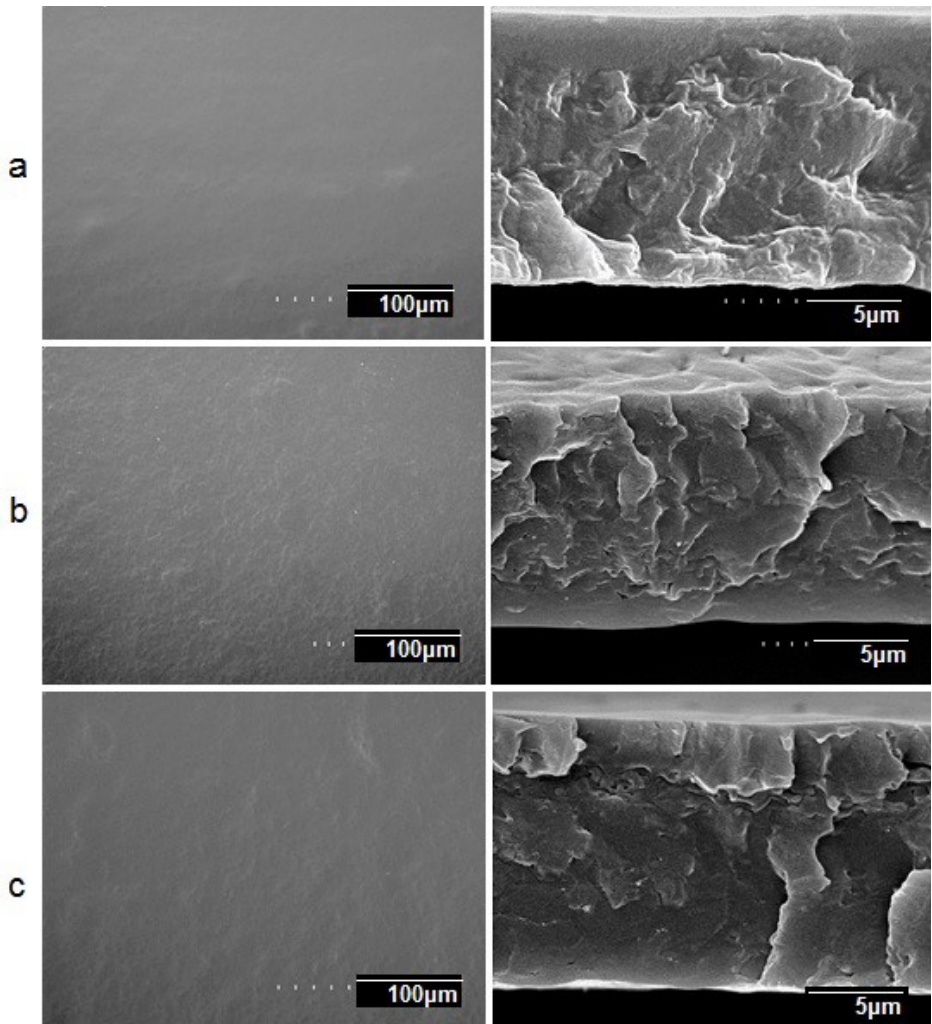


Fig. 3. Scanning electron microscopy (SEM) images taken on the surface view and cross-section: (a) EVOH film; (b) EVOH/CNC/PdNP film; (c) EVOH/TOCNC/PdNP film.

3.5. Transmission electron microscopy (TEM)

Transmission electron microscopy was used to characterize the dispersion and the spatial distribution of PdNP onto CNC and TEMPO-treated CNC. Figure 4 shows a typical TEM image obtained for the dried CNCs/PdNP solutions, where some agglomeration of CNCs could be seen probably resulting from the drying process. The particle size of PdNP is important in the context of catalysis; in general, smaller particle sizes entail larger surface areas, which tend to enhance the catalytic process [36]. In the present case, the diameter of PdNPs varied between 20 and 35 (± 5) nm and the CNCs acted as both the reducing agent and the support in the process. An analysis of the PdNP dispersion (Figure 4a and 4b) clearly showed the observed difference. In Figure 4a, the PdNPs were sparsely located on the CNC with partial aggregation; in comparison, the PdNPs supported by TOCNC (Figure 4b) were homogeneously distributed on the surface of CNC. This result confirmed the interaction between the PdNPs and the dissociated carboxyl groups on the surface of TOCNC, where the C atom of carboxyl group accepted the electrons from Pd, thereby enabling a more uniform immobilization of the PdNP on the TOCNC support [37]. Figures 4c and 4d show TEM images taken on the nanocomposite films. From the images, CNC and PdNP can be observed to be intimately dispersed and distributed throughout the polymer matrix, being more evident in the TOCNC sample, as expected.

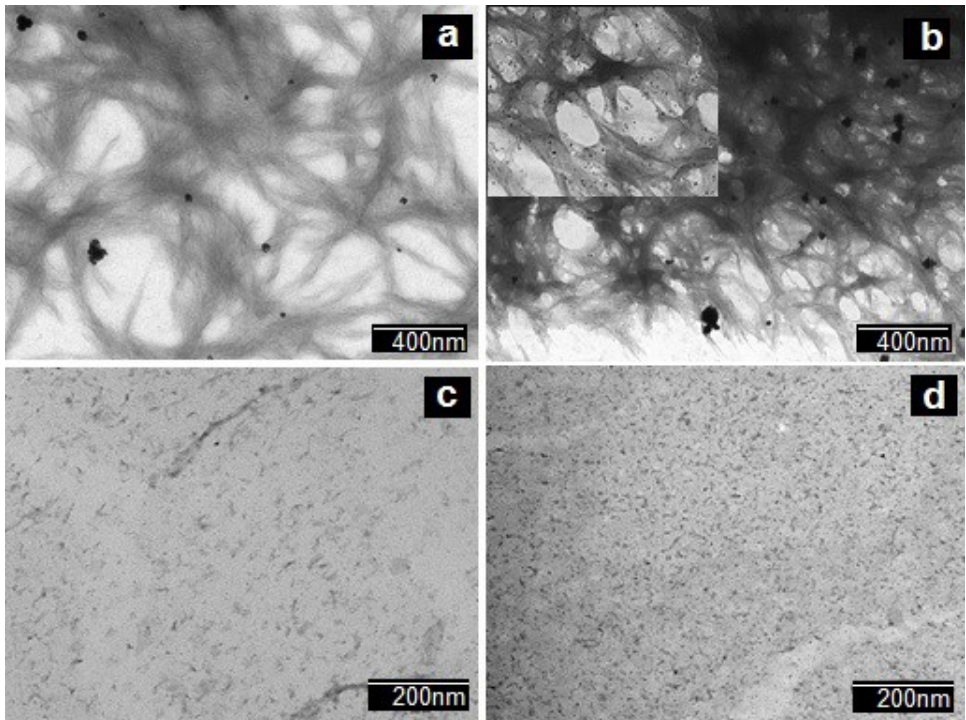


Fig. 4. Transmission electron microscopy (TEM) images taken directly from dried suspension of CNCs containing palladium nanoparticles (PdNPs): a) CNC, b) TOCNC; and TEM images taken from ultramicrotomed cross sections of the nanocomposite films: c) EVOH/CNC/PdNP Film and d) EVOH/TOCNC/PdNP Film.

3.6. FTIR analysis of the EVOH films

FTIR studies were conducted to investigate the changes in chemical structure of TOCNC and respective EVOH films with CNCs/PdNP addition (Figure 5). The IR spectrum for cellulose is well known, and some representative peaks can be found at $3200\text{--}3500\text{ cm}^{-1}$ (O-H stretching), $2850\text{--}3000\text{ cm}^{-1}$ (C-H stretching), and $1060\text{--}1162\text{ cm}^{-1}$

(C–O and C–O–C stretching bond); these peaks are not influenced by TO-mediated oxidation (Tang et al., 2017; Xiaodong Wu et al., 2013). When cellulose is selectively oxidized in position 6, the IR spectrum is known to change [38]. The most important change in the spectrum of modified nanocellulose can be observed by the appearance of new bands at 1605 cm^{-1} and 1730 cm^{-1} that could be attributed to $-\text{COONa}$ due to the C=O stretching of carboxyl groups and free carboxyl groups [39].

For EVOH film (Figure 5) the characteristic peaks can be found at 3340 cm^{-1} (–OH stretching), 2945 cm^{-1} (–CH₂ anti-symmetric stretching) and 2912 cm^{-1} (–CH anti-symmetric stretching), 1417 cm^{-1} (–CH₂ asymmetric stretching) and 1336 cm^{-1} (–CH asymmetric stretching), 1092 cm^{-1} (C–O stretching), and 850 cm^{-1} (–CH out-of-plane deformation). Moreover, the peaks at 1650 and 850 cm^{-1} may possibly be associated with residual C=O or C=C group vibrations in EVOH [40]. The 1% CNCs and 1% of PdNP added to the EVOH polymeric matrix were not enough to produce changes, as was shown by Choo et al. (2016), where they prepared poly(vinyl alcohol) (PVOH)-chitosan (CS) polymeric blends with different contents of TO-oxidized cellulose nanofiber (TOCN) (0, 0.5, 1.0 and 1.5 wt %) via the solution casting method. They observed only minor changes due to the incorporation of TOCN that resulted from the low weight ratio of TOCN added to form the bio-nanocomposite films. Martínez-Sanz et al. (2013a) also observed that the characteristic bands from cellulose were only apparent for concentrations greater than 3 wt % bacterial CNCs in EVOH films.

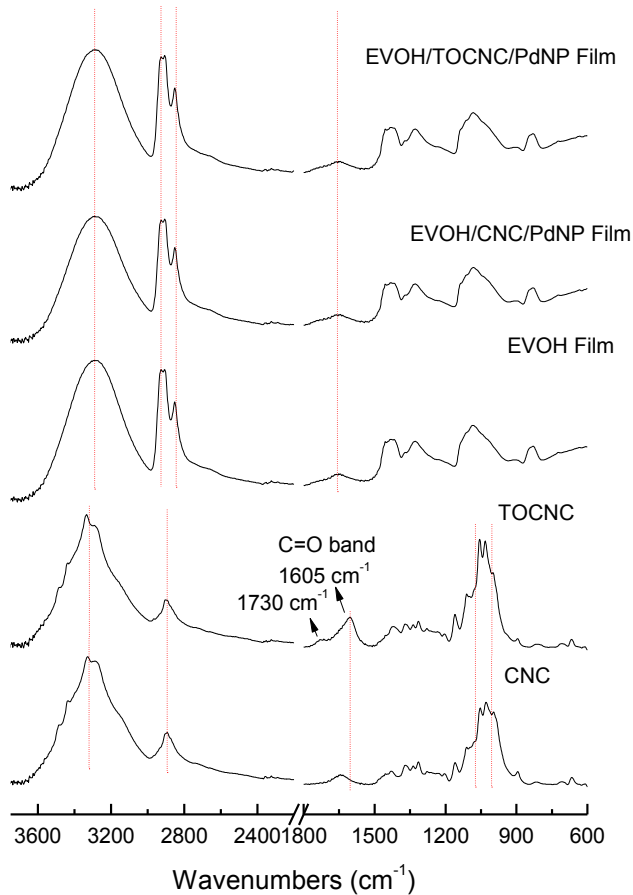


Fig. 5. ATR-FTIR spectra of the CNC, TOCNC, EVOH Film, EVOH/CNC/PdNP and EVOH/TOCNC/PdNP Films.

3.7. Thermal analysis

For an investigation of how CNCs/PdNP content affected the thermal stability of EVOH nanocomposite films, DSC and TGA analyses were performed. Table 2 shows the glass transition temperature (T_g),

melting temperature (T_m), and melting enthalpy (ΔH_m), and crystallization temperature (T_c) of the films as determined by DSC analysis of the dry samples. From the results, it can be seen that CNC reduces the polymer melting point, suggesting an antinucleating effect for the filler. This is confirmed by the observed reduction in crystallization temperature in the composites, which suggests that crystallization is hindered to some extent leading to smaller and more defective crystals. However, crystallinity was not observed to be reduced to a similar extent, suggesting that CNC does not impair crystallization but just leads to a more defective crystalline morphology, hence the lower melting point. The polymer T_g is also not affected to a significant extent by the presence of CNC.

Table 2. Thermal properties obtained by DSC in terms of glass transition (T_g), melting temperature (T_m), normalized melting enthalpy (ΔH_m), and crystallization temperature (T_c) for EVOH, EVOH/CNC/PdNP, and EVOH/TOCNC/PdNP films on first heating and subsequent crystallization runs.

Sample	T_m	ΔH_m	T_c	T_g
EVOH	166.6±2.1	29.0±3.0	160.2±2.0	46.7±0.8
EVOH/CNC PdNP	145.0±1.4	29.8±2.8	145.9±3.8	45.2±1.0
EVOH/TOCNC-PdNP	146.9±1.1	26.6±1.5	141.6±3.5	45.3±2.7

The thermal stability of EVOH nanocomposite films evaluated by TGA is shown in Figure 6 and Table 3. The EVOH nanocomposite films

presented a two-step degradation pattern similar to that of neat EVOH; however, greater thermal resistance was observed for the EVOH nanocomposites, which indicated that the presence of CNCs/PdNP significantly influenced the thermal degradation patterns of the EVOH nanocomposite films.

In the TGA curves, an initial weight loss was observed for all samples, corresponding to the elimination of the absorbed moisture. Similar results were reported for EVA membranes by Puente et al. (2015), where the initial weight loss (~100 °C) was related to the water tightly bound to the polymer structure. In the DTG curves (Figure 6d), a low temperature shoulder peak could be seen, which indicated the presence of some free water [41].

A decrease was observed in the maximum degradation rate for EVOH/TOCNC/PdNP film at 366 °C (Figure 6d). The maximum degradation temperature for neat EVOH film was near 381 °C and for EVOH/CNC/PdNP film 394°C, representing a decrease in the temperature of degradation about 15 °C and 28 °C, respectively. Fraschini et al. (2017) studied the thermal behavior of CNCs before and after oxidation, where an increase in the carboxyl content caused a gradual decrease in the thermal stability of the oxidized CNC samples. This was probably because the presence of charged groups on CNCs induced their earlier degradation during heating [42]. For all the samples, the residual

weight of the nanocomposite films at 800 °C was consistent with the theoretical values.

An important observation was the onset decomposition temperature of EVOH/CNCs/PdNP nanocomposites, which was slightly higher than that of the neat EVOH film and EVOH/CNCs films (Figure 6d), suggesting that the thermal stability of CNCs could be improved by the incorporation of the palladium nanoparticles.

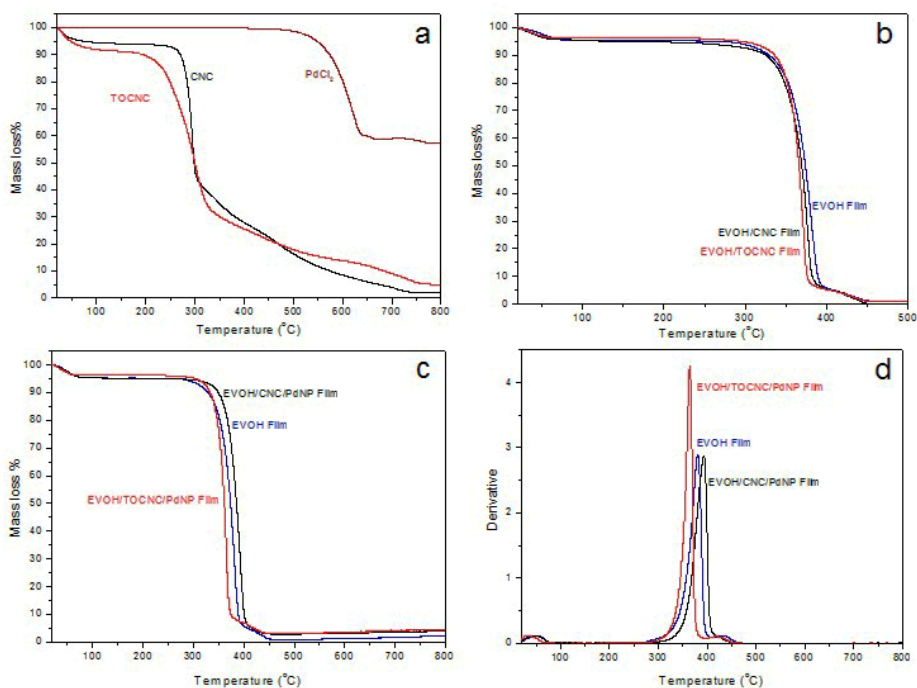


Fig. 6. Thermogravimetric analysis (TGA) curves for a) CNC, TOCNC, PdCl₂, b) EVOH/CNC, EVOH/TOCNC films and c) EVOH film, EVOH/CNC/PdNP and EVOH/TOCNC/PdNP films, and d) DTG curves for EVOH film, EVOH/CNC/PdNP and EVOH/TOCNC/PdNP films.

Table 3. Assessments of thermal stability obtained from thermogravimetric analysis (TGA) curves for CNC, TOCNC, EVOH/CNC, EVOH/TOCNC films, EVOH film EVOH/CNC/PdNP and EVOH/TOCNC/PdNP films, including degradation temperature at 5% of mass loss ($T_{5\%}$), maximum degradation temperature of the two degradation peaks (T_{d1} , T_{d2}), and residual mass at 800 °C (R_{800}).

Film sample	$T_{5\%}$ (°C)	T_{d1} (°C)	T_{d2} (°C)	R_{800} (%)
CNC	219.3	298.8	-	-
TOCNC	158.7	312.2	-	-
EVOH/CNC Film	256.2	387.0	458.9	1.9
EVOH/TOCNC Film	285.3	377.4	457.6	2.1
EVOH Film	270.5	381.0	452.3	2.2
EVOH/CNC/PdNP Film	285.1	394.3	445.1	3.9
EVOH/TOCNC /PdNP Film	301.6	365.6	445.5	4.5

3.8. Water Vapor Permeability (WVP)

Table 4 shows the WVP value for the EVOH film and EVOH/CNCs/PdNP nanocomposites. The results indicated that EVOH films containing CNCs/PdNP structures were not significantly different from neat EVOH film in terms of WVP values. Similar behavior was previously reported when bacterial cellulose CNCs incorporated into EVOH films showed a slight decrease in the water permeability of the nanocomposites, although the effect was not statistically significant for most of the samples [43]. However, Fortunati et al. (2013) obtained higher

reduction in water permeability value (59%) for systems loaded with modified-CNCs (PLA/1s-CNC/1Ag and PLA/5s-CNC/1Ag), highlighting the beneficial effect of cellulose modification on the WVP barrier properties. The reason for the permeability observations here could be related to the distortion of the crystalline morphology anticipated by the above DSC results. Crystals are typically impermeable to the transport of low molecular weight compounds, and smaller and more defective crystals can result in reduced chain immobilization factor and hence increased amorphous density for the permeants to diffuse through [44]. The effects of CNC and PdNP in the nanocomplex, however, can be more complex.

Table 4. Water vapor permeability (WVP) for EVOH film, EVOH/CNC/PdNP film and EVOH/TOCNC/PdNP film.

Sample	WVP x 10 ⁻¹⁴ (Kg·m·m ⁻² · s ⁻¹ ·Pa ⁻¹)*
EVOH Film	1.28 (2.3) ^a
EVOH/CNC/PdNP Film	1.33 (3.3) ^a
EVOH/TOCNC /PdNP Film	1.45 (2.6) ^a

* Mean value (standard error). The same superscript letter represents no statistically significant differences among the three samples (p < 0.05).

3.9. Oxygen scavenging activity

Figure 7 shows the oxygen scavenging rate (OSR) for neat EVOH and EVOH CNCs/PDNP films. The oxygen absorption of the multilayer structures was studied at 23 °C, with an initial oxygen concentration of

1.0 % in the headspace of the measuring flasks and 100% RH. The EVOH/TOCNC/PdNP film led to a faster and more significant decrease of O₂ rate. For EVOH/CNCs/PdNP (0.3/0.6 and 1%) films, the oxygen absorption (as expected) increased at nearly the same ratio as the oxygen scavenging content.

The TEM images (Figure 4) suggested that the PdNPs were dispersed on the surface of CNC, but showed greater dispersion in the case of TOCNC for which the average particle size slightly decreased. For CNCs, PdNPs were also sparsely located with more nanoparticles agglomerated. For TOCNC, the abundant carboxylic acid groups made them available to interact with PdNP; thus, the EVOH film with TOCNC/PdNP showed faster oxygen activity compared with EVOH/CNC/PdNP film. In a previous work, a higher dispersion of the nanoparticles due to surfactant addition was shown to improve the O₂ depletion rate [45]. In a further study of the topic, the oxygen scavenging of the PdNPs was enhanced by incorporating them within polycaprolactone, a more oxygen permeable material [46]. The use of capping agents can reduce or prevent aggregation but also tends to decrease the reactivity of the surface, thereby decreasing the catalytic activity of the stabilized nanoparticles. Thus, CNC can be employed as an alternative to minimize aggregation without blocking access to the reactive surface atoms [47].

Another important aspect of OSR is the effect of humidity. Water molecules that are absorbed by EVOH at high RH levels are believed to

interact with OH groups in the polymer matrix and weaken the hydrogen bonding among polymer molecules [48]. Because samples were exposed at 100% RH, the hydrophilic nature of the substrate materials presumably contribute to an accelerated water adsorption on the surface, which in turn might also promote the catalytic reaction of palladium [49].

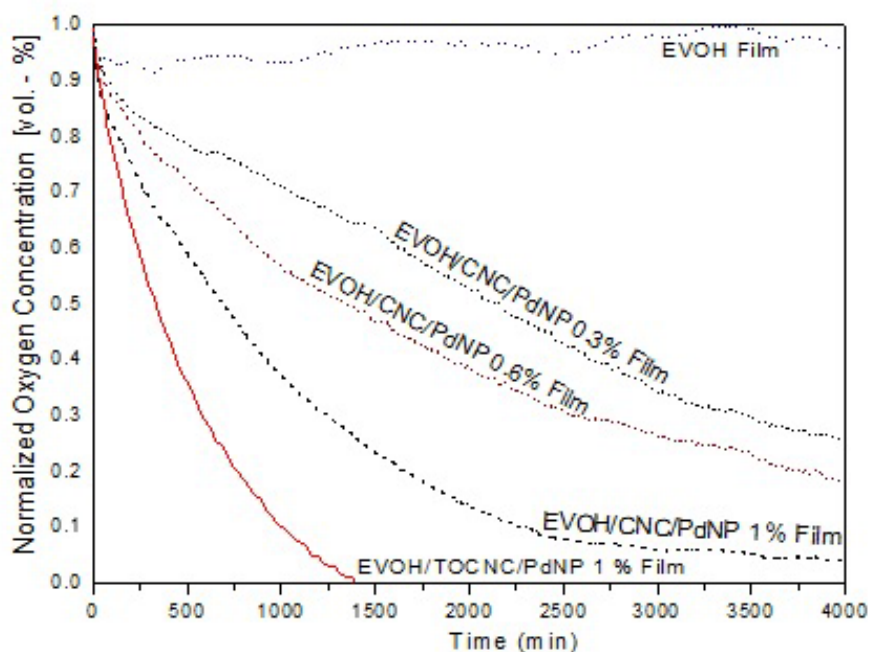


Fig. 7. Oxygen depletion for EVOH film without palladium nanoparticles (PdNPs), EVOH/CNC/PdNP (0.3, 0.6 and 1 wt. %), EVOH/TOCNC/PdNP (1 wt.%) films. Values were measured at 100% relative humidity (RH).

4. Conclusions

In this work, several techniques were employed in order to produce a novel active packaging material that could scavenge oxygen effectively. CNC was a critical component in the nanocomposite because it acted not only as reducing agent for PdCl₂ but also as support for the deposition of PdNP on EVOH. PdNP absorbed oxygen and furnished the beneficial function of oxygen scavenging for the packaging film. EVOH was chosen as the polymer matrix because it is a water-soluble polymer that is often used as oxygen barrier in packaging. Oxidation of CNC with TEMPO improved oxygen absorption. The resulting nanocomposite films seem to have promising active packaging properties.

Acknowledgements Adriane Cherpinski would like to thank the Brazilian Council for Scientific and Technological Development (CNPq) of the Brazilian Government for supporting her stay at USDA Peoria laboratories. This study would not have been possible without the financial support of her predoctoral grant (205955/2014-2). Eduardo Espinosa is grateful to the Spanish Ministry of Science and Education for support his research through the National Program FPU (grant number FPU14/02278). The authors would also like to acknowledge the funding by the MINECO project of the Spanish Government AGL2015-63855-C2-1-R.

The authors acknowledge the expert technical assistance of Jason Adkins at USDA. Mention of trade names or commercial products in this publication is solely for the purpose of providing specific information and does not imply recommendation or endorsement by the U.S. Department of Agriculture. USDA is an equal opportunity provider and employer. Mention of trade names or commercial products in this publication is solely for the purpose of providing specific information and does not imply recommendation or endorsement by the U.S. Department of Agriculture. USDA is an equal opportunity provider and employer.

6. References

1. Damaj, Ziad, Catherine Joly, and Emmanuel Guillon. "Toward New Polymeric Oxygen Scavenging Systems: Formation of Poly (Vinyl Alcohol) Oxygen Scavenger Film." *Packaging Technology and Science* 28, no. 4 (2015): 293-302.
2. Arvanitoyannis, Ioannis. *Modified Atmosphere and Active Packaging Technologies*: CRC Press, 2012.
3. Wilson, Charles L. *Intelligent and Active Packaging for Fruits and Vegetables*: CRC Press, 2007.
4. Farber, JN, LJ Harris, ME Parish, LR Beuchat, TV Suslow, JR Gorney, EH Garrett, and FF Busta. "Microbiological Safety of Controlled and Modified Atmosphere Packaging of Fresh and Fresh-Cut Produce." *Comprehensive reviews in food science and food safety* 2 (2003): 142-60.
5. Shin, Yangjai, Joongmin Shin, and Youn Suk Lee. "Preparation and Characterization of Multilayer Film Incorporating Oxygen Scavenger." *Macromolecular research* 19, no. 9 (2011): 869.
6. Dainelli, Dario, Nathalie Gontard, Dimitrios Spyropoulos, Esther Zondervan-van den Beuken, and Paul Tobback. "Active and Intelligent Food Packaging: Legal Aspects and Safety Concerns." *Trends in Food Science & Technology* 19 (2008): S103-S12.

7. Kundu, Subrata. "A New Route for the Formation of Au Nanowires and Application of Shape-Selective Au Nanoparticles in Sers Studies." *Journal of Materials Chemistry C* 1, no. 4 (2013): 831-42.
8. Mayer, A, and M Antonietti. "Investigation of Polymer-Protected Noble Metal Nanoparticles by Transmission Electron Microscopy: Control of Particle Morphology and Shape." *Colloid and Polymer Science* 276, no. 9 (1998): 769-79.
9. Masmoudi, Fatma, Atef Bessadok, Mohamed Dammak, Mohamed Jaziri, and Emna Ammar. "Biodegradable Packaging Materials Conception Based on Starch and Polylactic Acid (Pla) Reinforced with Cellulose." *Environmental Science and Pollution Research* 23, no. 20 (2016): 20904-14.
10. Arora, Amit, and GW Padua. "Nanocomposites in Food Packaging." *Journal of Food science* 75, no. 1 (2010): R43-R49.
11. Wróblewska-Krepsztul, Jolanta, Tomasz Rydzkowski, Gabriel Borowski, Mieczysław Szczypiński, Tomasz Klepka, and Vijay Kumar Thakur. "Recent Progress in Biodegradable Polymers and Nanocomposite-Based Packaging Materials for Sustainable Environment." *International Journal of Polymer Analysis and Characterization* 23, no. 4 (2018): 383-95.
12. Cirtiu, Ciprian M, Alexandre F Dunlop-Briere, and Audrey Moores. "Cellulose Nanocrystallites as an Efficient Support for Nanoparticles of Palladium: Application for Catalytic Hydrogenation and Heck Coupling under Mild Conditions." *Green Chemistry* 13, no. 2 (2011): 288-91.
13. Chakrabarty, Arindam, and Yoshikuni Teramoto. "Recent Advances in Nanocellulose Composites with Polymers: A Guide for Choosing Partners and How to Incorporate Them." *Polymers* 10, no. 5 (2018): 517.
14. Islam, MS, L Chen, J Sisler, and KC Tam. "Cellulose Nanocrystal (Cnc)–Inorganic Hybrid Systems: Synthesis, Properties and Applications." *Journal of Materials Chemistry B* 6, no. 6 (2018): 864-83.
15. Wu, Xinyun, Zengqian Shi, Sidong Fu, Jialu Chen, Richard M Berry, and Kam C Tam. "Strategy for Synthesizing Porous

- Cellulose Nanocrystal Supported Metal Nanocatalysts." *ACS Sustainable Chemistry & Engineering* 4, no. 11 (2016): 5929-35.
16. Wu, Xiaodong, Canhui Lu, Wei Zhang, Guiping Yuan, Rui Xiong, and Xinxing Zhang. "A Novel Reagentless Approach for Synthesizing Cellulose Nanocrystal-Supported Palladium Nanoparticles with Enhanced Catalytic Performance." *Journal of Materials Chemistry A* 1, no. 30 (2013): 8645-52.
 17. Tang, Zuwu, Wenyan Li, Xinxing Lin, He Xiao, Qingxian Miao, Liulian Huang, Lihui Chen, and Hui Wu. "Tempo-Oxidized Cellulose with High Degree of Oxidation." *Polymers* 9, no. 9 (2017): 421.
 18. Kaushik, Madhu, and Audrey Moores. "Nanocelluloses as Versatile Supports for Metal Nanoparticles and Their Applications in Catalysis." *Green Chemistry* 18, no. 3 (2016): 622-37.
 19. Carbone, Marilena, Domenica Tommasa Donia, Gianfranco Sabbatella, and Riccarda Antiochia. "Silver Nanoparticles in Polymeric Matrices for Fresh Food Packaging." *Journal of King Saud University-Science* 28, no. 4 (2016): 273-79.
 20. Kango, Sarita, Susheel Kalia, Annamaria Celli, James Njuguna, Youssef Habibi, and Rajesh Kumar. "Surface Modification of Inorganic Nanoparticles for Development of Organic-Inorganic Nanocomposites—a Review." *Progress in Polymer Science* 38, no. 8 (2013): 1232-61.
 21. Müller, Kerstin, Elodie Bugnicourt, Marcos Latorre, Maria Jorda, Yolanda Echegoyen Sanz, José M Lagaron, Oliver Miesbauer, Alvise Bianchin, Steve Hankin, and Uwe Bözl. "Review on the Processing and Properties of Polymer Nanocomposites and Nanocoatings and Their Applications in the Packaging, Automotive and Solar Energy Fields." *Nanomaterials* 7, no. 4 (2017): 74.
 22. Rosa, Morsyleide F, Bor-sen Chiou, Eliton S Medeiros, Delilah F Wood, Luiz HC Mattoso, William J Orts, and Syed H Imam. "Biodegradable Composites Based on Starch/Evoh/Glycerol Blends and Coconut Fibers." *Journal of Applied Polymer Science* 111, no. 2 (2009): 612-18.

23. Gavara, Rafael, Ramón Catalá Moragrega, Gracia López Carballo, Josep Pascual Cerisuelo, Irene Domínguez, Virginia Muriel Galet, and Pilar Hernández Muñoz. "Use of Evoh for Food Packaging Applications." (2017).
24. Mokwena, K Khanah, and Juming Tang. "Ethylene Vinyl Alcohol: A Review of Barrier Properties for Packaging Shelf Stable Foods." *Critical reviews in food science and nutrition* 52, no. 7 (2012): 640-50.
25. Isogai, Akira, and Yumiko Kato. "Preparation of Polyuronic Acid from Cellulose by Tempo-Mediated Oxidation." *Cellulose* 5, no. 3 (1998): 153-64.
26. Lin, Ning, Cécile Bruzzese, and Alain Dufresne. "Tempo-Oxidized Nanocellulose Participating as Crosslinking Aid for Alginate-Based Sponges." *ACS applied materials & interfaces* 4, no. 9 (2012): 4948-59.
27. Montanari, Suzelei, Mohamad Roumani, Laurent Heux, and Michel R Vignon. "Topochemistry of Carboxylated Cellulose Nanocrystals Resulting from Tempo-Mediated Oxidation." *Macromolecules* 38, no. 5 (2005): 1665-71.
28. Saito, Tsuguyuki, Satoshi Kimura, Yoshiharu Nishiyama, and Akira Isogai. "Cellulose Nanofibers Prepared by Tempo-Mediated Oxidation of Native Cellulose." *Biomacromolecules* 8, no. 8 (2007): 2485-91.
29. Segal, LGJMA, JJ Creely, AE Martin Jr, and CM Conrad. "An Empirical Method for Estimating the Degree of Crystallinity of Native Cellulose Using the X-Ray Diffractometer." *Textile Research Journal* 29, no. 10 (1959): 786-94.
30. Serra, Albert, Israel González, Helena Oliver-Ortega, Quim Tarrès, Marc Delgado-Aguilar, and Pere Mutjé. "Reducing the Amount of Catalyst in Tempo-Oxidized Cellulose Nanofibers: Effect on Properties and Cost." *Polymers* 9, no. 11 (2017): 557.
31. Martins, Guilherme BC, Marcelo R dos Santos, Marcus VR Rodrigues, Renata R Sucupira, Luisa Meneghetti, Adriano L Monteiro, and Paulo AZ Suarez. "Cellulose Oxidation and the Use of Carboxyl Cellulose Metal Complexes in Heterogeneous Catalytic Systems to Promote Suzuki-Miyaura Coupling and Co

- Bond Formation Reaction." *Journal of the Brazilian Chemical Society* 28, no. 11 (2017): 2064-72.
32. Meng, Fanrong, Guoqing Wang, Xueyu Du, Zhifen Wang, Shuying Xu, and Yucang Zhang. "Extraction and Characterization of Cellulose Nanofibers and Nanocrystals from Liquefied Banana Pseudo-Stem Residue." *Composites Part B: Engineering* 160 (2019): 341-47.
 33. French, Alfred D. "Idealized Powder Diffraction Patterns for Cellulose Polymorphs." *Cellulose* 21, no. 2 (2014): 885-96.
 34. Fortunati, E., F. Luzi, A. Jiménez, D. A. Gopakumar, D. Puglia, S. Thomas, J. M. Kenny, A. Chiralt, and L. Torre. "Revalorization of Sunflower Stalks as Novel Sources of Cellulose Nanofibrils and Nanocrystals and Their Effect on Wheat Gluten Bionanocomposite Properties." *Carbohydrate Polymers* 149 (2016): 357-68.
 35. Demir, Mustafa M, Mehmet A Gulgun, Yusuf Z Menciloglu, Burak Erman, Sergei S Abramchuk, Elena E Makhaeva, Alexei R Khokhlov, Valentina G Matveeva, and Mikhail G Sulman. "Palladium Nanoparticles by Electrospinning from Poly (Acrylonitrile-Co-Acrylic Acid)- PdCl₂ Solutions. Relations between Preparation Conditions, Particle Size, and Catalytic Activity." *Macromolecules* 37, no. 5 (2004): 1787-92.
 36. Chen, Yan, Shiyan Chen, Baoxiu Wang, Jingjing Yao, and Huaping Wang. "Tempo-Oxidized Bacterial Cellulose Nanofibers-Supported Gold Nanoparticles with Superior Catalytic Properties." *Carbohydrate Polymers* 160 (2017): 34-42.
 37. da Silva Perez, Denilson, Suzelei Montanari, and Michel R Vignon. "Tempo-Mediated Oxidation of Cellulose Iii." *Biomacromolecules* 4, no. 5 (2003): 1417-25.
 38. Karim, Zoheb, Minna Hakalahti, Tekla Tammelin, and Aji P Mathew. "In Situ Tempo Surface Functionalization of Nanocellulose Membranes for Enhanced Adsorption of Metal Ions from Aqueous Medium." *RSC Advances* 7, no. 9 (2017): 5232-41.
 39. Wang, Hualin, Heng Zhang, Baicheng Niu, Suwei Jiang, Junfeng Cheng, and Shaotong Jiang. "Structure and Properties of the Poly (Vinyl Alcohol-Co-Ethylene)/Montmorillonite-Phosphorylated

- Soybean Protein Isolate Barrier Film." *RSC Advances* 6, no. 35 (2016): 29294-302.
40. Puente, Jorge A Soto, Kateryna Fatyeyeva, Stéphane Marais, and Eric Dargent. "Multifunctional Hydrolyzed Eva Membranes with Tunable Microstructure and Water Barrier Properties." *Journal of Membrane Science* 480 (2015): 93-103.
 41. Fraschini, Carole, Grégory Chauve, and Jean Bouchard. "Tempo-Mediated Surface Oxidation of Cellulose Nanocrystals (Cncs)." *Cellulose* 24, no. 7 (2017): 2775-90.
 42. Mariano, Marcos, Nadia El Kissi, and Alain Dufresne. *Cellulose Nanomaterials: Size and Surface Influence on the Thermal and Rheological Behavior*. Vol. 28, 2018.
 43. Martínez-Sanz, Marta, Amparo Lopez-Rubio, and Jose M Lagaron. "Nanocomposites of Ethylene Vinyl Alcohol Copolymer with Thermally Resistant Cellulose Nanowhiskers by Melt Compounding (Ii): Water Barrier and Mechanical Properties." *Journal of Applied Polymer Science* 128, no. 3 (2013): 2197-207.
 44. Lagarón, J-M. "Multifunctional and Nanoreinforced Polymers for Food Packaging." In *Multifunctional and Nanoreinforced Polymers for Food Packaging*, 1-28: Elsevier, 2011.
 45. Cherpinski, Adriane, Melike Gozutok, Hilal Sasmazel, Sergio Torres-Giner, and Jose Lagaron. "Electrospun Oxygen Scavenging Films of Poly (3-Hydroxybutyrate) Containing Palladium Nanoparticles for Active Packaging Applications." *Nanomaterials* 8, no. 7 (2018): 469.
 46. Cherpinski, Adriane, Piotr K. Szewczyk, Adam Gruszczyński, Urszula Stachewicz, and Jose M. Lagaron. "Oxygen-Scavenging Multilayered Biopapers Containing Palladium Nanoparticles Obtained by the Electrospinning Coating Technique." *Nanomaterials* 9, no. 2 (2019): 262.
 47. Rezayat, Marzieh, Rebecca K Blundell, Jason E Camp, Darren A Walsh, and Wim Thielemans. "Green One-Step Synthesis of Catalytically Active Palladium Nanoparticles Supported on Cellulose Nanocrystals." *ACS Sustainable Chemistry & Engineering* 2, no. 5 (2014): 1241-50.

Chapter VI

48. Zhang, Zhongbin, Ian J Britt, and Marvin A Tung. "Permeation of Oxygen and Water Vapor through Evoh Films as Influenced by Relative Humidity." *Journal of Applied Polymer Science* 82, no. 8 (2001): 1866-72.
49. Yildirim, Selçuk, Bettina Röcker, Nadine Rüegg, and Wolfgang Lohwasser. "Development of Palladium-Based Oxygen Scavenger: Optimization of Substrate and Palladium Layer Thickness." *Packaging Technology and Science* 28, no. 8 (2015): 710-18.

4. General discussion

4. General discussion

In the conventional sense, packaging has been used for the purpose of conditioning and protecting the food, thereby constituting inert barriers. In recent years, adaptation to the new demands of consumers including maintenance of the quality, freshness and safety of the packaged product that goes beyond enclosing and protecting the products, have undergone major changes. The development of active packaging is the way industry meets these requirements. Noteworthy is the tendency of these active packages to be developed from natural and renewable materials, incorporating the functional additives into the polymer matrix, along with their inherent biodegradable properties. Polyhydroxyalkanoate polymers (PHAs) produced by microbial fermentation, such as polyhydroxybutyrate (PHB) and poly (hydroxybutyrate-co-valerate) (PHBV); as well as materials derived from polysaccharides (cellulose, starch, etc) have been used as interesting substitutes to petroleum based plastics in packaging. However, these biopolymers have shown some drawbacks with respect to conventional plastics, they have excessive rigidity, relative small processing windows and either low gas barrier or strong moisture sensitivity. This means less degree of protection, compromising the most important function of the packaging. Nevertheless, the use of the electrospinning technique to produce electrospun nanobiofibers, so called in this PhD biopapers, and multilayer composite structures obtained by different means, have significantly contributed to achieve additional functionalities and improved the

General discussion

functional properties of currently existing biodegradable packaging. Therefore, the main objective of this work was to incorporate nanoparticles, with active oxygen absorption capability, into the polymer matrix to obtain a biodegradable film with water barrier and with good oxygen scavenging properties, allowing the application of this active films as coating layers on cellulose based papers. In short, the development and characterization of hydrophobic coatings with active oxygen scavenging properties for fiber-based packaging applications was targeted.

For this purpose, in **Chapter I**, the influence of fibers alignment and post-processing by different physical treatments were studied. The electrospun fibers were randomly deposited over an static collector and aligned using a rotating drum collector. The influence of processing conditions on the degree of crystallinity, optical, mechanical and barrier properties was assessed. After inspecting different annealing temperatures, 160°C was selected to evaluate the effect of annealing time and cooling treatments on the films properties. The inspected time and cooling process conditions were: I) (t 0, 5, 10, 15 and 20 min) in air at room temperature; II) (t 0 and 5 min) in water at 25°C; III) (t 0 and 5 min) in ice and IV) slow cooling without temperature within the hydraulic hot-press. The morphology of samples cooled in air at room temperature for short time showed more compactness and less porosity while increasing the time led to higher porous structures, indicating that 5 min of annealing time was more than enough to obtain continuous and transparent films.

Later in the work, it was found that shorter times, i.e. 5 seconds, can also work. About the cooling conditions, only sample t0 in ice showed more porosity, while others did not show any significant differences. Compared to films obtained by fast cooling, PHB films with slowest cooling rate exhibited the lowest values for water and aroma permeability. The PHB samples collected on the rotating drum showed higher transparency, indicating greater homogeneity and packing. The storage modulus and tensile strength were higher for the oriented PHB sample which indicates somewhat higher rigidity of the system. No significant changes in thermal properties like melting and crystallization temperature were observed. Consequently, in **Chapter II**, the optimal conditions found out in the previous chapter, were applied to prepare mono- and multilayers based on electrospun biopolymers deposited on an uncoated paper substrate. Oriented PHB nanofibers showed enhanced adhesion to paper. For monolayers, it was also seen that in the lab experiments done in this work, a thickness dependence for the barrier properties were observed, annealed fiber mats with thicknesses above 30 μm resulted in lower permeability for water and limonene. Similar results were found for oxygen permeability, where increasing film thickness (above 80 μm) resulted in significantly reduced permeability. More importantly, the values for the water permeance of the multilayer paper/PHB showed a significant decrease for all samples in relation to uncoated paper. Some differences in performance between samples obtained by rotating or plate collector were observed for water

permeance, in particular, random multilayer structures of paper/PLA/PHB film and paper/PVOH/PHB film presented slightly higher barrier, because the thickness was higher in the latter case. In conclusion, the multilayers of paper/PLA/PHB and paper/PVOH/PHB delivered the best balance in gas and water vapour barrier performance.

Following the previous experiments, **Chapter III** was set to develop multilayer structures based on annealed electrospun biopolyesters to improve the water barrier properties of nanopapers, i.e. papers based on nanocellulose. The inherent hydrophilicity of cellulose nanopapers which generates poor resistance to water and humidity is an issue jeopardizing their application. To obtain the multilayer structures, two electrospun PHA grades, i.e. PHB and PHBV, were coated on both sides of nanopaper films made of cellulose nanofibrils (CNFs) and lignocellulose nanofibrils (LCNFs). In relation to the PHA coatings, the PHB grade was seen to produce slightly smoother surfaces compared to the PHBV coating. The effect of the lignin presence was assessed in the morphology study, thus while CNF showed fiber diameters of about 20 nm, for LCNF this was reduced to ~12 nm. The presence of globular nanoparticles in the LCNF sample between the nanofibrils was seen to reduce the interlayer distance and yielded an improved layered structure. After coating and annealing, the LCNF samples showed higher interlayer adhesion, effect that was attributed to the potentially higher binding effect of lignin. Moreover, the LCNF sample exhibited a smoother surface, which was attributed to the

reduced size of the fibers diameter for this sample. Regarding surface wettability, contact angles of 39° and 47° were measured for CNF and LCNF nanopapers films, respectively, with a slightly better performance for LCNF, ascribed to the presence of lignin. After coating, the multilayers showed higher contact angle, i.e. in the range of 75°–85°, indicating a reduction in surface wettability.

Moreover, the incorporation of electrospun PHA coatings reduced the overall mechanical stiffness and tensile strength of the multilayers but retained the sample ductility to a significant extent.

Finally, the double side coated nanopapers were seen to exhibit significantly reduced water vapor permeance as expected and also improved oxygen barrier. In doing so, the PHA coated multilayer nanopapers successfully achieved the targeted requirements.

In order to obtain films with active oxygen scavenging properties, **Chapter IV** was targeted at the incorporation of palladium nanoparticles to a matrix of PHB. Due to the large surface to volume ratio presented by nanomaterials, metal nanoparticles have a tendency to agglomerate. Thus, to optimize the distribution and dispersion of PdNP, the use of two surfactants permitted for food contact applications, hexadecyltrimethylammonium bromide (CTAB) and tetraethyl orthosilicate (TEOS), were utilized. As expected, the annealed electrospun film without surfactant exhibited more aggregation of the PdNP in the biopolyester matrix. Both surfactants used led to a more homogenous

General discussion

distribution of the nanoparticles, but the dispersion was found higher when the CTAB was used. In relation to the thermal properties, the presence of PdNP promoted a slight decrease in melting temperature and melting enthalpy, attributed to the formation of more imperfect crystals due to an anti-nucleating effect. The thermal degradation occurred in two steps for all samples, however, the films containing PdNP and surfactants presented a slight increase in thermal stability. The presence of PdNP also resulted in an enhancement of the mechanical resistance without altering the ductility and toughness characteristics of PHB.

Upon addition of PdNP, the results showed that the presence of the catalyst nanoparticles in the films led to an overall increase in WVP, but this was less pronounced for the sample containing CTAB in agreement with the morphology results. Limonene permeability was also seen to increase in the nanocomposites. Finally, the oxygen scavenging properties were also measured at 50% and 100% relative humidity (RH) for the PHB/PdNP fibers. All electrospun mats presented a significantly lower oxygen scavenging activity at 50%RH, as expected. At 100% RH, only the electrospun nanocomposite fibers containing surfactants, were able to fully reduce the oxygen levels in the headspace during the time span analysed. However, the annealed films also measured at 100% RH, did not show such strong oxygen scavenging capacity due to the reduced porosity. The best sample in terms of headspace oxygen depletion rate was the PHB/PdNP/CTAB as expected.

Albeit, the PdNP were seen to be efficient in the fibers, they were less efficient in film form. As a result, **Chapter V**, was aimed at finding a more efficient oxygen scavenging structure. PCL was selected to be a more suitable system, since it is less barrier to oxygen than PHB and is still biodegradable.

Electrospun PCL fibers containing PdNP were also carried out. These materials were coated together with PHA for facilitate degradation and water barrier over an uncoated paper substrate. Initially, the electrospun fibers were analysed by FIB-SEM to assess the distribution of the PdNP in the polymer matrix. The particles were seen to be mostly homogeneously aligned but agglomerated along the core of the PCL fibers, the dispersion of these was found to be higher than for PHA. Additional TEM studies also suggested that a fraction of the PdNP was also highly dispersed and distributed across the polymer matrix. Interestingly, the PdNP were seen to enhance the thermal stability of the two biopolymers.

Different multilayers were produced with PCL, PHA and PdNP. For the multilayer structures, the sample with the two electrospun coatings subjected to post processing by annealing, presented the expected porosity reduction, and as a result exhibited the lowest water barrier permeability. However, the optimal oxygen scavenging was found to be the best, even at 50 %RH, for the multilayers paper/PHB fibers/PCL-PdNP film and paper/PHB-PdNP fibers/PCL-PdNP film. The results suggest that as PHA is a higher barrier to oxygen than PCL, an optimal system would probably be just a PCL coating with PdNP.

In the final chapter of the PhD, a more complex high barrier layer comprising passive and active properties was aimed to be developed by the more traditional route of solvent casting, to be proposed as a potential model technology for paper coating. Thus, the aim of **Chapter VI**, was to obtain EVOH films with active oxygen scavenging properties by incorporating PdNP and CNCs. In a potential application case, this cast layer could be protected from moisture by using electrospun PHA.

In this study, the CNC were subjected to a TEMPO-mediated oxidation (TO) treatment yielding an increased carboxylate content in the nanomaterial. A three times increase in the cationic demand for CNC treated with TO was observed in comparison with the untreated CNC. Due to the increase in the carboxyl content, a gradual decrease in the thermal stability of the TOCNC samples was observed. Considering the hydrophilic nature and the good dispersion that CNCs exhibit in EVOH, nanocomposites films were produced using unmodified CNC and TOCNC as reducing supports for the creation of PdNP. The nanocomposite films produced showed good contact transparency after addition of CNCs/PdNP, which concentration was increased from 0.3 to 1%. A better dispersion of the nanofillers was inferred from the morphology data for the TOCNC sample. It was also found that PdNP were able, as observed above for the other two biopolymers, to enhance the thermal stability of the CNCs.

In terms of water barrier, the values obtained for the neat EVOH and the nanocomposites showed similar behaviour. The oxygen scavenging capacity was seen to increase in the TOCNC sample, since the increasing presence of carboxyl groups favoured a better distribution of the PdNP, accelerating the catalytic reaction.

The results presented here offer a proof that the various biopapers coatings and layers developed in this study could have significant potential to constitute new property enhanced and more sustainable solutions to coat paper of application interest in food packaging applications.

5. Conclusions

5. Conclusions

- I. A PHB fiber based biopaper made by electrospinning was developed and optimized. A subsequent post-processing annealing step was carried out. Optimal conditions for the annealing process to reduce interfiber porosity were found to be 160°C and slow cooling.
- II. The PHB biopaper developed exhibited similar barrier properties to conventional compression-molded PHB films but with improved optical properties. Within the experimental conditions carried out in this study, the minimal thickness found for the PHB biopaper to have high barrier to moisture and aroma was 30 microns while for oxygen was 80 microns.
- III. Different multilayer structures were developed where electrospun oxygen barrier PVOH was coated onto a paper substrate. To provide water barrier, PLA or PHB electrospun layers were also laminated onto both paper and paper coated PVOH. Good adhesion was found in between the various electrospun layers and to the paper, regardless of polymer chemistry.
- IV. The best barrier properties to water and limonene were achieved for the multilayer made of paper/PVOH/PHB.

Conclusions

- V. PHB and PHBV double side coatings were used to provide water barrier performance to two different nanopapers, made of cellulose nanofibrils (CNFs) and lignocellulose nanofibrils (LCNF). The interlayer adhesion was seen to be enhanced for the multilayer films based on LCNF. This observation was ascribed to the potentially higher binding effect of lignin.
- VI. The water barrier properties were seen higher for the nanopapers coated with PHBV as compared to PHB. In comparison to the neat nanopaper, the PHBV/LCNF/PHBV multilayer film, additionally showed the highest oxygen permeance reduction, ca. 35%.
- VII. Oxygen scavenging films made of PHB and PdNP were obtained by electrospinning followed by a post-processing annealing. Two food contact permitted surfactants, i.e. CTAB and TEOS, were used to improve the PdNP dispersion. The CTAB surfactant was seen to be more efficient in terms of improving the dispersion and distribution of PdNP within the biopolyester matrix.
- VIII. The best oxygen scavenging performance was found for the PHB electrospun fibers at 100%RH. The films obtained by annealing substantially reduced the oxygen scavenging rate due to a decreased accessibility of the reagents.

- IX. To further enhance to oxygen absorption capacity, incorporation of PdNP was carried out in a PCL matrix, which is a lower oxygen and water barrier material compared to PHA. Coatings of PCL and PHB active nanocomposites containing PdNP were applied onto conventional cellulose uncoated paper. Even at medium relative humidity, the higher fractional free volume of the PCL, resulted in a much faster oxygen absorption rate, compared to PHB.

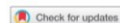
- X. The best water barrier and oxygen scavenging multilayer structure produced was found to be for the system paper/PHB film/PCL-PdNP film.

- XI. An oxygen superbarrier solvent cast layer was developed which was made of EVOH, as high oxygen barrier polymer, and CNC, as a reducing support to obtain in situ PdNP. The dispersion and oxygen scavenging capacity of the CNC-PdNP in the nanocomposites was found to be higher for the CNC that underwent TEMPO oxidation, due to the increased number of carboxyl groups created.

6. Annexes

Annex A: List of publications

ARTICLE



Post-processing optimization of electrospun submicron poly(3-hydroxybutyrate) fibers to obtain continuous films of interest in food packaging applications

Adriana Cherpinski^a, Sergio Torres-Giner ^a, Luis Cabedo^b and Jose M. Lagaron^a

^aNovel Materials and Nanotechnology Group, Institute of Agrochemistry and Food Technology (IATA), Spanish Council for Scientific Research (CSIC), Paterna, Spain; ^bPolymers and Advanced Materials Group (PIMA), Universitat Jaume I (UJI), Castellón, Spain

ABSTRACT

Polyhydroxyalkanoates (PHAs) are one of the most researched family of biodegradable polymers based on renewable materials due to their thermoplastic nature and moisture resistance. The present study was targeted to investigate the preparation and characterization of poly(3-hydroxybutyrate) (PHB) films obtained through the electrospinning technique. To convert them into continuous films and then to increase their application interest in packaging, the electrospun fiber mats were subsequently post-processed by different physical treatments. Thus, the effect of annealing time and cooling method on morphology, molecular order, thermal, optical, mechanical, and barrier properties of the electrospun submicron PHB fibers was studied. Annealing at 160°C, well below the homopolymer melting point, was found to be the minimum temperature at which homogeneous transparent films were produced. The film samples that were cooled slowly after annealing showed the lowest permeability to oxygen, water vapor, and limonene. The optimally post-processed electrospun PHB fibers exhibited similar rigidity to conventional compression-molded PHA films, but with enhanced elongation at break and toughness. Films made by this electrospinning technique have many potential applications, such as in the design of barrier layers, adhesive interlayers, and coatings for fiber- and plastic-based food packaging materials.

ARTICLE HISTORY

Received 10 April 2017
Accepted 10 July 2017

KEYWORDS



Barrier properties; coatings; electrospinning; packaging; polyhydroxyalkanoates

Introduction

The use of plastic materials in the food packaging area has been steadily increasing over recent decades due to a number of advantages (cost, versatility, lightness, etc.). However, their extensive use has created some challenges for waste management treatment procedures. In this regard, the use of bio-based and biodegradable polymers has recently received increased attention because of their potential as substitutes for petroleum-based polymers in a broad range of applications (Tharanathan 2003; Shah et al. 2014). The use of bio-based biodegradable and compostable polymers ('biopolymers') can lead to improved management of the plastic residues, as well as a reduction in dependency on fossil oil. However, one of the main disadvantages arising from the implementation of biopolymers based on renewable resources is that they present either low barrier performance or strong dependence of

physical properties on moisture, which can potentially compromise both food quality and safety. Thus, depending on the application, different material characteristics are needed: for fresh produce, selective gas-permeable materials are essential, while high-barrier materials are needed for oxygen-sensitive products (Lagaron 2011; Bhardwaj et al. 2014; Rujnić-Sokele and Pilipović 2017).

Among biopolymers, there has been particular interest in the use of polyhydroxyalkanoates (PHAs) (Plackett and Siro 2011). However, the use of PHAs in the plastic industry has been limited by several drawbacks such as the high production costs, brittleness, and low thermal stability in the molten state. One of the most extensively studied biopolymers within the PHA family is poly(3-hydroxybutyrate) (PHB). Its biocompatibility with the human body makes PHB also suitable for a number of biomedical applications (such as implants, surgical plasters, drug delivery systems, and

CONTACT Jose M. Lagaron  lagaron@iata.csic.es  Novel Materials and Nanotechnology Group, Institute of Agrochemistry and Food Technology (IATA), Spanish Council for Scientific Research (CSIC), Calle Catedrático Agustín Escardón Benlloch 7, Paterna, Spain

© 2017 Informa UK Limited, trading as Taylor & Francis Group

Multilayer structures based on annealed electrospun biopolymer coatings of interest in water and aroma barrier fiber-based food packaging applications

Adriane Cherpinski ¹, Sergio Torres-Giner ¹, Luis Cabedo ², Jose Alberto Méndez ³,
 Jose M. Lagaron ¹

¹Novel Materials and Nanotechnology Group, Institute of Agrochemistry and Food Technology (IATA), Spanish Council for Scientific Research (CSIC), Calle Catedrático Agustín Escardino Benlloch 7, Paterna 46980, Spain

²Polymers and Advanced Materials Group (PIMA), Universitat Jaume I (UJI), Avenida de Vicent Sos Baynat s/n, Castellón 12071, Spain

³Department of Chemical Engineering, LEPAMAP Group, University of Girona, Ma Aurèlia Capmany 61, Girona 17003, Spain

Correspondence to: J. M. Lagaron (E-mail: lagaron@iata.csic.es)

ABSTRACT: In this research work, for the first time, a fiber-based packaging material was coated by annealed electrospun ultrathin fibers of poly(3-hydroxybutyrate), poly(vinyl alcohol), and polylactide. The resultant mono- and multilayer structures self-adhered to the paper substrate and were characterized in terms of morphology, optical, and barrier properties. Additionally, the use of a static flat plate and rotating mandrel collector as well as the application of different electrospinning deposition times were analyzed. The thermally treated electrospun biopolymers yielded totally transparent films while, due to the opaque nature of the uncoated paper substrate, the developed packaging materials were also opaque but with a glossier surface finish provided by the bioplastic coating. The annealed films obtained from random electrospun fibers, that is, the mats of ultrathin fibers collected on the static plate, presented higher transparency and thickness and also enhanced barrier performance. On the overall, the developed annealed electrospun biopolymer coatings resulted in a significant improvement of the paper barrier properties to water and limonene vapors, being the paper/poly(vinyl alcohol)/poly(3-hydroxybutyrate) film the best performing multilayer packaging structure. © 2017 Wiley Periodicals, Inc. *J. Appl. Polym. Sci.* **2017**, *134*, 45501.

KEYWORDS: biopolymers and renewable polymers; coatings; electrospinning; optical properties; packaging

Received 11 May 2017; accepted 29 June 2017

DOI: 10.1002/app.45501

INTRODUCTION

Lightweight, renewability, and recyclability represent the main advantages of fiber-based packaging, which is highly used in the food packaging industry. The concept of fiber-based packaging, habitually referred for simplicity as paper, includes different types of materials such as sulfite paper, Kraft paper, grease-free paper, paperboards, and laminated paper.¹ This material is mainly made of cellulosic pulp fibers that are derived from renewable resources, including wood and nonwood lignocellulosic materials.² After processing, the paper surface habitually remains rather rough and porous. Filling paper with a color-containing pigment is an excellent method to improve certain qualities, including weight, surface smoothness, opacity, gas permeability, and ink absorbency.³ However, the porosity and hydrophilic nature of paper, which are intrinsically ascribed to the hydroxyl groups (O–H) of cellulose, create some limitations for its use on food packaging applications. These are mainly related to the high permeation of moisture, organic vapors, and

gases, and to the adsorption of oils. This certainly makes uncoated paper unable to retain its proper shape, resulting in a loss of quality and organoleptic properties for the packaged products.⁴

The limitations described above can be reduced by the application of plastic coatings to paper that can advantageously increase paper stiffness too. Nevertheless, these plastic materials are habitually based on polymers obtained from monomers derived from petroleum that certainly limits intrinsic sustainability aspects of fiber-based packaging materials such as recyclability, biodegradability, carbon footprint, etc.⁵ In contrast to traditional petroleum-based plastics, biopolymers certainly represent a promising alternative as paper coatings due to their environmentally friendly nature both in terms of natural origin and biodegradability.⁶ Indeed, the association of biopolymers to paper provides interesting functionalities while maintaining the environmentally friendly characteristics of the packaging material.⁷ In particular, biodegradable polymers can enhance

© 2017 Wiley Periodicals, Inc.

*Materials
Views*

WWW.MATERIALSVIEWS.COM

45501 (1 of 11)

J. APPL. POLYM. SCI. **2017**, DOI: 10.1002/APP.45501



Improving the water resistance of nanocellulose-based films with polyhydroxyalkanoates processed by the electrospinning coating technique

Adriane Cherpinski · Sergio Torres-Giner · Jari Vartiainen · Maria Soledad Peresin · Panu Lahtinen · Jose M. Lagaron

Received: 23 August 2017 / Accepted: 2 January 2018 / Published online: 11 January 2018
© Springer Science+Business Media B.V., part of Springer Nature 2018

Abstract Polyhydroxyalkanoates (PHAs) comprise a family of biodegradable aliphatic polyesters with enhanced sustainable profile and high water vapor barrier. As environmentally friendly materials, nanostructured cellulose-based films, also called nanopapers, such as films made of cellulose nanofibrils (CNFs) and lignocellulose nanofibrils (LCNFs), are also of growing interest due to their high mechanical strength and outstanding oxygen barrier properties at dry conditions. Unfortunately, nanopapers are highly hydrophilic, lacking of sufficient moisture resistance for uses in, for instance, food packaging. The present study reports, for the first time, on the effect of electrospun poly(3-hydroxybutyrate) (PHB) and poly(3-hydroxybutyrate-co-3-hydroxyvalerate) (PHBV) double side coatings on the morphology, water contact angle, mechanical properties, and barrier performance of CNF and LCNF films. The

resultant multilayer structures showed significantly improved water contact resistance, more balanced mechanical properties, and higher barrier performance against water vapor in comparison to the neat nanopapers. Although the PHA-coated nanopapers presented slightly lower aroma barrier due to the intrinsic affinity of PHA for limonene uptake, these sustainable multilayer films further improved the oxygen performance of the nanopapers, showing significant potential as barrier materials even at high humidity conditions. As a result, the here-developed novel films, based on nanopapers double side coated with electrospun PHB and PHBV layers, appear as a very promising fully bio-based material concept for food packaging applications due to their outstanding water vapor and oxygen barrier performance.

Keywords PHB · PHBV · Nanopaper · Nanocellulose · Electrospinning · Barrier packaging

A. Cherpinski · S. Torres-Giner · J. M. Lagaron (✉)
Novel Materials and Nanotechnology Group, Institute of Agrochemistry and Food Technology (IATA), Spanish Council for Scientific Research (CSIC), Paterna, Spain
e-mail: lagaron@iata.csic.es

J. Vartiainen · M. S. Peresin · P. Lahtinen
VTT Technical Research Centre of Finland Ltd, Espoo, Finland

M. S. Peresin
Forest Products Development Center, School of Forestry and Wildlife Sciences, Auburn University, Auburn, AL, USA



Introduction

There is a remarkable trend in the packaging industry toward more sustainable packaging materials that are biodegradable, not interfering with the end-of-life or recovery schemes and helping to avoid plastic waste accumulation (Babu et al. 2013). Simultaneously, there is a considerable interest in bio-based polymers, which can serve to develop sustainable polymer



Article

Electrospun Oxygen Scavenging Films of Poly(3-hydroxybutyrate) Containing Palladium Nanoparticles for Active Packaging Applications

Adriane Cherpinski ¹, Melike Gozutok ¹, Hilal Turkoglu Sasmazel ² , Sergio Torres-Giner ¹ 
and Jose M. Lagaron ^{1,*} 

¹ Novel Materials and Nanotechnology Group, Institute of Agrochemistry and Food Technology (IATA), Spanish Council for Scientific Research (CSIC), Calle Catedrático Agustín Escardino Benlloch 7, 46980 Paterna, Spain; adricherpinski@iata.csic.es (A.C.); melikegozutok@gmail.com (M.G.); storresginer@iata.csic.es (S.T.-G.)

² Department of Metallurgical and Materials Engineering, Atilim University, Incek, Golbasi, 06830 Ankara, Turkey; hilal.sasmazel@atilim.edu.tr

* Correspondence: lagaron@iata.csic.es; Tel.: +34-96-3900022; Fax: +34-96-3636301

Received: 29 May 2018; Accepted: 21 June 2018; Published: 27 June 2018



Abstract: This paper reports on the development and characterization of oxygen scavenging films made of poly(3-hydroxybutyrate) (PHB) containing palladium nanoparticles (PdNPs) prepared by electrospinning followed by annealing treatment at 160 °C. The PdNPs were modified with the intention to optimize their dispersion and distribution in PHB by means of two different surfactants permitted for food contact applications, i.e., hexadecyltrimethylammonium bromide (CTAB) and tetraethyl orthosilicate (TEOS). Analysis of the morphology and characterization of the chemical, thermal, mechanical, and water and limonene vapor barrier properties and the oxygen scavenging capacity of the various PHB materials were carried out. From the results, it was seen that a better dispersion and distribution was obtained using CTAB as the dispersing aid. As a result, the PHB/PdNP nanocomposites containing CTAB provided also the best oxygen scavenging performance. These films offer a significant potential as new active coating or interlayer systems for application in the design of novel active food packaging structures.

Keywords: polyhydroxyalkanoates; palladium nanoparticles; packaging; electrospinning

1. Introduction

An important increasing quantity of plastic waste is being generated yearly for which the precise needed time for its biodegradation is certainly unknown. This environmental awareness has driven the development and improvement of new biodegradable polymers, especially for single-use plastic items [1]. In this sense, polyhydroxyalkanoates (PHAs) are well-known biopolymers that can be produced microbially by a variety of microorganisms as an energy storage mechanism. They exhibit similar performance in terms of mechanical, thermal, and barrier properties than petroleum-derived polymers and, thus, they can potentially replace conventional thermoplastics (e.g., polyolefins) in a wide range of applications [2]. In particular, barrier properties are of fundamental importance for food packaging applications. For instance, there are many food products that are very sensitive to oxidation and, to overcome this issue, packages with reduced oxygen permeability are desirable. Additionally, the water resistance is also important, particularly for plastic materials intended for direct contact with high moisture foodstuff as well as materials to be applied in high humidity conditions during storage and/or transport [3].



Article

Oxygen-Scavenging Multilayered Biopapers Containing Palladium Nanoparticles Obtained by the Electrospinning Coating Technique

Adriane Cherpinski ¹, Piotr K. Szewczyk ², Adam Gruszczyński ², Urszula Stachewicz ² and Jose M. Lagaron ^{1,*}

¹ Novel Materials and Nanotechnology Group, Institute of Agrochemistry and Food Technology (IATA), Spanish Council for Scientific Research (CSIC), Calle Catedrático Agustín Escardino Benlloch 7, 46980 Paterna, Spain; adricherpinski@iata.csic.es

² AGH University of Science and Technology, International Centre of Electron Microscopy for Materials Science, Faculty of Metals Engineering and Industrial Computer Science, Al. A. Mickiewicza 30, 30-059 Kraków, Poland; pszew@agh.edu.pl (P.K.S.); gruszcz@agh.edu.pl (A.G.); ustachew@agh.edu.pl (U.S.)

* Correspondence: lagaron@iata.csic.es; Tel.: + 34-96-3900-022; Fax: +34-96-3636-301

Received: 11 January 2019; Accepted: 11 February 2019; Published: 14 February 2019



Abstract: The main goal of this study was to obtain, for the first time, highly efficient water barrier and oxygen-scavenging multilayered electrospun biopaper coatings of biodegradable polymers over conventional cellulose paper, using the electrospinning coating technique. In order to do so, poly(3-hydroxybutyrate) (PHB) and polycaprolactone (PCL) polymer-containing palladium nanoparticles (PdNPs) were electrospun over paper, and the morphology, thermal properties, water vapor barrier, and oxygen absorption properties of nanocomposites and multilayers were investigated. In order to reduce the porosity, and to enhance the barrier properties and interlayer adhesion, the biopapers were annealed after electrospinning. A previous study showed that electrospun PHB-containing PdNP did show significant oxygen scavenging capacity, but this was strongly reduced after annealing, a process that is necessary to form a continuous film with the water barrier. The results in the current work indicate that the PdNP were better dispersed and distributed in the PCL matrix, as suggested by focus ion beam-scanning electron microscopy (FIB-SEM) experiments, and that the Pd enhanced, to some extent, the onset of PCL degradation. More importantly, the PCL/PdNP nanobiopaper exhibited much higher oxygen scavenging capacity than the homologous PHB/PdNP, due to most likely, the higher oxygen permeability of the PCL polymer and the somewhat higher dispersion of the Pd. The passive and active multilayered biopapers developed here may be of significant relevance to put forward the next generation of fully biodegradable barrier papers of interest in, for instance, food packaging.

Keywords: polyhydroxyalkanoates; polycaprolactone; biopapers; palladium nanoparticles; oxygen scavengers; electrospinning; fiber based packaging

1. Introduction

Active technologies, when applied to packaging refer to the incorporation of certain additives into the packaging structure. These additives may be loose as sachets within the design, attached to the inside part or, more recently, dispersed as an additive within the packaging materials, in order to maintain or even extend product quality and shelf-life [1].

Permeated or head space oxygen in packaged foods, beverages, and pharmaceuticals can promote a range of oxidative degradation reactions and support microbial growth, ultimately impacting on

Annex B: Additional work

ACS7 – Novel Topcoat Functionality

Date/Time: Sunday, April 15th 11:00am – 12:30 pm

ACS7: High Performance Active Electrospun Polyhydroxyalkanoate Based Coatings

Adriane Cherpinski¹, Christian Kossel², Sergio Torres-Giner¹ and Jose Maria Lagaron¹.

¹ Novel Materials and Nanotechnology Group, IATA-CSIC, Paterna, Spain.

² PTS Papiertechnische Stiftung, Munich, Germany

Summary

The present study describes the development and characterization of a paper coated by the electrospinning coating technique with a bilayer structure based on poly(vinyl alcohol) (PVOH) and poly(3-hydroxybutyrate) (PHB) to provide a new multilayer system with enhanced physical and barrier performance. Using this innovative coating technique, non-woven nanofibers of the two polymers were deposited over the uncoated paper that later underwent a curing step to produce a continuous uniform layer by fibers coalescence.

Introduction

Innovation in food packaging is a key strategy to reduce both food waste and the environmental footprint of packaging materials, especially in short-term and disposable applications. Fiber-based packaging materials, habitually referred as paper, have many advantages over traditional plastics such as renewability, recyclability, and compostability (Guazzotti et al. 2014). However, their application is restricted due to the intrinsic high sensitivity to moisture of paper (Hult et al. 2013).

To prevent and/or minimize the loss of physical strength and to improve water resistance, the surface of fiber-based packaging materials can be coated with hydrophobic materials, typically plastics (Han et al. 2010). To still keep the intrinsic sustainability aspects of fiber-based packaging materials, biopolymers certainly represent a promising alternative over traditional petroleum-based plastics as paper coatings due to their natural origin and biodegradability (Fabra et al. 2013). On the one hand, poly(vinyl alcohol) (PVOH) is a petrochemical water soluble and biodegradable polymer with an outstanding oxygen barrier performance at dry conditions. In particular, its oxygen permeability varies from $1.7 \times 10^{-22} \text{ m}^3 \cdot \text{m} \cdot \text{m}^{-2} \cdot \text{Pa}^{-1} \cdot \text{s}^{-1}$, at 0% relative humidity (RH), to $9 \times 10^{-19} \text{ m}^3 \cdot \text{m} \cdot \text{m}^{-2} \cdot \text{Pa}^{-1} \cdot \text{s}^{-1}$, at 0% RH (Lagaron, 2011). On the other, bacterial aliphatic polyhydroxyalkanoates (PHAs), such as poly(3-hydroxybutyrate) (PHB), present excellent barrier properties to water vapor. For instance, PHB films in the range of 100–700 μm have reported to present a water vapor

permeability of approximately $1.70 \times 10^{-15} \text{ kg}\cdot\text{m}\cdot\text{m}^{-2}\cdot\text{Pa}^{-1}\cdot\text{s}^{-1}$ (Sanchez-Garcia et al. 2007).

Recent works of our research group have shown the potential of the so-called “electrospinning coating technology” to develop packaging structures of higher quality and safety, showing a high capacity to extend the shelf life of food products (Cherpinski et al. 2018; Cherpinski, Torres-Giner, Cabedo, Méndez et al. 2017). This technology is based on the application of a post-processing curing treatment, at a temperature below the biopolymer’s melting temperature (T_m) for few seconds, on electrospun mats (Cherpinski, Torres-Giner, Cabedo, Lagaron 2017). The present study describes the coating of paper with a bilayer PVOH/PHB electrospun film and shows for the first time the characterization of some relevant paper properties.

Material and Methods

Two grades of PVOH were tested, POVAL® 18-88 and 28-88, obtained from Kuraray Europe GmbH (Hattersheim, Germany). PHB homopolymer was P226F, supplied by Biomer (Krailling Germany). Kraft paper, of $120\text{g}/\text{m}^2$ in a basis weight, was purchased from Mondi Ltd. (United Kingdom, England). 2,2,2-trifluoroethanol (TFE) with 99% purity was obtained from Sigma-Aldrich S.A. (Madrid, Spain).

Film Preparation

The biopolymer solutions were prepared by dissolving PHB and PVOH under continuous stirring in TFE and distilled water at 80°C, respectively. The optimal weight contents (wt.-%) of each biopolymer in the solutions were 10 wt.-%, for PHB, and 12 wt.-%, for PVOH.

Electrospinning was performed using a Fluidnatek® LE10 coating lab line from Bioinicia S.L. (Valencia, Spain) with a variable high-voltage 0–30 kV power supply. Bioinicia also offers a contract manufacturing plant for industrial coating of paper rolls using this technology. The above lab device was equipped with a motorized injector that was scanning horizontally towards a rotating mandrel, aiming to obtain a homogeneous electrospun deposition. The different biopolymers solutions were transferred to a 30-mL plastic syringe, with an internal diameter of 22.5 mm, which was coupled by means of a Teflon tube to a stainless-steel needle ($\varnothing=0.9$ mm) while the needle tip was connected to the power supply. The paper substrate was placed on a rotating mandrel, rotating at 500 rpm. Out of the two PVOH grades, the 18-88 grade resulted in a more stable processing and hence this grade was selected for the coating. The selected PVOH grade was first electrospun on the paper substrate for 2h and, over the PVOH layer, PHB was then electrospun for 4h. For both PVOH grades, the applied voltage and flow-rate were 18 kV and 0.5 ml/h. In the case of PHB, the selected processing conditions were

set at 16 kV and 6 ml/h. Both biopolymer solutions were electrospun at room temperature, *i.e.* 25°C, while the tip-to-collector distance was 15 cm. The resultant electrospun mats and coated papers were subjected to a curing process using a hydraulic press 4122-model from Carver, Inc. (Wabash, IN, USA). The treatment was performed at 160°C for PHB and at 200°C for PVOH for few seconds, both without pressure. The resultant films were right after air cooled at room temperature. Fig. 1 shows a scheme illustrating the prepared mono- and multilayer structures. Prior to evaluation, the films were equilibrated in desiccators containing dried silica gel at constant temperature of 25°C for, at least, 1 week.

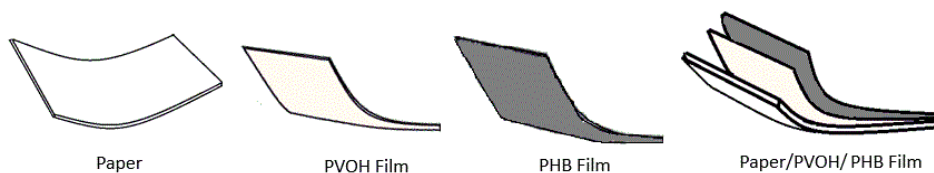


Fig. 1. Scheme of the mono- and multilayer structures based on paper and cured electrospun fibers of PVOH and PHB.

Characterization

The morphology of the electrospun fibers and the fracture surfaces of the cured films were observed by scanning electron microscopy (SEM) using an S-4800 from Hitachi (Tokyo, Japan). Cryo-fractures of the films were obtained from samples snap in liquid nitrogen. The samples were prior to observation sputtered with a mixture of gold-palladium under vacuum and observed using an accelerating voltage of 5 kV. Sizes were

determined by the software Image J 1.4 and at least 10 SEM micrographs were used for the measurements.

Thicknesses were measured using a digital micrometer series S00014, having ± 0.001 mm accuracy, from Mitutoyo Corporation (Kawasaki, Japan). Measurements were performed at three random positions and values were averaged.

The grease resistance of the film samples was evaluated according to the standard method Tappi T559 pm-96 (Ham-Pichavant, Sèbe, Pardon, & Coma, 2005). For this, a series of solutions with different Kit numbers (1–12) were used, which contained specific proportions of three reagents: castor oil, toluene, and *n*-heptane. Oil number 1 was the least aggressive oil, *i.e.* with the highest surface energy while oil number 12 was the most aggressive oil, *i.e.* with the lowest surface energy. The various liquids were dropped onto the paper surface from a predetermined height. After 15 s, the oils were removed with tissue. The highest numbered liquid that remained on the film surface without causing staining, was reported as the Kit value for the paper. A paper with a Kit test 12 indicates the fattest resistant surface.

Water absorption of paperboard was recorded as the Cobb value, according to ISO535, Paper and Board – Determination of Water Absorptiveness – Cobb Method. This was defined as the amount of water in grams per square meter that was absorbed over the test area under a water pressure of 10 mm for 60 seconds.

The surface tension and contact angle are characteristic variables to determine the wettability and potential adhesion of coatings on the paper surface. Contact angle was measured using the DAT1100 Dynamic Contact Angle Tester from FIBRO System AB (Stockholm, Sweden). The surface tension was derived from the contact angle measurements.

Determination of the surface roughness was performed by using the Bendtsen apparatus, according to ISO8791-2:2013, Paper and board determination of roughness/smoothness (air leak methods)—part 2: Bendtsen method.

Determination of foldability and scoring characteristics were performed according to DIN 55437-2. This describes the ability of the coated paper to get creased without occurrence of any cracks on the coating.

The water vapor permeability of the individual layers and the permeance of the multilayers were determined according to the ASTM E96 gravimetric method using Payne permeability cups as described in previous works (A. Cherpinski, S; Cabedo, L; Méndez, J.A; and Lagaron, J.M., 2017). Each film sample was sealed to a permeation cell containing liquid water and the cells were weighed regularly under controlled environmental conditions until the steady-state was reached. Measurements were performed in triplicate and averaged.

Results and discussion

The SEM images included in Fig. 2 show the morphologies of the neat paper (top view), the electrospun fibers of the individual layers, and the multilayer film (fracture surface view). The surface view of the Kraft paper, shown in Fig. 2a, indicates that this consisted of microfibers as expected. These cellulosic fibers presented a mean cross-section diameter of $60 \pm 35 \mu\text{m}$, which clearly contribute to the high level of porosity of paper. As opposite, in Fig. 2b and 2c, one can observe that the electrospinning process generated mats composed of non-woven ultrathin fibers. The PVOH and PHB nanofibers presented mean cross-section fiber diameters of approximately $258 \pm 25 \text{ nm}$ and $220 \pm 20 \text{ nm}$, respectively. In Fig. 2d, the cross-section of the multilayer structure revealed that the curing process resulted in a phenomenon of nanofibers coalescence, leading to a packing rearrangement of the electrospun fibers into a continuous film that was strongly adhered to the paper surface. The combined thickness of the resultant electrospun bilayer coating presented a mean thickness of *ca.* $50 \mu\text{m}$ out of which $10 \mu\text{m}$ were of PVOH. It was not feasible to discern one layer from the other, hence supporting the strong interadhesion of the hydrophobic to the hydrophilic electrospun nanofiber based layers after curing.

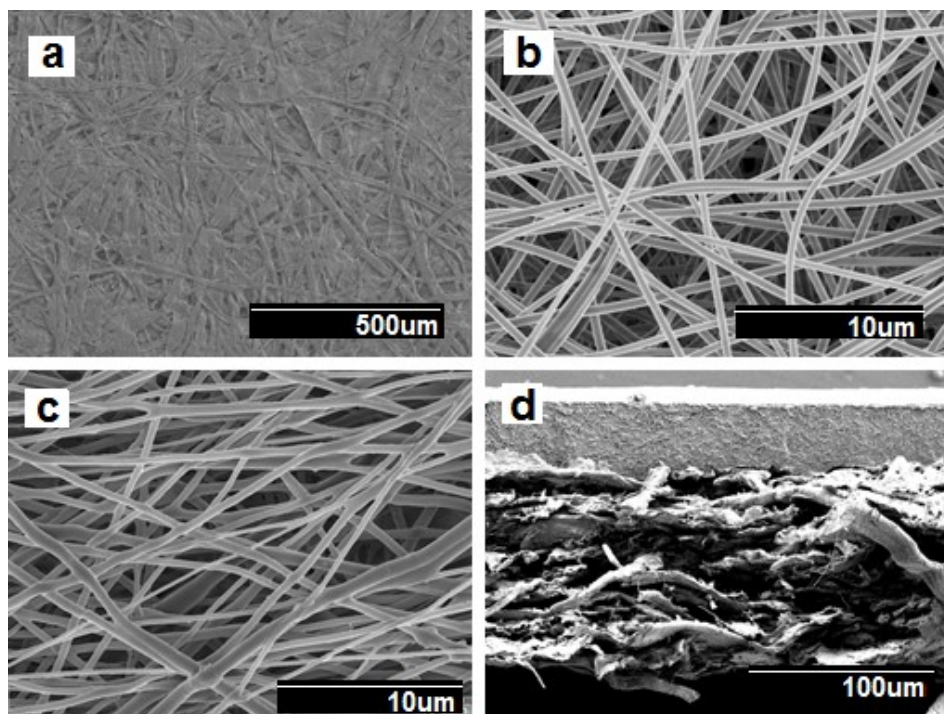


Fig. 2. Scanning electron microscopy (SEM) micrographs of: (a) Paper; (b) electrospun PVOH fibers; (c) electrospun PHB fibers; (d) cross-section of the annealed Paper/PVOH/PHB film.

Table 1 shows some relevant parameters typically used to characterize paper of the neat the paper and multilayer film. The grease resistance test showed that the electrospun bilayer film offers a high repellence capacity against fat and oil. In particular, it reached the highest possible value, *i.e.* 12. In comparison, the uncoated paper resulted in values of only 1, *i.e.* a very poor repellence ability.

Water absorption values, determined by the Cobb Test, were 29 g/m² and 1 g/m², for the uncoated paper and the multilayer film, respectively.

Therefore, the presence of the PVOH/PHB bilayer electrospun film provided a low water absorption ability to the system. The water contact angle of the barrier layer is habitually considered one of the most important factors predicting standard coatability. From this measurement we can observed that the multilayer has higher hydrophobicity and lower oleophobicity as expected.

In relation to roughness, the results show that by coating the kraft paper with the electrospun PVOH/PHB bilayer film, the surface became significantly smoother. Moreover, it can be seen that in the machine direction (MD) as well as in the cross-section direction (CD) the electrospun coating did not impair the foldability of the substrate.

Table 1. Summary of technical parameters obtained for neat paper and the multilayer film.

Property	Units/Method	Structure		Summary
		Paper	Paper/PVOH /PHB Film	
Grease resistance	KIT- Test TAPPI T559	<1	>12	High resistance
Water absorptiveness	[g/m ²] Cobb-Test	29	1	Low water absorption

Surface tension	[mN/m]	39	21	Wettability decreases
Contact angle	[°] PTS-PP:103/85	H ₂ O: 68	H ₂ O: 110	>90° +
		Formamide: 89	Formamide: 57	<90° -
Foldability and scoring characteristics	[µm] DIN 55437-2	CD: 7 MD: 7	CD: 7 MD: 5	No influence
Roughness	[ml/min] Bendtsen	504	64	<100ml/min ~Smooth

Finally, Fig. 3 shows the water vapor permeance of the neat paper and of the multilayer film. From this, it can be observed that the water vapour transmission rate was found to be 10 times lower in the paper after the incorporation of the electrospun bilayer coating, reaching a permeance value of ca. $2 \times 10^{-10} \text{ kg}\cdot\text{m}^{-2}\cdot\text{Pa}^{-1}\cdot\text{s}^{-1}$. The above reduction in water vapour transmission rate can be explained by the much lower water vapor permeability measured in the neat cured electrospun PHB film, *i.e.* $2.1 \times 10^{-15} \text{ kg}\cdot\text{m}\cdot\text{m}^{-2}\cdot\text{Pa}^{-1}\cdot\text{s}^{-1}$, in comparison to both the permeability of the neat

cured electrospun PVOH film and of the uncoated paper, *i.e.* 29 and $340 \times 10^{-15} \text{ kg}\cdot\text{m}\cdot\text{m}^{-2}\cdot\text{Pa}^{-1}\cdot\text{s}^{-1}$, respectively. Oxygen permeability experiments will also be carried out in the multilayers in the near future to assess if the PVOH and PHB combined layers can additionally lead to a reduced oxygen transmission rate, as would be expected from the known high oxygen barrier of PVOH when protected from direct moisture content.

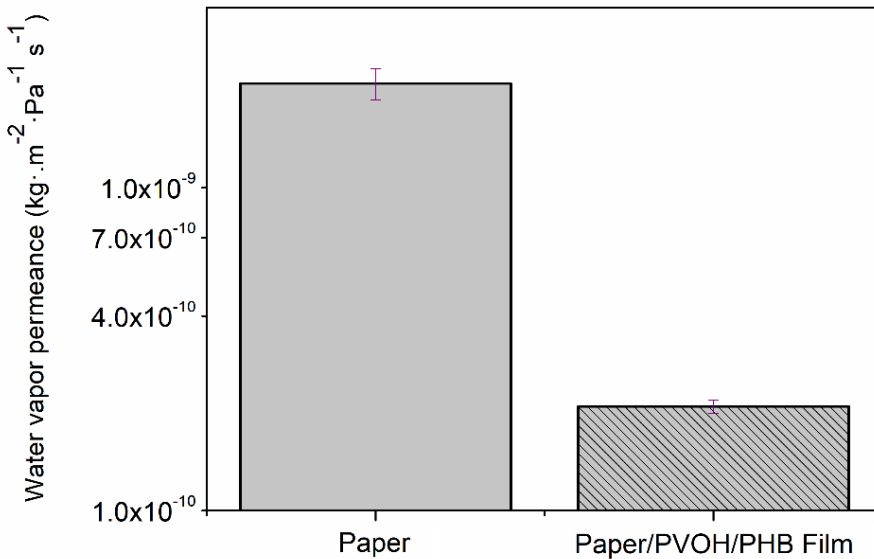


Fig. 3. Water vapor permeance of Paper and of the multilayer Paper/PVOH/PHB film.

Conclusion

The above results showed the potential of the electrospinning coating technique to generate strongly adhered, smooth and water and grease resistant coatings based on combining hydrophilic and hydrophobic biodegradable polymers on paper. It was also found that the water transmission rate dropped by ca. one order of magnitude by coating paper with PVOH and PHB layers, leading to a multilayer with potential application interest in food packaging applications.

Acknowledgements

The authors would like to thank the Spanish Ministry of Economy and Competitiveness (MINECO) project AGL2015-63855-C2-1-R and to the H2020 EU project YPACK for funding. A. Cherpinski is also supported by the Brazilian Council for Scientific and Technological Development (CNPq) of the Brazilian Government with a predoctoral scholarship (205955/2014-2).

References

- Cherpinski, A., Torres-Giner, S., Cabedo, L., Lagaron, J.M. (2017). Post-processing optimization of electrospun submicron poly(3-hydroxybutyrate) fibers to obtain continuous films of interest in food packaging applications. *Food Additives & Contaminants: Part A*, 34, 1817-1830.
- Cherpinski, A., Torres-Giner, S., Vartiainen, J., Peresin, M. S., Lahtinen, P., Lagaron, J.M. (2018). Improving the water resistance of nanocellulose-based films with polyhydroxyalkanoates processed by the

electrospinning coating technique. Cellulose, DOI: 10.1007/s10570-018-1648-z.

Cherpinski, A., Torres-Giner, S., Cabedo, L, Méndez, J.A, Lagaron, J.M. (2017). Multilayer Structures Based on Annealed Electrospun Biopolymer Coatings of Interest in Water and Aroma Barrier Fiber-Based Food Packaging Applications. *Journal of Applied Polymer Science*, 134, 45501.

Fabra, M.J., Busolo, M.A., Lopez-Rubio, A., Lagaron, J.M. (2013). Nanostructured biolayers in food packaging. *Trends in Food Science & Technology*, 31(1), 79-87.

Guazzotti, V., Marti, A., Piergiovanni, L., Limbo, S. (2014). Bio-based coatings as potential barriers to chemical contaminants from recycled paper and board for food packaging. *Food Addit Contam Part A Chem Anal Control Expo Risk Assess*, 31, 402-413.

Ham-Pichavant, F., Sèbe, G., Pardon, P., Coma, V. (2005). Fat resistance properties of chitosan-based paper packaging for food applications. *Carbohydrate Polymers*, 61, 259-265.

Han, J., Salmieri, S., Le Tien, C., Lacroix, M. (2010). Improvement of water barrier property of paperboard by coating application with biodegradable polymers. *J. Agric. Food Chem.*, 58, 3125-3131.

Hult, E.-L., Ropponen, J., Poppius-Levlin, K., Ohra-Aho, T., Tamminen, T. (2013). Enhancing the barrier properties of paper board by a novel lignin coating. *Industrial Crops and Products*, 50, 694-700.

Lagaron, J.M. (2011). In: Multifunctional and nanoreinforced polymers for food packaging. In *Multifunctional and Nanoreinforced Polymers for Food Packaging* (pp. 1-28). Cambridge, UK: Woodhead Publishing.

Sanchez-Garcia, M.D., Gimenez, E., Lagaron, J. M. (2007). Novel PET Nanocomposites of Interest in Food Packaging Applications and Comparative Barrier Performance With Biopolyester Nanocomposites. *Journal of Plastic Film & Sheeting*, 23, 133-148.

